Appendix

Appendix A

Characterization of 2-Methylglyceric Acid Oligomers in Secondary Organic Aerosol Formed from the Photooxidation of Isoprene using Trimethylsilylation and Gas Chromatography/Ion Trap Mass Spectrometry*

---

*This chapter is reproduced by permission from "Characterization of 2-Methylglyceric Acid Oligomers in Secondary Organic Aerosol Formed from the Photooxidation of Isoprene using Trimethylsilylation and Gas Chromatography/Ion Trap Mass Spectrometry" by Rafal Szmigielski, Jason D. Surratt, Reinhilde Vermeylen, Katarzyna Szmigielska, Jesse H. Kroll, Nga L. Ng, Shane M. Murphy, Armin Sorooshian, John H. Seinfeld, and Magda Claeys, *Journal of Mass Spectrometry*, 42 (1), 101–116, 2007. Copyright 2007 John Wiley & Sons, Ltd.

JOURNAL OF MASS SPECTROMETRY
J. Mass Spectrom. 2007; **42**: 101–116
DOI: 10.1002/jms.1146

Characterization of 2-methylglyceric acid oligomers in secondary organic aerosol formed from the photooxidation of isoprene using trimethylsilylation and gas chromatography/ion trap mass spectrometry

Rafal Szmigielski,[1] Jason D. Surratt,[2] Reinhilde Vermeylen,[1] Katarzyna Szmigielska,[1] Jesse H. Kroll,[3,4] Nga L. Ng,[4] Shane M. Murphy,[4] Armin Sorooshian,[4] John H. Seinfeld[3,4] and Magda Claeys[1]*

[1] Department of Pharmaceutical Sciences, University of Antwerp (Campus Drie Eiken), Universiteitsplein 1, BE-2610 Antwerp, Belgium
[2] Department of Chemistry, California Institute of Technology, Pasadena, CA 91125, USA
[3] Department of Environmental Science and Engineering, California Institute of Technology, Pasadena, CA 91125, USA
[4] Department of Chemical Engineering, California Institute of Technology, Pasadena, CA 91125, USA

Received 12 July 2006; Accepted 24 October 2006

In the present work, we have characterized in detail the chemical structures of secondary organic aerosol (SOA) components that were generated in a smog chamber and result from the photooxidation of isoprene under high-NO$_x$ conditions typical for a polluted atmosphere. Isoprene high-NO$_x$ SOA contains 2-methylglyceric acid (2-MG) and oligoester derivatives thereof. Trimethylsilylation, in combination with capillary gas chromatography (GC)/ion trap mass spectrometry (MS) and detailed interpretation of the MS data, allowed structural characterization the polar oxygenated compounds present in isoprene SOA up to 2-MG trimers. GC separation was achieved between 2-MG linear and branched dimers or trimers, as well as between the 2-MG linear dimer and isomeric mono-acetate derivatives thereof. The electron ionization (EI) spectra of the trimethylsilyl derivatives contain a wealth of structural information, including information about the molecular weight (MW), oligoester linkages, terminal carboxylic and hydroxymethyl groups, and esterification sites. Only part of this information can be achieved with a soft ionization technique such as electrospray (ESI) in combination with collision-induced dissociation (CID). The methane chemical ionization (CI) data were used to obtain supporting MW information. Interesting EI spectral differences were observed between the trimethylsilyl derivatives of 2-MG linear and branched dimers or trimers and between 2-MG linear dimer mono-acetate isomers. Copyright © 2006 John Wiley & Sons, Ltd.

KEYWORDS: isoprene; 2-methylglyceric acid; oligomers; secondary organic aerosol; trimethylsilylation; gas chromatography/mass spectrometry; oligoesters

INTRODUCTION

Isoprene (2-methyl-1,3-butadiene, C_5H_8) is a volatile organic compound (VOC) that is emitted in large amounts by terrestrial vegetation, estimated at about 500 Tg/year worldwide.[1] In the past, isoprene was assumed not to contribute significantly to secondary organic aerosol (SOA) formation because of the high volatility of its first-generation oxidation products (i.e. methacrolein, methyl vinyl ketone and formaldehyde).[2] However, during the past 3 years evidence from both field[3–7] and laboratory[4,8–13] studies has been obtained that isoprene is photooxidized to polar oxygenated products which are present in the aerosol phase. The aerosol yields from photooxidation of isoprene are rather low (maximum about 3%);[11,12] a recent modeling study, however, shows that this aerosol source is quite significant on a global scale.[14] Knowledge of the detailed chemical structures of isoprene oxidation products is required in order to gain insights into the underlying photochemical oxidation mechanisms of isoprene, which so far are only partially understood.

In a recent work,[10] we characterized the chemical structures of SOA components that were produced in a smog chamber from photooxidation of isoprene under both high- and low-NO$_x$ conditions. A combination of several mass spectrometric techniques was used, including electrospray ionization (ESI), matrix-assisted laser desorption ionization (MALDI), aerosol mass spectrometry (MS), and derivatization gas chromatography (GC). It was shown in that study that isoprene high-NO$_x$ SOA contains 2-methylglyceric acid (2-MG), formed by further photooxidation of methacrolein, a

---

*Correspondence to: Magda Claeys, Department of Pharmaceutical Sciences, University of Antwerp (Campus Drie Eiken), Universiteitsplein 1, BE-2610 Antwerp, Belgium.
E-mail: magda.claeys@ua.ac.be

first-generation oxidation product of isoprene, and oligoester derivatives of 2-MG.

Soft ionization techniques such as ESI and MALDI are widely used currently in the analysis of oligomers and polymers, including oligomeric substances formed by photooxidation of biogenic and anthropogenic hydrocarbons such as isoprene,[13] α-pinene,[15–18] cycloalkenes[16] and trimethylbenzene.[19] Combination of these techniques with collision-induced dissociation (CID) and tandem MS techniques generally only partially provide the structural information that is needed for elucidation of unknown multifunctional compounds. In the case of the oligomeric isoprene SOA compounds studied here, partial structural information was obtained by (−/+)ESI-ion trap MS and by upfront CID mode of analysis on a LC/ESI-MS instrument.[10] The major fragmentation observed for 2-MG oligomers was loss of 102 Da 2-MG residue(s), likely corresponding to 2-hydroxy-2-methylpropiolactone and formed through a nucleophilic reaction directed by the negative charge on the terminal ionized carboxylic acid function. In the present study, we demonstrate that additional structural information can be achieved on oligomeric isoprene SOA compounds by trimethylsilylation in combination with GC/ion trap MS and detailed interpretation of the electron ionization (EI) spectra.

A derivatization protocol based on methylation of carboxylic acid functions prior to trimethylsilylation of neutral hydroxyl groups has been successfully applied in a previous work[20] to the analysis of polar oxygenated compounds present in organic aerosol. In the present work, preference was given to a one-step trimethylsilylation procedure that converts neutral and acidic hydroxyl functions to trimethylsilyl (TMS) ether or ester functions and allows the analysis of polar multifunctional compounds in the EI and/or chemical ionization (CI) mode. The EI mass spectra of trimethylsilylated compounds generally contain a wealth of structural information but often provide insufficient molecular weight (MW) information.[6,20,21] The latter shortcoming can however be overcome by recording spectra in the CI mode. In the EI mode, information can be obtained on functional groups and their locations owing to the fragmentation-directing effect of ionized trimethylsilylated hydroxyl groups. Rearrangement reactions of the trimethylsilyl group may occur, rendering EI mass spectra quite complex and difficult to interpret, but have the merit that they can yield structurally characteristic ions.

The isoprene high-NO_x SOA examined in the present study contains 2-MG, 2-MG dimers, 2-MG dimer monoacetate derivatives, and 2-MG trimers. We will first discuss the EI fragmentation behaviors of the 2-MG monomer and its oligomeric derivatives. In addition, we will examine the fragmentation behaviors of the ethyl ester derivatives that are formed by subjecting isoprene high-NO_x SOA to acidic hydrolysis in ethanol. Part of this work has been briefly presented in our previous study dealing with the overall chemical composition and mechanism of SOA formed from the photooxidation of isoprene under low- and high-NO_x conditions.[10]

EXPERIMENTAL

Aerosol samples and workup

SOA was generated from isoprene (500 ppb) in Caltech's indoor 28 m^3 Teflon chambers using hydrogen peroxide as the OH radical precursor and 800 ppb NO; the oxidation reaction was initiated by UV irradiation,[11,12] and the SOA was collected on Teflon filters. Full details about SOA generation from isoprene are given in our previous study.[10] The SOA sample used in the present study was from a high-NO_x isoprene nucleation (seed-free) experiment (Experiment 5). 2-MG and a branched and linear dimer thereof were prepared by reacting methacrylic acid (250 µl; purity, 99%; Sigma, St. Louis, MI, USA) with hydrogen peroxide (250 µl; 50% aqueous solution) in the presence of formic acid (125 µl) for ten days at room temperature, following a procedure adapted from a previously reported one.[4] The yield of 2-MG, as determined by trimethylsilylation GC with flame ionization detection and using glyceric acid (Sigma) as an internal recovery standard, was 222 mg; the 2-MG linear and branched dimer were produced in small yield (combined yield estimated at about 3.3 mg assuming a similar EI response as 2-MG), and the ratio branched/linear 2-MG dimer was 1 : 10.

The sample workup of the isoprene SOA sample consisted of extraction of the filter with methanol under ultrasonic agitation and derivatization. The extract was divided into two parts; one part was trimethylsilylated, while the other part was subjected to a hydrolysis/ethylation procedure. For analysis of the methacrylic acid reaction products, 2 µl of the 30 times diluted reaction mixture (with methanol) was dried and trimethylsilylated. Trimethylsilylation was performed by reacting the extract residue with 40 µl of a mixture containing 1 ml *N*-methyl-*N*-trimethylsilyltrifluoroacetamide (+1% trimethylchlorosilane) (Pierce, Rockford, IL, USA) and 500 µl of dry pyridine (Merck) for an hour at 70 °C. The reagent employed for deuterium labeling of the TMS methyl groups, *N*,*O*-bis(trimethyl-$^2H_9$-silyl)acetamide, was obtained from Cambridge Isotope Laboratories (Andover, MA, USA). The hydrolysis/ethylation procedure involved reaction of the extract residue with 40 µl of analytical-grade ethanol and 8 µl of trimethylchlorosilane (Supelco, Bellafonte, PA, USA) for 1 h at 60 °C. Aliquots of 1 µl were used for GC/MS analysis and were injected in the splitless mode.

GC/ion trap MS

GC/MS analyses were performed with a system comprising a TRACE GC2000 gas chromatograph, which was coupled to a Polaris Q ion trap mass spectrometer equipped with an external ionization source (ThermoElectron, San Jose, CA, USA). A Heliflex AT-5MS fused-silica capillary column (5% phenyl, 95% methylpolysiloxane, 0.25 µm film thickness, 30 m × 0.25 mm i.d.) preceded by a deactivated fused-silica precolumn (2 m × 0.25 mm i.d.) (Alltech, Deerfield, IL, USA) was used to separate the derivatized extracts. Helium was used as the carrier gas at a flow rate of 1.2 ml/min. The temperature program was as follows: isothermal hold at 50 °C for 5 min, temperature ramp of 3 °C/min up to 200 °C, isothermal hold at 200 °C for 2 min, temperature ramp of

DOI: 10.1002/jms

30 °C/min up to 310 °C; and isothermal hold at 310 °C for 2 min. The analyses were performed in the full-scan mode (mass range: *m/z* 50–800), and were first carried out in the EI mode and subsequently in the CI mode. The ion source was operated at an electron energy of 70 eV and temperatures of 200 °C and 140 °C in the EI and CI modes, respectively. The temperatures of the GC injector and the GC/MS transfer line were 250 °C and 280 °C, respectively. For CI, methane was introduced as the reagent gas at a flow rate of 1.8 ml/min. We present here mainly data collected in the EI mode; data collected in the CI mode was used to obtain supporting MW information.

For CID experiments, the ions of interest were activated by applying a percentage of a 5-V supplementary a.c. potential to the end-caps of the ion trap at the resonance frequency of the selected ion [referred to as *collision energy level* (CEL)]. The CEL was 16%, while the excitation time was 15 ms. Helium was introduced as damping and collision gas at a flow rate of 1.1 ml/min. In some cases, MS/MS experiments were performed on several mass-selected precursor ions sequentially during the same chromatographic run. For this purpose, the width of the isolation waveform at which the ion trap separation of the precursor ions turned out to be the best was determined; the optimized value ranged between 3.5 and 5 a.m.u. For each precursor ion, the excitation time was 12 ms.

RESULTS AND DISCUSSION

Figure 1 shows a GC/MS total ion current chromatogram (TIC) obtained for SOA produced from the photooxidation of isoprene under high-NO_x conditions. Compound **1** was identified as the dihydroxymonocarboxylic acid, 2-MG (where 2-methylglyceric acid is its common name), which has retained part of the isoprene skeleton. This compound was reported for the first time in rural $PM_{2.5}$ aerosol collected at K-puszta, Hungary, during a 2003 summer field campaign,[4] and has since been reported in several field studies.[5,7,8] In addition, it was shown in smog chamber studies that 2-MG is formed by photooxidation of isoprene[8] and, more specifically, by further oxidation of methacrolein, which is a first-generation photooxidation product of isoprene.[10] Compound **2a** was characterized in our previous laboratory study as a linear oligoester dimer of 2-MG (denoted as 2-MG linear dimer), using a combination of several MS techniques, including ESI-MS, MALDI-MS, aerosol-MS, and trimethylsilylation GC/MS.[10] In the present work, we discuss the EI behavior of the TMS derivative of the 2-MG linear dimer in more detail and compare it with that of the branched dimer (**2b**), which is not formed during photooxidation of isoprene under high-NO_x conditions (and therefore is not shown in Fig. 1) but which together with the 2-MG linear dimer is produced as a minor reaction product during the acid-catalyzed oxidation of methacrylic acid with hydrogen peroxide. The 2-MG branched dimer was found to elute at an earlier retention time (RT = 50.37 min) compared to the linear dimer (RT = 51.59 min) (GC/MS TIC not shown). No conclusions can be drawn about the relative amounts of 2-MG and its oligoester derivatives in the samples since it is possible that 2-MG oligoester derivatives are partially degraded owing to hydrolysis during the trimethylsilylation procedure which uses an acidic catalyst (i.e. trimethylchlorosilane). Figure 2 shows the *m/z* 219 mass chromatogram obtained after subjecting the isoprene high-NO_x SOA extract to acidic hydrolysis in ethanol, an experiment that was performed to obtain evidence for ester linkages in the 2-MG oligomers. Compounds identified are the ethyl ester derivatives of 2-MG (**1-Et**), a branched (**2b-Et**) and linear 2-MG dimer (**2a-Et**), and a branched (**3b-Et**) and linear 2-MG trimer (**3a-Et**). In a following section, we will first discuss in detail the rather complex fragmentation behavior of the TMS derivatives of 2-MG (**1**) and its ethyl derivative (**1-Et**) and will limit the discussion to diagnostic ions with *m/z* values >140. In subsequent sections, we will then use this information to derive

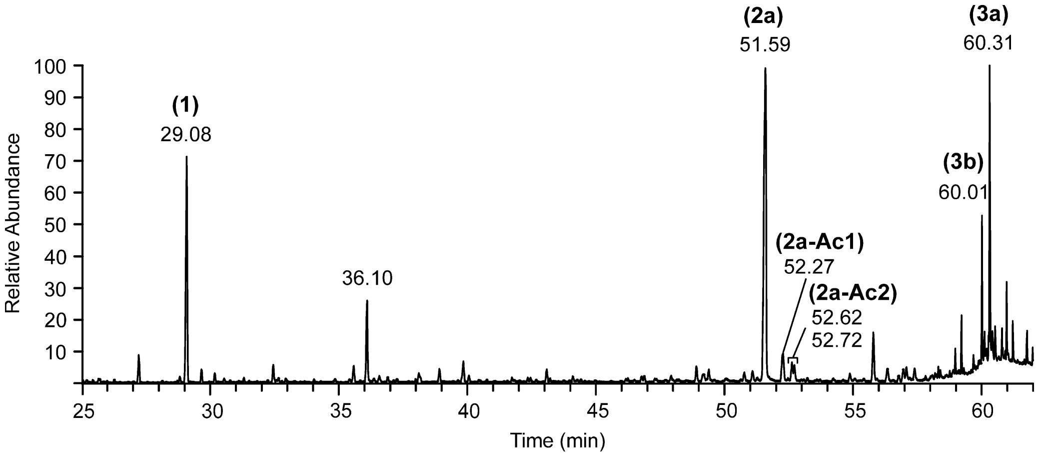

Figure 1. GC/MS TIC obtained for a trimethylsilylated extract of isoprene high-NO_x SOA. Peak identifications: **1**, 2-MG; **2a**, 2-MG linear dimer; **2a-Ac1** and **2a-Ac2**, 2-MG linear dimer mono-acetates; **3a**, 2-MG linear trimer; **3b**, 2-MG branched trimer. The peak eluting at 36.10 min is not discussed in the present work; it was found to correspond to an oxidation product of isoprene but not to be related to 2-MG, and was tentatively identified as 2-hydroxymethyl-3-ketopropanoic acid. Other peaks not marked were also found in a control filter and were identified as fatty acids and monoglycerides thereof. Reprinted from *J. Phys. Chem. A*, **110**, Surratt JD *et al*., Chemical composition of secondary organic aerosol formed from the photooxidation of isoprene, 9665, Copyright (2006), with permission from American Chemical Society.

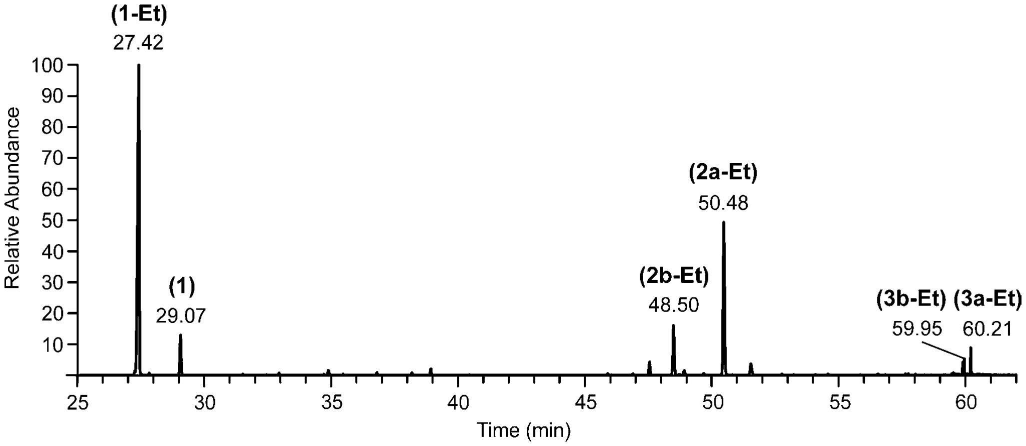

Figure 2. GC/MS extracted ion chromatogram (*m/z* 219) obtained for an extract of isoprene high-NO$_x$ SOA subjected to a hydrolysis/ethylation procedure prior to trimethylsilylation. Reprinted from *J. Phys. Chem. A*, **110**, Surratt JD *et al.*, Chemical composition of secondary organic aerosol formed from the photooxidation of isoprene, 9665, Copyright (2006), with permission from American Chemical Society.

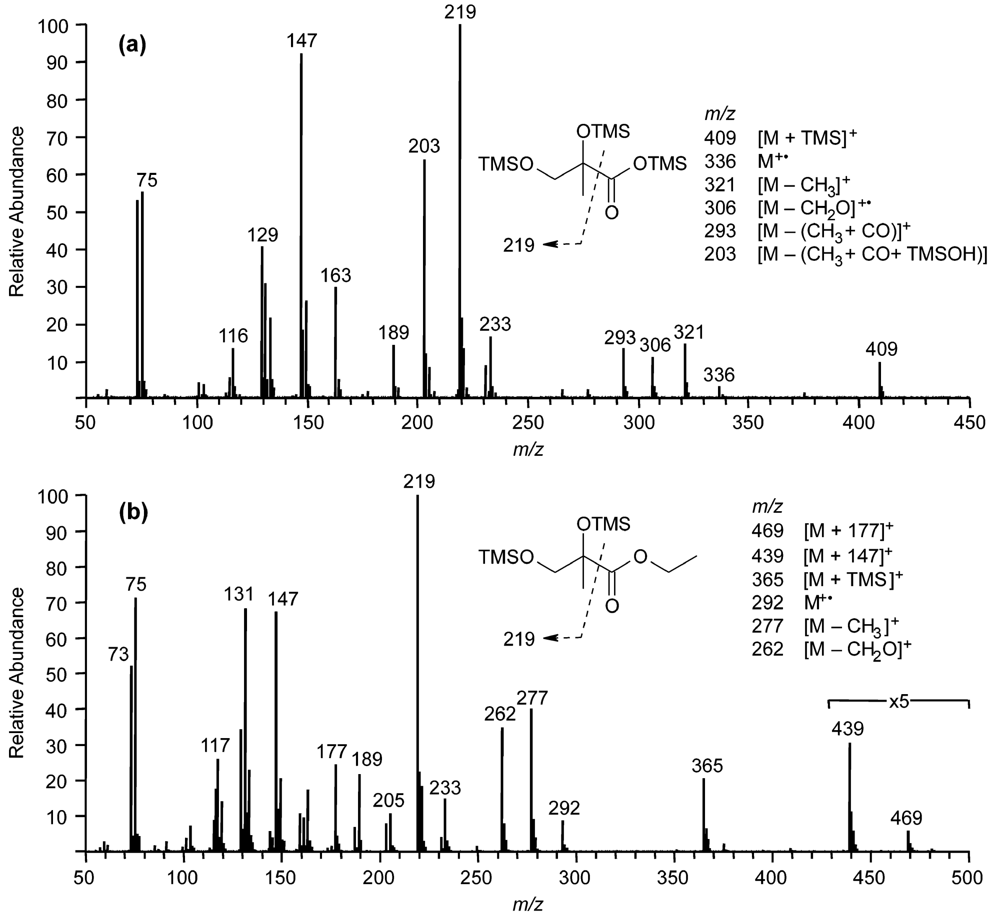

Figure 3. EI mass spectra for the TMS derivatives of (a) 2-MG (**1**) and (b) its ethyl ester derivative (**1-Et**). Part (a) reprinted from *J. Phys. Chem. A*, **110**, Surratt JD *et al.*, Chemical composition of secondary organic aerosol formed from the photooxidation of isoprene, 9665, Copyright (2006), with permission from American Chemical Society.

structural information for 2-MG dimers (**2a,b**), 2-MG trimers (**3a,b**), the ethyl derivatives of 2-MG dimers (**2a,b-Et**), as well as mono-acetate derivatives of the 2-MG linear dimer (**2a-Ac1,2**). In order to support fragmentation pathways, ion trap MS/MS experiments were used; only in the case of the 2-MG monomer was deuterium labeling of the TMS groups carried out.

Fragmentation behavior of 2-methylglyceric acid and its ethyl ester derivative

Figure 3 shows the EI mass spectra of the TMS derivatives of (a) 2-MG (**1**) and (b) its ethyl ester derivative (**1-Et**). The fragmentation pathways of the TMS derivative of 2-MG are summarized in Schemes 1 and 2; all pathways supported by an MS^2 ion trap experiment are indicated

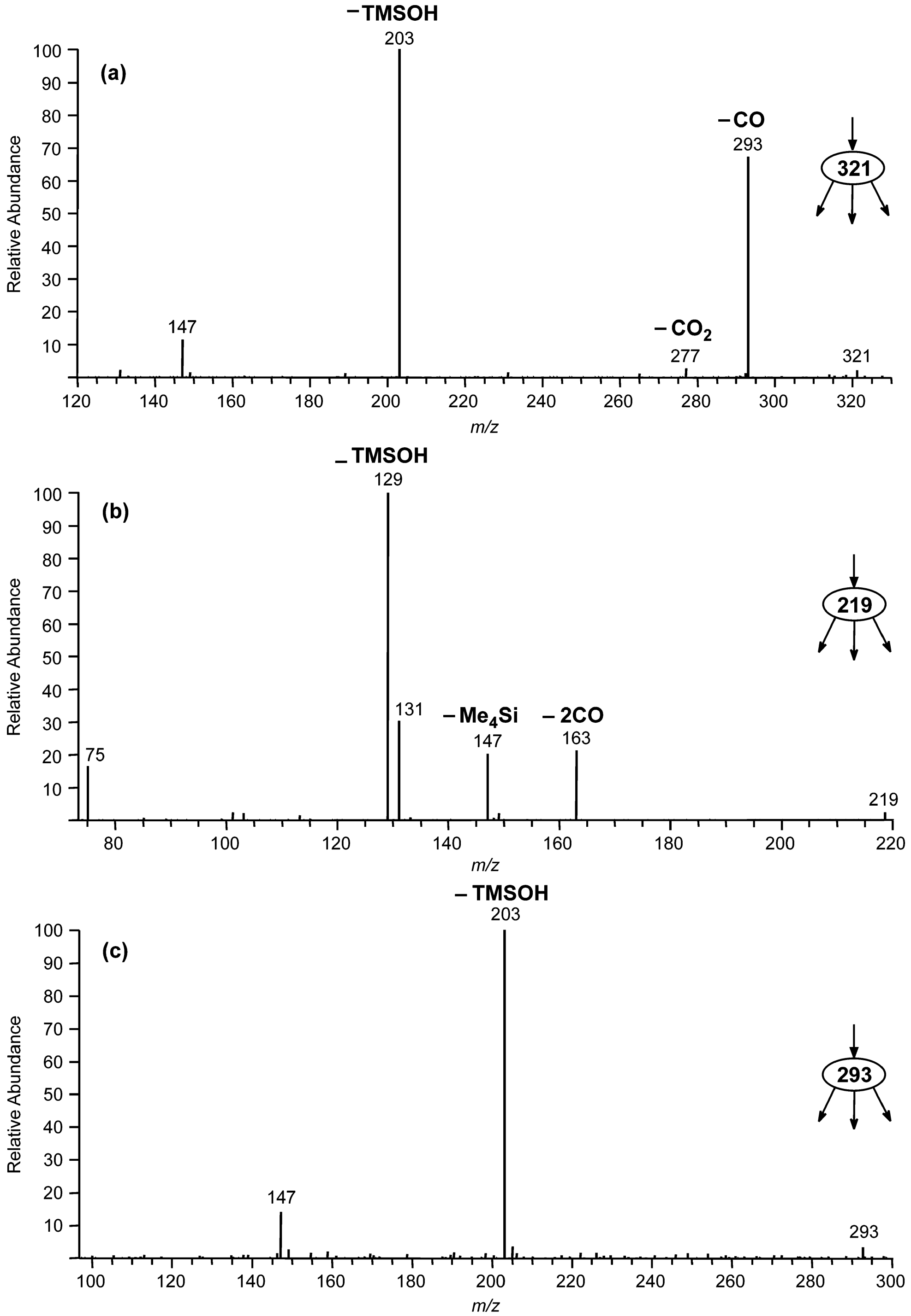

Figure 4. MS^2 ion trap spectra for selected ions of the TMS derivative of 2-MG: (a) *m/z* 321, (b) *m/z* 219 and (c) *m/z* 293.

with an asterisk, while mass shifts obtained by introducing a deuterium labeled TMS group are given in parentheses. The molecular ion ($M^{+\bullet}$; *m/z* 336) of the TMS derivative of 2-MG is very weak, as is generally the case for TMS derivatives of compounds containing multiple hydroxyl groups.[6,21] The molecular ion region has a signature that is characteristic of a trimethylsilylated carboxylic acid, i.e. the $[M - CH_3]^+$ ion (*m/z* 321) and the $[M - (CH_3 + CO)]^+$ ion (*m/z* 293). Proof that *m/z* 321 is the precursor of *m/z* 293 was obtained through an MS^2 ion trap experiment on *m/z* 321 (Fig. 4(a)). Besides the $M^{+\bullet}$ ion, other useful ions for inferring the MW (336) are the $[M - CH_3]^+$ ion (*m/z* 321) and the $[M + TMS]^+$ ion (*m/z* 409). In addition, the molecular ion region contains a $[M - CH_2O]^{+\bullet}$ ion (*m/z* 306), which is indicative of a terminal trimethylsilylated hydroxymethyl function and can be explained via a rearrangement reaction of a TMS group to the ionized ester function as outlined in Scheme 3.

The ion at *m/z* 219 is the base peak in the mass spectrum and can be explained by a homolytic α-cleavage (Scheme 2). Fragmentation of *m/z* 219 (Fig. 4(b)) yields the specific signature that was previously reported for the *m/z* 219 ion of trimethylsilylated 2-methyltetrols,[21]

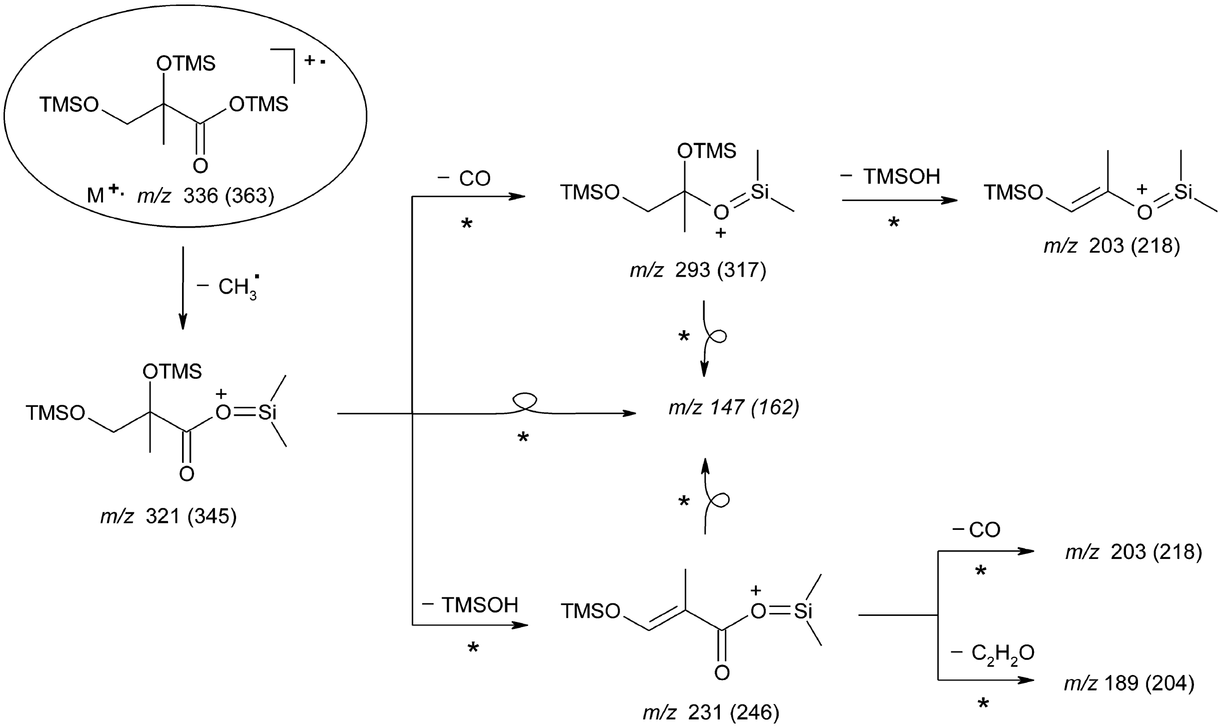

Scheme 1. Main fragmentation pathways for the TMS derivative of 2-methylglyceric acid. All pathways supported by an MS^2 ion trap experiment are indicated with an asterisk.

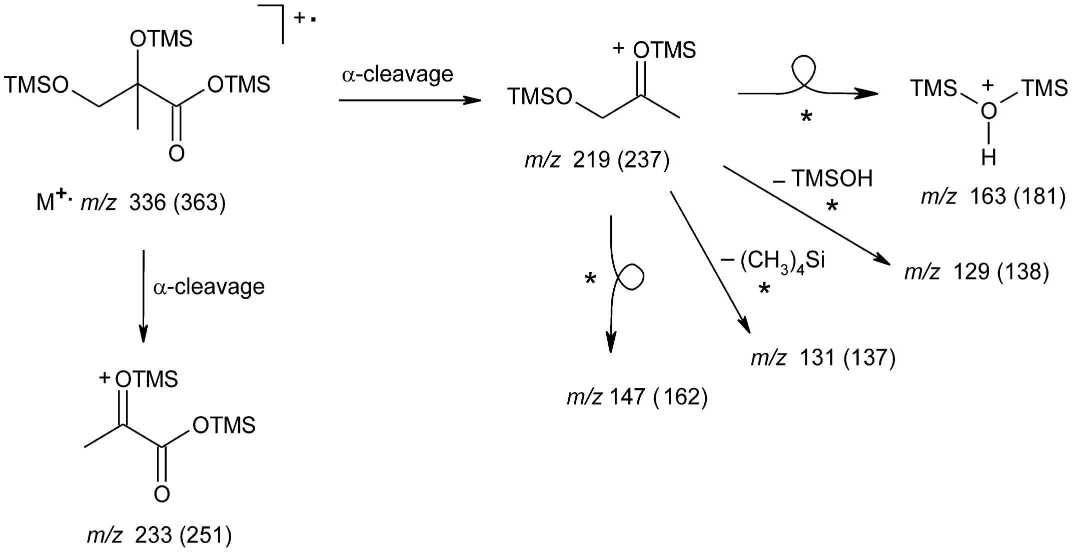

Scheme 2. Proposed pathways for *m*/*z* 233 and 219 formed from the TMS derivative of 2-MG and pathways for formation of *m*/*z* 219.

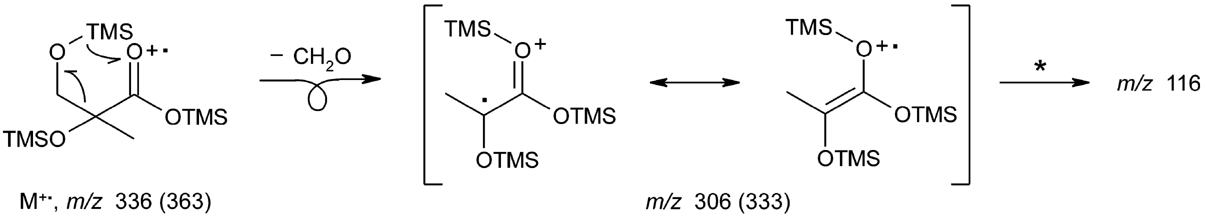

Scheme 3. Postulated gas-phase rearrangement process for the TMS derivative of 2-MG resulting in a resonance-stabilized *m*/*z* 306 ion.

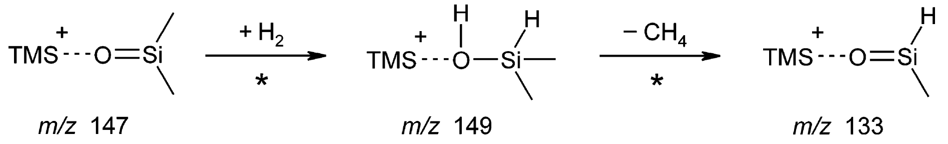

Scheme 4. Hydrogenation reaction of m/z 147 occurring in the ion trap resulting in m/z 149 and 133.

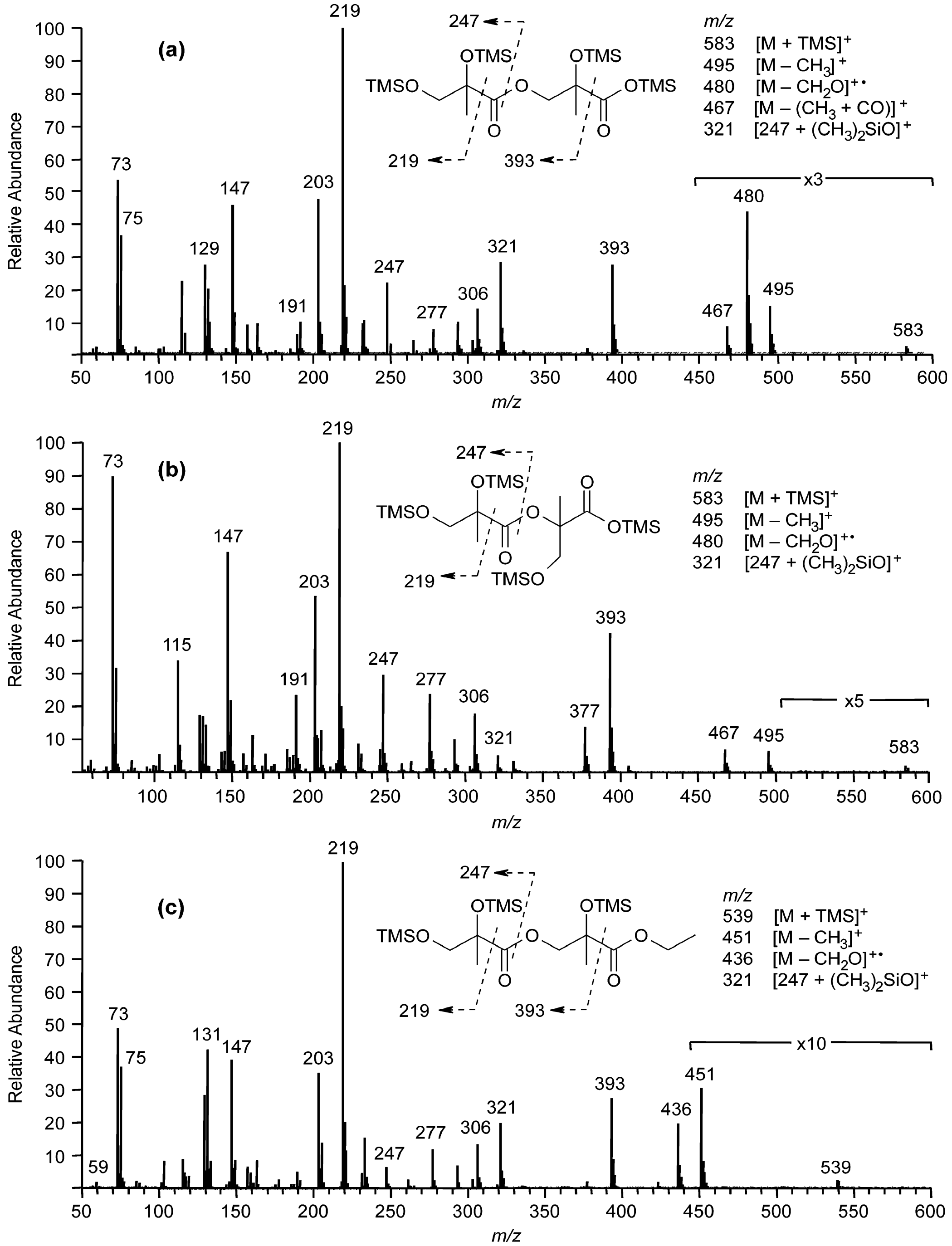

Figure 5. EI mass spectra of the TMS derivatives (a) 2-MG linear dimer (**2a**), (b) 2-MG branched dimer (**2b**), and (c) 2-MG linear dimer ethyl ester (**2a-Et**). Part (a) reprinted from *J. Phys. Chem. A*, **110**, Surratt JD *et al.*, Chemical composition of secondary organic aerosol formed from the photooxidation of isoprene, 9665, Copyright (2006), with permission from American Chemical Society.

and is therefore consistent with a trimethylsilylated 1,2-dihydroxy-2-methylethyl group in the molecule. The *m/z* 203 ion can be explained by loss of TMSOH from *m/z* 293 (Scheme 1; Fig. 4(c)), while the *m/z* 147 ion corresponding to $(CH_3)_2Si = O^+ - TMS$ is due to interaction between two TMSO groups[22] and indicates that the molecule contains at least two TMSO groups. The *m/z* 147 ion is accompanied by a *m/z* 149 ion which was shown to be formed from the *m/z* 147 ion, and is explained by addition of hydrogen in the ion trap, and fragments to *m/z* 133 through loss of methane (Scheme 4).

Comparison of the spectra of the TMS derivatives of 2-MG (Fig. 3(a)) and its ethyl ester (Fig. 3(b)) shows that ethylation results in the expected mass shifts but has little effect on the fragmentation pathways. MW information is provided by the $M^{+\bullet}$ ion (*m/z* 292), the $[M - CH_3]^+$ ion (*m/z* 277), and the $[M + TMS]^+$ ion (*m/z* 365). It is worth noting that the higher *m/z* region contains additional adduct ions at *m/z* 439 $[M + 147]^+$ and *m/z* 469 $[M + 177]^+$. Of these ions, *m/z* 439 can be explained by adduct formation of the 2-MG ethyl ester molecule with *m/z* 147, which is an abundant ion in the spectrum. The formation of *m/z* 177 likely involves the further addition of formaldehyde (30 Da), which is generated in the formation of *m/z* 262 $[M - CH_2O]^+$. The latter ion supports a terminal trimethylsilylated hydroxymethyl function, while the base peak at *m/z* 219 is consistent with a trimethylsilylated 1,2-dihydroxy-2-methylethyl group.[21]

Fragmentation behavior of 2-MG dimers and their ethyl ester derivatives

Figure 5 shows the EI mass spectra of the TMS derivatives of (a) the linear (**2a**) and (b) branched dimer of 2-MG (**2b**) and (c) the ethyl ester derivative of the 2-MG linear dimer (**2a-Et**). Examination of the *m/z* range 450–600 provides information about the MW. In the case of the 2-MG linear dimer (Fig. 5(a); MW 510), these ions include *m/z* 583 $[M + TMS]^+$, *m/z* 495 $[M - CH_3]^+$, and *m/z* 467 $[M - (CH_3 + CO)]^+$. The latter ion supports the presence of a terminal COOTMS group in the molecule as has been discussed above for 2-MG (Scheme 1). In the case of the 2-MG linear dimer ethyl ester (Fig. 5(c)), the MW (466) is supported by *m/z* 539 $[M + TMS]^+$ and *m/z* 451 $[M - CH_3]^+$. The ion at *m/z* 393 detected for both of the 2-MG linear and branched dimers and their ethyl esters can be readily explained by a homolytic α-cleavage reaction as depicted in Scheme 5.

The mass spectra of the TMS derivatives of the 2-MG linear dimer as well as of its ethyl ester display an abundant $[M - CH_2O]^{+\bullet}$ ion (*m/z* 480 and *m/z* 436, respectively), which is consistent with a terminal trimethylsilylated hydroxymethyl function as has been discussed above for the 2-MG monomer (Scheme 2). Subsequent elimination of a neutral (130 Da) through a rearrangement of a TMS group leads to *m/z* 306, an ion that is also observed for the 2-MG monomer (Fig. 3(a)) and is stabilized by resonance (Scheme 6).

Comparison of the EI spectrum of the TMS derivative of the 2-MG linear dimer (Fig. 5(a)) with that of the branched dimer (Fig. 5(b)) reveals some interesting differences. It can be seen that the $[M - CH_2O]^{+\bullet}$ ion (*m/z* 480) is absent in the case of the 2-MG branched dimer. However, it is noted that a *m/z* 306 ion is also present in the 2-MG branched dimer, suggesting that the internal TMS group rearrangement (shown for **2a** in Scheme 6) occurs prior to

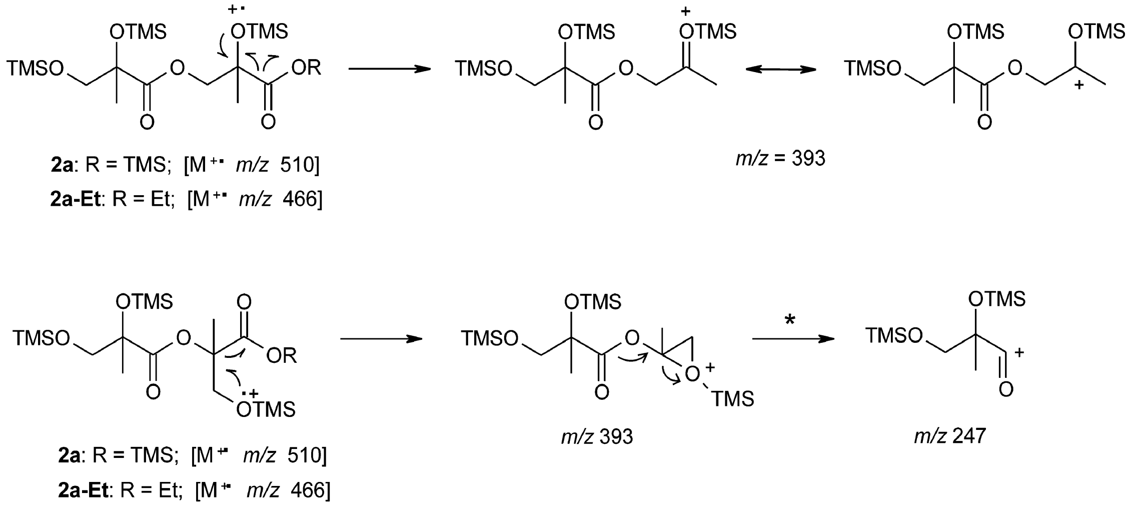

Scheme 5. Formation of the *m/z* 393 characteristic of the 2-MG linear and branched dimers and their ethyl esters via a homolytic α-cleavage reaction.

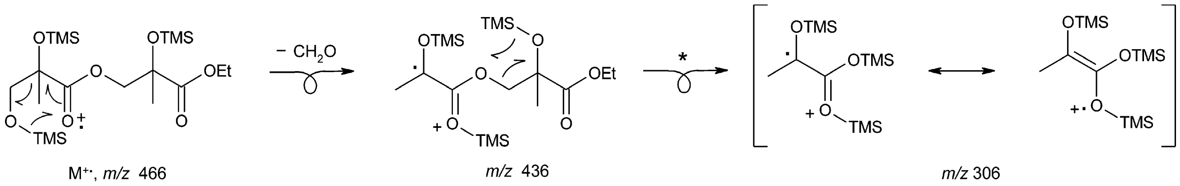

Scheme 6. Plausible mechanisms for the formation of *m/z* 436 and 306 from the TMS derivative of 2-MG linear dimer ethyl ester.

CH_2O loss. Furthermore, it can be seen that there is an additional ion at *m/z* 377 in the latter case, which corresponds to $[M - (CH_3 + CO + TMSOH)]^+$. An MS/MS experiment confirmed that *m/z* 467 is the precursor for *m/z* 377; a possible explanation is a favorable 1,3-elimination of TMSOH in the branched carboxylic acid-containing 2-MG residue.

Figure 6 shows the *m/z* 393 product ion spectra for the two isomeric 2-MG dimers. Interesting differences can be noted, with *m/z* 247 being most abundant in the branched case; this information will be used in the following section to establish an esterification site in the 2-MG branched trimer. In the case of the 2-MG branched dimer, *m/z* 247 can be readily formulated through a charge-directed loss of trimethylsilylated hydroxyacetone (Scheme 5).

Other structurally informative ions in the EI spectra of the TMS derivatives of the 2-MG linear and branched dimers worth discussing are *m/z* 247 and 321. The *m/z* 247 ion is explained by an α-cleavage relative to the ester C = O bond (Scheme 7) but can also be formed by other pathways (e.g. from *m/z* 393; Scheme 5) and is characteristic for the presence of an ester linkage in the molecule. The ion at *m/z* 247 fragments further to *m/z* 231, 219, 203, and 157, as confirmed

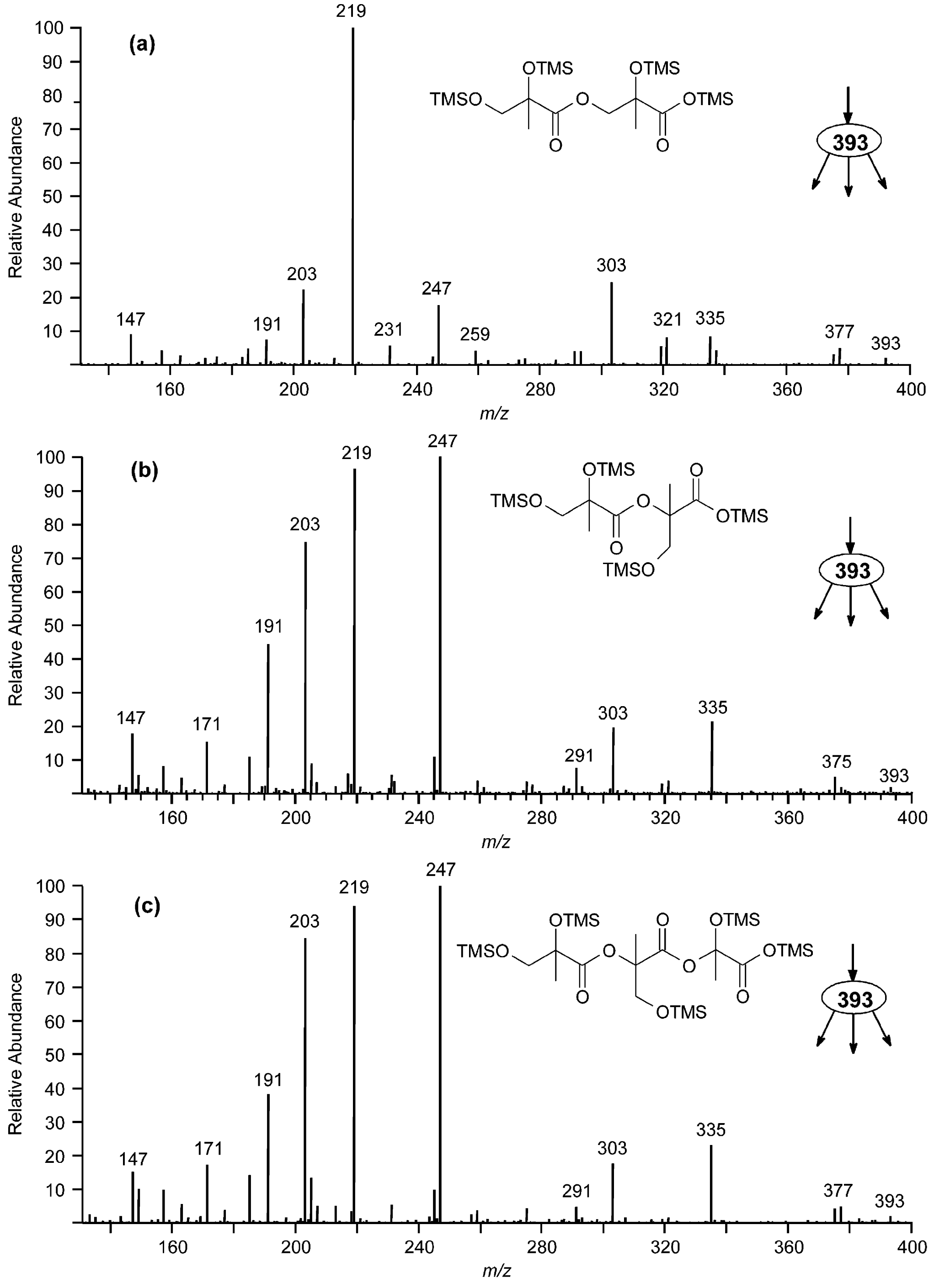

Figure 6. MS^2 ion trap spectra for *m/z* 393 of the TMS derivative of (a) the 2-MG linear dimer, (b) the 2-MG branched dimer and (c) the 2-MG branched trimer.

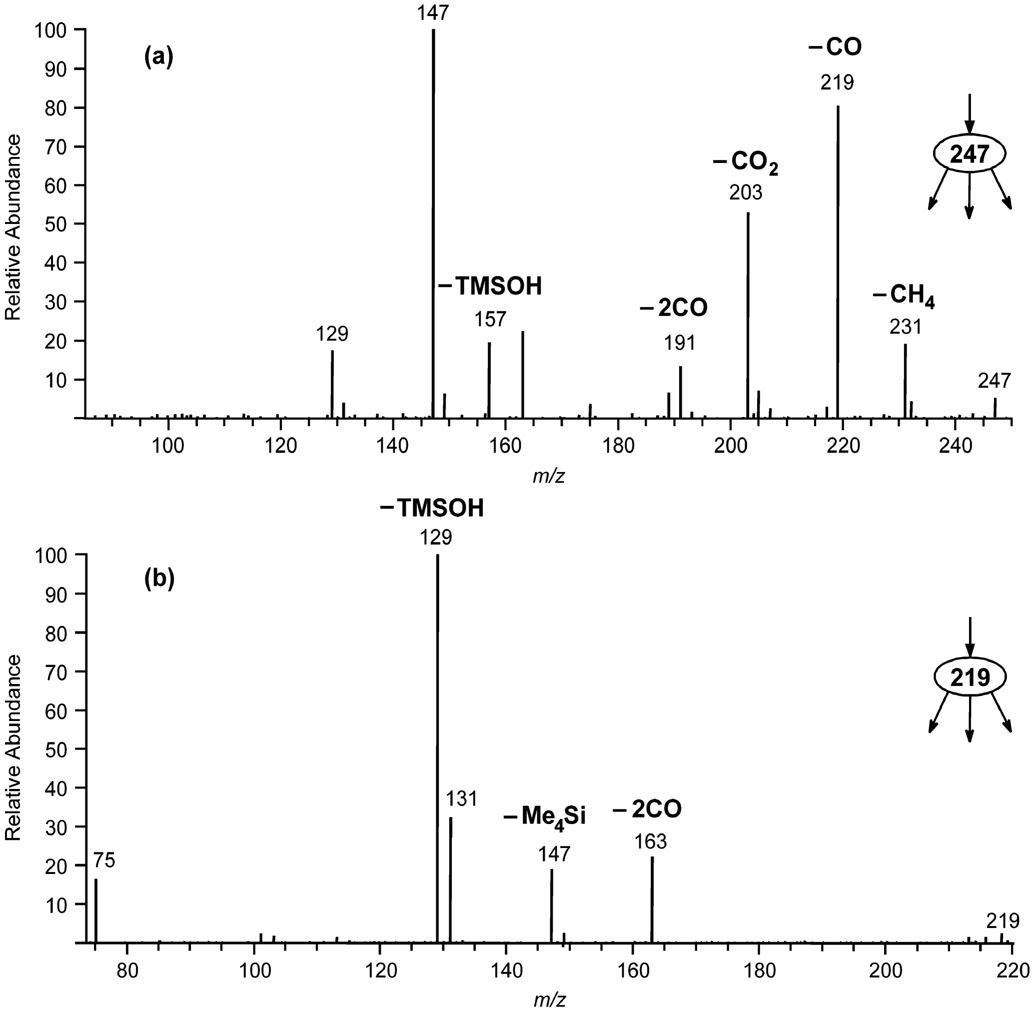

Figure 7. MS^2 ion trap spectra for selected ions of the TMS derivative of the 2-MG linear dimer: (a) *m/z* 247 and (b) *m/z* 219.

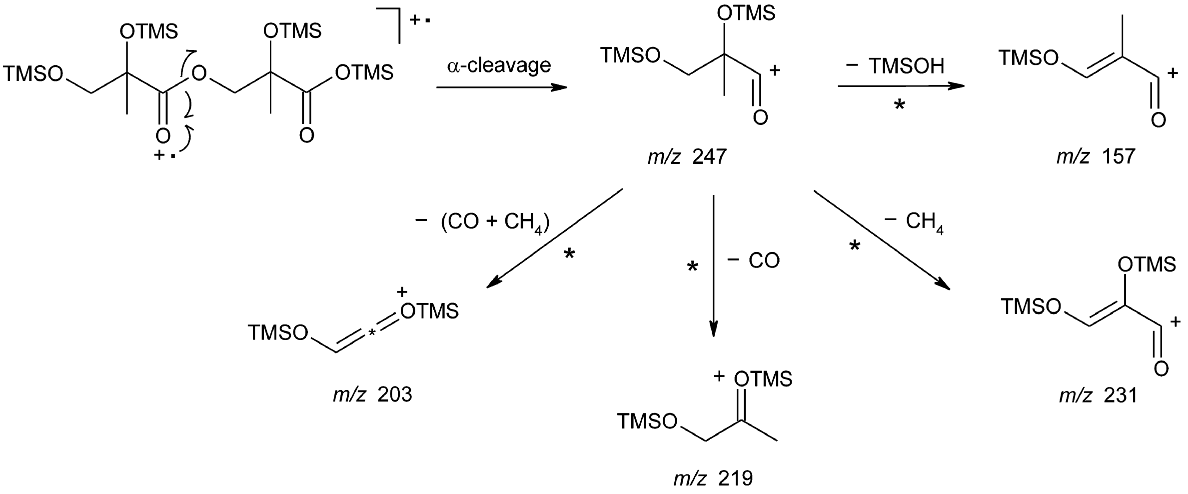

Scheme 7. A plausible formation mechanism for *m/z* 247 and its further fragmentation as confirmed by MS^2 ion trap experiments.

by MS^2 experiments (Fig. 7(a); Scheme 7). The MS^2 ion trap spectrum of *m/z* 219 (Fig. 7(b)) unambiguously proves that its structure is consistent with a trimethylsilylated 1,2-dihydroxy-2-methylethyl group,[21] which has already been discussed above in the case of 2-MG and its ethyl ester derivative.

Fragmentation behavior of 2-MG trimers and their ethyl esters

Figure 8(a) and (b) shows the EI mass spectra of the TMS derivatives of the two isomeric trimers of 2-MG that were detected in the GC/MS TIC of high-NO_x isoprene SOA (Fig. 1). Since both spectra display the same set of ions

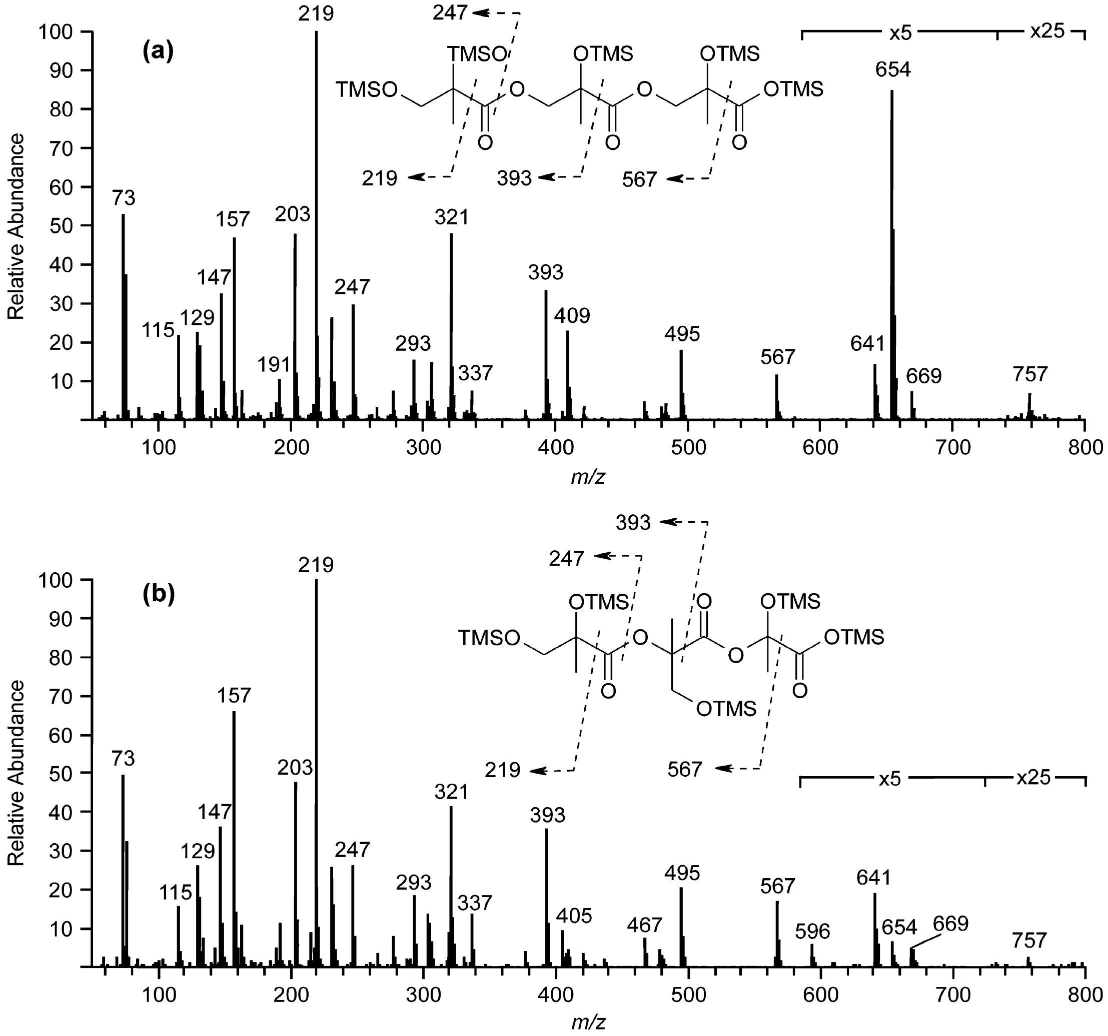

Figure 8. EI mass spectra of the TMS derivatives of 2-MG (a) linear (**3a**) and (b) branched trimer (**3b**).

differing only in terms of their relative abundances, one can conclude that they represent isomeric compounds. The most abundant compound which elutes at the latest retention time (RT = 60.31 min) is attributed to the linear trimer (**3a**), while the other one (RT = 60.01 min) is attributed to a branched trimer (**3b**), given that under the GC conditions employing a nonpolar stationary phase, branched isomers, which have a more compact structure than their linear forms, elute at an earlier retention time. As will be discussed below, evidence for a branched internal 2-MG residue was obtained. However, we have no evidence for the esterification site in the terminal carboxylic acid-containing 2-MG residue and assume that after dimer formation, esterification proceeds by reaction with a terminal hydroxymethyl group of a 2-MG molecule, thus resulting in a linear form, since the formation of linear forms is sterically less hindered.

As in the case of the 2-MG dimers, examination of the high *m*/*z* range enables us to infer the MW (684). Both isomers reveal a very weak $[M + TMS]^+$ adduct ion (*m*/*z* 757) as well as $[M - CH_3]^+$ ion (*m*/*z* 669) and $[M - (CH_3 + CO)]^+$ ions (*m*/*z* 641). The latter ion also supports a terminal carboxyl group in the underivatized molecules. It can be seen that the abundance of the $[M - CH_2O]^{+\bullet}$ ion (*m*/*z* 654) is strikingly different and is more abundant for the linear system compared to the branched one. The same observation was made for the $[M - CH_2O]^{+\bullet}$ ion (*m*/*z* 610) in the mass spectra of the 2-MG dimers and the ethyl derivatives of 2-MG trimers (results not shown). A possible explanation for this phenomenon is given in Scheme 8. A TMS group transfer may not only proceed from the terminal $TMSOCH_2$ group but also from an internal $TMSOCH_2$ group, involve different geometries of the transition state, and take place at a different rate. The interaction between the terminal $TMSOCH_2$ group and a neighboring ester function involves a 6-centered transition state, while that between the internal $TMSOCH_2$ group of the branched isomer and a neighboring ester function involves a 7-centered state which is less favorable but may be formed faster.

The *m*/*z* 393 ion can be explained by an α-cleavage directed by the ionized internal TMSO group of the inner 2-MG residue. Figure 6(c) shows that the *m*/*z* 393 product ion profile of the branched trimer is very similar to that of the branched dimer (Fig. 6(b)), suggesting that the branched 2-MG trimer contains an inner branched 2-MG residue. In the following discussion, attention will be given to structurally informative ions, which were not present in the case of the 2-MG dimers. Both the linear and branched 2-MG trimer reveal an ion at *m*/*z* 495 which can be explained

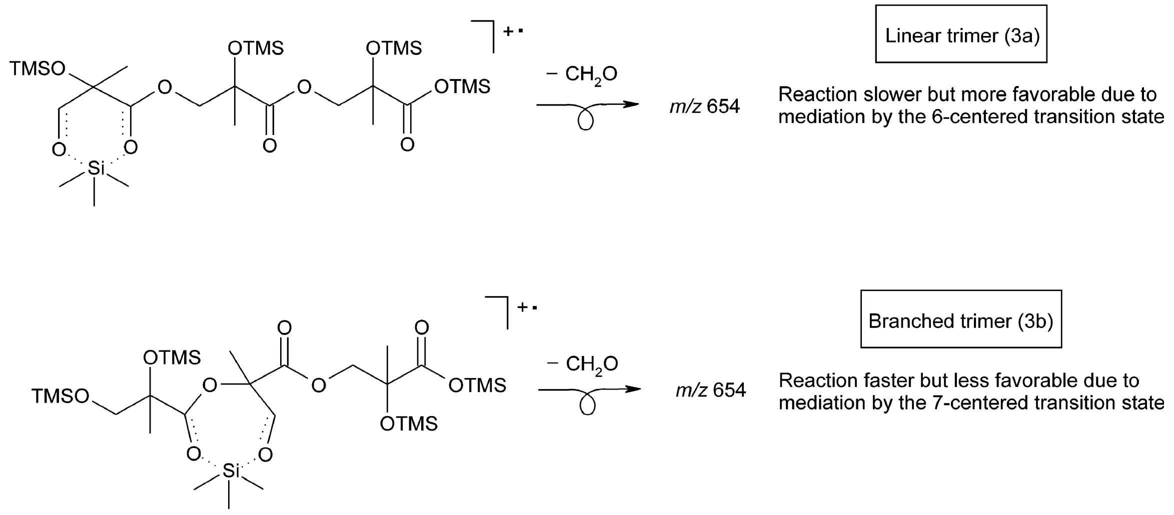

Scheme 8. Differences in the geometry of the transition state providing a rational explanation for the more favorable loss of formaldehyde from the $M^{+\bullet}$ ion of the TMS derivative of the 2-MG linear trimer compared to that of the branched form.

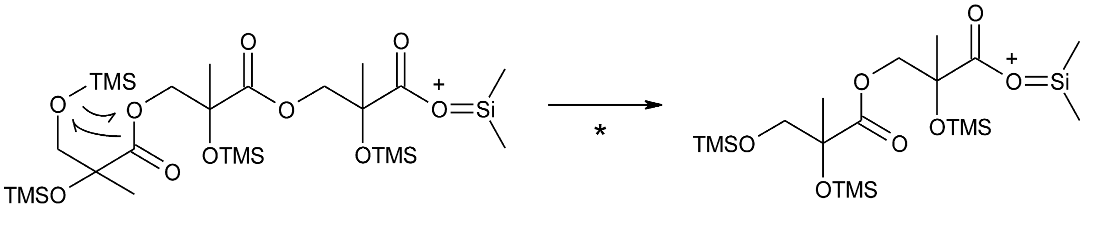

3a: linear form; *m/z* 669

m/z 495

Scheme 9. Formation of *m/z* 495 in the case of the TMS derivative of the 2-MG linear trimer. The same mechanism can be proposed for the 2-MG branched trimer.

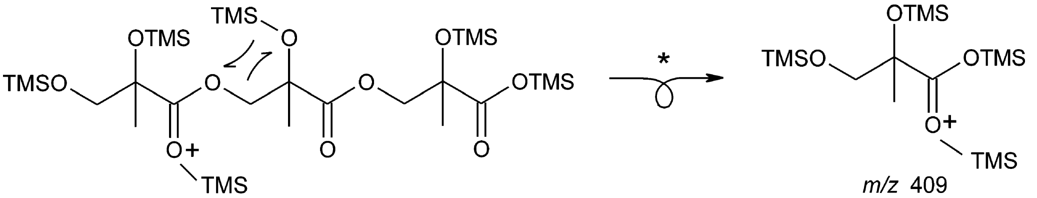

m/z 409

3a: linear form; *m/z* 757

Scheme 10. Pathway leading to *m/z* 409 in the TMS derivative of the 2-MG linear trimer.

from the $[M - CH_3]^+$ ion by loss of a neutral (174 Da) from the terminal 2-MG residue through a rearrangement of a TMS group (Scheme 9). In addition, ions are present, which are isomer-specific. In the case of the 2-MG linear trimer, an ion can be seen at *m/z* 409, while the 2-MG branched trimer reveals an ion at *m/z* 596. The *m/z* 409 ion can be generated from the $[M + TMS]^+$ adduct ion by an internal rearrangement of a TMS group resulting in the $[2\text{-MG} + TMS]^+$ adduct ion (Scheme 10). The *m/z* 596 ion characteristic of the 2-MG branched trimer is believed to result from a favorable interaction in the $M^{+\bullet}$ ion between the trimethylsilylated hydroxymethyl group of the branched unit and a trimethylsilylated hydroxyl group, leading to loss of $(CH_3)_4Si$ (88 Da).

Fragmentation behavior of 2-MG linear dimer mono-acetate derivatives

The two small peaks in the GC/MS TIC of high-NO_x isoprene SOA (Fig. 1) eluting just after the 2-MG linear dimer (**2a**) were identified as isomeric 2-MG linear dimer mono-acetates (**2a-Ac1,2**). These products were already partially characterized in our previous study using (−) ESI-MS, and are formed by esterification between the 2-MG linear dimer and acetic acid, which is also generated from isoprene in the smog chamber under high-NO_x conditions.[10] As will be discussed below, a more complete characterization of the isomeric 2-MG linear dimer mono-acetates was possible by detailed interpretation of the EI mass spectral data. The EI spectra of the TMS derivatives of the isomeric 2-MG linear dimer mono-acetates are shown in Fig. 9. The peak eluting at a RT of 52.3 min was characterized as the isomer containing an internal acetate group (**2a-Ac1**), while the peak at a RT of 52.6 min was attributed to the isomer containing a terminal acetate group (**2a-Ac2**). The partial splitting noted in the latter chromatographic peak can be explained by diastereoisomerism.

Examination of the high *m/z* range enables us to infer the MW (480); the EI spectra of the TMS derivatives of both

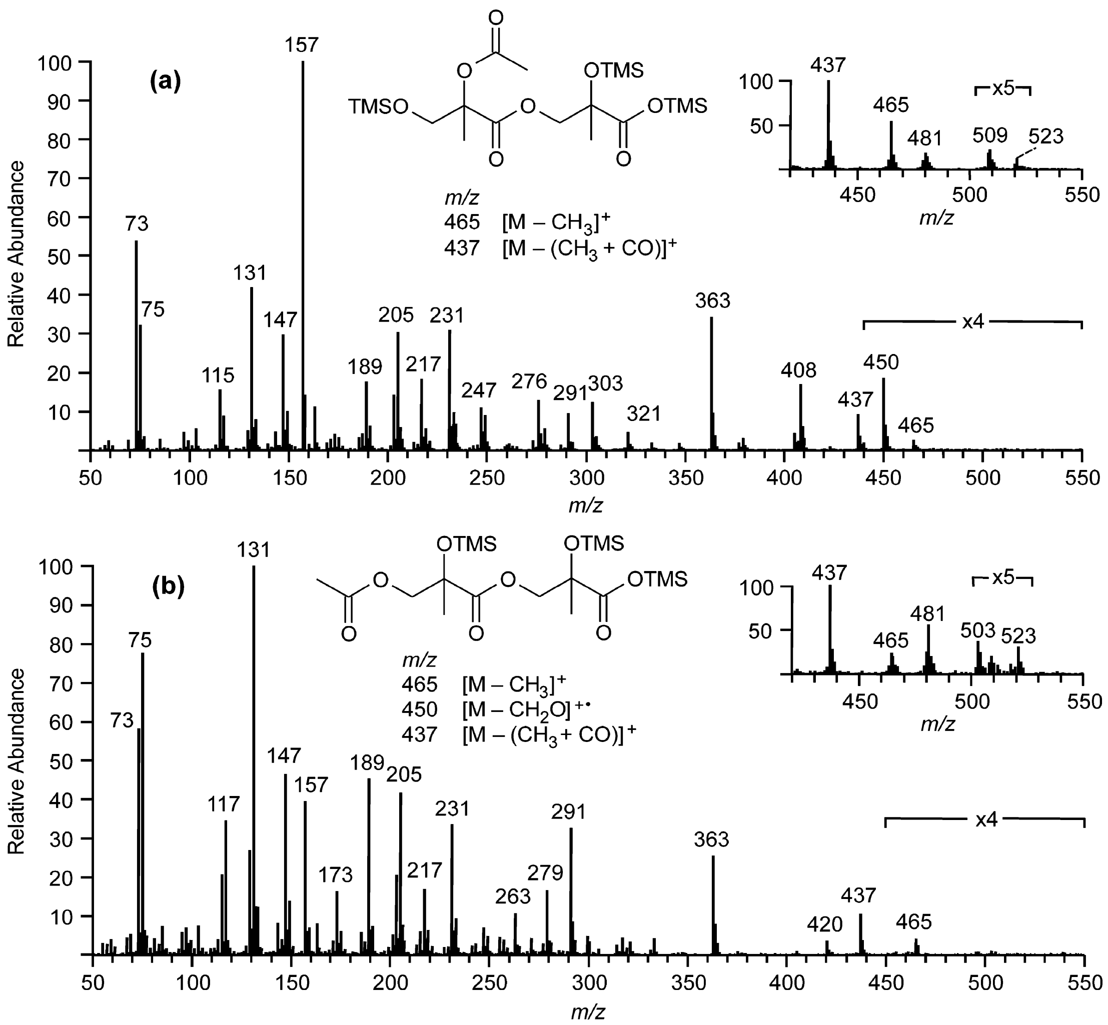

Figure 9. EI mass spectra of the TMS derivatives of 2-MG linear dimer mono-acetates bearing the acetate group at (a) the terminal hydroxymethyl group (**2a-Ac1**) and (b) an internal hydroxyl group (**2a-Ac2**). Insets: CI (methane) data.

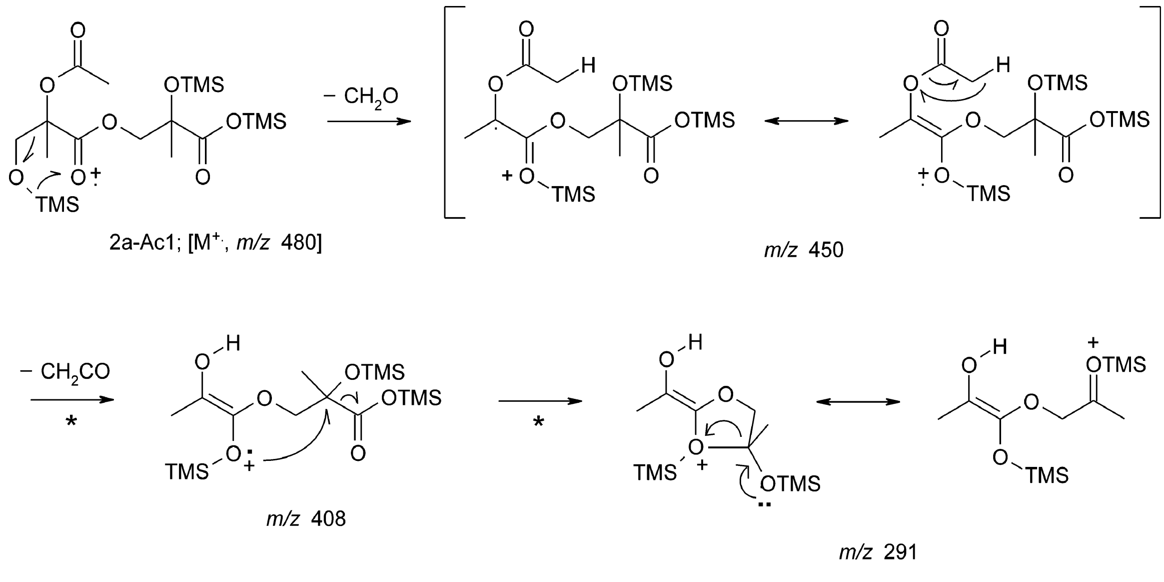

Scheme 11. Mechanisms proposed for the formation of *m/z* 450, 408, and 291 present in the EI spectrum of the TMS derivative of the 2-MG dimer mono-acetate isomer eluting at RT 52.3 min (**2a-Ac1**).

2-MG linear dimer mono-acetates show $[M - CH_3]^+$ (*m/z* 465) and $[M - (CH_3 + CO)]^+$ ions (*m/z* 437). Supporting MW information was derived from the CI (methane) spectra (insets in Fig. 9), which reveal $[M + H]^+$ (*m/z* 481), $[M + C_2H_5]^+$ (*m/z* 509), and $[M + C_3H_7]^+$ (*m/z* 523) ions as well as $[MH - CH_4]^+$ ions (*m/z* 465). It can be

DOI: 10.1002/jms

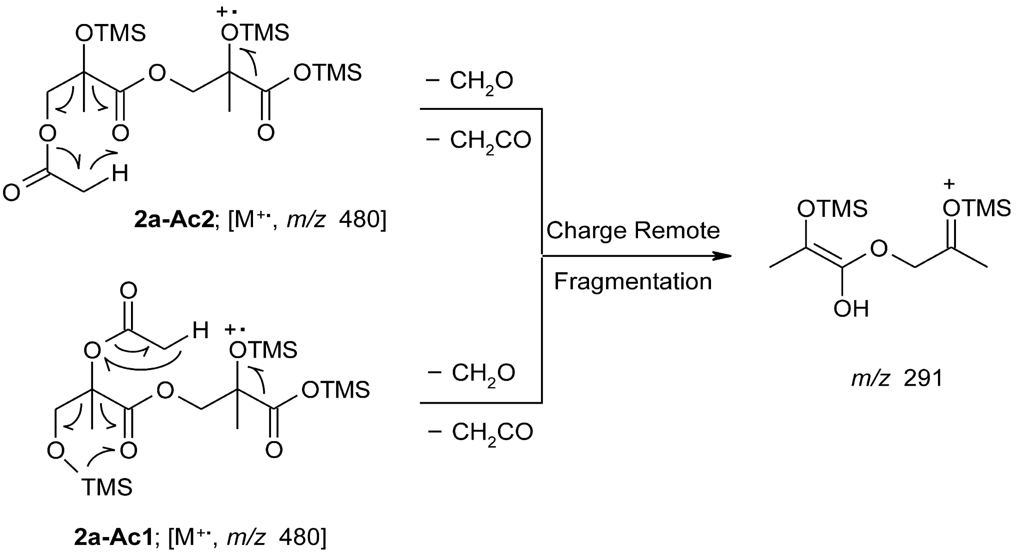

Scheme 12. Possible formation pathways for *m/z* 291 in the TMS derivatives of both 2-MG dimer mono-acetate isomers through charge-remote fragmentation reactions.

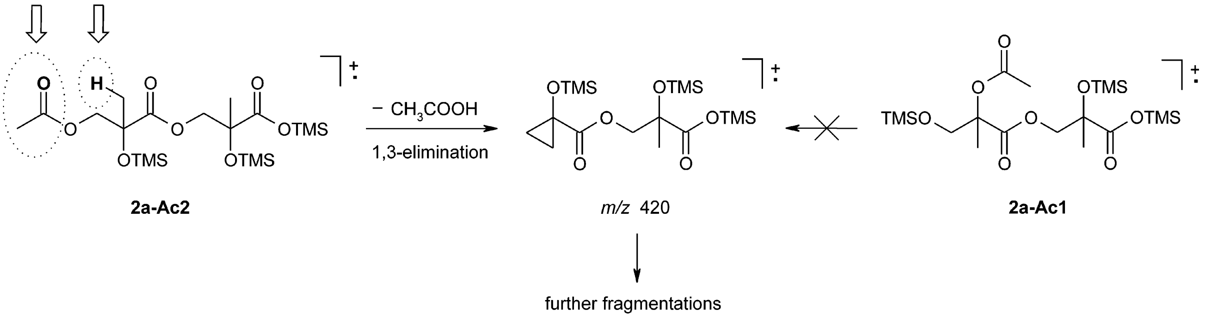

Scheme 13. Mechanism proposed for the formation of *m/z* 420, an ion characteristic of the TMS derivative of the 2-MG dimer mono-acetate bearing an acetyl group at the terminal hydroxymethyl group of the non-carboxylic acid-containing 2-MG residue (**2a-Ac2**). Parts of the molecule engaged in the elimination process are circled.

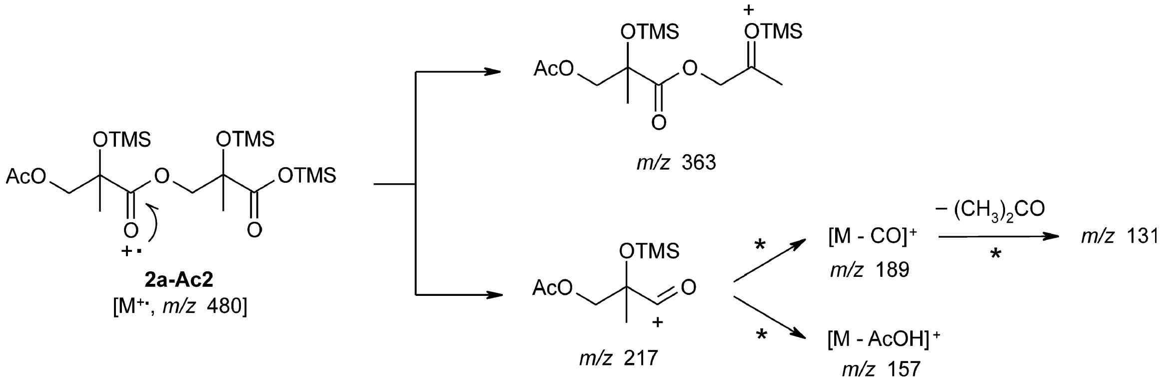

Scheme 14. Mechanisms proposed for formation of *m/z* 363, 217, 189, 157, and 131 in the TMS derivative of an 2-MG linear dimer mono-acetate (**2a-Ac2**). The same mechanisms hold for the isomer **2a-Ac1**.

seen that the spectrum of the first-eluting isomer (**2a-Ac1**) contains an ion at *m/z* 450, corresponding to the $[M - CH_2O]^{+\bullet}$ ion formed through a rearrangement of a TMS group (Scheme 11). This ion firmly supports the presence of a terminal trimethylsilylated hydroxymethyl group in the non-carboxylic acid-containing 2-MG residue and is consistent with a nonbranched carboxylic acid-containing 2-MG residue. Following the loss of formaldehyde, *m/z* 450 fragments by loss of ketene (42 Da) from the acetate group, resulting in *m/z* 408. Further fragmentation of *m/z* 408 through loss of a $TMSO(CO)^{\bullet}$ radical leads to *m/z* 291. It can be seen that *m/z* 291 is also present in the case of the 2-MG dimer mono-acetate isomer eluting at a RT of 52.6 min (**2a-Ac2**); an alternative explanation for *m/z* 291 in both 2-MG dimer mono-acetate isomers through charge-remote rearrangement reactions involving neutral loss of both ketene (42 Da) and formaldehyde (30 Da) is outlined in Scheme 12.

The EI spectrum of the compound corresponding to the 2-MG dimer mono-acetate isomer eluting at a RT of 52.6 min (**2a-Ac2**) (Fig. 9(b)) shows a unique ion at *m/z* 420, which is explained by loss of acetic acid from the $M^{+\bullet}$ ion (Scheme 13). This favorable elimination of acetic acid involves a hydrogen at a 3-position relative to the acetate group[23] and does not occur in the other isomer (RT 52.3 min) in which only hydrogen atoms at the 2-position are available.

Ions present in the spectra of the TMS derivatives of both isomeric 2-MG linear dimer mono-acetates worth discussing are *m/z* 363, 217, 189, 157, and 131. Their formation mechanisms are given in Scheme 14. The formation of *m/z* 217 and 189 in both isomers is consistent with the presence of an acetate group in the non-carboxylic acid-containing 2-MG residue. As expected, *m/z* 157 is more prominent in the case of the 2-MG dimer mono-acetate bearing an acetyl group at the terminal hydroxymethyl group because of the favorable 1,3-elimination of acetic acid. On the other hand, the formation of *m/z* 131 due to loss of acetone from *m/z* 189 seems to be a favored pathway in the case of the 2-MG dimer mono-acetate bearing an internal acetyl group.

CONCLUSIONS

Detailed interpretation of the EI mass spectral data of the TMS derivatives of 2-MG and oligoester derivatives thereof allows one to obtain key structural features of the molecules and as such to elucidate their chemical structures and differentiate isomeric compounds. The *m/z* 219 ion containing the trimethylsilylated 1,2-dihydroxy-2-methylethyl group is a characteristic ion of 2-MG and its oligomers. Evidence for an ester function in the 2-MG dimers and trimers is indicated by the *m/z* 247 ion formed by an α-cleavage in the ester group linking the non-carboxylic acid-containing 2-MG residue to the remaining part of the molecules. In addition, evidence for an inner branched 2-MG residue in the case of the 2-MG branched trimer was obtained, while the 2-MG linear and branched dimers could be readily differentiated. Characteristic ions of the terminal carboxyl group are the $[M - CH_3]^+$ and $[M - (CH_3 + CO)]^+$ ions, while the terminal hydroxymethyl group was found to give rise to a $[M - CH_2O]^{+\bullet}$ ion in linear 2-MG oligomers. Furthermore, it was possible to differentiate isomeric mono-acetates of the 2-MG linear dimer containing an acetyl group in the non-carboxylic acid-containing 2-MG residue and locate the position of the acetyl group. We can conclude that the EI spectra of the TMS derivatives contain a wealth of structural information, including information about the MW, ester linkages, terminal carboxylic and hydroxymethyl groups, and esterification sites.

Acknowledgements

Research at the University of Antwerp was supported by the Belgian Federal Science Policy Office through the BIOSOL project (contract SD/AT/02A) and a visiting postdoctoral fellowship to Rafal Szmigielski, and by the Research Foundation – Flanders (FWO) (grant number G.0091.06). Research at Caltech was funded by the U.S. Environmental Protection Agency under the Science to Achieve Results (STAR) Program grant number RD-83107501-0, managed by EPA's Office of Research and Development (ORD), National Center for Environmental Research (NCER), and by the U.S. Department of Energy, Biological, and Environmental Research Program DE-FG02-05ER63983; this work has not been subjected to the EPA's required peer and policy review and therefore does not necessarily reflect the views of the Agency and no official endorsement should be inferred. Jason Surratt was supported in part by the United States Environmental Protection Agency (EPA) under the STAR Graduate Fellowship Program.

REFERENCES

1. Guenther A, Hewitt CN, Erickson D, Fall R, Geron C, Graedel T, Harley P, Klinger L, Lerdau M, Mckay WA, Pierce T, Scholes B, Steinbrecher R, Tallamraju R, Taylor J, Zimmerman P. A global model of natural volatile organic compound emissions. *J. Geophys. Res.* 1995; **100**: 8873.
2. Pandis SN, Paulson SE, Seinfeld JH, Flagan RC. Aerosol formation in the photooxidation of isoprene and β-pinene. *Atmos. Environ.* 1991; **25A**: 997.
3. Claeys M, Graham B, Vas G, Wang W, Vermeylen R, Pashynska V, Cafmeyer J, Guyon P, Andreae MO, Artaxo P, Maenhaut W. Formation of secondary organic aerosols through photooxidation of isoprene. *Science* 2004; **303**: 1173.
4. Claeys M, Wang W, Ion AC, Kourtchev I, Gelencsér A, Maenhaut W. Formation of secondary organic aerosols from isoprene and its gas-phase oxidation products through reaction with hydrogen peroxide. *Atmos. Environ.* 2004; **38**: 4093.
5. Ion AC, Vermeylen R, Kourtchev I, Cafmeyer J, Chi X, Gelencsér A, Maenhaut W, Claeys M. Polar organic compounds in rural $PM_{2.5}$ aerosols from K-puszta, Hungary, during a 2003 summer field campaign: sources and diel variations. *Atmos. Chem. Phys.* 2005; **5**: 1805.
6. Wang W, Kourtchev I, Graham B, Cafmeyer J, Maenhaut W, Claeys M. Characterization of oxygenated derivatives of isoprene related to 2-methyltetrols in Amazonian aerosols using trimethylsilylation and gas chromatography/ion trap mass spectrometry. *Rapid Commun. Mass Spectrom.* 2005; **19**: 1343.
7. Kourtchev I, Ruuskanen T, Maenhaut W, Kulmala M, Claeys M. Observation of 2-methyltetrols and related photo-oxidation products of isoprene in boreal forest aerosols from Hyytiälä, Finland. *Atmos. Chem. Phys.* 2005; **5**: 2761.
8. Edney EO, Kleindienst TE, Jaoui M, Lewandowski M, Offenberg JH, Wang W, Claeys M. Formation of 2-methyl tetrols and 2-methylglyceric acid in secondary organic aerosol from laboratory irradiated isoprene/NO_x/SO_2/air mixtures and their detection in ambient $PM_{2.5}$ samples collected in the eastern United States. *Atmos. Environ.* 2005; **39**: 5281.
9. Böge O, Miao Y, Plewka A, Herrmann H. Formation of secondary organic particle phase compounds from isoprene gas-phase oxidation products: an aerosol chamber and field study. *Atmos. Environ.* 2006; **40**: 2501.
10. Surratt JD, Murphy SM, Kroll JH, Ng NL, Hildebrandt L, Sorooshian A, Szmigielski R, Vermeylen R, Maenhaut W, Claeys M, Flagan RC, Seinfeld JH. Chemical composition of secondary organic aerosol formed from the photooxidation of isoprene. *J. Phys. Chem. A* 2006; **110**: 9665.
11. Kroll JH, Ng NL, Murphy SM, Flagan RC, Seinfeld JH. Secondary organic aerosol formation from isoprene photooxidation under high-NO_x conditions. *Geophys. Res. Lett.* 2005; **32**: L18808, Doi:10.1029/2005GL023637.
12. Kroll JH, Ng NL, Murphy SM, Flagan RC, Seinfeld JH. Secondary organic aerosol formation from isoprene photooxidation. *Environ. Sci. Technol.* 2006; **40**: 1867, Doi:10.1021/es054301.
13. Dommen J, Metzger A, Duplissy J, Kalberer M, Alfarra MR, Gascho A, Weingartner E, Prevot ASH, Verheggen B, Baltensperger U. Laboratory observation of oligomers in the aerosol

from isoprene/NO_x photooxidation. *Geophys. Res. Lett.* 2006; **33**: L13805, Doi:10.1029/2006GL026523.

14. Henze DK, Seinfeld JH. Global secondary organic aerosol from isoprene oxidation. *Geophys. Res. Lett.* 2006; **33**: L09812, Doi:10.1029/2006GL025976.
15. Iinuma Y, Böge O, Gnauk T, Herrmann H. Aerosol-chamber study of the α-pinene/O_3 reaction: influence of particle acidity on aerosol yields and products. *Atmos. Environ.* 2004; **38**: 761.
16. Gao S, Keywood M, Ng NL, Surratt JD, Varutbangkul V, Bahreini R, Flagan RC, Seinfeld JH. Low-molecular-weight and oligomeric components in secondary organic aerosol from the ozonolysis of cycloalkenes and alpha-pinene. *J. Phys. Chem. A* 2004; **108**: 10147.
17. Gao S, Ng NL, Keywood M, Varutbangkul V, Bahreini R, Nenes A, He J, Yoo KY, Beauchamp JL, Hodyss RP, Flagan RC, Seinfeld JH. Particle phase acidity and oligomer formation in secondary organic aerosol. *Environ. Sci. Technol.* 2004; **38**: 6582.
18. Tolocka MP, Jang M, Ginter JM, Cox FJ, Kamens RM, Johnston MV. Formation of oligomers in secondary organic aerosol. *Environ. Sci. Technol.* 2004; **38**: 1428.
19. Kalberer M, Paulsen D, Sax M, Steinbacher M, Dommen J, Prevot ASH, Fisseha R, Weingartner E, Frankevich V, Zenobi R, Baltensperger U. Identification of polymers as major compounds of atmospheric organic aerosols. *Science* 2004; **308**: 1659.
20. Jaoui M, Kleindienst TE, Lewandowski M, Edney EO. Identification and quantification of aerosol polar oxygenated compounds bearing carboxylic acid or hydroxy groups. 1. Method development. *Anal. Chem.* 2004; **76**: 4765.
21. Wang W, Vas G, Dommisse R, Loones K, Claeys M. Fragmentation study of diastereoisomeric 2-methyltetrols, oxidation products of isoprene, as their trimethylsilyl ethers, using gas chromatography/ion trap mass spectrometry. *Rapid Commun. Mass Spectrom.* 2004; **18**: 1787.
22. Maenhaut-Claeys M, Vandewalle M. Studies in organic mass spectrometry XIX. The fragmentation of the trimethylsilyl derivatives of some 2,3-diakyl-1,4-cyclopentanediols. *Bull. Soc. Chim. Belges* 1974; **83**: 343.
23. Liptak M, Heerma W. Fast atom bombardment mass spectrometric study of some *N*-glycosides and *S*-glycosides of acetylated hexose isomers. *Rapid Commun. Mass Spectrom.* 1993; **7**: 676.

Appendix B

Characterization of Polar Organic Components in Fine Aerosols in the Southeastern United States: Identity, Origin, and Evolution*

---

*This chapter is reproduced by permission from “Characterization of Polar Organic Components in Fine Aerosols in the Southeastern United States: Identity, Origin, and Evolution” by Song Gao, Jason D. Surratt, Eladio M. Knipping, Eric S. Edgerton, Mona Shahgholi, and John H. Seinfeld, *Journal of Geophysical Research - Atmospheres*, 111 (D14), D14314, 2006. Copyright 2006 by the American Geophysical Union.

JOURNAL OF GEOPHYSICAL RESEARCH, VOL. 111, D14314, doi:10.1029/2005JD006601, 2006

Characterization of polar organic components in fine aerosols in the southeastern United States: Identity, origin, and evolution

Song Gao,[1] Jason D. Surratt,[2] Eladio M. Knipping,[3] Eric S. Edgerton,[4] Mona Shahgholi,[2] and John H. Seinfeld[1]

Received 19 August 2005; revised 13 December 2005; accepted 28 February 2006; published 27 July 2006.

[1] Filter samples of fine aerosols collected in the Southeastern United States in June 2004 were analyzed for the characterization of polar organic components. Four analytical techniques, liquid chromatography −mass spectrometry, ion trap mass spectrometry, laser desorption ionization mass spectrometry, and high-resolution mass spectrometry, were used for identification and quantification. Forty distinct species were detected, comprising on average 7.2% and 1.1% of the total particulate organic mass at three inland sites and a coastal site, respectively. The relative abundance of these species displays a rather consistent distribution pattern in the inland region, whereas a different pattern is found at the coastal site. Chemical and correlation analyses suggest that the detected species are secondary in nature and originate from terpene oxidation, with possible participation of NO_x and SO_2. It is estimated that polar, acidic components in fine aerosols in the Southeastern United States cover a molecular weight range of 150−400 Da and do not appear to be oligomeric. Other components with MW up to 800 Da may also be present. The detected polar organic species are similar to humic-like substances (HULIS) commonly found in fine aerosols in other rural areas. We present the first, direct evidence that atmospheric processing of biogenic emissions can lead to the formation of certain HULIS species in fine aerosols, and that this may be a typical pathway in the background atmosphere in continental regions; nevertheless, a natural source for HULIS, such as from aquatic and/or terrestrial humic/fulvic acids and their degradation products, cannot be precluded.

Citation: Gao, S., J. D. Surratt, E. M. Knipping, E. S. Edgerton, M. Shahgholi, and J. H. Seinfeld (2006), Characterization of polar organic components in fine aerosols in the southeastern United States: Identity, origin, and evolution, *J. Geophys. Res.*, *111*, D14314, doi:10.1029/2005JD006601.

1. Introduction

[2] A subject of intense interest is the composition, sources and formation pathways of organic aerosols because of their role in climate forcing and their adverse effects on human health. The Southeastern United States (SE US) is of particular interest from a global point of view for its generally rural environment interspersed with a number of urban areas. Ample subtropical vegetation provides a constant source of biogenic volatile organic compounds (VOC), such as isoprene, monoterpenes and sesquiterpenes, in this large region. Also present are several urban areas, varying from small cities to metropolitan ones, and burgeoning industrial activities including coal-fired power plants, petroleum processing and maritime shipping, all contributing to background and heightened levels of SO_2, NO_x and anthropogenic VOC. Together with biogenic emissions, these emissions can contribute to the formation of ozone and particulate matter (PM). Prevailing winds can bring different source air masses to inland regions versus coastal areas. A number of field measurements have been carried out to study this region, including the Atlanta Supersite Experiment [e.g., *Lim and Turpin*, 2002] and the Southeastern Aerosol and Visibility Study (SEAVS) [e.g., *Yu et al.*, 2005]. The Southeastern Aerosol Research and Characterization Study (SEARCH) was initiated in mid-1998 to carry out systematic measurements of temporal and spatial variability of PM, in particular $PM_{2.5}$ (i.e., aerosols with aerodynamic diameter less than 2.5 μm, also commonly called fine aerosols), gases relevant to secondary O_3 formation, and surface meteorology. Among the myriad of measurements and analyses to date, the organic composition of $PM_{2.5}$ has been explored, such as a source apportionment analysis by *Zheng et al.* [2002]. Zheng et al. concluded that the major source contributors to organic PM were wood combustion (25–66%), diesel exhaust (14–30%), meat cooking (5–12%) and gasoline-powered motor vehicle exhaust (0–10%). Altogether, the individual components identified and quantified by the gas chromatography−mass

---

[1] Departments of Environmental Science and Engineering and Chemical Engineering, California Institute of Technology, Pasadena, California, USA.

[2] Department of Chemistry, California Institute of Technology, Pasadena, California, USA.

[3] Electric Power Research Institute, Palo Alto, California, USA.

[4] Atmospheric Research and Analysis, Inc., Cary, North Carolina, USA.

0148-0227/06/2005JD006601$09.00

spectrometry (GC-MS) account for on average 12% of the total organic mass in $PM_{2.5}$. An immediate question arises as to the identity of the nearly 90% of the $PM_{2.5}$ organic mass. Since GC-MS is intrinsically amenable to identifying relatively nonpolar species (unless derivatization techniques are employed), and it is speculated that secondary organic aerosol (SOA) formation occurs more substantially in the summer, one central goal of this work is to understand the chemical nature, sources and evolution pathways of the relatively polar species in $PM_{2.5}$ in the SE US.

[3] Answers to these questions, and indeed, more detailed knowledge of the organic composition of $PM_{2.5}$ in the SE US, can have broader impacts on several fronts. Polar, more oxidized species may play important roles in determining the hygroscopicity and cloud condensation nuclei (CCN) activity of aerosols [*Cruz and Pandis*, 1998, 2000; *Choi and Chan*, 2002]. The detection of oligomers in SOA from recent chamber experiments, attributed tentatively to acid catalysis, poses the possibility that oligomers may be present in ambient aerosols [*Kalberer et al.*, 2004; *Tolocka et al.*, 2004; *Gao et al.*, 2004a, 2004b; *Baltensperger et al.*, 2005]. To date, no definitive detection of oligomers in ambient aerosols has been reported. There are limitations of laboratory chamber experiments, such as the insufficient aging time. The longest duration of SOA evolution was ~30 hours for *Kalberer et al.* [2004], which is less than that in the ambient air (e.g., about 1 week for $PM_{2.5}$ in the SE US). Oxidation and even decomposition of oligomers may take place in the latter stage of aging. In addition, the hydrocarbon concentrations used in chamber experiments tend to be about an order of magnitude higher than those in the atmosphere, and synergistic effects of multiple reactants and oxidants generally have not been simulated yet in laboratory experiments. Theoretical calculations do not seem to support the stable presence of species formed via accretion reactions alone [*Barsanti and Pankow*, 2004]. Answers to whether oligomers are present in $PM_{2.5}$ in the SE US and whether particle acidity plays a role in affecting aerosol composition are of great interest in bridging the gap between laboratory studies and ambient realities.

[4] In rural areas worldwide, a large number of organic species have been detected in aerosols, as well as fog and cloud water [e.g., *Kavouras et al.*, 1999; *Krivacsy et al.*, 2001; *Pio et al.*, 2001; *Kiss et al.*, 2003; *Cappiello et al.*, 2003]. These species have been found to be generally rather polar and even water-soluble; however, their chemical identity remains elusive. The ensemble of these species is often referred to as humic-like substances (HULIS), and hypothesis has been made as to a direct link between HULIS species in atmospheric aerosols, with MW estimated to be on the order of several hundreds, and humic/fulvic acids naturally occurring in terrestrial and aquatic environments [*Gelencser et al.*, 2002]. Interestingly, a secondary photochemical source for HULIS has never been precluded, although direct evidence for this pathway has been lacking. A better understanding of the $PM_{2.5}$ composition in the SE US may shed further light on the sources and evolution pathways for the much-speculated HULIS species.

[5] This work addresses these questions by analyzing the organic fraction, especially the polar components, in fine aerosols in the SE US. A suite of analytical instruments are used concurrently for this purpose. Back trajectories of specific samples and correlations among chemical and field variables are also examined. Possible sources and evolution pathways of the identified organic species are then discussed.

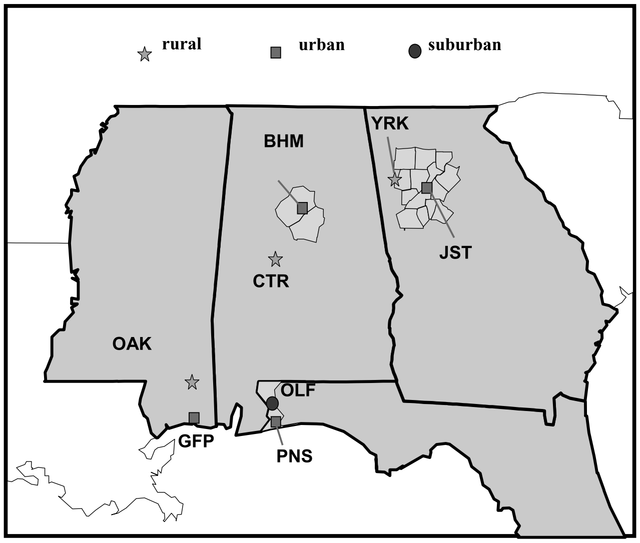

Figure 1. SEARCH network. Atlanta (JST), north Birmingham (BHM), Centreville (CTR), and Pensacola (PNS) are the four sampling sites used for analysis in this work.

2. Experiment

2.1. Filter Sampling and Field Measurements

[6] The quartz and Teflon filters used for this work were collected at four different sites in the SEARCH network on 4 days in June 2004. Twenty-four-hour composite samples were taken; owing to this long sampling time, the contribution of adsorbed compounds to the total organic aerosol mass can be assumed to be relatively low [*Turpin et al.*, 1994]. Detailed descriptions of the four sites, including their terrain, vegetation, industrial and transportation sources and surrounding environment, are described in a SEARCH overview paper [*Hansen et al.*, 2003]. Briefly, JST (Jefferson Street, near downtown Atlanta, Georgia) and BHM (North Birmingham, Alabama) are both urban sites with mainly industrial and residential settings. CTR (Centreville, Alabama) is a rural site with a heavily wooded forest setting approximately 80 km southwest of BHM. PNS (Pensacola, Florida) is an urban site with a mainly residential setting. Figure 1 shows the location of these four sites, along with other SEARCH sites. It is worth noting that JST, BHM and CTR are all inland sites, whereas PNS is a coastal site subject to frequent prevailing winds from the Gulf of Mexico.

[7] Detailed descriptions of the measurements of gas-phase species, particulate sulfate, nitrate, ammonium, major metal oxides, total organic matter (TOM) and black carbon (BC) are also provided by *Hansen et al.* [2003], and will not be reiterated here. In particular, the TOM mass is estimated from the total organic carbon mass (section 3.5), which, in turn, is derived from thermal evolution measurements of

total carbon and aethalometer measurements of BC with further corrections from the backup filter data.

2.2. Filter Extraction and Sample Preparation

[8] Quartz and Teflon filters collected from each of the four SEARCH sites were extracted in HPLC-grade methanol by 40 min of sonication. The filters were then removed from the methanol sample extract and stored at −20°C with dichloromethane added for archiving purposes. In order to remove soot and filter media residues, the filter extracts were centrifuged for 10 min at 4500 rpm and then filtered through a PALL Life Sciences Acrodisc CR 25-mm syringe filter (PTFE membrane, 0.2-μm pore size) into a scintillation vial. Because these samples usually contain a high concentration of inorganic ions such as sulfate, a solid phase extraction (SPE) technique was applied to desalt and further pretreat the sample extracts. This procedure used 3-mL Supleco Discovery C_{18} reverse phase SPE tubes. Following the sonication, centrifuging and filtering steps outlined above, filter extracts were blown to near dryness with a gentle stream of N_2 and were reconstituted with 5 mL of 1% acetic acid in water. The 1% acetic acid buffer was used to adjust the pH of the extracts to allow many organic species to become protonated and thus better retained on the C_{18} material upon sample addition to the SPE tube. Three milliliters of water was then washed through the SPE tube to desalt the sample. Organic species were then gradually eluted off the SPE tube with 5 mL of methanol. This eluate was collected, blown dry, and reconstituted with 0.1% acetic acid in 50% water/50% methanol. Field blank filters and lab control filters were extracted and pretreated the same way as the samples. Aliquots of each filter extract were subsequently analyzed by the following four analytical techniques.

2.3. LC-MS Analysis

[9] A Hewlett-Packard 1100 Series HPLC−single quadrupole MS system, equipped with an electrospray ionization (ESI) source, was used to identify and quantify relatively polar, acidic species in SEARCH 2004 aerosol samples, under the negative ion mode. A Waters Nova-Pak C_{18} column (3.9 × 300 mm) was used to separate the organic species before the MS detection. The eluents used were 0.1% acetic acid in water (A) and methanol (B). A 40-min gradient elution program was used, where eluent B increased from 10% to 90% in the first 35 min and then decreased to 10% in 5 min. During full spectrum MS mode of analysis, the fragmentor voltage was set at 60 V and most species were detected as their molecular ions. During the upfront CID (i.e., collision-induced dissociation) mode of analysis, the fragmentor was set at 110 V resulting in partial fragmentation of the molecular ions. By comparing the two sets of MS data and their different fragmentation patterns, some structural information on the analyzed species was gleaned.

2.4. Ion Trap MS (ITMS) Analysis

[10] Another aliquot of the filter extract was analyzed by a Finnigan LCQ ion trap mass spectrometer (equipped with an ESI source) without chromatographic separation. Under the negative ion mode, relatively polar species with MW up to 1200 were detected. Under the positive ion mode, a broader range of compounds with MW up to 1600 Da were detected as mainly Na^+adducts. By comparing the detection under both ion modes, aerosol components of different polarity and acidity can be assessed. In addition, specific ions of interest were isolated from the rest of the sample matrix and were further fragmented to produce tandem mass spectra, aiding structure elucidation.

2.5. LDI MS Analysis

[11] A third aliquot of the filter extract was analyzed by laser desorption/ionization mass spectrometry (LDI MS) on porous silicon (i.e., DIOS). In DIOS, a porous Si surface serves as LDI matrix while in standard matrix-assisted LDI (MALDI), a UV-light absorbing species is the matrix. DIOS-LDI MS was used in favor of MALDI in order to avoid interferences from MALDI matrix ions. After the extract was dried on the DIOS chip, the sample plate was analyzed by a Voyager-DE PRO MALDI time-of-flight (TOF) mass spectrometer in order to assess the MW range of aerosol components. Analyses were performed in the linear mode with delayed extraction on. The laser intensity was adjusted at ∼10% above ionization threshold to permit detection without inducing fragmentation. Usually, 900 laser shots were summed to get a representative spectrum of a sample.

2.6. High-Resolution MS Analysis

[12] A fourth aliquot of the filter extract was analyzed by a Waters LCT Premier electrospray time-of-flight mass spectrometer in the Department of Chemistry at the University of California, Irvine, operated in the negative ion mode using W geometry. Initial calibration used sodium formate clusters with a known compound spiked into the analytical sample for lock-mass corrections to obtain accurate mass for the ions with *m*/*z* 294.

[13] For further confirmation, a JEOL JMS-600H double-focusing, high-resolution, magnetic sector mass spectrometer at Caltech was also used for accurate mass measurements of the ion with *m*/*z* 294. The sample was analyzed by Fast Atom Bombardment (FAB) in the negative ion mode with instrument resolving power set to 3000, using the 10% valley definition. For these experiments the instrument was first externally calibrated with polyethylene glycol (PEG) clusters in the negative ion mode. The sample was mixed with glycerol, and glycerol cluster ions were used for internal calibration of the mass spectrum.

3. Results and Discussion

3.1. Identification of Organic Components in Fine Aerosols

[14] All four analytical methods described in section 2 were used to identify organic species in the fine aerosols in the SE US. As we demonstrate next, these measurements indicate possible structures of specific species and reveal a consistent picture of the organic aerosol composition.

[15] Figure 2 shows the total ion chromatogram (TIC) and several (*m*/*z* 171, 185, 294, 313) extracted ion chromatograms (EIC) of a typical $PM_{2.5}$ sample collected during SEARCH 2004. Background signals from field blanks are subtracted from all aerosol samples for identification and quantification. It is noticeable that multiple peaks are present in the EIC of certain ions, such as those with *m*/*z*

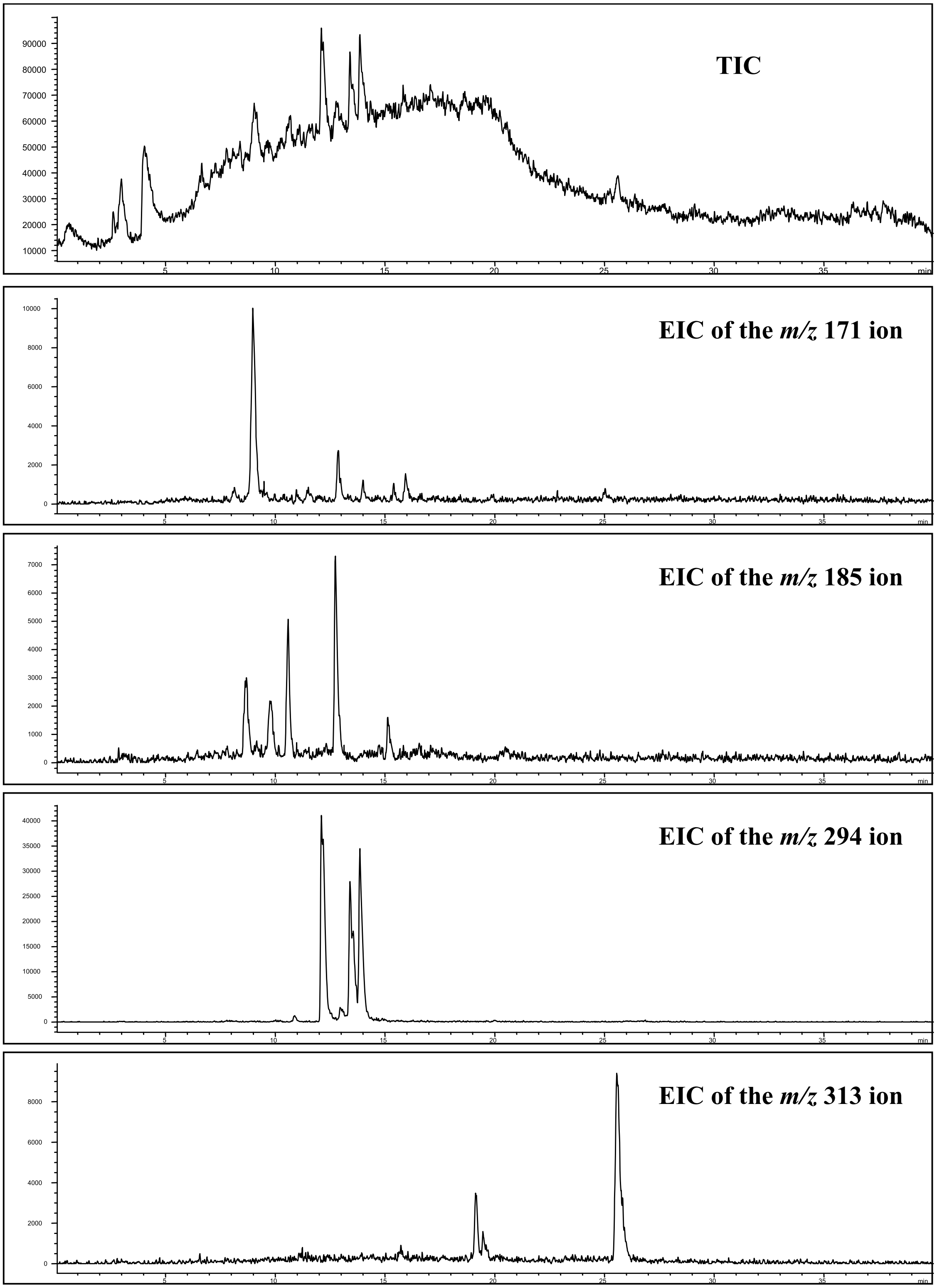

Figure 2. TIC and several EIC of the extract of the $PM_{2.5}$ sample collected at the BHM site on 23 June 2004. The *y* axis is intensity for the TIC and all EICs.

171, 185, 187, 294, 313, and 342. These same-nominal mass species could have either different elemental compositions or different isomeric structures with the same elemental composition, which is not possible to pinpoint owing to the unit mass resolution in the quadrupole MS. Throughout this paper, each set of these same-mass species detected by the LC-MS shall be called "isobaric species" or "isobaric compounds," terms commonly used in the mass

Table 1. Abundance and Occurrence of Detected Organic Species in $PM_{2.5}$ in the Southeast United States in June 2004[a]

			JST				CTR				BHM				PNS			
[M-H]-Ion	Standard or Surrogate Standard	Number of Occurrences	14 June 2004	17 June 2004	23 June 2004	29 June 2004	14 June 2004	17 June 2004	23 June 2004	29 June 2004	14 June 2004	17 June 2004	23 June 2004	29 June 2004	14 June 2004	17 June 2004	23 June 2004	29 June 2004
157	adipic acid	9			6.3				8.1	5.6	7.9	13.2	6.1		3.6	5.2		3.7
165	trans-norpinic acid	7		21.9		29.9					2.4	19.0		17.9		5.5		7.9
171	trans-norpinic acid[b]	16	20.9	29.5	15.8	19.5	22.1	40.0	20.4	16.2	18.3	31.8	20.6	12.5	0.9	3.9	4.0	4.5
175	adipic acid	4	8.7	6.6			7.7	6.3										
179	trans-norpinic acid	5		5.7		6.3					1.4	7.5				0.6		
183	cis-pinonic acid[b]	13		4.6	3.5		3.5	4.8	4.4	4.8	9.1	8.5	3.2		2.4	2.6	3.1	3.4
185	pinic acid[b]	14	9.2	42.7	28.2	30.6	16.2	43.2	30.2	21.0	16.6	42.3	26.8	19.1		1.3		1.2
187	2-isopopylmalic acid, azelaic acid[b]	16	119.2	26.9	16.6	9.0	46.3	28.4	16.0	10.7	47.6	20.5	24.1	2.0	0.5	6.8	0.7	1.1
189	2-isopropylmalic acid	5	23.5				26.5		14.3		14.1		24.1					
197	sebacic acid	8		1.9			1.5	3.5	1.4		1.6	2.1	1.1				0.9	
199	trans-norpinic acid	3						7.5	8.0		2.5							
201	sebacic acid[b]	5				10.2		0.9	4.1	5.4				10.0				
203	trans-norpinic acid	13	62.9	50.1	15.7	29.2	48.6	66.6	21.8	20.5	20.6	47.1	31.8	21.5		12.0		
215	2-ketogulonic acid hydrate, trans-norpinic acid	13	24.5	48.9	2.3	17.8	26.2	60.3	15.4	10.2	9.4	48.5	8.1	3.3		1.9		
231	sinapic acid	3	9.6				9.1				1.8							
241	sebacic acid	4		1.2			1.2	2.2				1.6						
253	sebacic acid	11		3.5	2.7	1.2		3.8	3.0	2.8	2.0	2.9	2.4			0.8	1.5	
255	azelaic acid	4		2.4				0.7				4.5	2.2					
294	sinapic acid, suberic acid	12	139.6	81.5	87.4	39.4	58.0	131.1	72.9	27.1	94.6	99.1	117.2	44.6				
296	trans-norpinic acid	4			5.5			19.3			4.1		9.3					
310	sinapic acid	4					8.6		10.7		8.1		11.8					
311	undecandioic acid	6		4.2	1.5			4.2				0.2				1.5	2.1	
313	undecandioic acid	5						3.5	2.9				6.1			3.8		1.6
339	undecandioic acid	9		1.7				5.8	3.5	3.5		1.8	1.4			2.7	1.2	2.4
342	sinapic acid	11	11.6	12.6	15.6	10.0	53.1	13.8	18.0		14.5	7.1	21.1	6.3				

Table 1. (continued)

[M-H]-Ion	Standard or Surrogate Standard	Number of Occurrences	JST				CTR				BHM				PNS			
			14 June 2004	17 June 2004	23 June 2004	29 June 2004	14 June 2004	17 June 2004	23 June 2004	29 June 2004	14 June 2004	17 June 2004	23 June 2004	29 June 2004	14 June 2004	17 June 2004	23 June 2004	29 June 2004
382	undecandioic acid	3			1.5				0.04				1.7					
387	sinapic acid	6	4.1	5.7	7.3	6.6	2.8				7.6							
Totals			14 June 2004	17 June 2004	23 June 2004	29 June 2004	14 June 2004	17 June 2004	23 June 2004	29 June 2004	14 June 2004	17 June 2004	23 June 2004	29 June 2004	14 June 2004	17 June 2004	23 June 2004	29 June 2004
Total identified organic mass,^{c} ng/m^3			466.3	351.6	212.1	209.6	357.5	453.1	271.1	131.8	293.4	358.0	346.8	137.1	7.3	62.6	16.3	25.8
Mass of total organic matter (TOM) in PM$_{2.5}$, ng/m^3			7119.5	5315.9	3124.3	6076.5	3566.6	3465.7	3006.1	3148.1	4496.7	4705.8	3265.1	5385.3	592.2	3678.6	1623.3	6154.1
Percent of TOM mass identified			6.5	6.6	6.8	3.4	10.0	13.1	9.0	4.2	6.5	7.6	10.6	2.5	1.2	1.7	1.0	0.4

[a] Values are in terms of molecular ion's *m/z*. Species with their [M-H]-*m/z* of 173, 217, 265, 269, 271, 285, 299, 312, 315, 326, 329, and 353 occur in no more than two samples and comprise, on average, less than 4% of the total identified organic mass. These species are not included in this table. A blank cell indicates the corresponding species was below detection limits.

[b] Indicates the standard used matches the retention time and mass spectrum of one or more of the isobaric species.

[c] Mass concentrations of the 1–2 occurrence species are included in the total identified organic mass, even though they are not listed above.

spectrometry community. We note that this chemical definition of isobaric (of equal molecular weight) is different from and should not be confused with the meteorological definition of isobaric (of equal atmospheric pressure). The presence of these isobaric species indicates the complexity of the organic fraction of PM$_{2.5}$ in the SE US, and they can originate from either isomerization through a single reaction pathway or multiple sources and reaction pathways. We will discuss these isobaric species further in section 3.2.

[16] A series of standard compounds were analyzed by the LC-MS to obtain their retention times and ESI (negative ion mode) mass spectra. The reproducibility of these retention times is mostly within 0.05 min and never exceeds 0.1 min. The details of standard calibration on the same LC-MS and the relationship between retention time and compound structure are discussed in detail by *Gao et al.* [2004a]. Owing to the "soft" nature of the ESI source, all standard compounds are detected as deprotonated molecular ions [M-H]$^-$ and display no or minimal fragmentation in the mass spectra. Earlier work has shown that acidic compounds with MW below 600 tend to form only singly charged ions (mainly [M-H]$^-$) in the ESI-MS [*Leenheer et al.*, 2001; *Kiss et al.*, 2003]. It is then reasonable to assume that the detected organic species in the fine aerosols in SEARCH 2004 are mostly in the form of [M-H]$^-$. Each chromatographic peak in the TIC in Figure 2 represents either a single species or several convoluted species due to co-eluting. From the EIC, 40 distinct species are detected in the 16 SEARCH 2004 PM$_{2.5}$ samples, which are listed in Table 1 except for those species that are detected in only one or two samples (i.e., occurrence < 3). Some individual isobaric species are not listed in this table for two reasons. The analytical techniques in this work cannot pinpoint the exact structures of most of these isobaric species. In addition, as will be shown in section 3.2, in the sampling region in June 2004, there is a rather constant mass distribution pattern of each set of isobaric species, rendering a summation within each set still a good representation of a specific species.

[17] It is of great interest to understand the molecular structures of these species, which can shed light on their sources and formation pathways. For a species that matches the retention time and mass spectrum of a certain standard compound, the structure of the standard is assigned to the corresponding species. For example, certain isobaric species of *m*/*z* 171, 183, and 185 (all detected as [M-H]$^-$) correspond to the standards of norpinic acid, pinonic acid, and pinic acid, respectively. The two-stage tandem mass spectra by the ITMS (MS/MS) of these species are similar to those of the standards, further confirming their structures. Previous work has shown that these organic acids are some of the dominant low-MW products from gas-phase monoterpene oxidation, such as α-pinene ozonolysis [*Yu et al.*, 1999; *Glasius et al.*, 2000; *Gao et al.*, 2004b]. Considering the substantial presence of terpene-emitting vegetation, such as mixed conifer and deciduous forests, in the SE US, terpene oxidation is a very likely pathway to form these species in PM$_{2.5}$ there.

[18] There are other species detected by the LC-MS for which standards are not available for comparison, making elucidation of their structures more difficult. However, as will be discussed in section 3.4, there is good correlation between many other species (e.g., *m*/*z* 203, 215, 253, 294,

$[M-H]^-$ ion (*m/z*)	Species (common name, if available)	Molecular Structure
157	157 A (norpinolic acid)	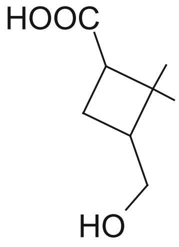
165	165 A	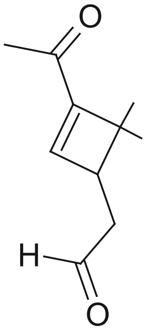
	165 B	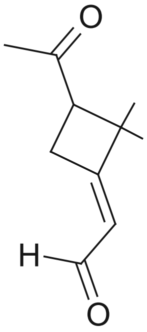
171	171 A (norpinic acid)	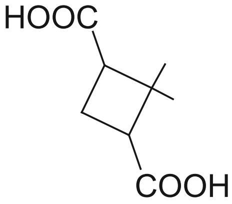
	171 B (pinolic acid)	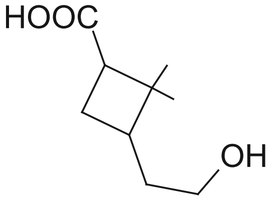

Figure 3. Identified and proposed molecular structures of some detected species (MW < 250 Da) in $PM_{2.5}$ in the SE United States in June 2004 (all drawn in the form of neutral species).

and 339 ions) and those likely with a biogenic source (e.g., *m/z* 171, 183, and 185 ions). This suggests that the former may also come from terpene oxidation, at least for selected isobaric species. Most of them appear to contain carboxyl groups, as revealed by the MS/MS fragmentation patterns. Their rather early retention times on the C_{18} reversed-phase column, compared with those of known standards, suggest they are highly oxidized species. For species with MW below 250 Da, we propose possible structures based on their MS/MS fragmentation patterns and mechanistic consideration of monoterpene oxidation (Figure 3). Some of these structures have been proposed before, such as by

173	173 A	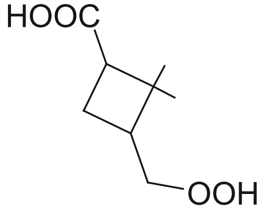
183	183 A (pinonic acid)	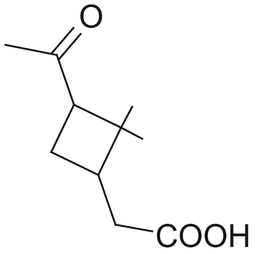
	183 B (hydroxyl pinonaldehyde)	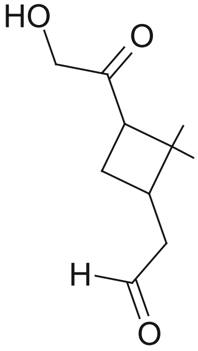
	183 C (hydroxyl pinonaldehyde)	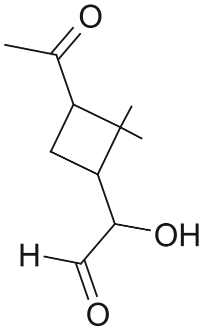
	183 D (hydroxyl pinonaldehyde)	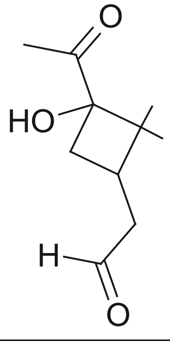

Figure 3. (continued)

Winterhalter et al. [2003], but they require further confirmation such as by the high-resolution MS. For species with MW above 250 Da, it is generally difficult to even propose possible structures. However, since the *m*/*z* 294 ion is almost always the most abundant species (except for the PNS site), comprising 19–41% (28% on average) of the total identified organic mass, we attempt to elucidate its structure by several other approaches.

[19] The fact that the *m*/*z* 294 molecular ion is even-numbered suggests, at first glance, that it may be a

185	185 A (pinic acid)	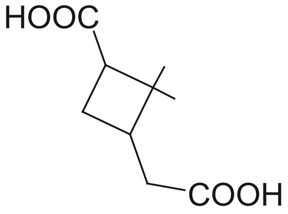
	185 B (pinalic peroxo acid)	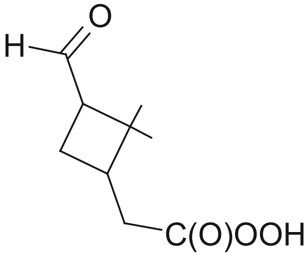
	185 C	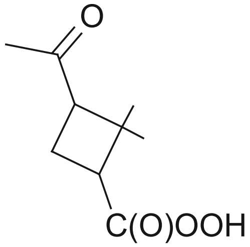
187	187 A (azelaic acid)	HOOC–$(CH_2)_7$–COOH
	187 B (norpinic peroxy acid)	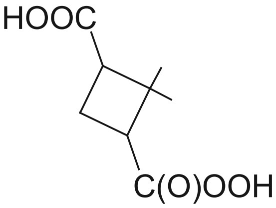
197	197 A (keto-pinonic acid)	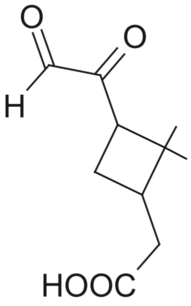
	197 B (keto-pinonic acid)	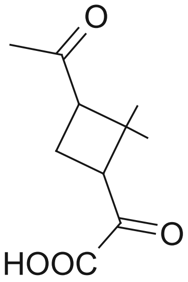

Figure 3. (continued)

199	199 A (hydroxyl pinonic acid) 199 B (hydroxyl pinonic acid) 199 C (hydroxyl pinonic acid)	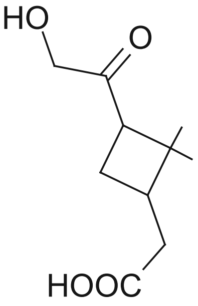 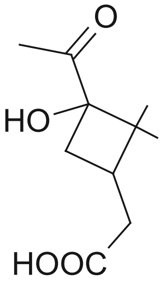 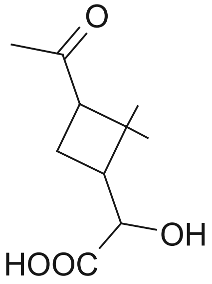
201	201 A (sebacic acid) 201 B (peroxo pinic acid)	$HOOC-(CH_2)_8-COOH$ 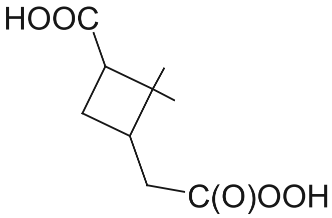
203	203 A (norpinic diperoxy acid)	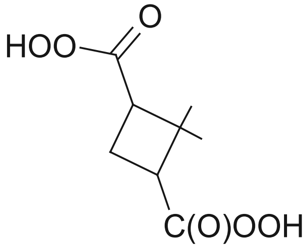

Figure 3. (continued)

nitrogen-containing species. This hypothesis is supported by the MS/MS data. Figure 4 shows the ion trap MS/MS of the *m*/*z* 294 ion from the same samples as shown in Figure 2, where all isobaric species were isolated and fragmented simultaneously. The most abundant fragment ion (*m*/*z* = 231) corresponds to a loss of 63, which is likely HNO_3. Another fragment ion (*m*/*z* = 247) corresponds to a loss of 47, which is likely HNO_2. As will be discussed in section 3.4, there is good correlation between the abundance of the *m*/*z* 294 ion and that of the *m*/*z* 171, 185, 187, 197, 203 and 215 ions, the latter likely formed via terpene oxidation. It follows that *m*/*z* 294 ion

215	215 A (undecanedioic acid)	$HOOC-(CH_2)_9-COOH$
	215 B (hydroxy pinonic peroxy acid)	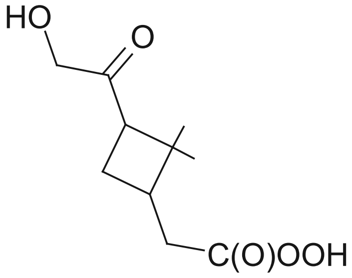
	215 C (hydroxy pinonic peroxy acid)	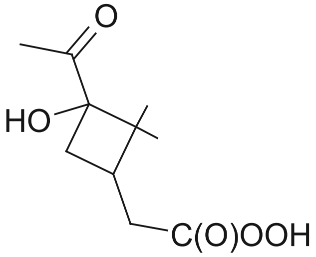
	215 D (hydroxy pinonic peroxy acid)	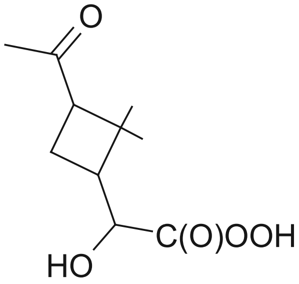
217	217 A (hydroxy pinic peroxy acid)	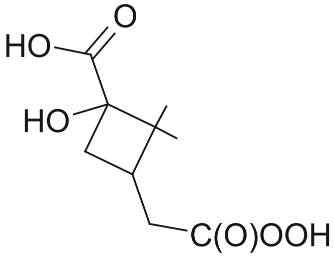
	217 B (hydroxy pinic peroxy acid)	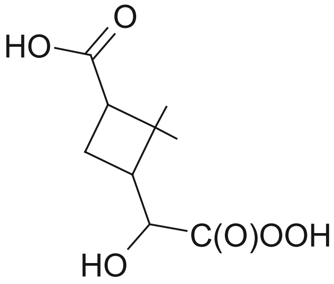

Figure 3. (continued)

may also come from terpene oxidation, but with the participation of NO_x to account for the presence of HNO_2 and HNO_3 in its structures. It is worth noting that *Kiss et al.* [2003] also observed an *m*/*z* 294 ion in their LC-MS analysis of rural fine aerosols, which they concluded as different from the HULIS fraction that exhibited a polyconjugated nature similar to aquatic fulvic acids [*Kiss et al.*, 2001]. The secondary formation scheme

231	231 A (hydroperoxy pinonic peroxy acid)	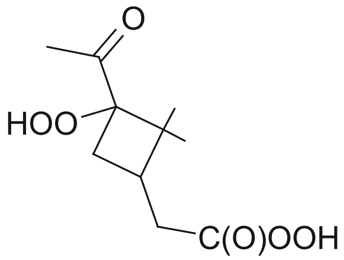
	231 B (hydroperoxy pinonic peroxy acid)	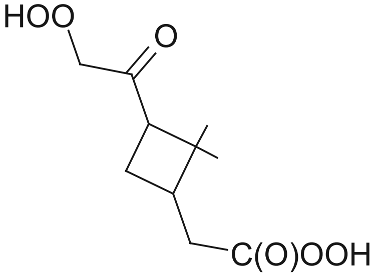
	231 C (hydroperoxy pinonic peroxy acid)	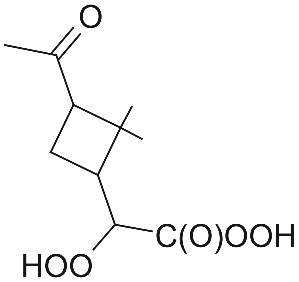

Figure 3. (continued)

proposed here appears to be a viable pathway. Since the organic eluent used by *Kiss et al.* [2003] was isopropanol, whereas it is methanol in this work, this is confirmation that the *m*/*z* 294 ion is not an eluent adduct.

[20] The upfront CID MS/MS analysis of the *m*/*z* 294 ion by the LC-MS provides a consistent picture. Figure 5 shows the EIC of the *m*/*z* 294 ion and the upfront CID mass spectra of the three main chromatographic peaks, with the fragmentor voltage set at 110V. It can be seen that the *m*/*z* 247 ion is a major fragment ion in peak 1 and peak 2, while the *m*/*z* 231 ion is a major fragment ion in peak 3. This suggests HONO is a dominant loss from the *m*/*z* 294 ion eluting in the first two peaks, while $HONO_2$ is a dominant loss from the species eluting in the third peak. In the full spectrum mode of the LC-MS analysis (fragmentor voltage = 60V) as shown in Figure 6, the *m*/*z* 294 ion elutes similarly in three main peaks, but with much higher intensities due to much less fragmentation. Strikingly, in addition to the dominant molecular ion, isotopic ions with *m*/*z* of 295 and 296 are always present in the mass spectra. The distinct pattern of isotopic distribution strongly suggests the *m*/*z* 294 ion is also a sulfur-containing species. Also strikingly, the *m*/*z* 96 ion is always the dominant ion in the upfront CID mass spectra of the *m*/*z* 294 ion, next to a smaller *m*/*z* 97 ion. These two fragment ions are probably attributed to SO_4^- and its isotope (or HSO_4^-), which are also seen in the ion trap MS/MS spectrum (Figure 4). However, neither is present in the full spectrum mode LC-MS spectra. This strongly suggests that there is an SO_4 structure in the *m*/*z* 294 species, and it is likely covalently bonded with the rest of the *m*/*z* 294 ion. Upon CID fragmentation, SO_4^- comes off as a radical ion, which has been suggested to react with monoterpenes to form SO_4^- adducts in oxygen-poor conditions [*Buxton et al.*, 2000]. Other ions such as those with *m*/*z* 171, 185, 203 and 215 only have a small *m*/*z* 97 daughter ion, which probably comes from externally mixed HSO_4^- in the $PM_{2.5}$ that entered the ion trap together with the organic parent ion.

[21] The high-resolution MS measurements on the LCT electrospray TOF instrument show the accurate mass of the *m*/*z* 294 ion in the sample in Figure 2 to be 294.0638 Da. This mass is consistent with the measurements on the magnetic sector instrument using FAB ionization. We emphasize that because there is no separation of the *m*/*z* 294 ions before the MS detection, this is the average mass of all possible *m*/*z* 294 ions present. Considering the likely presence of both N and S, one possible molecular formula, with the smallest difference between the measured and calculated mass, is $C_{10}H_{16}NO_7S$, which gives rise to the six possible structures listed in Figure 7. The attack of OH

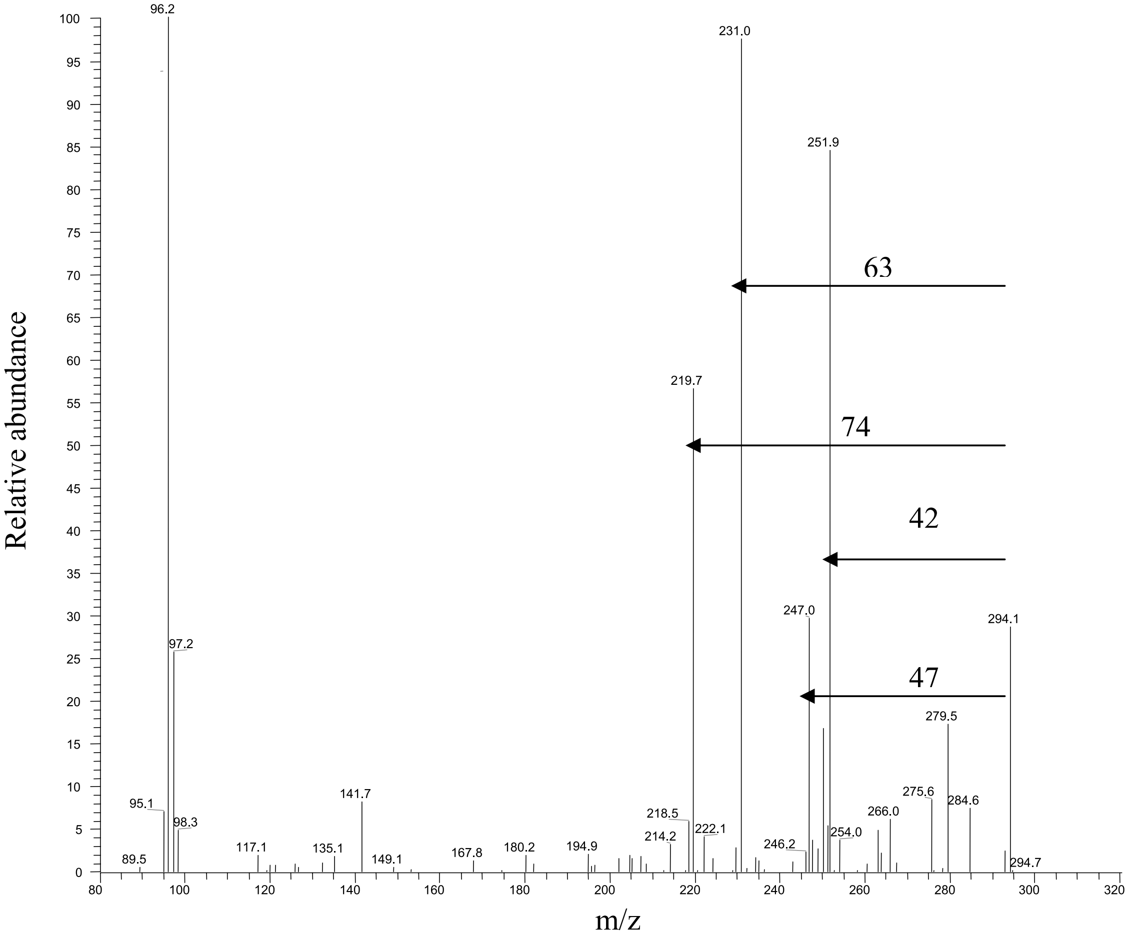

Figure 4. Ion trap MS/MS spectrum of the *m*/*z* 294 ion (containing all isobaric species) from the same sample as shown in Figure 2.

to NO and NO_2 and the attack of H to NO_2 and NO_3 in these structures would lead to the loss of HNO_2 and HNO_3, respectively, explaining the *m*/*z* 247 and *m*/*z* 231 fragment ions in the ion trap MS/MS (Figure 4), upfront CID mass spectra (Figure 5), and the high-resolution MS/MS. Known monoterpene oxidation pathways can explain the formation of these species quite nicely. For example, the Criegee intermediate from α-pinene ozonolysis can further react with NO_x and SO_2 at the end carbon and α-carbon to form N, S-containing species. Further oxidation of S is expected to eventually form the SO_4 or SO_3 groups in the proposed structures. Again, the high-resolution MS shows an isotopic distribution pattern of *m*/*z* 294, 295 and 296 ions that is characteristic of sulfur. However, until exact masses are obtained for each isobaric ion with *m*/*z* 294, we can only propose tentative structures such as those in Figure 7.

[22] Recent chamber experiments conducted jointly with the U.S. Environmental Protection Agency (E. Edney, T. Kleindienst) show that secondary organic aerosols readily form from the photooxidation of varying combinations of α-pinene, toluene and isoprene. These SOA have been analyzed by the same LC-MS method as in this work. Strikingly, when SO_2 and NO_x are both present and the precursors include α-pinene, the *m*/*z* 294 ion is always detected as an SOA component. The three main peaks of the *m*/*z* 294 isobaric ions elute at the same retention times as in the SEARCH samples. However, the *m*/*z* 294 ion is not present in the SOA in the absence of either SO_2 or α-pinene. Furthermore, the *m*/*z* 247 and *m*/*z* 231 ions are the major fragment ions in the upfront CID mass spectra of the three main 294 chromatographic peaks, again similar to the SEARCH samples. These results strongly support the hypothesis that the *m*/*z* 294 ions are formed via monoterpene oxidation with the participation of NO_x and SO_2. Of course, the exact nature of the reactions (the roles of ozonolysis and photooxidation as well as the distinction between gas-phase, particle-phase and heterogeneous reactions) remains to be investigated.

[23] Most of these species detected by the LC-MS are also detected by the ion trap MS in the negative ion mode. Figure 8 shows the ITMS of the extract of the same sample as shown in Figure 2. It can be seen that *m*/*z* 171, 185, 187, 203, 215, 253, 281, 294, 313 and 342 ions are the molecular ions of the dominant species, which are also detected by the LC-MS (Table 1). The relative abundances of these species also agree well between these two sets of measurements. Together, they indicate that the relatively polar organic species in the SE US in June 2004 cover a MW range of 150–400 Da. This is rather consistent with the earlier estimate of the average MW (i.e., 215–345) of polar organic components in rural fine aerosols in Hungary [*Kiss et al.*, 2003].

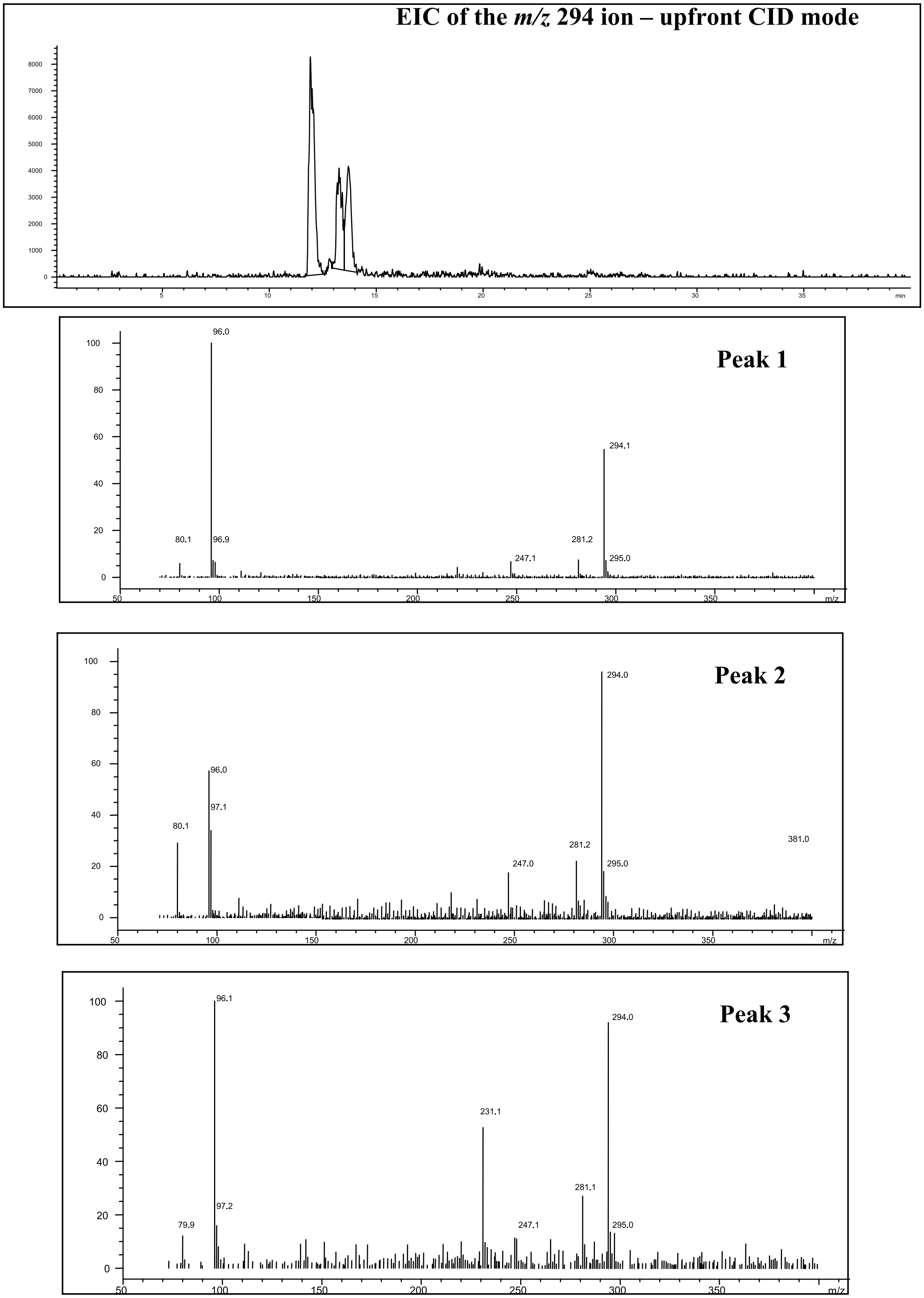

Figure 5. EIC of the *m*/*z* 294 ion in the same sample as shown in Figure 2 with the fragmentor set at 110V (upfront CID mode), and the upfront CID mass spectra of the three main peaks (retention times = 12.0, 13.3 and 13.7 min for Peak 1, 2 and 3, respectively). The *y* axis is intensity and relative abundance for the EIC and the mass spectra, respectively.

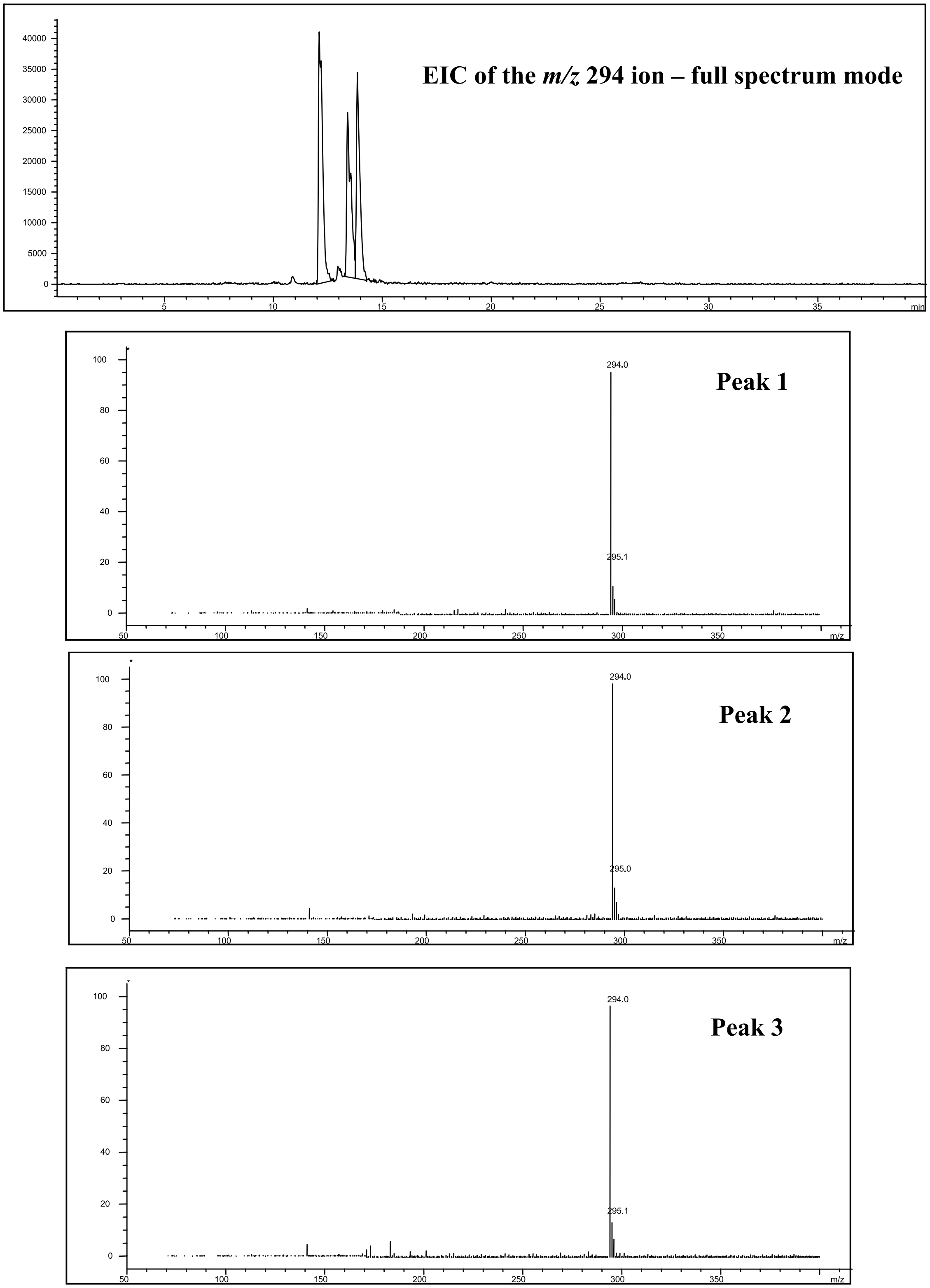

Figure 6. EIC of the *m*/*z* 294 ion in the same sample as shown in Figure 2 with the fragmentor set at 60 V (full spectrum MS mode), and the mass spectra of the three main peaks (retention times = 12.0, 13.3 and 13.7 min for Peak 1, 2 and 3, respectively). The *y* axis is intensity and relative abundance for the EIC and the mass spectra, respectively.

Proposed Structure	Neutral Loss
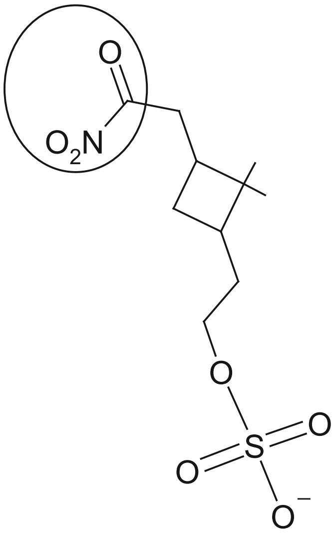	$O_2N–C=O$ (74)
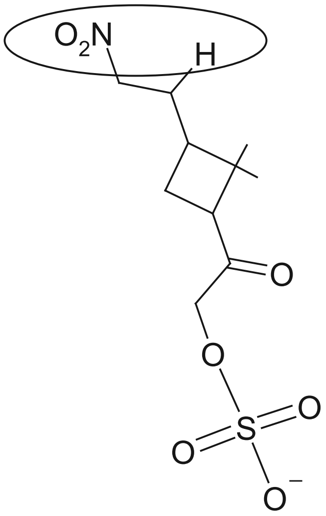	HNO_2 (47)
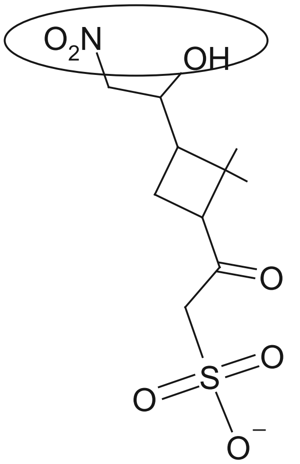	HNO_3 (63)

Figure 7. Proposed structures of the *m*/*z* 294 ion, based on the accurate mass measurements and the MS/MS fragmentation pattern in the ITMS and the upfront CID MS.

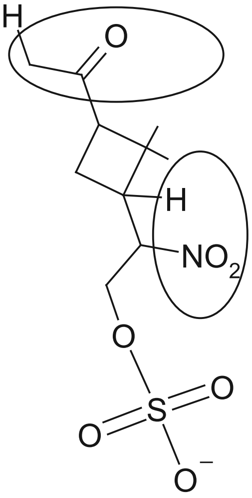	HNO_2 (47) $H_2C{=}C{=}O$ (42)
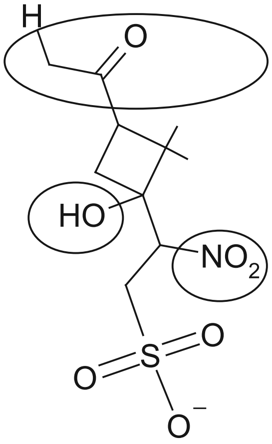	HNO_3 (63) $H_2C{=}C{=}O$ (42)
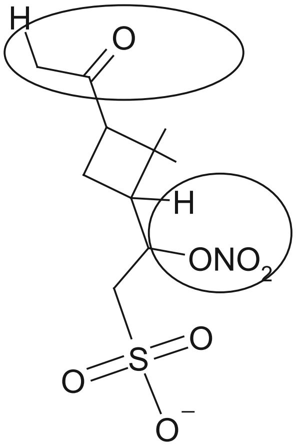	HNO_3 (63) $H_2C{=}C{=}O$ (42)

Figure 7. (continued)

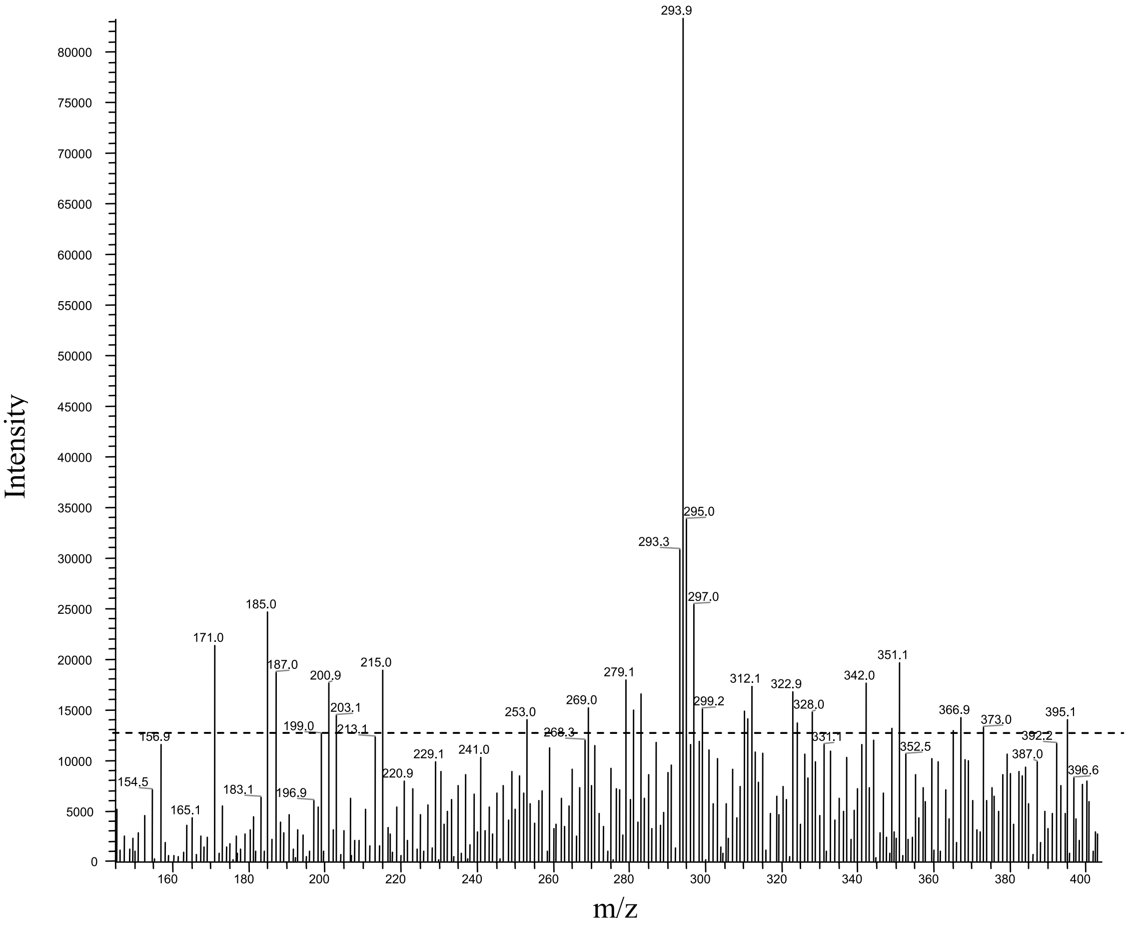

Figure 8. Ion trap mass spectrum (negative ion mode) of the same sample as shown in Figure 2. The detection limit was determined from field blanks and was ~14,000 as shown by the dashed line.

[24] In addition, LDI MS analyses of SEARCH 2004 samples also suggest that the majority of the detected organic species in $PM_{2.5}$ cover the MW range of 150–400 Da. For example, the LDI mass spectrum of the quartz filter sample collected at the JST site on 14 June 2004 is shown in auxiliary Figure S1[1]. A series of peaks separated by 14 Da and 16 Da are abundantly detected in the 150 to 350 mass range, and species with *m*/*z* above 400 can be seen sporadically but at very low intensities. This is consistent with other ambient aerosol measurements by LDI MS, such as by *Samburova et al.* [2005]. Species with MW from 400 to 700 Da detected in their study comprise only a small fraction of the total ion intensities, and these could be due to their distinct aerosol source (urban background).

[25] It is of particular interest to examine whether these identified species have an oligomeric nature, which is suggested recently for urban aerosols [*Samburova et al.*, 2005]. As we have mentioned earlier, species with MW below 250 Da are very likely oxidation products of monoterpenes, based on chemical and correlation analyses (section 3.4). Ion trap MS/MS analyses show that 18, 32, and 44 are the most common, dominant neutral losses from these species, which suggests they do not have a monomeric unit. Of species with MW from 250 to 400 Da, again, ion trap MS/MS analyses show that the dominant neutral losses are usually small, such as 18, 44, 47, 63 and 74. This does not support the presence of oligomers and corresponding monomeric fragments in the MS/MS spectra, such as those demonstrated by *Gao et al.* [2004a, 2004b]. A cautionary note here is that even though there is apparently regular mass difference (e.g., 14 and 16 Da) between identified species, such as the series of ions with *m*/*z* 157, 171, 185/187, 201/203, and 215, or the series of ions with *m*/*z* 294, 310, 326 and 342, these species may simply be oxidation products that differ by CH_2 (14), O (16) and H_2O (18), arising from the complicated reaction pathways common in atmospheric oxidation. Species with MW above 250 Da can, for example, come from oxidation of sesquiterpenes and even larger precursors. The ultimate criterion for the existence of oligomers should be whether repeating monomer (though not necessarily identical) units exist. Accordingly, in the LDI MS data (e.g., auxiliary Figure S1), the regularly spaced peaks with 14 and 16 Da mass differences are mainly due to the various oxidation products differed by groups such as CH_2 and O. Therefore the polar organic species detected in $PM_{2.5}$ in the SE US (MW 150–400 Da) do not appear to be oligomeric in nature. Similar species detected in rural aerosols and fogwater in Europe by other groups [e.g., *Krivacsy et al.*, 2001; *Kiss et al.*, 2003; *Cappiello et al.*, 2003], often referred to as HULIS, are likely not oligomeric as well. However, for species with

---

[1] Auxiliary material is available at ftp://ftp.agu.org/apend/jd/2005jd006601.

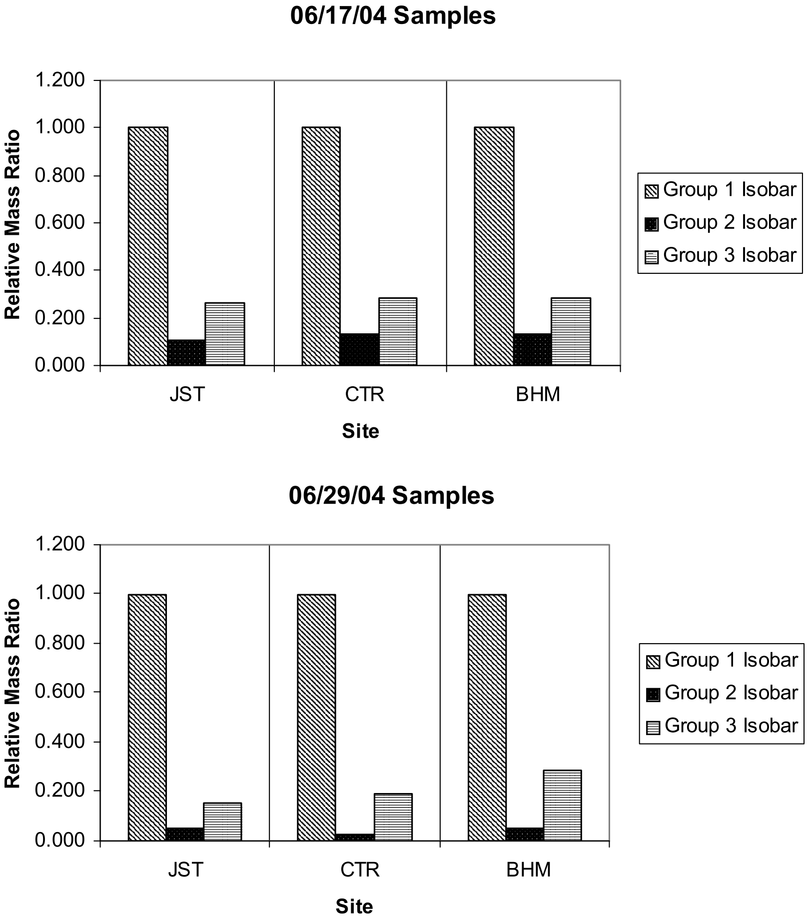

Figure 9. Relative abundance of three groups of 294 isobaric species, displaying a rather consistent distribution pattern.

MW above 400 Da, we cannot yet preclude the possibility that some are oligomers, originating from the first-generation oxidation products through the pathways suggested recently [*Kalberer et al.*, 2004; *Tolocka et al.*, 2004; *Gao et al.*, 2004a, 2004b]. This will be discussed further in sections 3.4 and 3.5.

3.2. Quantification of Organic Components in Fine Aerosols

[26] Calibration factors were determined for each standard compound by carrying out a five-point calibration. These calibration factors are then used to quantify the detected species in the $PM_{2.5}$ samples collected in the SEARCH network in June 2004. For those species matching the exact retention time (RT) and mass spectrum of a standard, that standard is used to quantify the mass concentration of the species. For example, cis-pinonic acid, pinic acid, and azelaic acid are used to quantify the *m/z* 183 ion (RT = 14.0 min), one of the *m/z* 185 isobaric ion (RT = 12.8 min) and one of the *m/z* 187 isobaric ion (RT = 15.8 min), respectively. For those species without a match of standards, surrogate standards with similar retention times and molecular weights are used to quantify. More than 80% of the detected species have retention times within 1.0 min of their surrogate standards, while the rest lie within 2.0 min. Since the standards cover the MW range of 103 (C_3 diacid) to 215 (C_{11} diacid), species with MW between 250 and 400 Da have relatively larger uncertainties in their quantification. Additional standards need to be analyzed in the future to reduce this uncertainty.

[27] For isobaric compounds, various surrogate standards are chosen for the best match in both RT and structures. As an example, sinapic acid (a common compound found in plant cells) is chosen to quantify the *m/z* 294 isobaric peaks eluting before 13.0 min, while suberic acid (a C_8 diacid) is chosen to quantify the 294 peaks eluting after 13.0 min. The RT discrepancies between these peaks and the surrogate standards are always less than 0.5 min. Isobaric species with closest RT can be grouped together, and these groups of isobaric species display a rather constant mass distribution pattern in the SE US in June 2004. For example, Figure 9 shows that on 17 and 29 June 2004, the first group of the *m/z* 294 isobaric species always has the highest abundance while the second always has the lowest, at all three inland sites. Therefore the summation of these groups is still a good representation of the abundance of all individual isobaric species. With this in mind, we report in Table 1 the mass concentration (ng/m^3 air) of each detected and quantified species from the quartz filter analyses, without differentiating the isobaric species.

[28] During June 2004, PTFE membrane filters were collected in the SEARCH network with the same sampling protocol as the quartz filters, and they were analyzed by the same LC-MS method. By comparison, the most abundant

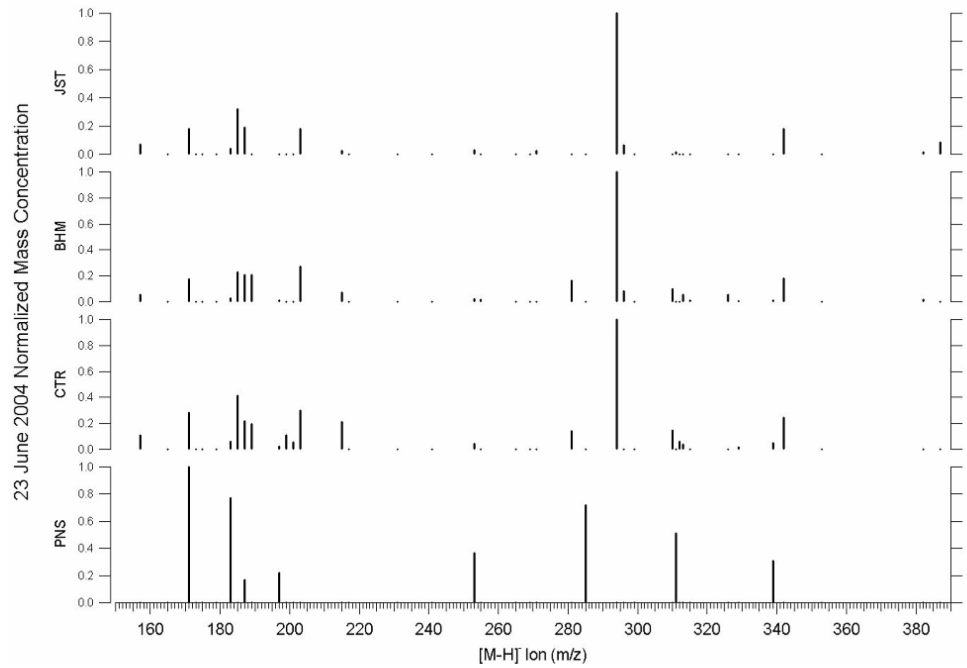

Figure 10. Mass distribution pattern at four sampling sites on 23 June 2004.

species detected on both filters are the same, and the mass distribution pattern of various species in each site is similar. However, the mass concentrations derived from PTFE filters are in general lower, which may be partly due to their generally higher blank filter background. Therefore the type of filters used can have an effect on the measured concentrations of aerosol components, but does not influence the qualitative assessment of aerosol composition. The discussion in this paper is based on quartz filters, which have cleaner blanks. Background signals from blank filters are used to correct for the quantification of field samples.

[29] Some common species are consistently detected as the most abundant species at BHM, CTR, and JST sites, such as the *m*/*z* 171, 185, 187, 203, 215, 294 and 342 ions (all molecular ions $[M\text{-}H]^-$). This suggests there are common sources leading to the formation of these species at these continental sites. In comparison, the PNS site has somewhat different aerosol composition, such as the absence of *m*/*z* 294 and 342 ions and the relatively higher abundance of 285 and 157 ions on some days. This coastal site may receive emission impacts from different sources in comparison to the inland sites. To better understand this difference, we will examine next the spatial and temporal distribution patterns of the detected $PM_{2.5}$ components in detail.

3.3. Mass Distribution and Regional Signature of Detected Organic Species

[30] As will be discussed in section 3.5, these detected species comprise only a modest fraction (on average 7.2% for the three inland sites and 1.1% for the PNS site) of the total organic matter in the $PM_{2.5}$ in the SE US. Since they are relatively polar species, they may be important in determining the hygroscopicity and CCN activation behavior of aerosols. In addition, as will be discussed in section 3.4, some of these can be tracers for $PM_{2.5}$ and secondary formation pathways in that region. For each sample, we normalize the mass concentrations of all species to that of the most abundant species. Such a plot displays the mass distribution pattern of the detected $PM_{2.5}$ components.

[31] For each sampling date, mass distributions at the four sites are plotted in one figure to examine the spatial variation of the detected species across the SE US. As an example, Figure 10 shows the spatial mass distribution pattern on 23 June 2004. Except for the PNS site, the *m*/*z* 171, 185, 187, 203, 294 and 342 ions (all $[M\text{-}H]^-$) are the dominant species, and the relative abundance of these species is rather consistent on this day. In fact, on each sampling day, there is a rather consistent mass distribution pattern across the JST, BHM and CTR sites. And on all four days, the dominant species remain the same with rather modest variation in their relative abundance from day to day (see another example in auxiliary Figure S2). This regional signature of organic matter in $PM_{2.5}$ strongly suggests that there are common sources in the inland region of the SE US.

[32] Analyses of back trajectories generated using the National Oceanic and Atmospheric Administration (NOAA) HYbrid Single-Particle Lagrangian Integrated Trajectory (HYSPLIT) Model, version 4.7 (http://www.arl.noaa.gov/ready/hysplit4.html) reveal that meteorological conditions from 14 to 29 June in 2004 are generally similar at the three inland sites. As an illustration, Figure 11 shows the 3-day back trajectories for 23 June while those of the other 3 days are shown in auxiliary Figures S3, S4 and S5. BHM and CTR sites have essentially the same back trajectories due to their close proximity. On 14 June the trajectories originated mostly from the southeast near the vicinity of Florida panhandle. On 17 June the trajectories extended from the South across southern Louisiana, Mississippi, Alabama and the Florida panhandle (depending on start time and trajectory height during the 24-hour period). On 23 and 29 June the trajectories originated mainly from the southwest crossing eastern Texas, Mississippi and Alabama. In addition, the JST site had trajectories very similar to BHM and CTR sites

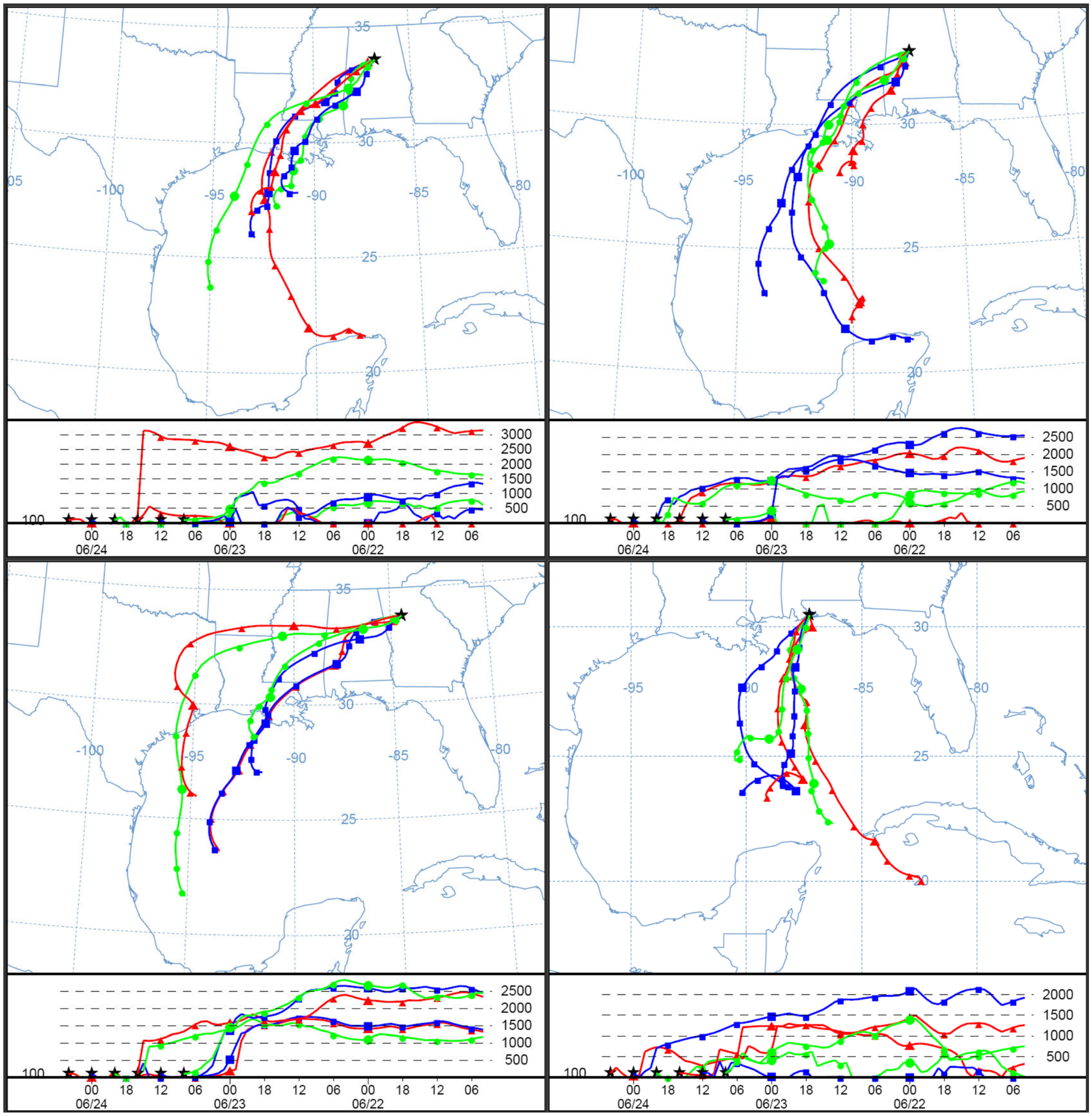

Figure 11. Three-day back trajectories on 23 June 2004 (clockwise from top left: BHM, CTR, PNS, and JST). The start height was 100 m. Back trajectories started every 4 hours starting at 1200 am EDT.

on 17 and 23 June, while on 14 and 29 June the back trajectories extended from SE Georgia/NE Florida and mixed sources, respectively. Owing to the presence of several coal-fired powered plants, extensive industrial activity in the Gulf Coast, and large metropolitan areas near (Atlanta, Birmingham) and upwind of the sampling sites (Houston, New Orleans–Baton Rouge, Mobile-Pensacola, Jacksonville, Orlando, and Tampa–St. Petersburg), all sets of trajectories transported NO_x and SO_2 within a rich, biogenic VOC background en route. All over the SE US, there is a ubiquitous distribution of lush vegetation, much of which emits terpenes abundantly year round, but with higher emissions rates during the summer. Such similar source gases and meteorological conditions would then provide a regional environment for common in situ reactions, in particular terpene oxidations, with possible participation of NO_x and SO_2 as proposed earlier based on chemical analysis. Owing to the lower volatility of the products, secondary organic aerosols can subsequently form and contribute significantly to the regional aerosol mass loading. The remarkable similarity in the organic aerosol composition of $PM_{2.5}$ at JST, BHM and CTR sites on 17 and 23 June (auxiliary Figure S2 and Figure 10) strongly supports such a scheme of SOA formation in the inland region.

[33] In comparison, PNS is a coastal site on the northern edge of the Gulf of Mexico, and experienced mainly southerly flows from the Gulf in June 2004 according to back trajectory analyses (Figure 11 and auxiliary Figures S3, S4 and S5). Such flows and geographical location probably

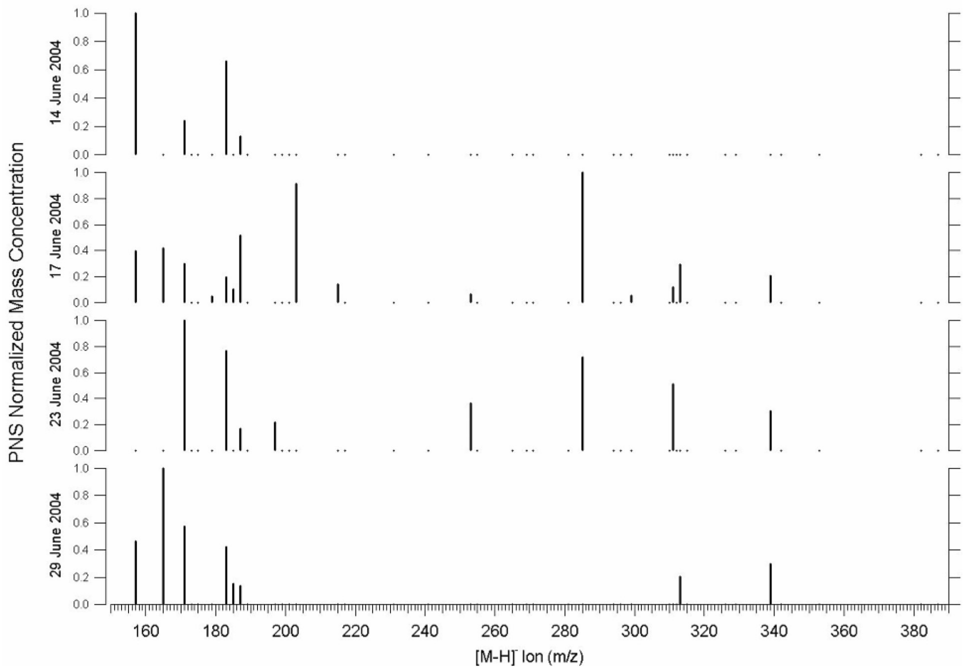

Figure 12. Mass distribution pattern on four sampling dates at the PNS site.

led to a decreased concentration of terpenes, making it difficult to form the *m*/*z* 294 ion according to our proposed scheme. In addition, such trajectories would make it difficult to provide enough SO_2 en route to the sampling site, again suppressing formation of the *m*/*z* 294 ion. Indeed, this species is never identified in the $PM_{2.5}$ samples at the PNS site, despite emissions of NO_x and VOC from local transportation sources. Furthermore, back trajectory analyses reveal distinctly different flows on the four sampling dates, i.e., south-southeasterly flow (originating from the vicinity of Cuba) on 14 June, southeasterly flow (originating from middle Florida) on 17 June, southerly flow (from the vicinity of the Yucatan peninsula in Mexico) on 23 June and stagnant south-southeasterly flow on 29 June. If primary, oceanic sources from the Gulf of Mexico were mainly responsible for $PM_{2.5}$ at the PNS site, then the aerosol composition would have been similar on all four sampling days. However, this is not the case as seen in Figure 12, where the temporal mass distribution pattern at the PNS site is shown. Neither the most abundant species nor their relative abundance displays a consistent pattern. Therefore either other primary sources or secondary processes during the onshore transport appear to have played a role in influencing the $PM_{2.5}$ composition at this site in June 2004. Among the four sites, the fraction of identified organics in the total $PM_{2.5}$ organic matter is the lowest at the PNS site (0.4–1.7%). In contrast, 5.8–9.1% (temporal average for each site) of the total organic matter is identified for the other three sites (Table 1), and the temporal distribution pattern for identified species is, again, rather consistent. An example is shown in Figure 13, where only the 29 June case for the BHM site has somewhat different mass distribution. Interestingly, the identified organic fraction in this case is 2.5%, the lowest of all 12 continental samples. There was primarily flow from the southwest in near stagnant conditions mainly over Mississippi and Louisiana but originating from the center of the Gulf of Mexico. This unique meteorological condition, and consequently the aerosol evolution, was likely responsible for the above observations on 29 June. On other days, however, it appears there is a rather stable June signature of the $PM_{2.5}$ composition at the BHM site. This is also true for the JST and CTR sites.

[34] The mass distribution pattern shown in Figure 10 from the LC-MS analyses resembles a typical mass spectrum, and can be readily compared with the corresponding ion trap mass spectrum, such as the Figure 8 for the BHM sample collected on 23 June. These two spectra show very similar distribution patterns, detecting ions with *m*/*z* 171, 185, 187, 203, 215, 281, 294, 313 and 342 (all are $[M-H]^-$) as the most abundant species. In other samples, such a comparison also yields similar mass distribution patterns, which indicates the consistency of our measurements and confirms the stable regional characteristics of fine particulate organic matter, especially the polar components being targeted here.

3.4. Sources and Evolution of Detected Organic Species: Correlation Study

[35] Another approach to understanding the sources of detected organic species in $PM_{2.5}$ is to examine the correlation between the abundances of these species. To account for the variation in the total organic mass in each sample, the mass concentration of an organic species is normalized by its corresponding total organic mass. Standard least-square linear regressions are then carried out between the normalized mass concentrations of two species, and their correlation during SEARCH 2004, if statistically significant, indicates that they likely share common sources and evolution pathways. Such a correlation analysis is also carried out between the mass concentration of a species and other field variables, such as the degree of neutraliza-

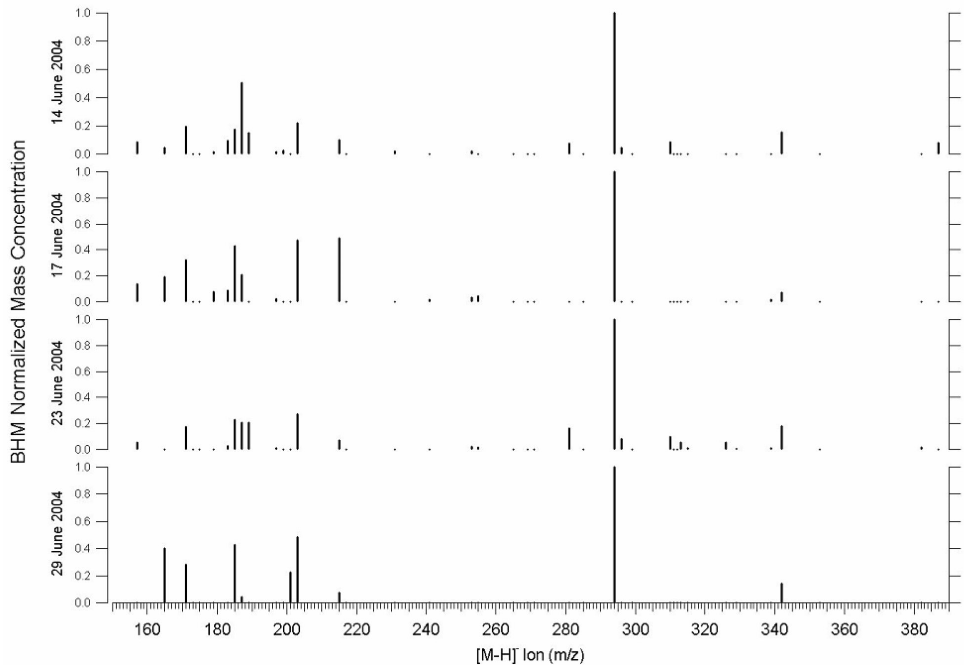

Figure 13. Mass distribution pattern on four sampling dates at the BHM site.

tion of the particle (a proxy for particle acidity), mean wind speed, relative humidity and temperature to examine other possible effects on aerosol composition.

[36] As discussed earlier, the *m*/*z* 171, 183 and 185 ions are very likely oxidation products of monoterpenes. Their ubiquitous presence in $PM_{2.5}$ in the SE US in June 2004 strongly suggests that terpene oxidation is a common secondary source for some $PM_{2.5}$ components, and these three species can serve as tracers for such a biogenic source. We next examine the correlation between the abundances of other species and these tracer species. In the MW range of 150–250 Da, 197, 203 and 215 ions are also commonly detected. Table 2 shows the calculated coefficients of determination (R^2) values of the normalized mass concentrations of these species with that of *m*/*z* 171 and 185 ions, respectively. Also listed are the numbers of data pairs with positive detection and the corresponding threshold R^2 values to be statistically significant at the 5% level. Although alternative methods exist that can better determine the correlation of data sets taking into account measurement uncertainty, given the small number of data pairs, the significance of correlation is simply estimated as $(R^2_{\mathrm{calculated}} - R^2_{\mathrm{threshold}})/(1 - R^2_{\mathrm{threshold}})$, which varies from 0 (at the threshold for a significant correlation at the 5% level) to 100% (at a perfect correlation). It can be seen that the *m*/*z* 197, 203 and 215 ions all have good or strong correlations with the *m*/*z* 171 and 185 ions. Therefore terpene oxidation appears to be also a major source for the 197, 203 and 215 ions. Indeed, their ion trap MS/MS spectra are consistent with the structures we propose in Figure 3, and their formation can be explained by known reaction mechanisms, in some cases with peracid (RC(O)OOH) as an end product [e.g., *Yu et al.*, 1999; *Winterhalter et al.*, 2003; *Aschmann et al.*, 2003].

[37] Whether terpene oxidation can also be a source for higher-MW $PM_{2.5}$ species (MW above 250 Da) can be assessed by similar correlation analysis. We first examine the most abundant species in the three inland sites, the *m*/*z* 294 ion. Using *m*/*z* 171, 185, 187, 197, 203 and 215 ions as tracers, it can be seen that the *m*/*z* 294 ion is well correlated with all these species, as shown in Table 3. Combined with the earlier analyses of possible structures and reaction pathways of the *m*/*z* 294 ion in sections 3.1 and 3.3, there is strong evidence that terpene oxidation is probably a major source for the *m*/*z* 294 ion, at least for some of its isobaric species. In addition, some other frequently detected species, such as 253, 339 and 342 ions, are also reasonably well correlated with the tracer species,

Table 2. Correlation of Mass Concentrations of the *m*/*z* 197, 203, and 215 Ions With Those of the *m*/*z* 171 and 185 Ions

[M-H]-of $PM_{2.5}$ Species	R^2 With the Normalized Mass Concentration of Given Ion	Number of Data Pairs	Threshold of R^2 Value	Significance of Correlation, %
		171 Ion		
197	0.71	8	0.50	43
203	0.80	13	0.30	71
215	0.78	13	0.30	68
		185 Ion		
197	0.63	7	0.56	16
215	0.50	13	0.30	29

Table 3. Correlation of Mass Concentrations of the *m*/*z* 171 Ion, 185 *m*/*z* Ion, One of *m*/*z* 187 Isobars, *m*/*z* 197 Ion, *m*/*z* 203 Ion, and One of *m*/*z* 215 Isobars With That of the *m*/*z* 294 Ion

[M-H]-of $PM_{2.5}$ Species	R^2 With the Normalized Mass Concentration of the *m*/*z* 294 Ion	Number of Data Pairs	Threshold R^2 Values	Significance of Correlation, %
171	0.60	12	0.34	40
185	0.49	12	0.34	23
187A	0.70	8	0.50	39
197	0.59	7	0.56	7
203	0.44	12	0.34	15
215B	0.69	8	0.50	38

suggesting a biogenic, secondary source as well. Possible evolution pathways can be readily gleaned from the recent laboratory chamber experiments discussed in section 3.1. Not only is the *m*/*z* 294 ion present in the SOA from α-pinene photooxidation (with the participation of NO_x, SO_2 and sometimes other VOC precursors), but the *m*/*z* 171, 183, 185, 197, 203 and 215 ions are also present. They commonly have isobaric species, some of which elute the LC column at retention times similar to the same-mass $PM_{2.5}$ species in SEARCH. The upfront CID mass spectra of some of these species are also similar to their counterparts in the SEARCH samples, suggesting that α-pinene photooxidation is a possible pathway. Gas-phase data such as O_3, SO_2 and NO_x mixing ratios are needed to fully examine possible evolution pathways of the detected species in $PM_{2.5}$. Currently, these data are not yet available.

[38] Particle acidity (assessed by the degree of neutralization calculated as the mole-equivalent ratio of ammonium to sulfate and nitrate) is found to have no correlation with any detected species or other field variables obtained in the SEARCH network in June 2004. As discussed in section 3.1, in the MW range 150–400 Da, oligomers do not appear to be present in $PM_{2.5}$ in the SE US. Therefore acid catalysis and subsequent oligomer formation does not appear to be a main pathway to form major $PM_{2.5}$ components in this MW range. Rather, oxidation of monoterpenes and sesquiterpenes can readily lead to many of the polar species in $PM_{2.5}$. Although possibility exists that some species with MW above 400 Da are oligomeric in nature, this is less likely than a direct extrapolation from recent chamber experiments [*Kalberer et al.*, 2004; *Tolocka et al.*, 2004; *Gao et al.*, 2004b] would suggest. The polar nature of the detected species in $PM_{2.5}$ in the SE US suggests oxidation is an important pathway to form aerosol components, and these oxidation processes, both ozonolysis and photooxidation, can occur continuously in the atmosphere. Albeit unknown at this moment, it is also conceivable that oxidation may be one of the pathways to decompose oligomers. Indeed, as shown theoretically by *Barsanti and Pankow* [2004], most accretion reactions proposed from chamber studies do not appear to be thermodynamically favorable pathways to form oligomers or grow aerosol mass. It is possible that oligomers observed in chamber experiments, the longest of which lasted less than 30 hours [*Kalberer et al.*, 2004], decompose by various pathways at a prolonged aging time with complex atmospheric processing. The average aging time for tropospheric aerosols is roughly a week. Furthermore, the degradation scheme would suggest that smallest oligomers are most likely to survive in the fine aerosols (unless some large oligomers have highly conjugated structures), as they are near the end of degradation pathways. However, our observations reveal a lack of oligomers in the low MW range (150–400 Da). In all, little evidence exists that oligomers comprise a major fraction of $PM_{2.5}$ in the SE US in the summer. Rather, strong evidence exists that oxidation is a main pathway to form polar particulate species there. Since similar species have been observed in $PM_{2.5}$ elsewhere [*Gelencser et al.*, 2000, 2002; *Krivacsy et al.*, 2001; *Kiss et al.*, 2003], this terpene oxidation scheme is likely a ubiquitous pathway to form major organic species in $PM_{2.5}$ in rural, continental regions.

[39] Even though a detailed source apportionment study has not been carried out in this work, it is possible to estimate the source contribution of terpene oxidation to $PM_{2.5}$. Since most of the dominant organic species detected in this work are associated with terpene oxidation, together they can provide a lower-bound estimate of its source contribution to the total organic matter in $PM_{2.5}$ in the SE US, which is 1.1–9.1% in June 2004. This is comparable to the source contributions from diesel exhaust (14–30%), meat cooking (5–12%), and gasoline-powered motor vehicle exhaust (0–10%) in that region [*Zheng et al.*, 2002]. Since wood smoke makes a much smaller contribution (less than 30% in July 1999) to $PM_{2.5}$ organic matter in the summer [*Zheng et al.*, 2002], terpene oxidation ranks among the major regional sources during summer. Indeed, the speculation [*Zheng et al.*, 2002] that the exceptionally high ratio of unexplained OC to the total OC in the summer in the SE US is due to SOA formation is supported by this work. By the same approach, at JST, CTR, BHM and PNS sites in June 2004, terpene oxidation contributed to at least 0.2–5.2% of the total fine particulate mass.

3.5. Identified and Missing Fractions of Particulate Organic Matter

[40] Six categories of chemical species in $PM_{2.5}$ were measured in June 2004 in the SEARCH network by various techniques described by *Hansen et al.* [2003], i.e., sulfate, nitrate, ammonium, black carbon, organic matter and major metal oxides (including Al_2O_3, SiO_2, K_2O, CaO, TiO_2, Fe_2O_3). Together, they comprise 92.1 ± 6.9%, 95.4 ± 5.8%, 86.3 ± 7.0% and 78.2 ± 13.7% of the total $PM_{2.5}$ mass at JST, CTR, BHM and PNS sites, respectively. Of the six categories, total organic matter (TOM) mass, estimated from multiplying the measured total organic carbon (TOC) mass by the corresponding OM/OC ratio, comprise 36.8 ± 5.6 %, 42.7 ± 13.6%, 31.8 ± 2.4% and 20.5 ± 8.2% of the total $PM_{2.5}$ mass at JST, CTR, BHM and PNS sites, respectively. The OM/OC ratio of 1.6 is used for the three mainly urban sites (JST, BHM and PNS) while the ratio of 2.0 is used for the mostly rural site (CTR), as suggested by recent work [e.g., *Krivacsy et al.*, 2001; *Turpin and Lim*, 2001; *El-Zanan et al.*, 2005]. This is consistent with the relatively high (MW/carbon mass) ratios of many highly

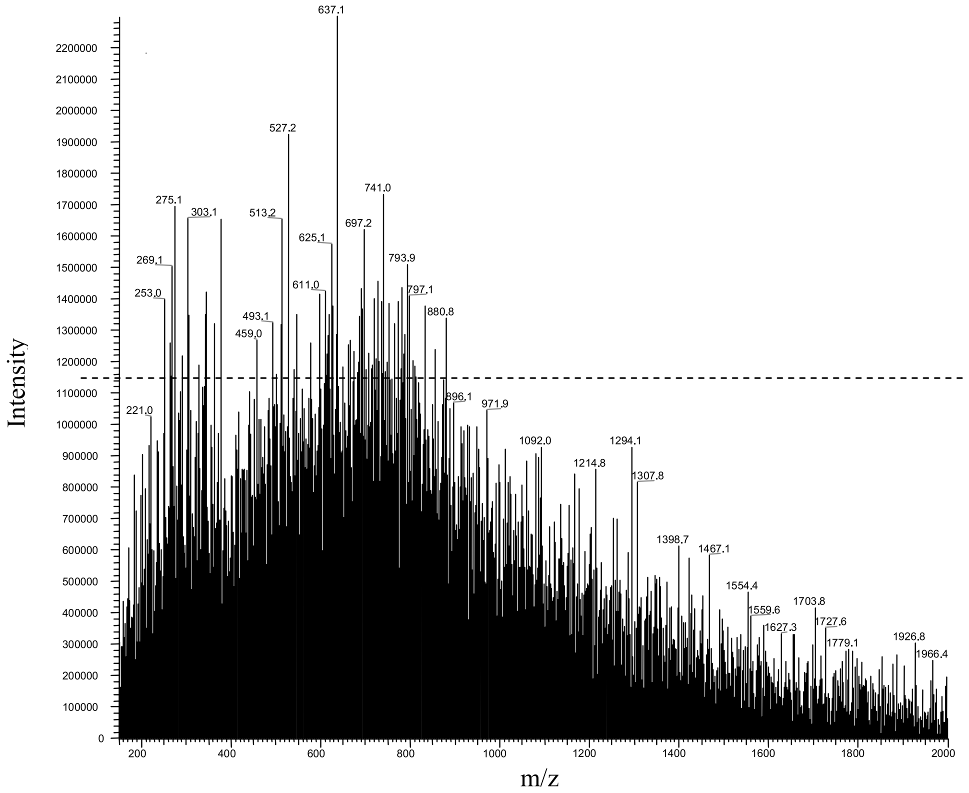

Figure 14. Ion trap MS (positive ion mode) of the extract of the $PM_{2.5}$ sample collected at the CTR site on 17 June 2004. $PM_{2.5}$ organic components cover a MW range of 200–850 (after the Na mass is subtracted). The detection limit was determined from field blanks and was ~1,120,000 as shown by the dashed line.

oxidized species identified in this study (e.g., as high as 2.46 for the *m*/*z* 294 species). Averaged over the four June samples, the total identified organic species (Table 1) account for 5.8%, 9.1%, 6.8% and 1.1% of the total particulate organic mass at the JST, CTR, BHM and PNS sites, respectively. Questions arise as to the nature of the unidentified organic species in $PM_{2.5}$.

[41] In the previous composition analysis and source apportionment study of $PM_{2.5}$ in the SE US, *Zheng et al.* [2002] detected 107 organic compounds, which accounted for no more than 12% of the total organic mass in $PM_{2.5}$. The majority of these detected compounds are rather nonpolar, such as alkanes, cycloalkanes, PAHs, steranes, hopanes, long-chain alkanoic acids and resin acids. This is due to the nature of the GC-MS employed by *Zheng et al.* [2002], which is amenable primarily to detecting relatively volatile and nonpolar species.

[42] By comparison, LC-MS is used in this work, which is suitable to detecting relatively polar and acidic species. Nonanedioic acid (azelaic acid) is the common diacid that is detected by both *Zheng et al.* [2002] and this work. Owing to the quantification of all *m*/*z* 187 isobaric species, the mass concentration of the 187 ion is higher in this study (30.63 ng/m^3, on average, for JST, BHM and CTR sites) than in *Zheng et al.* [2002] (6.28 ng/m^3). Interestingly, azelaic acid (C_9) is a well-known secondary oxidation product of unsaturated fatty acids [*Stephanou and Stratigakis*, 1993], again suggesting a secondary pathway for organic aerosols in the SE US. Smaller diacids (C_3 to C_8) were detected by the GC-MS, but they were not detected by the LC-MS, which is probably due to the loss during the water washing step of the SPE technique. The water effluents from SPE of all samples have been archived at −20°C, and can be analyzed if necessary. However, these diacids often have low occurrences [*Yu et al.*, 2005] in the SE US and are rarely more than 7 ng/m^3 in $PM_{2.5}$ [*Zheng et al.*, 2002]. In total, they are estimated to comprise only a small fraction of the total organic mass in $PM_{2.5}$, consistent with observations at other rural continental sites [e.g., *Sarvari et al.*, 1999]. The organic species detected in this work, most of which appear to originate from terpene oxidation, comprise on average 7.2% of the total organic mass in $PM_{2.5}$ at the three inland sites. Combining with the speciation results by *Zheng et al.* [2002], about 20% of the $PM_{2.5}$ organic matter has been quantitatively identified.

[43] Whereas the chemical nature of the unidentified organic species remains elusive, it is possible to estimate the MW range of these species. Under the positive ion mode in the ion trap MS, compounds with a broad range of polarity can be detected as their Na^+ adducts, as demonstrated by *Gao et al.* [2004b]. Figure 14 shows the ion trap mass spectrum of a $PM_{2.5}$ sample collected in the CTR site on 17 June 2004, which was extracted with the SPE technique applied. The detection limit is determined from the average and standard deviation of six field blanks with a signal-to-noise ratio of 3 applied. It can be seen that compounds with MW from ~200–850 Da are present in this sample. When SPE is not applied during filter extraction, most species increase in intensity by a factor of 2–3 and species with MW above 1000 are present, which is

probably due to the adduct formation between charged molecules and neutral ones and/or between metal ions and organic species [*Klaus et al.*, 2000; *Leenheer et al.*, 2001; *Plancque et al.*, 2001]. In the mass spectra where inorganic ions are mostly removed by SPE, such as the one shown in Figure 14, the chance of adduct formation has been minimized. Therefore the MW range of $PM_{2.5}$ organic matter is estimated to be 200–850 Da in this sample. Other samples are evaluated by the same approach. On average, organic species in $PM_{2.5}$ in the SE US in June 2004 cover a MW range of 150–800 Da. This is consistent with the recent estimate that the upper MW limit of HULIS in ambient urban aerosols is about 700 [*Samburova et al.*, 2005]. This latter estimate was based on two different analytical techniques, i.e., size exclusion chromatography-UV spectroscopy and LDI MS, providing some independent confirmation of this conclusion.

[44] It can be seen from Figure 14 that compounds with MW above 400 Da actually have higher abundances and number of species than those with MW below 400 Da. If similar response factors are assumed for all detected compounds, those with MW above 400 Da may comprise a major fraction of the total organic matter. This suggests that these relatively high-MW species, whose molecular structures are not yet known, may explain a substantial fraction of unidentified mass in $PM_{2.5}$. However, it is possible that there is large variation in response factors among species, especially the high-MW ones of which response factors are not well understood. In addition, despite the application of SPE, adduct formation in the ion trap MS is still likely which may have caused a shift in the MW range to larger numbers.

[45] Higher-MW, relatively polar, but unidentified species in $PM_{2.5}$ have been lumped together and named HULIS owing to a speculation of their origin as the humic (and/or fulvic) acids found in natural waters and soil [e.g., *Havers et al.*, 1998] (and references mentioned above). A primary source for HULIS (i.e., direct release of actual humic matter from the soil or natural waters) appears unlikely, owing to the ubiquitous presence of HULIS in the fine particle size range. It has been hypothesized that HULIS in continental $PM_{2.5}$ may be produced aloft from precursors emitted directly from terrestrial sources [*Gelencser et al.*, 2002]. However, calculation by the same authors show that this soil flux appears too low (by about 1 order of magnitude) to account for the observed total organic mass in $PM_{2.5}$. On the other hand, a photochemical secondary source for HULIS has also been speculated [*Gelencser et al.*, 2002; *Szidat et al.*, 2004; *Samburova et al.*, 2005]. To our knowledge, we have presented the first, direct evidence that some HULIS species are probably formed via atmospheric oxidation of VOC precursors. In the SE US, polar species with MW range 150–400 Da in $PM_{2.5}$ appear to originate from the oxidation of monoterpenes and sesquiterpenes. The ESI-mass spectra of $PM_{2.5}$ samples in the SE US bear resemblance to those of aerosol and fog water samples in previous studies, such as those of *Krivacsy et al.* [2001], *Kiss et al.* [2003] and *Cappiello et al.* [2003], suggesting that similar HULIS material is present in $PM_{2.5}$ in different regions. A biogenic, secondary source can be ubiquitous in the background atmosphere in many continental regions, leading to a multitude of relatively polar and acidic species in $PM_{2.5}$. The wide-ranging biogenic precursors and the complex reaction pathways can result in a series of secondary aerosol components with extremely similar but not identical structures. This would be consistent with the commonly observed co-elution of HULIS species on LC columns and regular mass differences seen in the mass spectra. Of course, the structural similarity between HULIS species in $PM_{2.5}$ and humic/fulvic acids in natural waters and soil [*Martin et al.*, 1994, 1995; *Gelencser et al.*, 2000; *Krivacsy et al.*, 2001] still indicates a possible link between them, yet direct evidence has yet to be found. Indeed, it is likely that both pathways exist and the resultant ensemble of species is the so-called HULIS in $PM_{2.5}$. Indirect evidence for this appears to exist, such as the somewhat different chemical nature between the *m*/*z* 294 ion and other species in rural fine aerosols as reported by *Kiss et al.* [2003]. In addition, it is possible that oligomerization may be another pathway in forming HULIS species in $PM_{2.5}$, such as those with MW above 400 Da that likely contain highly conjugated monomer units. Novel techniques to unravel the structures of higher-MW species and unambiguously detect oligomers should be pursued. The ability to quantify higher-MW species should also be pursued to achieve a better mass closure of organic matter in $PM_{2.5}$.

4. Summary and Conclusions

[46] Four analytical techniques have been used concurrently to identify and quantify polar organic components in $PM_{2.5}$ in the SE US. Forty distinct species are detected and together they comprise on average 7.2% and 1.1% of the total organic mass in $PM_{2.5}$ at three inland sites and a coastal site, respectively. These polar, acidic species cover a MW range of 150–400 Da and do not appear to be oligomeric in nature. The mass distribution pattern of these species is rather consistent in the inland region due to the rather uniform sources and meteorology, but this pattern varies in the coastal region owing to the more complex sources and meteorology.

[47] Chemical structure and correlation analyses strongly suggest that most of these polar species originate from terpene oxidation. Structures of some species are proposed on the basis of fragmentation patterns in the MS/MS spectra and known reaction mechanisms. In particular, the most dominant species ($[M\text{-}H]^-$ has *m*/*z* 294) is likely from monoterpene oxidation with the participation of NO_x and SO_2 from anthropogenic sources. It is estimated that terpene oxidation can be an important regional source for the organic fraction of $PM_{2.5}$ in the SE US, contributing to 1.1–9.1% of the total organic mass. Proposed oxidation pathways can lead to other polar and possibly higher-MW species in fine aerosols that have up to now evaded detection. There is no direct evidence that oligomerization or particle acidity plays a role in affecting the aged aerosol composition or mass. The sufficient aging in the atmosphere may decompose oligomers (if formed initially), which is yet difficult to simulate in laboratory chamber studies. Nevertheless, in the MW range of 400–800 Da where organic species are detected but unidentified, it cannot be precluded that oligomers may be present and could comprise a fraction of the total particulate organic mass.

[48] In rural areas in other parts of the world, terpene oxidation can also be an important regional source, leading to the formation of secondary organic aerosols. Indeed, a biogenic, secondary source is likely ubiquitous for $PM_{2.5}$ in

the background atmosphere in continental regions, forming some of the so-called HULIS species. We provide the first direct evidence for this hypothesis. The validity and relative importance of this source and the hypothetical natural source (terrestrial and/or aquatic humic/fulvic acids) for HULIS in fine aerosols await further investigation.

[49] **Acknowledgments.** This work was supported by the Electric Power Research Institute (EPRI). Jason Surratt was supported by an EPA Science to Achieve Results (STAR) Fellowship. We thank D. Alan Hansen of Electric Power Research Institute and John Jansen of Southern Company for helpful discussions. We also thank Mei Zheng at the Georgia Institute of Technology for preparing and shipping the quartz filter samples and John Greaves at the University of California, Irvine, for the accurate mass measurements on the ESI-TOF instrument.

References

Aschmann, S. M., E. C. Tuazon, J. Arey, and R. Atkinson (2003), Products of the gas-phase reaction of O_3 with cyclohexene, *J. Phys. Chem. A*, *107*, 2247–2255.
Baltensperger, U., et al. (2005), Secondary organic aerosols from anthropogenic and biogenic precursors, *Faraday Disc.*, *130*, 265–278.
Barsanti, K., and J. Pankow (2004), Thermodynamics of the formation of atmospheric organic particulate matter by accretion reactions: Part 1. Aldehydes and ketones, *Atmos. Environ.*, *38*, 4371–4382.
Buxton, G. V., G. A. Salmon, and J. E. Williams (2000), The reactivity of biogenic monoterpenes towards OH center dot and SO4-center dot radicals in de-oxygenated acidic solution, *J. Atmos. Chem.*, *36*, 111–134.
Cappiello, A., E. De Simoni, C. Fiorucci, F. Mangani, P. Palma, H. Trufelli, S. Decesari, M. C. Facchini, and S. Fuzzi (2003), Molecular characterization of the water-soluble organic compounds in fogwater by ESIMS/MS, *Environ. Sci. Technol.*, *37*, 1229–1240.
Choi, M., and C. Chan (2002), The effects of organic species on the hygroscopic behaviors of inorganic aerosols, *Environ. Sci. Technol.*, *36*, 2422–2428.
Cruz, C., and S. Pandis (1998), The effect of organic coatings on the cloud condensation nuclei activation of inorganic atmospheric aerosol, *J. Geophys. Res.*, *103*, 13,111–13,123.
Cruz, C., and S. Pandis (2000), Deliquescence and hygroscopic growth of mixed inorganic-organic atmospheric aerosol, *Environ. Sci. Technol.*, *34*, 4313–4319.
El-Zanan, H. S., D. H. Lowenthal, B. Zielinska, J. C. Chow, and N. Kumar (2005), Determination of the organic aerosol mass to organic carbon ratio in IMPROVE samples, *Chemosphere*, *60*, 485–496.
Gao, S., M. Keywood, N. L. Ng, J. Surratt, V. Varutbangkul, R. Bahreini, R. C. Flagan, and J. H. Seinfeld (2004a), Low-molecular-weight and oligomeric components in secondary organic aerosol from the ozonolysis of cycloalkenes and alpha-pinene, *J. Phys. Chem. A*, *108*, 10,147–10,164.
Gao, S., et al. (2004b), Particle phase acidity and oligomer formation in secondary organic aerosol, *Environ. Sci. Technol.*, *38*, 6582–6589.
Gelencser, A., T. Meszaros, M. Blazso, G. Kiss, Z. Krivacsy, A. Molnar, and E. Meszaros (2000), Structural characterisation of organic matter in fine tropospheric aerosol by pyrolysis-gas chromatography-mass spectrometry, *J. Atmos. Chem.*, *37*, 173–183.
Gelencser, A., A. Hoffer, Z. Krivacsy, G. Kiss, A. Molnar, and E. Meszaros (2002), On the possible origin of humic matter in fine continental aerosol, *J. Geophys. Res.*, *107*(D12), 4137, doi:10.1029/2001JD001299.
Glasius, M., M. Lahaniati, A. Calogirou, D. Di Bella, N. R. Jensen, J. Hjorth, D. Kotzias, and B. R. Larsen (2000), Carboxylic acids in secondary aerosols from oxidation of cyclic monoterpenes by ozone, *Environ. Sci. Technol.*, *34*, 1001–1010.
Hansen, D., E. S. Edgerton, B. E. Hartsell, J. J. Jansen, N. Kandasamy, G. M. Hidy, and C. L. Blanchard (2003), The southeastern aerosol research and characterization study: Part 1, Overview, *J. Air Waste Manage.*, *53*, 1460–1471.
Havers, N., P. Burba, J. Lambert, and D. Klockow (1998), Spectroscopic characterization of humic-like substances in airborne particulate matter, *J. Atmos. Chem.*, *29*, 45–54.
Kalberer, M., et al. (2004), Identification of polymers as major components of atmospheric organic aerosols, *Science*, *303*, 1659–1662.
Kavouras, I. G., N. Mihalopoulos, and E. G. Stephanou (1999), Formation and gas/particle partitioning of monoterpenes photooxidation products over forests, *Geophys. Res. Lett.*, *26*, 55–58.
Kiss, G., B. Varga, A. Gelencser, Z. Krivacsy, A. Molnar, T. Alsberg, L. Persson, H. C. Hansson, and M. C. Facchini (2001), Characterisation of polar organic compounds in fog water, *Atmos. Environ.*, *35*, 2193–2200.
Kiss, G., E. Tombacz, B. Varga, T. Alsberg, and L. Persson (2003), Estimation of the average molecular weight of humic-like substances isolated from fine atmospheric aerosol, *Atmos. Environ.*, *37*, 3783–3794.
Klaus, U., T. Pfeifer, and M. Spiteller (2000), APCI-MS/MS: A powerful tool for the analysis of bound residues resulting from the interaction of pesticides with DOM and humic substances, *Environ. Sci. Technol.*, *34*, 3514–3520.
Krivacsy, Z., et al. (2001), Study on the chemical character of water soluble organic compounds in fine atmospheric aerosol at the Jungfraujoch, *J. Atmos. Chem.*, *39*, 235–259.
Leenheer, J. A., C. E. Rostad, P. M. Gates, E. T. Furlong, and I. Ferrer (2001), Molecular resolution and fragmentation of fulvic acid by electrospray ionization/multistage tandem mass spectrometry, *Anal. Chem.*, *73*, 1461–1471.
Lim, H. J., and B. J. Turpin (2002), Origins of primary and secondary organic aerosol in Atlanta: Results of time-resolved measurements during the Atlanta supersite experiment, *Environ. Sci. Technol.*, *36*, 4489–4496.
Martin, F., F. J. Gonzalezvila, J. C. Delrio, and T. Verdejo (1994), Pyrolysis derivatization of humic substances: 1. Pyrolysis of fulvic-acids in the presence of tetramethylammonium hydroxide, *J. Anal. Appl. Pyrol.*, *28*, 71–80.
Martin, F., J. C. Delrio, F. J. Gonzalezvila, and T. Verdejo (1995), Pyrolysis derivatization of humic substances: 2. Pyrolysis of soil humic acid in the presence of tetramethylammonium hydroxide, *J. Anal. Appl. Pyrol.*, *31*, 75–83.
Pio, C. A., C. A. Alves, and A. C. Duarte (2001), Organic components of aerosols in a forested area of central Greece, *Atmos. Environ.*, *35*, 389–401.
Plancque, G., B. Amekraz, V. Moulin, P. Toulhoat, and C. Moulin (2001), Molecular structure of fulvic acids by electrospray with quadrupole time-of-flight mass spectrometry, *Rapid Commun. Mass. Spectrom.*, *15*, 827–835.
Samburova, V., M. Kalberer, and R. Zenobi (2005), Characterization of high molecular weight compounds in urban atmospheric particles, *Atmos. Chem. Phys. Disc.*, *5*, 437–454.
Sarvari, Z., Z. Krivacsy, U. Baltensperger, S. Nyeki, E. Weingartner, S. Wessel, and S. G. Jennings (1999), Low-molecular weight carboxylic acids in atmospheric aerosol at different European sites, *J. Aerosol Sci.*, *30*, S261–S262.
Stephanou, E. G., and N. Stratigakis (1993), Oxocarboxylic and alpha, omega-dicarboxylic acids—Photooxidation products of biogenic unsaturated fatty-acids present in urban aerosols, *Environ. Sci. Technol.*, *27*, 1403–1407.
Szidat, S., et al. (2004), Source apportionment of aerosols by C-14 measurements in different carbonaceous particle fractions, *Radiocarbon*, *46*, 475–484.
Tolocka, M. P., M. Jang, J. M. Ginter, F. J. Cox, R. M. Kamens, and M. V. Johnston (2004), Formation of oligomers in secondary organic aerosol, *Environ. Sci. Technol.*, *38*, 1428–1434.
Turpin, B. J., and H. J. Lim (2001), Species contributions to PM2.5 mass concentrations: Revisiting common assumptions for estimating organic mass, *Aerosol Sci. Technol.*, *35*, 602–610.
Turpin, B. J., J. J. Huntzicker, and S. V. Hering (1994), Investigation of organic aerosol sampling artifacts in the Los-Angeles basin, *Atmos. Environ.*, *28*, 3061–3071.
Winterhalter, R., R. Van Dingenen, B. R. Larsen, N. R. Jensen, and J. Hjorth (2003), LC-MS analysis of aerosol particles from the oxidation of a-pinene by ozone and OH-radicals, *Atmos. Chem. Phys. Disc.*, *3*, 1–39.
Yu, J. Z., D. R. Cocker, R. J. Griffin, R. C. Flagan, and J. H. Seinfeld (1999), Gas-phase ozone oxidation of monoterpenes: Gaseous and particulate products, *J. Atmos. Chem.*, *34*, 207–258.
Yu, L. E., M. L. Shulman, R. Kopperud, and L. M. Hildemann (2005), Characterization of organic compounds collected during Southeastern Aerosol and Visibility Study: Water-soluble organic species, *Environ. Sci. Technol.*, *39*, 707–715.
Zheng, M., G. R. Cass, J. J. Schauer, and E. S. Edgerton (2002), Source apportionment of PM2.5 in the southeastern United States using solvent-extractable organic compounds as tracers, *Environ. Sci. Technol.*, *36*, 2361–2371.

E. S. Edgerton, Atmospheric Research and Analysis, Inc., Cary, NC 27513, USA.

S. Gao and J. H. Seinfeld, Departments of Environmental Science and Engineering and Chemical Engineering, California Institute of Technology, 1200 East California Boulevard, MC 210-41, Pasadena, CA 91125, USA. (seinfeld@caltech.edu)

E. M. Knipping, Electric Power Research Institute, Palo Alto, CA 94304, USA.

M. Shahgholi and J. D. Surratt, Department of Chemistry, California Institute of Technology, Pasadena, CA 91125, USA.

Appendix C

Characterization of Organosulfates from the Photooxidation of Isoprene and Unsaturated Fatty Acids in Ambient Aerosol using Liquid Chromatography/(–)Electrospray Ionization Mass Spectrometry*

---

*This chapter is reproduced by permission from “Characterization of Organosulfates from the Photooxidation of Isoprene and Unsaturated Fatty Acids in Ambient Aerosol using Liquid Chromatography/(–)Electrospray Ionization Mass Spectrometry” by Yadian Gómez-González, Jason D. Surratt, Filip Cuyckens, Rafal Szmigielski, Reinhilde Vermeylen, Mohammed Jaoui, Michael Lewandowski, John H. Offenberg, Tadeusz E. Kleindienst, Edward O. Edney, Frank Blockhuys, Christian Van Alsenoy, Willy Maenhaut, and Magda Claeys, *Journal of Mass Spectrometry,* 43 (3), 371–382, 2008. Copyright 2008 by John Wiley & Sons, Ltd.

JOURNAL OF MASS SPECTROMETRY
J. Mass Spectrom. 2008; **43**: 371–382
DOI: 10.1002/jms.1329

Characterization of organosulfates from the photooxidation of isoprene and unsaturated fatty acids in ambient aerosol using liquid chromatography/(−) electrospray ionization mass spectrometry

Yadian Gómez-González,[1] Jason D. Surratt,[2] Filip Cuyckens,[3] Rafal Szmigielski,[1] Reinhilde Vermeylen,[1] Mohammed Jaoui,[4] Michael Lewandowski,[5] John H. Offenberg,[5] Tadeusz E. Kleindienst,[5] Edward O. Edney,[5] Frank Blockhuys,[6] Christian Van Alsenoy,[6] Willy Maenhaut[7] and Magda Claeys[1]*

[1] Department of Pharmaceutical Sciences, University of Antwerp (Campus Drie Eiken), Universiteitsplein 1, BE-2610 Antwerp, Belgium
[2] Department of Chemistry, California Institute of Technology, Pasadena, CA 91125, USA
[3] Global Preclinical Development, Johnson and Johnson Pharmaceutical R&D, Turnhoutseweg 30, BE-2340 Beerse, Belgium
[4] Alion Science and Technology, Research Triangle Park, NC 27709, USA
[5] National Exposure Research Laboratory, Office of Research and Development, United States Environmental Protection Agency, Research Triangle Park, NC 27711, USA
[6] Department of Chemistry, University of Antwerp (Campus Drie Eiken), Universiteitsplein 1, BE-2610 Antwerp, Belgium
[7] Department of Analytical Chemistry, Institute for Nuclear Sciences, Ghent University, Proeftuinstraat 86, BE-9000 Gent, Belgium

Received 20 July 2007; Accepted 17 September 2007

In the present study, we have characterized in detail the MS^2 and MS^3 fragmentation behaviors, using electrospray ionization (ESI) in the negative ion mode, of previously identified sulfated isoprene secondary organic aerosol compounds, including 2-methyltetrols, 2-methylglyceric acid, 2-methyltetrol mononitrate derivatives, glyoxal and methylglyoxal. A major fragmentation pathway for the deprotonated molecules of the sulfate esters of 2-methyltetrols and 2-methylglyceric acid and of the sulfate derivatives of glyoxal and methylglyoxal is the formation of the bisulfate $[HSO_4]^-$ anion, while the deprotonated sulfate esters of 2-methyltetrol mononitrate derivatives preferentially fragment through loss of nitric acid. Rational interpretation of MS^2, MS^3 and accurate mass data led to the structural characterization of unknown polar compounds in K-puszta fine aerosol as organosulfate derivatives of photooxidation products of unsaturated fatty acids, i.e. 2-hydroxy-1,4-butanedialdehyde, 4,5- and 2,3-dihydroxypentanoic acids, and 2-hydroxyglutaric acid, and of *α*-pinene, i.e. 3-hydroxyglutaric acid. The deprotonated molecules of the sulfated hydroxyacids, 2-methylglyceric acid, 4,5- and 2,3-dihydroxypentanoic acid, and 2- and 3-hydroxyglutaric acids, showed in addition to the $[HSO_4]^-$ ion (*m/z* 97) neutral losses of water, CO_2 and/or SO_3, features that are characteristic of humic-like substances. The polar organosulfates characterized in the present work are of climatic relevance because they may contribute to the hydrophilic properties of fine ambient aerosol. In addition, these compounds probably serve as ambient tracer compounds for the occurrence of secondary organic aerosol formation under acidic conditions.

KEYWORDS: isoprene; unsaturated fatty acids; hydroxyacids; organosulfates; humic-like substances; secondary organic aerosol; sulfate esters

INTRODUCTION

Considerable efforts have been undertaken in the last two decades to characterize the chemical composition of particulate matter in the atmosphere, especially of polar and water-soluble organic compounds (WSOC). The latter compounds account for 20–70% of the organic mass[1] and are of climatic relevance because they can enhance the capability of aerosols to act as cloud condensation nuclei.[2] Humic-like substances (HULIS) constitute a major fraction of WSOC[3] and have been studied by NMR,[3–5] UV/VIS,[6] infrared spectroscopy,[6] fluorescence spectroscopy,[6] pyrolysis gas chromatography/mass spectrometry[4,7] and electrospray ionization mass spectrometry in the negative ion mode [(−)ESI-MS].[8–11] Using the latter technique, it was shown in

---

*Correspondence to: Magda Claeys, Department of Pharmaceutical Sciences, University of Antwerp (Campus Drie Eiken), Universiteitsplein 1, BE-2610 Antwerp, Belgium.
E-mail: magda.claeys@ua.ac.be

recent work that ambient aerosol contains organosulfates (OSs) (i.e. sulfate esters and sulfate derivatives) from the photooxidation of isoprene and α-pinene, and it was proposed that this pathway is important for other biogenic terpenes and may be involved in the formation of HULIS in ambient aerosol.[12]

In the present study, liquid chromatography (LC) combined with (−)ESI-linear ion-trap MS is used to characterize in detail OSs from the photooxidation of isoprene, including sulfate derivatives of 2-methyltetrols,[13–15] 2-methylglyceric acid,[14–16] 2-methyltetrol mononitrates, glyoxal and methylglyoxal, in ambient $PM_{2.5}$ (particulate matter with an aerodynamic diameter <2.5 μm) aerosol from K-puszta, Hungary, and, for comparison, in laboratory-generated secondary organic aerosol (SOA) from the photooxidation of isoprene in the presence of acidified inorganic seed aerosol. A motivation for examining K-puszta $PM_{2.5}$ aerosol was that this aerosol contains high atmospheric concentrations of 2-methyltetrols, indicating the importance of isoprene emissions to organic aerosol formation in this region.[16] Furthermore, it is known that K-puszta aerosol has high inorganic sulfate concentrations (about 5 $\mu g\,m^{-3}$ or 25% of the PM_2)[17] and that the WSOC fraction of the $PM_{2.5}$ contains *ca* 20–50% HULIS.[6] In addition, we address the characterization of OSs of other polar oxygenated compounds with chromatographic properties similar to those of sulfated isoprene SOA. These polar OSs appear to originate mainly from the photooxidation of unsaturated fatty acids and represent a novel group of compounds that may contribute to the hydrophilic properties of ambient fine aerosol.

The OSs characterized in the present work are potential tracers for SOA formation occurring under acidic conditions.[12,18–20] In this respect, it is worth noting that the sulfate ester formation is a particle–phase reaction that has been observed to occur in both chamber-generated and ambient aerosol. These observations have prompted us to elucidate the detailed sulfate ester product structures, which in turn could provide a better understanding of sulfate ester formation and its role in SOA formation.

(−)ESI-linear ion-trap MS offers considerable advantages as regards detection of polar OSs compared to (−)ESI-MS techniques using classical ion-trap and quadrupole mass analyzers. The enhanced sensitivity of the linear ion trap[21] allows the recording of first-order mass spectra and MS^2 and higher-order MS^3 product-ion spectra for individual compounds in a single chromatographic run. On the basis of the interpretation of the MS^2 and MS^3 ion-trap data and accurate mass data, plausible structures are proposed for unknown organosulfate compounds.

EXPERIMENTAL

Chemicals

HPLC grade methanol was purchased from Biosolve (Valkenswaard, The Netherlands), acetic acid analytical reagent grade from Merck (Darmstadt, Germany) and 0.45-μm Teflon syringe filters from Alltech (Deerfield, IL, USA). Demineralised water was further purified with a Milli-Q system (Millipore, Milford, MA, USA). The following chemicals were purchased from Sigma (St. Louis, MI, USA): 2-hydroxyglutaric acid Na_2-salt (purity >95%), allylacetic (purity >98%), 2-pentenoic (purity >98%), and 3-pentenoic acid (purity >95%). Malic acid (purity >99%) was purchased from Sigma–Aldrich (Steinheim, Germany). Synthesized 3-hydroxyglutaric acid was available from a previous study.[22] 2-Pentenoic, 3-pentenoic and 4-pentenoic acids were converted to their dihydroxyacids (2,3-, 3,4- and 4,5-dihydroxypentanoic acids, respectively) by oxidation with hydrogen peroxide and acid-catalyzed hydrolysis following the procedure reported for the preparation of 2-methylglyceric acid in previous work.[23]

Aerosol samples

Archived $PM_{2.5}$ aerosol samples were used. The collection substrates were quartz fiber filters for the ambient samples, and a Teflon filter for the smog chamber sample. The ambient samples were collected at K-puszta, Hungary, a mixed deciduous/coniferous forest site, during a 2003 summer campaign.[24] The smog chamber sample was obtained by irradiating isoprene in the presence of air, NO_x, and SO_2 (provides particle–phase acidity by its photochemical conversion to H_2SO_4), as reported in previous work.[14]

Sample preparation

For the ambient samples, sections of quartz fiber filters from different days and/or nights (containing in all between 30 and 80 μg organic carbon) were extracted 3 times for 30 min in an ultrasonic bath with 20 ml of methanol. The extracts were combined and concentrated in a rotary evaporator at 35 °C and 200 mbar to approximately 1 ml and filtered through a Teflon filter (0.45 μm), then evaporated to dryness under a nitrogen stream and redissolved in 200 μl of water. In the case of the smog chamber sample, one half of the Teflon filter was used and worked up in the same way as described above.

Liquid chromatography

The LC system consisted of a Surveyor Plus system (pump and autosampler) (Thermo Fisher, San Jose, USA) and a data system using Xcalibur version 2.0 software. An Atlantis dC18 column (3 μm; 2.1 × 150 mm) (Waters, Milford, USA) was employed. The mobile phases consisted of acetic acid 0.1% (v/v) (A) and methanol (B). The applied 45-min gradient elution program was as follows: the concentration of eluent B was kept at 3% for 2 min, then increased to 90% in 18 min, kept at 90% for 10 min, then decreased to 3% in 5 min, and kept at 3% for 10 min. The injection volume and flow rate were 5 μl and 0.2 ml min^{-1}, respectively.

With respect to the choice of the LC column, it was found in preliminary trials that the Atlantis dC18 column, which contains difunctionally bonded C_{18} alkyl residues preventing stationary phase collapse when an aqueous mobile phase is used, provides increased retention of the polar OSs compared to a classical C18 column (ODS Hypersil; 3 μm; 3 × 250 mm; Thermo Fisher). On the Atlantis dC18 column, a separation was obtained between inorganic sulfate (detected at m/z 195 as the adduct H_2SO_4: HSO_4^-), which eluted first from the column (Fig. 1(a); RT 2.2 min), and the OSs of 2-methyltetrols (RTs 3.1 and 3.4 min). It should be noted that this separation was not achieved in a prior study by Surratt *et al.*[12]; therefore, this result further confirms that the initial identifications made by Surratt *et al.*[12] were not artifacts formed in the mass spectrometer due to coelution.

Mass spectrometry

A linear ion-trap mass spectrometer (LXQ, Thermo Fisher) was operated under the following conditions: sheath gas flow (nitrogen), 50 arbitrary units; auxiliary gas flow (nitrogen), 5 arbitrary units; source voltage, −4.5 kV; capillary temperature, 350 °C; and maximum ion injection time, 200 ms. For MS^2 and MS^3 experiments, an isolation width of 2 m/z units and a normalized collision energy level of 35% were applied. A strong influence of the capillary temperature on the $[M - H]^-$ signal sensitivity was observed owing to formation of acetic acid adduct ions (m/z 119) at lower temperatures. The $[M - H]^-$ signal optimization was done by introducing a 50 µg ml^{-1} malic acid standard solution.

Accurate mass measurements were carried out using an LTQ-Orbitrap mass spectrometer (Thermo Fisher, Bremen, Germany) equipped with a Waters Alliance 2695 HPLC system (Waters, Milford, Massachusetts, USA). The LTQ-Orbitrap mass spectrometer was equipped with an ESI source operated in the negative ion mode under the same conditions as described above for the ion-trap experiments. The mass resolution was set at 100 000 in the MS^1 mode and 7500 in the MS^2 and MS^3 modes. The source parameters were tuned for maximum sensitivity using a 50 µg ml^{-1} malic acid standard solution. For MS^2 and MS^3 experiments, an isolation width of 5 units and a normalized collision energy level of 35% were applied. Accurate mass measurements were obtained using external calibration. Data were acquired and processed using Xcalibur 2.0 software. The mass accuracy was better than 1 mDa. Accurate mass measurements were only carried out for K-puszta $PM_{2.5}$ aerosol (pooled day- and night-time samples).

Theoretical calculations

All calculations were performed on isolated molecules in C_1 symmetry using the Gaussian 03[25] suite of programs applying the density functional (DFT) level of theory, using the B1B95[26] functional and the aug-cc-pVTZ basis set, as it is implemented in Gaussian 03. The energies were not corrected for the basis set superposition error (BSSE).

RESULTS AND DISCUSSION

Figure 1 shows the base peak chromatograms (BPCs) obtained for (a) K-puszta $PM_{2.5}$ aerosol (pooled day- and night-time sample) and (b) SOA that was generated from an isoprene/NO_x/SO_2/air mixture. In this work, we focus on the mass spectrometric characterization of the early eluting compounds (RTs <12 min), which include SOA compounds from the photooxidation of isoprene. It is noted that the K-puszta aerosol sample also contains abundant compounds eluting after 12 min; these compounds (marked with an asterisk in Fig. 1) include the known terpenoic acids, norpinic, pinic and pinonic acids,[18] and compounds that have only been recently identified, e.g. OSs of α-pinene SOA containing a nitrate group.[12,20,27] Similar BPCs were obtained for other separately pooled day- and night-time K-puszta samples analyzed, except that the OSs of α-pinene SOA containing a nitrate group were enhanced in the night-time samples compared to the day-time ones, consistent with recent work by Iinuma *et al.*[20] These compounds will not be considered in the present work.

Figures 2 and 3 show corresponding extracted ion chromatograms (EICs) for selected abundant ions detected in K-puszta $PM_{2.5}$ aerosol and isoprene SOA, respectively. In the following discussion, we will first consider OSs that are formed from isoprene SOA, which have been partially characterized in previous work by Surratt *et al.*[12] Subsequently, we will address the characterization of

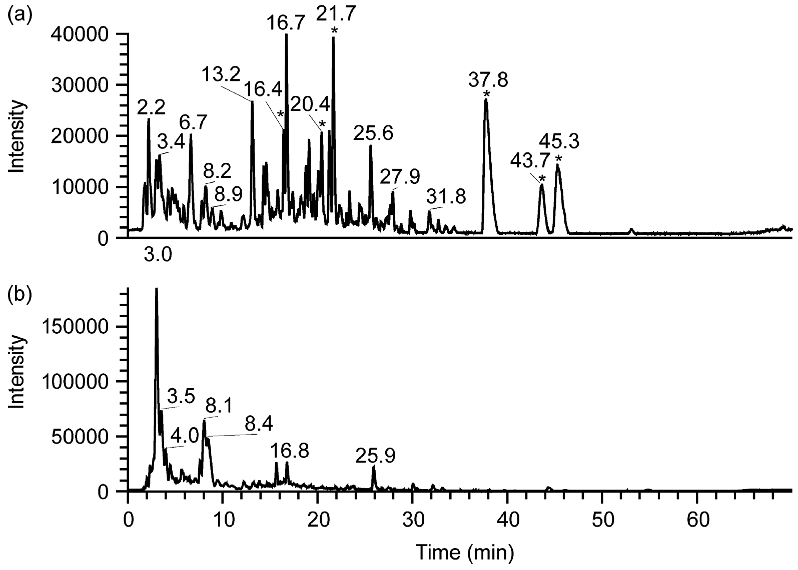

Figure 1. LC/(−) ESI-MS BPCs obtained for methanol extracts of $PM_{2.5}$ aerosol: (a) K-puszta aerosol collected during a 2003 summer campaign; (b) SOA from an isoprene/NO_x/air/SO_2 irradiation experiment. Peaks marked with an asterisk correspond to known terpenoic acids (i.e. norpinic acid, RT 16.4 min; pinic acid, RT 20.4 min; pinonic acid, RT 21.7 min) and α-pinene SOA compounds containing both a sulfate and a nitrate group (RTs 37.8, 43.7, and 45.3 min).

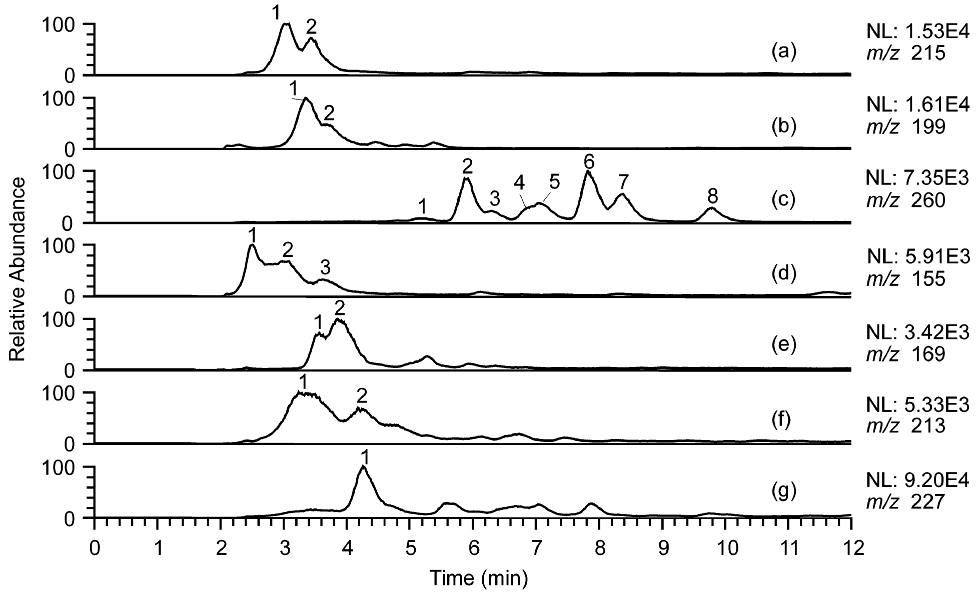

Figure 2. LC/(−) ESI-MS EICs obtained for K-puszta aerosol. Ions extracted: (a) *m/z* 215 (2-methyltetrol OS isomers); (b) *m/z* 199 (2-methylglyceric acid OS + unknown); (c) *m/z* 260 (2-methyltetrol mononitrate OS isomers); (d) *m/z* 155 (glyoxal OS); (e) *m/z* 169 (methylglyoxal OS); (f) *m/z* 213 (unknown OSs); and (g) *m/z* 227 (unknown OS).

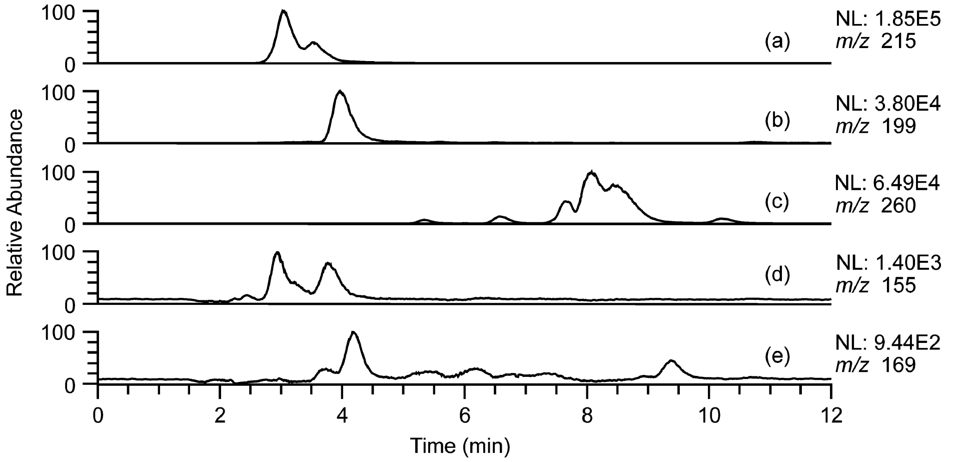

Figure 3. LC/(−) ESI-MS EICs obtained for SOA from the photooxidation of isoprene in the presence of NO_x, SO_2 and air. Ions extracted: (a) *m/z* 215 (2-methyltetrol OS isomers); (b) *m/z* 199 (2-methylglyceric acid OS); (c) *m/z* 260 (2-methyltetrol mononitrate OS isomers); (d) *m/z* 155 (glyoxal OS); and (e) *m/z* 169 (methylglyoxal OS).

additional unknown OSs with MW 200, 214 and 228, which elute during the first 12 min, are very polar, and have similar hydrophilic properties as isoprene SOA. It should be mentioned that other unknown abundant early eluting OSs could be detected in K-puszta aerosol (MWs 212, 226, 230 and 240), of which the chemical structures remain to be elucidated in future work.

Two types of OSs are considered in the present study: (1) sulfate esters formed by esterification of a compound containing one or more hydroxyl groups and sulfuric acid or sulfur trioxide[28]; and (2) sulfate derivatives, i.e. α-hydroxysulfate esters,[12,29] formed between a compound containing an aldehyde or keto group and sulfuric acid. These derivatives can be explained by gem-diol formation and subsequent sulfation of one of the two hydroxyl groups. We also considered the possible formation of sulfate derivatives of the noncovalent type and performed theoretical calculations to address this issue. The energies of the α-hydroxysulfate ester of glyoxal on the one hand, and of three noncovalent sulfate adducts of glyoxal, in which the HSO_4^- moiety was positioned in a number of different orientations with respect to the glyoxal molecule, on the other, were calculated. In all cases the energy of the noncovalent adduct was more than 10 kcal mol^{-1} higher than that of the α-hydroxysulfate ester, indicating that the latter is the preferred form.

MASS SPECTROMETRIC CHARACTERIZATION OF OSs OF ISOPRENE SOA

The 2-methyltetrol OSs detected at m/z 215 correspond to the major early eluting compounds (Fig. 2(a)). Two partially resolved peaks can be noted; however, it is not possible to assign these peaks to isomeric forms since many isomeric forms are possible owing to a different stereochemistry at the C(2) and C(3) positions of the 2-methyltetrol skeleton (i.e. *threo* and *erythro* diastereoisomerism) [Scheme 1(a) (**1**)] and the four possible positions of the hydroxyl groups that can be sulfated. From a mechanistic formation point of view, however, it is more likely that the terminal primary hydroxyl groups will be more readily sulfated than the inner secondary and tertiary hydroxyl groups at the C(3) and C(2) positions, respectively.[28] The *m/z* 215 MS^2 product-ion spectra are very simple and only exhibit a $[HSO_4^-]$ anion (*m/z* 97) (only shown for peak 1; Fig. 4(a)), which is consistent with the neutral nature of the 2-methyltetrols and with previous work.[12] On the basis of the detailed study by Attygalle

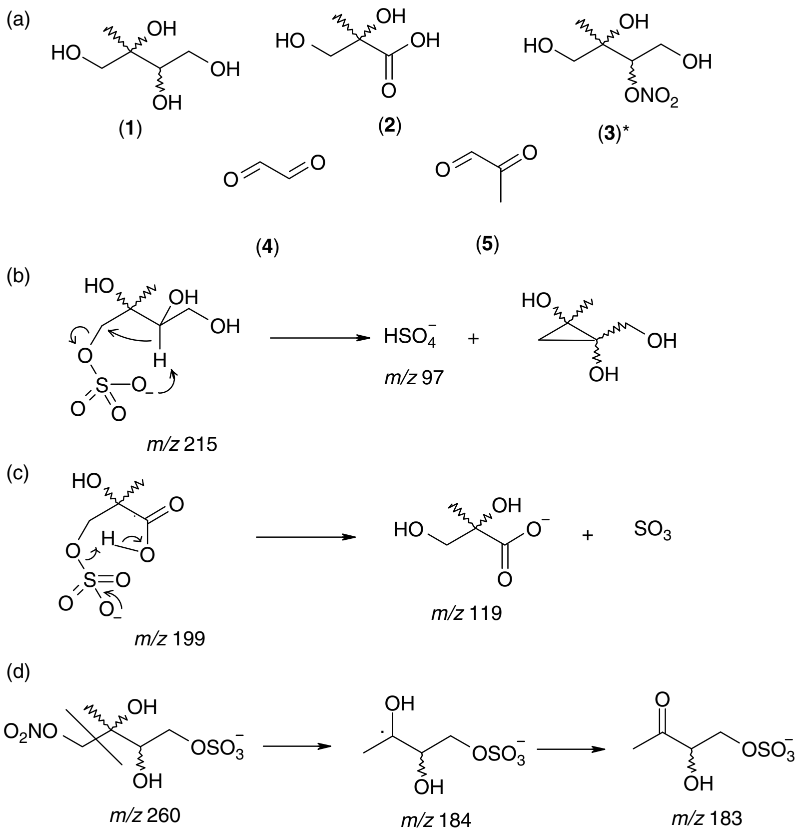

Scheme 1. (a) Structures of photooxidation products of isoprene: (**1**) 2-methyltetrols; (**2**) 2-methylglyceric acid; (**3**) 2-methyltetrol mononitrates* in which the nitrate group can occupy different positions; (**4**) glyoxal and (**5**) methylglyoxal. Proposed fragmentation pathways of (b) *m/z* 215 leading to *m/z* 97, (c) *m/z* 199 leading to *m/z* 119, and (d) *m/z* 260 leading to *m/z* 184 and 183.

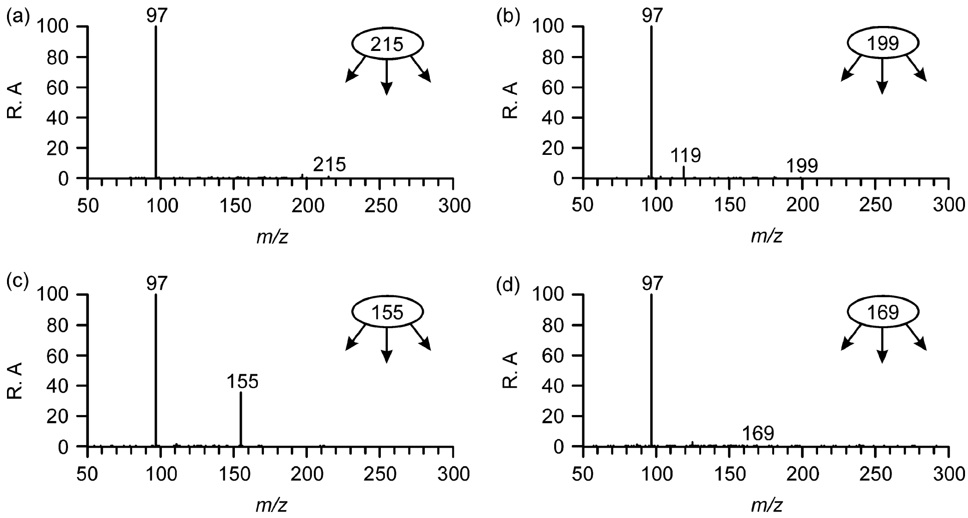

Figure 4. Selected MS^2 product-ion spectra obtained for organosulfates related to the photooxidation of isoprene present in K-puszta aerosol: (a) *m/z* 215 MS^2 (2-methyltetrol OS, peak 1); (b) *m/z* 199 MS^2 (2-methylglyceric acid OS, peak 2); (c) *m/z* 155 MS^2 (glyoxal OS, peak 3); and (d) *m/z* 169 MS^2 (methylglyoxal OS, peak 1).

et al.,[30] formation of the bisulfate [HSO_4^-] anion is believed to involve a hydrogen atom from a C(2) or more distant position in addition to a C–O bond cleavage (Scheme 1(b)).

The OS of 2-methylglyceric acid corresponds to the second minor partially resolved peak detected at m/z 199 in K-puszta aerosol (peak 2; Fig. 2). Compared to the 2-methyltetrol OSs, the 2-methylglyceric acid OS (Fig. 4(b)) shows a different MS^2 fragmentation behavior. More specifically, loss of 80 u (SO_3) is observed giving rise to deprotonated 2-methylglyceric acid (m/z 119). This neutral loss can be regarded as a diagnostic fragmentation of OSs containing an additional carboxylic group since it will only occur if the negative charge following SO_3 loss can be accommodated by an acidic group (Scheme 1(c)). Two possible structures with a chiral center at C(2) can be suggested for the organosulfate derivatives of 2-methylglyceric acid with the sulfate group at the C(2) or C(3) positions. The MS data do not allow to locate the sulfate group with certainty although sulfation at the terminal C(3) position appears more likely since in the case of sulfation at the C(2) position, elimination of formaldehyde can occur and loss of SO_3 may be less favorable. Furthermore, from a mechanistic formation point of view, it is likely that a primary hydroxyl group at C(3) will more readily undergo sulfation than the tertiary one at C(2).[28]

A number of peaks due to OSs of 2-methyltetrol mononitrates detected at m/z 260 could be observed in both K-puszta aerosol (Fig. 2(c)) and isoprene SOA (Fig. 3(c)). It is noted that a different isomeric composition is observed for the ambient and smog chamber sample. As in the case of the OSs of 2-methyltetrols, it is not feasible to assign isomeric forms owing to the many different possible isomeric forms that are even more numerous than in the case of the 2-methyltetrols because of the additional nitrate group. The m/z 260 MS^2 product-ion spectra only reveal some subtle differences and are shown for the eight peaks observed in K-puszta aerosol (Fig. 5). The main fragmentation pathway corresponds to a neutral loss of 63 u (HNO_3) resulting in m/z 197 as a base peak. Minor peaks at m/z 97 ([HSO_4^-]), 142, 183 and 184 can be observed in some of the m/z 260 MS^2 product-ion spectra. The m/z 142 ion is attributed to a $O_2N{-}OSO_3^-$ ion, pointing to a close proximity of the nitrate and sulfate groups. The formation m/z 183 and 184 ions involves the loss of a terminal $CH_2{-}ONO_2$ group at the branched site of the 2-methyltetrol skeleton as outlined in Scheme 1(d). The corresponding m/z 260 → 197 MS^3 product-ion spectra (Fig. 5) show the [HSO_4^-] ion (m/z 97) as the major product ion; these spectra provide additional information and reveal more pronounced isomeric differences compared to the m/z 260 MS^2 product ion spectra. Product ions are observed at m/z 167, 153 and 139, corresponding to neutral losses of 30 u (CH_2O), 44 u ($CH_4 + CO$) and 58 u ($CH_2O + CH_2{=}CH_2$), respectively.

Both K-puszta aerosol and isoprene SOA show early eluting m/z 155 and 169 compounds (Figs 2(d), (e) and 3(d), (e)), which have been attributed in the previous work to covalent sulfate adducts of glyoxal and methylglyoxal, respectively, i.e. α-hydroxysulfate esters.[12] The corresponding MS^2 product-ion spectra (illustrated for K-puszta aerosol in Fig. 4(c), (d)) reveal the [HSO_4^-] ion (m/z 97) as the major product-ion, consistent with the neutral nature of both glyoxal and methylglyoxal. It is noted that multiple peaks are observed for both the m/z 155 and 169 compounds. A possible explanation for the multiple peaks in the case of the m/z 155 compounds is that the glyoxal sulfate derivative has partially degraded during sample preparation and is also present in the free form, which in LC/MS coelutes with inorganic sulfate and gives rise to sulfate adduct formation in the ion source. Indeed, for the first-eluting m/z 155 compound coelution with inorganic sulfate (m/z 195) could be observed. The two partially resolved m/z 169 peaks (Figs 2(e) and 3(e)) that elute later than inorganic sulfate can be explained by sulfation of the gem-diol form involving the terminal aldehyde or 2-keto group of methylglyoxal.

STRUCTURE CHARACTERIZATION OF ADDITIONAL UNKNOWN COMPOUNDS IN K-PUSZTA AEROSOL

MW 200 compound, identified as an OS adduct of 2-hydroxy-1,4-butanedialdehyde

K-puszta aerosol shows in addition to the 2-methylglyceric acid OS m/z 199 peak a more abundant early eluting m/z 199 peak (peak 1, Fig. 2(b)). The m/z 199 MS^2 product-ion spectrum (Fig. 6) reveals a neutral loss of 44 u (C_2H_4O), while the m/z 199 → m/z 155 MS^3 product-ion spectrum shows the [HSO_4^-] ion (m/z 97), pointing to a sulfate group. It can be observed that the m/z 199 → m/z 155 MS^3 product-ion spectrum is similar to the m/z 155 MS^2 spectrum of glyoxal OS. On the basis of its MS behavior, the unknown compound is attributed to a sulfate derivative of 2-hydroxy-1,4-butanedialdehyde. The neutral loss of C_2H_4O in the deprotonated molecule can be explained as outlined in Scheme 2.

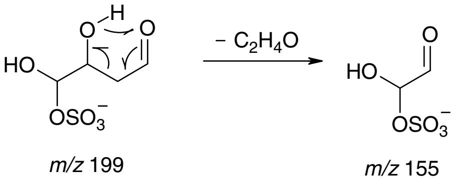

Scheme 2. Explanation for the loss of C_2H_4O (44 u) observed in the m/z 199 MS^2 spectrum of the major m/z 199 compound, identified as an OS derivative of 2-hydroxy-1,4-butanedialdehyde.

The C_4-hydroxydialdehyde, 2-hydroxy-1,4-butanedialdehyde, is believed to be an intermediate in the formation of malic acid, which occurs at significant concentrations in K-puszta $PM_{2.5}$ aerosol[24] and is known to result from the photooxidation of unsaturated fatty acids.[31,32]

MW 214 compounds, identified as OSs of dihydroxypentanoic acids

Figure 7 shows MS^2 and MS^3 data for the major early eluting m/z 213 compounds detected in K-puszta aerosol (peak 1; Fig. 2(f)). Since this peak was found to be heterogeneous, m/z 213 MS^2 spectra are given for two sections of the peak. The base peak (in the first section of the peak) in the m/z 213 MS^2 spectra is m/z 133, corresponding to the neutral loss of SO_3 which indicates that the molecule contains a carboxyl group that can readily accommodate the negative

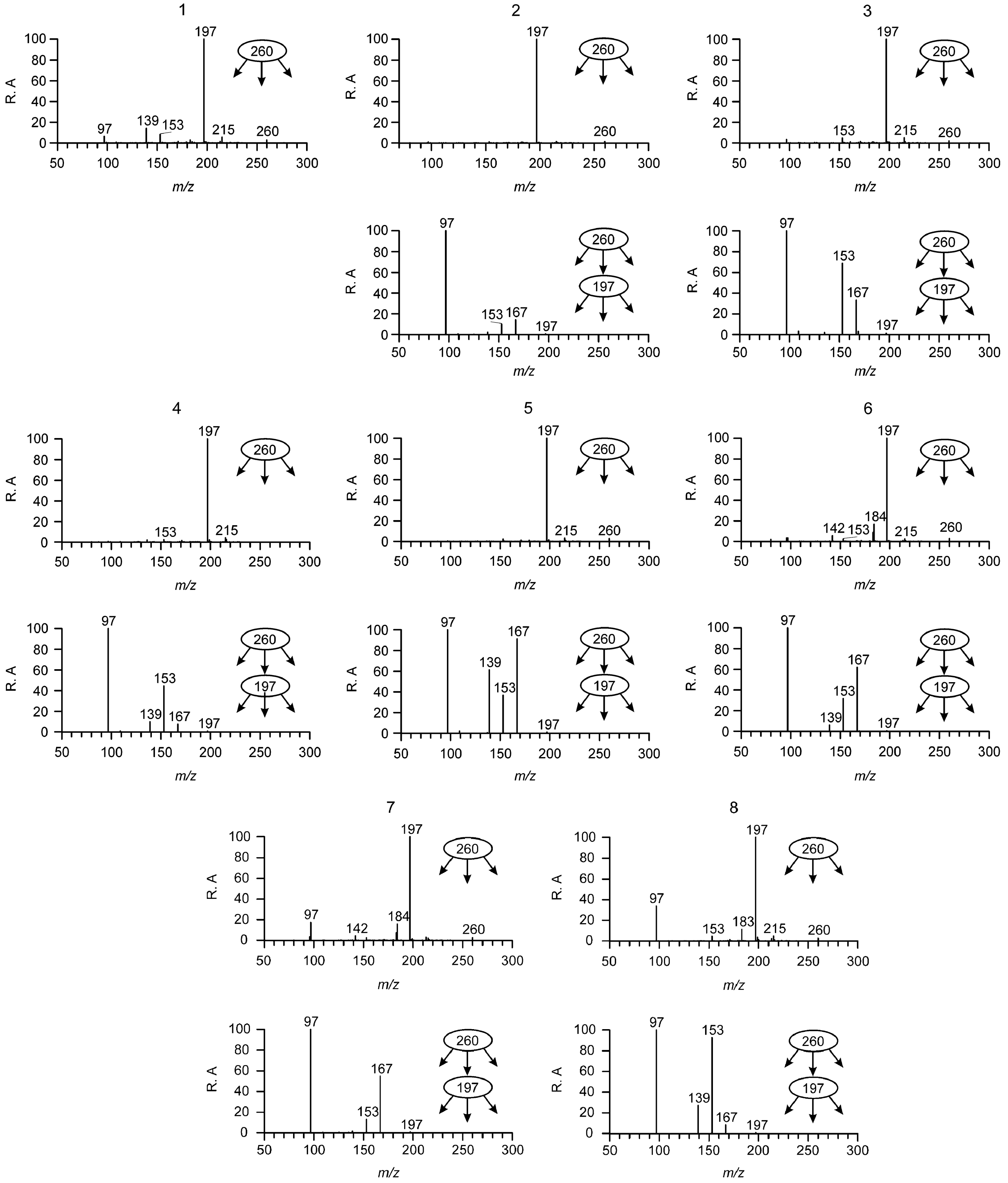

Figure 5. MS^2 and MS^3 product-ion spectra for OSs of 2-methyltetrol mononitrates (MW 261) present in K-puszta aerosol. A *m/z* 260 → *m/z* 193 MS^3 spectrum could not be obtained for the minor peak 1.

charge. Furthermore, the loss of 44 u (CO_2; *m/z* 169) is also in agreement with a carboxyl group. A candidate for the unknown compound was malic acid since this hydroxyacid is a major tracer compound in K-puszta aerosol[24]; however, malic acid could be ruled out because its *m/z* 133 MS^2 spectrum (not shown) did not match with the *m/z* 213 → 133 MS^3 spectrum of the unknown compounds (Fig. 7(c)), and also on the basis of the accurate mass data which indicated $C_5H_9O_7S^-$ as the elemental composition of *m/z* 213. Comparison of the *m/z* 213 → 133 MS^3 spectrum with the *m/z* 133 MS^2 spectra of synthesized reference compounds (Fig. 7(d)), i.e. 2,3-, 3,4-, and 4,5-dihydroxypentanoic acids, led to the characterization of the *m/z* 213 compounds as isomeric OSs of 4,5-dihydroxypentanoic acid. The *m/z* 213 → 133 MS^3 spectrum for the unknown compounds matched with the *m/z* 133 MS^2 spectrum of 4,5-dihydroxypentanoic

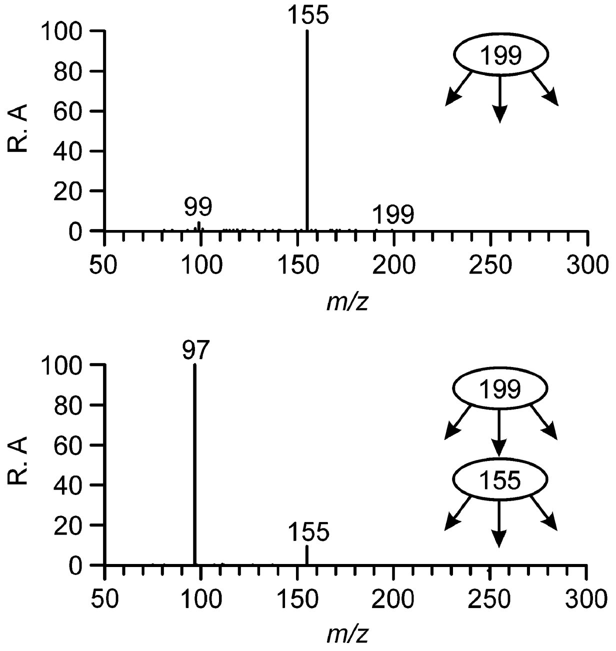

Figure 6. MS^2 (*m/z* 199) and MS^3 (*m/z* 199 → *m/z* 155) product-ion spectra for the unknown MW 200 compound present in K-puszta aerosol, identified as an OS derivative of 2-hydroxy-1,4-butanedialdehyde.

acid (Fig. 7(d)). On the basis of the detailed interpretation of the *m/z* 213 MS^2 spectra, the sulfate groups could be located at the C(5) and C(4) positions for the first- and second-eluting 4,5-dihydroxypentanoic acid OS compounds within peak 1, respectively (Scheme 3(a)). The second-eluting compound is attributed to the isomer with the sulfate group at the C(4) position based on the loss of formaldehyde (30 u). In addition, the loss of H_2O in the *m/z* 213 → 133 MS^3 spectrum could also be readily interpreted as outlined in Scheme 3(b).

A possible VOC precursor for 4,5-dihydroxypentanoic acid is 4-pentenal (Scheme 3(d)), which to our knowledge has not been reported in the atmosphere. It is hypothesized that the latter unsaturated aldehyde is formed through oxidative decay of unsaturated fatty acids; more specifically, it is probably an intermediate in the formation of malic acid, which is a known photooxidation product of unsaturated fatty acids.[31,32]

Figure 8 shows the *m/z* 213 MS^2 spectrum and corresponding *m/z* 213 → *m/z* 133 MS^3 spectrum for peak 2 which is only partially resolved from peak 1 (Fig. 2(f)). Despite the spectra being not of high quality owing to interferences from peak 1, a suggestion can be made about the structure of the corresponding unknown organosulfate. The latter compound is tentatively attributed to an organosulfate of 2,3-dihydroxypentanoic acid, based on the presence of *m/z* 75 in its *m/z* 213 → 133 MS^3 spectrum. The *m/z* 133 MS^2 spectrum of 2,3-dihydroxypentanoic acid shows that *m/z* 75 is a characteristic ion (Fig. 8(c); Scheme 3(c)).

A possible VOC precursor for 2,3-dihydroxypentanoic acid is 2-pentenal, which has been reported as a photolysis product of Z-3-hexenal,[33] a plant-leaf volatile which in turn results from enzyme (i.e. lipoxygenase and hydroperoxide lyase)-mediated oxidation of unsaturated fatty acids.[34]

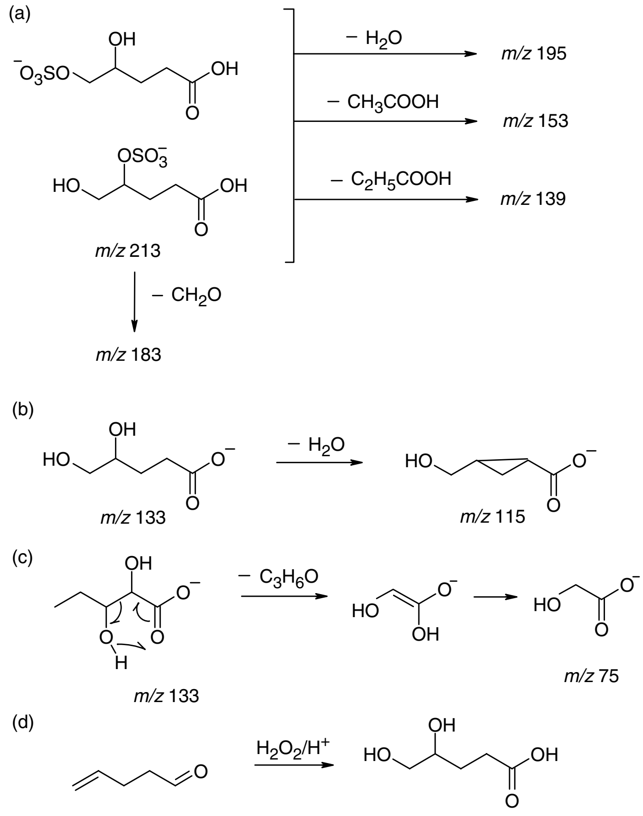

Scheme 3. (a) Possible explanations for the losses of 18, 30, 60 and 74 u observed in the MS^2 spectra of the early eluting *m/z* 213 compounds (peak 1; Fig. 2) and (b) water from *m/z* 133 (other structures are also possible). (c) Pathway leading to *m/z* 75 in the case of deprotonated 2,3-dihydroxypentanoic acid. (d) Formation of 3,4-dihydroxypentanoic acid through oxidation of 4-pentenal, a possible intermediate in the oxidative decay of unsaturated fatty acids.

MW 228 compounds, identified as a mixture of OSs of 2-and 3-hydroxyglutaric acid

Figure 9 presents the *m/z* 227 MS^2 and *m/z* 227 → *m/z* 147 MS^3 spectra for the unknown MW 228 compounds present in K-puszta aerosol. On the basis of the interpretation of the MS data this compound could be assigned to a mixture of OSs of 2- and 3-hydroxyglutaric acids (Scheme 4(a)), hydroxydicarboxylic acids which are present at significant concentrations in K-puszta aerosol.[18] The loss of water (*m/z* 209) and SO_3 (*m/z* 147) are consistent with the presence of a hydroxyl and carboxyl function, respectively (Fig. 9(a)). The *m/z* 227 → *m/z* 147 MS^3 spectrum of the unknown compound shows the loss of water (*m/z* 129) characteristic of 2-hydroxyglutaric acid (Fig. 9(b), (c)) as well as *m/z* 85 characteristic of 3-hydroxyglutaric acid (Fig. 9(d)). Explanations for the loss of water (*m/z* 129) in the case of 2-hydroxyglutaric acid and the combined loss of water and CO_2 (*m/z* 85) in the case of 3-hydroxyglutaric acid are given in Scheme 4(b).

Considering that 2-hydroxyglutaric acid is a homolog of malic acid, a known photooxidation product of unsaturated fatty acids,[31,32] it is reasonable to suggest that it may also result from the latter oxidative decay process. It is worth noting that the isomer 3-hydroxyglutaric acid is a recently elucidated photooxidation product of α-pinene.[18]

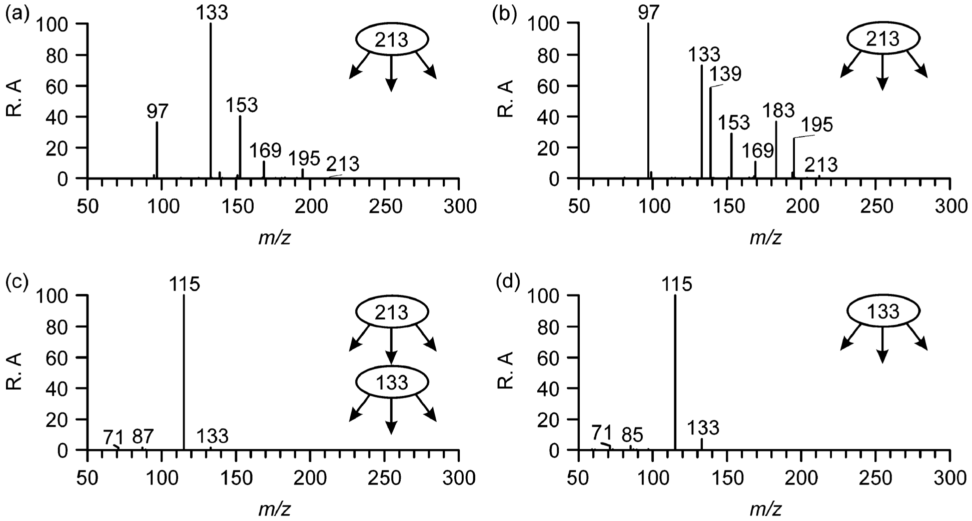

Figure 7. MS^2 (*m/z* 213) product-ion spectra of unknown early eluting MW 214 compounds (peak 1; Fig. 2) present in K-puszta aerosol, identified as OSs of 4,5-dihydroxypentanoic acid: spectrum averaged between (a) 2.6 and 3 min; and (b) 3.4 and 3.8 min. (c) The MS^3 (*m/z* 213 → 155) spectrum (averaged between 2.6 and 3.8 min) was found to be the same for the two compounds. (d) MS^2 (*m/z* 133) spectrum of 4,5-dihydroxypentanoic acid.

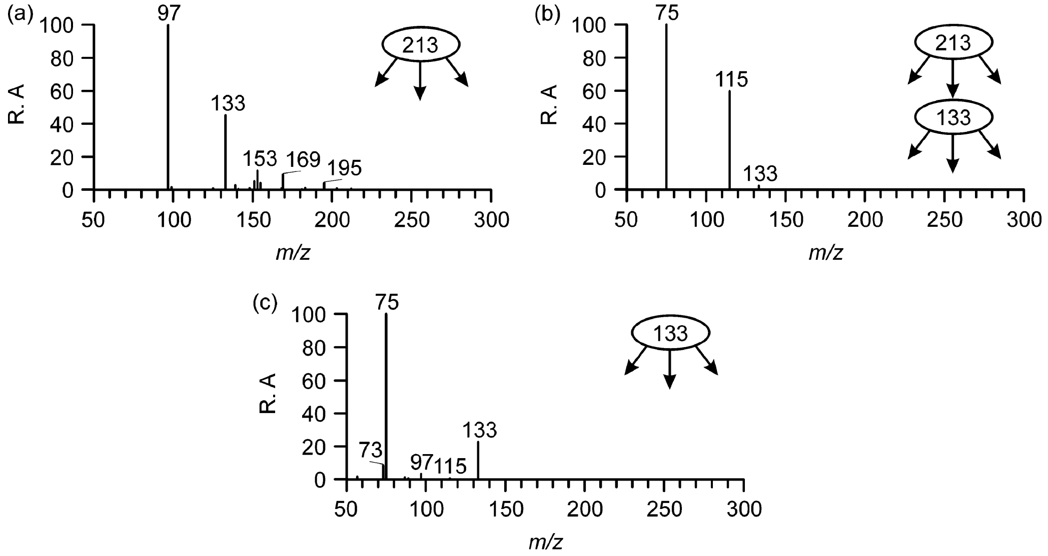

Figure 8. MS data for the unknown early eluting MW 214 compound (peak 2; Fig. 2) present in K-puszta aerosol, tentatively identified as an OS of 2,3-dihydroxypentanoic acid: (a) MS^2 (*m/z* 213) spectrum; (b) corresponding MS^3 (*m/z* 213 → *m/z* 133) spectrum. (c) MS^2 (*m/z* 133) spectrum obtained for 2,3-dihydroxypentanoic acid.

CONCLUSIONS AND PERSPECTIVES

We have characterized in detail the MS^2 and MS^3 fragmentation behaviors of sulfated isoprene SOA compounds, including sulfated 2-methyltetrols, 2-methylglyceric acid, 2-methyltetrol mononitrate derivatives, glyoxal and methylglyoxal. A major fragmentation pathway for the deprotonated sulfate esters of the 2-methyltetrols and 2-methylglyceric acid and the sulfate derivatives of glyoxal and methylglyoxal is the formation of the bisulfate $[HSO_4]^-$ anion, while the deprotonated sulfate esters of 2-methyltetrol mononitrate derivatives preferentially fragment through loss of nitric acid. Rational interpretation of MS^2, MS^3 and accurate mass data led to the structural characterization of unknown polar compounds in K-puszta fine aerosol as organosulfate derivatives of compounds that originate from the photooxidation of unsaturated fatty acids, i.e. 2-hydroxy-1,4-butanedialdehyde, 4,5-dihydroxypentanoic acid, 2,3-dihydroxypentanoic acid and 2-hydroxyglutaric acid, and of α-pinene, i.e. 3-hydroxyglutaric acid. The deprotonated molecules of the sulfated hydroxyacids, 4,5-, and 2,3-dihydroxypentanoic acids, and 2- and 3-hydroxyglutaric acids, show in addition to the $[HSO_4]^-$ ion (*m*/*z* 97) neutral losses of water, CO_2 and/or SO_3, features that are characteristic of HULIS.[10] Using the same mass spectrometric approaches, we hope to elucidate in future work the chemical structures of additional polar OSs in ambient fine aerosol, considering that the latter compounds may contribute to the hydrophilic properties of fine ambient aerosol and as such enhance the capability of the aerosol particles to act

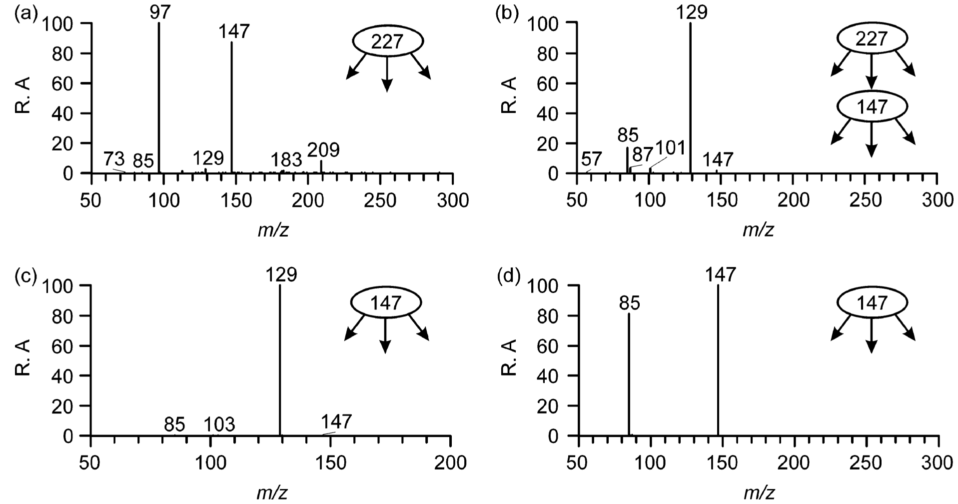

Figure 9. (a) MS^2 (*m/z* 227) and (b) MS^3 (*m/z* 227 → *m/z* 147) product-ion spectra for unknown MW 228 compounds present in K-puszta aerosol, identified as a mixture of OSs of 2- and 3-hydroxyglutaric acids. MS^2 (*m/z* 147) spectra of (c) 2- and (d) 3-hydroxyglutaric acid.

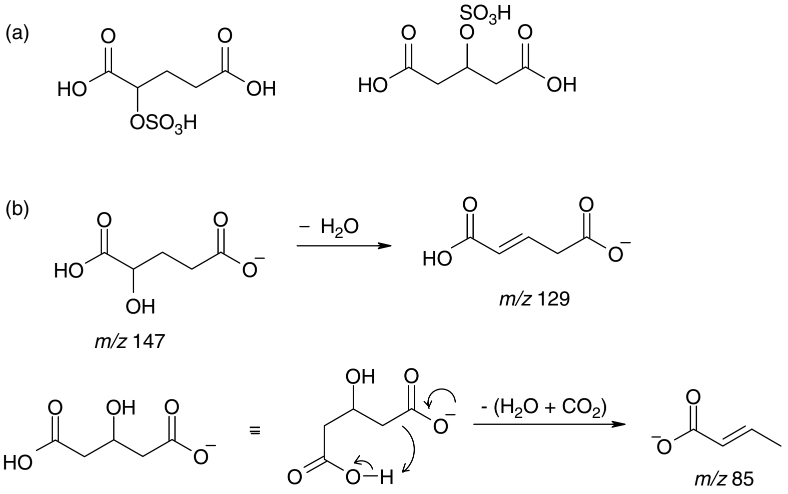

Scheme 4. (a) Proposed structures for the unknown MW 228 compounds. (b) Explanations for the loss of water (*m/z* 129) in the case of 2-hydroxyglutaric acid and the combined loss of water and CO_2 (*m/z* 85) in the case of 3-hydroxyglutaric acid.

as cloud condensation nuclei. With regard to the cloud condensation nuclei properties of the compounds characterized in the present study, it is worth mentioning that glyoxal and methylglyoxal have been considered in recent work by Matsunaga *et al.*[35] Sulfation provides a mechanism by which polar compounds containing hydroxyl groups or carbonyl compounds (after conversion to gem-diols) become associated with the particle phase and can contribute to its cloud condensation nuclei properties.

It has been stated in 1990 by MacCarthy *et al.*[36] that the term 'structure of humic substances' must not be interpreted in the conventional chemical context because such microscopic detail was simply beyond reach at that time. Owing to the considerable developments of mass spectrometric techniques based on ESI, tandem MS and high resolution MS, during the last two decades, the analytical tools are now available to efficiently address the polyfunctional chemical structures of polar HULIS in complex mixtures.

Acknowledgements

Research at the Universities of Antwerp and Ghent was supported by the Belgian Federal Science Policy Office (contract SD/AT/02A), the Research Foundation – Flanders (FWO) and the Special Research Funds of the Universities of Antwerp and Ghent. The U.S. Environmental Protection Agency through its Office of Research and Development funded and collaborated in the research described here under Contract EP-D-05-065 to Alion Science and Technology. The manuscript has been subjected to external peer review and has been cleared for publication. Mention of trade names or commercial products does not constitute an endorsement or recommendation for use. Jason Surratt was supported in part by the United States Environmental Protection Agency (EPA) under the Science to Achieve Results (STAR) Graduate Fellowship Program. Rafal Szmigielski was supported by a Marie Curie Intra-European fellowship (contract No. 039787-SOAMASS).

REFERENCES

1. Saxena P, Hildemann LM. Water-soluble organics in atmospheric particles: a critical review of the literature

and application of thermodynamics to identify candidate compounds. *Journal of Atmospheric Chemistry* 1996; **24**: 57.

2. Facchini MC, Mircea M, Fuzzi S, Charlson RJ. Cloud albedo enhancement by surface-active organic solutes in growing droplets. *Nature* 1999; **401**: 257.
3. Decesari S, Facchini MC, Fuzzi S, Tagliavini E. Characterization of water-soluble organic compounds in atmospheric aerosol: a new approach. *Journal of Geophysical Research* 2000; **105**: 1481.
4. Subbalakshmi Y, Patti AF, Lee GSH, Hooper MA. Structural characterisation of macromolecular organic material in air particulate matter using Py-GC-MS and solid state ^{13}C-NMR. *Journal of Environmental Monitoring* 2000; **2**: 561.
5. Suzuki Y, Kawamaki M, Akasaka K. ^{1}H NMR application for characterizing water-soluble organic compounds in urban atmospheric particles. *Environmental Science and Technology* 2001; **35**: 2656.
6. Zappoli S, Andracchio A, Fuzzi S, Facchini MC, Gelencsér A, Kiss G, Krivácsy Z, Molnár A, Mészáros E, Hansson HC, Rosman K, Zebühr Y. Inorganic, organic and macromolecular components of fine aerosol in different areas in Europe in relation to their water solubility. *Atmospheric Environment* 1999; **33**: 2733.
7. Gelencsér A, Mészáros T, Blazsó M, Kiss G, Krivácsy Z, Molnár A, Mészáros E. Structural characterization of organic matter in fine tropospheric aerosol by pyrolysis-gas chromatography-mass spectrometry. *Journal of Atmospheric Chemistry* 2000; **37**: 173.
8. Cappiello A, De Simoni E, Fiorucci C, Mangani F, Palma P, Trufelli H, Decesaro S, Facchini MC, Fuzzi S. Molecular characterization of the water-soluble organic compounds in fogwater by ESI-MS/MS. *Environmental Science and Technology* 2003; **37**: 1229.
9. Kiss G, Tombácz E, Varga B, Alsberg T, Persson L. Estimation of the average molecular weight of humic-like substances isolated from fine atmospheric aerosol. *Atmospheric Environment* 2003; **37**: 3783.
10. Romero F, Oehme M. Organosulfates – a new component of humic-like substances in atmospheric aerosols? *Journal of Atmospheric Chemistry* 2005; **52**: 283.
11. Reemtsma T, These A, Venkatachari P, Xia XJ, Hopke PK, Springer A, Linscheid M. Identification of fulvic acids and sulfated and nitrated analogues in atmospheric aerosol by electrospray ionization Fourier transform ion cyclotron resonance mass spectrometry. *Analytical Chemistry* 2006; **78**: 8299.
12. Surratt JD, Kroll JH, Kleindienst TE, Edney EO, Claeys M, Sorooshian A, Ng NL, Offenberg JH, Lewandowski M, Jaoui M, Flagan RC, Seinfeld JH. Evidence for organosulfates in secondary organic aerosol. *Environmental Science and Technology* 2007; **41**: 517.
13. Claeys M, Graham B, Vas G, Wang W, Vermeylen R, Pashynska V, Cafmeyer J, Guyon P, Andreae MO, Artaxo P, Maenhaut W. Formation of secondary organic aerosols through photooxidation of isoprene. *Science* 2004; **303**: 1173.
14. Edney EO, Kleindienst TE, Jaoui M, Lewandowski M, Offenberg JH, Wang W, Claeys M. Formation of 2-methyl tetrols and 2-methylglyceric acid in secondary organic aerosol from laboratory irradiated isoprene/NO_X/SO_2/air mixtures and their detection in ambient PM2.5 samples collected in the eastern United States. *Atmospheric Environment* 2005; **39**: 5281.
15. Surratt JD, Murphy SM, Kroll JH, Ng NL, Hildebrandt L, Sorooshian A, Szmigielski R, Vermeylen R, Maenhaut W, Claeys M, Flagan RC, Seinfeld JH. Chemical composition of secondary organic aerosol formed from the photooxidation of isoprene. *Journal of Physical Chemistry A* 2006; **110**: 9665.
16. Claeys M, Wang W, Ion AC, Kourtchev I, Gelencsér A, Maenhaut W. Formation of secondary organic aerosols from isoprene and its gas-phase oxidation products through reaction with hydrogen peroxide. *Atmospheric Environment* 2004; **38**: 4093.
17. Ocksay R, Salma I, Wang W, Maenhaut W. Characterization and diurnal variation of size-resolved inorganic water-soluble ions at a rural background site. *Journal of Environmental Monitoring* 2006; **8**: 300.
18. Surratt JD, Lewandowski M, Offenberg JH, Jaoui M, Kleindienst TE, Edney EO, Seinfeld JH. Effect of acidity on secondary organic aerosol from isoprene. *Environmental Science and Technology* 2007; **41**: 517.
19. Iinuma Y, Müller C, Böge O, Gnauk T, Herrmann H. The formation of organic sulfate esters in the limonene ozonolysis secondary organic aerosol (SOA) under acidic conditions. *Atmospheric Environment* 2007; doi:10.1016/j.atmosenv.2007.03.007.
20. Iinuma Y, Müller C, Berndt T, Claeys M, Herrmann H. Evidence for organosulfates in secondary organic aerosol from β-pinene ozonolysis and ambient aerosol. *Environmental Science and Technology* 2007; **41**: 6678.
21. Douglas DJ, Frank AJ, Mao D. Linear ion traps in mass spectrometry. *Mass Spectrometry Reviews* 2005; **24**: 1.
22. Claeys M, Szmigielski R, Kourtchev I, Van der Veken P, Vermeylen R, Maenhaut W, Jaoui M, Kleindienst TE, Lewandowski M, Offenberg JH, Edney EO. Hydroxydicarboxylic acids: Markers for secondary organic aerosol from the photooxidation of α-pinene. *Environmental Science and Technology* 2007; **41**: 1628.
23. Szmigielski R, Surratt JD, Vermeylen R, Szmigielska K, Kroll JH, Ng NL, Murphy SM, Sorooshian A, Seinfeld JH, Claeys M. Characterization of 2-methylglyceric acid oligomers in secondary organic aerosol formed from the photooxidation of isoprene using trimethylsilylation and gas chromatography/ion trap mass spectrometry. *Journal of Mass Spectrometry* 2007; **42**: 101.
24. Ion AC, Vermeylen R, Kourtchev I, Cafmeyer J, Chi X, Gelencsér A, Maenhaut W, Claeys M. Polar organic compounds in rural $PM_{2.5}$ aerosols from K-puszta, Hungary, during a 2003 summer field campaign: sources and diel variations. *Atmospheric Chemistry and Physics* 2005; **5**: 1805.
25. Frisch MJ, Trucks GW, Schlegel HB, Scuseria GE, Robb MA, Cheeseman JR, Montgomery JA Jr, Vreven T, Kudin KN, Burant JC, Millam JM, Iyengar SS, Tomasi J, Barone V, Mennucci B, Cossi M, Scalmani G, Rega N, Petersson GA, Nakatsuji H, Hada M, Ehara M, Toyota K, Fukuda R, Hasegawa J, Ishida M, Nakajima T, Honda Y, Kitao O, Nakai H, Klene M, Li X, Knox JE, Hratchian HP, Cross JB, Adamo C, Jaramillo J, Gomperts R, Stratmann RE, Yazyev O, Austin AJ, Cammi R, Pomelli C, Ochterski JW, Ayala PY, Morokuma K, Voth GA, Salvador P, Dannenberg JJ, Zakrzewski VG, Dapprich S, Daniels AD, Strain MC, Farkas O, Malick DK, Rabuck AD, Raghavachari K, Foresman JB, Ortiz JV, Cui Q, Baboul AG, Clifford S, Cioslowski J, Stefanov BB, Liu G, Liashenko A, Piskorz P, Komarom I, Martin RL, Fox DJ, Keith T, Al-Laham MA, Peng CY, Nanayakkara A, Challacombe M, Gill PMW, Johnson B, Chen W, Wong MWC, Gonzalez C, Pople JA. *Gaussian 03, Revision C.02*. Gaussian: Wallingford, 2004.
26. Becke AD. Density-functional thermochemistry 4. A new dynamical correlation functional and implications for exact-exchange mixing. *Journal of Chemical Physics* 1996; **104**: 1040.
27. Gao S, Surratt JD, Knipping EM, Edgerton ES, Shahgholi M, Seinfeld JH. Characterization of polar organic components in fine aerosols in the southeastern United States: identity, origin, and evolution. *Journal of Geophysical Research* 2006; **111**: D14314, doi:10.1029/2005JD006601.
28. Gilbert EE. *Sulfonation and Related Reactions*. Interscience: New York, 1965; 339.
29. Liggio J, Li SM. Organosulfate formation during the uptake of pinonaldehyde on acidic sulfate aerosols. *Geophysical Research Letters* 2006; **33**: L13808, doi:10.1029/2006GL026079.
30. Attygalle AB, Garcia-Rubio S, Ta J, Meinwald J. Collisionally-induced dissociation mass spectra of organic sulfate anions. *Journal of the Chemical Society, Perkin Transactions 2*, 2001; 498.
31. Kawamura K, Ikushima K. Seasonal changes in the distribution of dicarboxylic acids in the urban atmosphere. *Environmental Science and Technology* 1993; **27**: 2227.
32. Kawamura K, Sakaguchi F. Molecular distributions of water soluble dicarboxylic acids in marine aerosols over the

Pacific Ocean including tropics. *Journal of Geophysical Research [Atmospheres]* 1999; **104**: 3501.

33. O'Connor MP, Wenger JC, Mellouki A, Wirtz K, Munoz A. The atmospheric photolysis of E-2-hexenal, Z-3-hexenal and E,E-2,4-hexadienal. *Physical Chemistry Chemical Physics* 2006; **8**: 5236.
34. Hatanaka A. The biogeneration of green odour by green leaves. *Phytochemistry* 1993; **34**: 1201.
35. Matsunaga SN, Guenther AB, Izawa Y, Wiedinmyer C, Greenberg JP, Kawamura K. Importance of wet precipitation as a removal and transport process for atmospheric water soluble carbonyls. *Atmospheric Environment* 2007; **41**: 790.
36. MacCarthy P, Bloom PR, Clapp CE, Malcolm RL. Humic substances in soil and crop sciences: an overview. *Humic Substances in Soil and Crop Sciences: Selected Readings*. American Society of Agronomy: Madison, 1990; 261.

DOI: 10.1002/jms

Appendix D

Secondary Organic Aerosol (SOA) Formation from Reaction of Isoprene with Nitrate Radicals (NO_3)*

---

*This chapter is reproduced by permission from "Secondary Organic Aerosol (SOA) Formation from Reaction of Isoprene with Nitrate Radicals (NO_3)" by Nga L. Ng, Alan J. Kwan, Jason D. Surratt, Arthur W. H. Chan, Puneet S. Chhabra, Armin Sorooshian, Havala O. T. Pye, John D. Crounse, Paul O. Wennberg, Richard C. Flagan, and John H. Seinfeld, *Atmospheric Chemistry and Physics*, 8 (14), 4117–4140, 2008. Copyright 2008 by Authors. This work is licensed under a Creative Commons License.

Atmos. Chem. Phys., 8, 4117–4140, 2008
www.atmos-chem-phys.net/8/4117/2008/

Atmospheric
Chemistry
and Physics

Secondary organic aerosol (SOA) formation from reaction of isoprene with nitrate radicals (NO_3)

N. L. Ng[1], **A. J. Kwan**[2], **J. D. Surratt**[1], **A. W. H. Chan**[1], **P. S. Chhabra**[1], **A. Sorooshian**[1], **H. O. T. Pye**[1], **J. D. Crounse**[1], **P. O. Wennberg**[2,3], **R. C. Flagan**[1,2], **and J. H. Seinfeld**[1,2]

[1]Division of Chemistry and Chemical Engineering, California Institute of Technology, Pasadena, CA 91125, USA
[2]Division of Engineering and Applied Science, California Institute of Technology, Pasadena, CA 91125, USA
[3]Division of Geological and Planetary Sciences, California Institute of Technology, Pasadena, CA 91125, USA

Received: 3 January 2008 – Published in Atmos. Chem. Phys. Discuss.: 15 February 2008
Revised: 3 July 2008 – Accepted: 3 July 2008 – Published: 1 August 2008

Abstract. Secondary organic aerosol (SOA) formation from the reaction of isoprene with nitrate radicals (NO_3) is investigated in the Caltech indoor chambers. Experiments are performed in the dark and under dry conditions (RH$<$10%) using N_2O_5 as a source of NO_3 radicals. For an initial isoprene concentration of 18.4 to 101.6 ppb, the SOA yield (defined as the ratio of the mass of organic aerosol formed to the mass of parent hydrocarbon reacted) ranges from 4.3% to 23.8%. By examining the time evolutions of gas-phase intermediate products and aerosol volume in real time, we are able to constrain the chemistry that leads to the formation of low-volatility products. Although the formation of ROOR from the reaction of two peroxy radicals (RO_2) has generally been considered as a minor channel, based on the gas-phase and aerosol-phase data it appears that RO_2+RO_2 reaction (self reaction or cross-reaction) in the gas phase yielding ROOR products is a dominant SOA formation pathway. A wide array of organic nitrates and peroxides are identified in the aerosol formed and mechanisms for SOA formation are proposed. Using a uniform SOA yield of 10% (corresponding to $M_o \cong 10\,\mu g\,m^{-3}$), it is estimated that ~2 to 3 Tg yr^{-1} of SOA results from isoprene+NO_3. The extent to which the results from this study can be applied to conditions in the atmosphere depends on the fate of peroxy radicals in the nighttime troposphere.

1 Introduction

Isoprene is the most abundant non-methane hydrocarbon emitted into the atmosphere with a global emission of ~500 Tg yr^{-1} (Guenther et al., 1995; Guenther et al., 2006). In the troposphere, isoprene reacts with hydroxyl radicals (OH), ozone (O_3), and nitrate radicals (NO_3). Owing to its high concentration and reactivity with OH radicals, isoprene plays an important role in the photochemistry occurring within the atmospheric boundary layer. Recently, it has been shown that the photooxidation of isoprene leads to the formation of low volatility species that condense to form SOA (Claeys et al., 2004; Edney et al., 2005; Kroll et al., 2005; Dommen et al., 2006; Kroll et al., 2006; Surratt et al., 2006); SOA yields as high as ~3% have been observed (Kroll et al., 2005; Kroll et al., 2006). Global SOA production from isoprene photooxidation has been estimated to be about 13 Tg yr^{-1} (Henze et al., 2007).

Although emission of isoprene from vegetation is triggered by sunlight and increases with light intensity and temperature (e.g. Sharkey et al., 1996), the isoprene mixing ratio has been observed to peak in early evening in several field studies, with a measured mixing ratio up to a few ppb (Curren et al., 1998; Starn et al., 1998; Stroud et al., 2002; Steinbacher et al., 2005). After sunset, the isoprene mixing ratio drops rapidly, and it has been suggested that the reaction with nitrate radicals, NO_3, is a major contributor to isoprene decay at night (Curren et al., 1998; Starn et al., 1998; Stroud et al., 2002; Steinbacher et al., 2005). Typical NO_3 radical mixing ratios in boundary layer continental air masses range between ~10 to ~100 ppt (Platt and Janssen, 1995; Smith et al., 1995; Heintz et al., 1996; Carslaw et al., 1997). However, concentrations as high as

---

Correspondence to: J. H. Seinfeld
(seinfeld@caltech.edu)

several hundred ppt have been observed over northeastern USA and Europe (Platt et al., 1981; von Friedeburg et al., 2002; Brown et al., 2006; Penkett et al., 2007). Given the rapid reaction rate between isoprene and NO_3 radicals (k_{NO_3}=7×10^{-13} cm^3 molecule^{-1} s^{-1} at T=298 K, IUPAC), it is likely that NO_3 radicals play a major role in the nighttime chemistry of isoprene.

The kinetics and gas-phase products of the isoprene-NO_3 reaction have been the subject of several laboratory and theoretical studies (Jay and Stieglitz, 1989; Barnes et al., 1990; Skov et al., 1992; Kwok et al., 1996; Berndt and Böge, 1997; Suh et al., 2001; Zhang et al., 2002; Fan et al., 2004). In many studies, C_5-nitrooxycarbonyl is identified as the major first-generation gas-phase reaction product (Jay and Stieglitz, 1989; Skov et al., 1992; Kwok et al., 1996; Berndt and Böge, 1997). Other compounds such as C_5-hydroxynitrate, C_5-nitrooxyhydroperoxide, and C_5-hydroxycarbonyl have also been identified (Kwok et al., 1996); C_5-hydroxynitrate has also been measured in ambient air with concentrations in the lower ppt range at a few ng m^{-3} (Werner et al., 1999). According to the experimental study by Barnes et al. (1990), the yield for nitrate-containing compounds from the reaction of isoprene and NO_3 radicals can be as high as 80%. A recent modeling study in conjunction with observations from the ICARTT field campaign suggests that ~50% of the total isoprene nitrates production occurs via reaction of isoprene and NO_3 radicals (Horowitz et al., 2007).

Little is known beyond the formation of the first-generation products of the reaction of NO_3 with isoprene. The isoprene nitrates and other first-generation products still contain a double bond, and it is likely that the further oxidation of these species will lead to low volatility products that can contribute to SOA formation at nighttime.

In this work, SOA formation from the reaction of isoprene with NO_3 radicals is investigated. Laboratory chamber experiments are performed in the dark using N_2O_5 as a source of NO_3 radicals. Aerosol yields are obtained over a range of initial isoprene concentrations (mixing ratios). By examining the time evolutions of aerosol volume and different intermediate gas-phase products, we are able to constrain the chemistry that leads to the formation of low-volatility products. Mechanisms for SOA formation are proposed and chemical composition data of the SOA formed are also presented.

2 Experimental section

Experiments are carried out in the Caltech dual 28 m^3 Teflon chambers. A detailed description of the facility is provided elsewhere (Cocker et al., 2001; Keywood et al., 2004). Before each experiment, the chambers are flushed continuously for over 24 h. Aerosol number concentration, size distribution, and volume concentration are measured by a Differential Mobility Analyzer (DMA, TSI model 3081) coupled with a condensation nucleus counter (TSI model 3760). All aerosol growth data are corrected for wall loss, in which size-dependent particle loss coefficients are determined from inert particle wall loss experiments (Keywood et al., 2004). Temperature, relative humidity (RH), O_3, NO, and NO_x are continuously monitored. Experiments are performed in the dark at room temperature (20–21°C) and under dry conditions (RH$<$10%).

In most experiments, seed aerosols are introduced into the chamber to act as a substrate onto which the gas-phase products may condense. Seed aerosols are generated by atomizing an aqueous solution with a constant-rate atomizer. The seed solution consists of 0.015 M $(NH_4)_2SO_4$. In a few experiments, acidic seed is used, consisting of 0.03 M $MgSO_4$ and 0.05 M H_2SO_4. The initial particle number concentration is ~20 000 particles cm^{-3}, with a geometric mean diameter of ~50 nm. The initial seed volume is 10–12 μm^3 cm^{-3}. In some experiments, no seed particles are added and aerosols are formed via nucleation. After introduction of the seed aerosols (in seeded experiments), a known volume of isoprene (Aldrich, 99%) is injected into a glass bulb and introduced into the chamber by an air stream. The mixing ratio of isoprene is monitored with a gas chromatograph equipped with a flame ionization detector (GC-FID, Agilent model 6890N). The column used is a bonded polystyrene-divinylbenzene based column (HP-PLOT Q, 15 m×0.53 mm, 40 μm thickness, J&W Scientific). The oven temperature is held at 60°C for 0.5 min, ramped at 35°C min^{-1} to 200°C, and held constant for 3.5 min.

The thermal decomposition of N_2O_5 serves as a source of NO_3 radicals in these experiments. N_2O_5 is prepared and collected offline by mixing a stream of nitric oxide ($\geq$99.5%, Matheson Tri Gas) with a stream of ozone in a glass bulb (Davidson et al., 1978):

$$NO + O_3 \rightarrow NO_2 + O_2 \quad (1)$$

$$NO_2 + O_3 \rightarrow NO_3 + O_2 \quad (2)$$

$$NO_2 + NO_3 \leftrightarrow N_2O_5 \quad (3)$$

Ozone is generated by flowing oxygen through an ozonizer (OREC model V10-0, Phoenix, AZ) at ~1 L min^{-1}. The mixing ratio of ozone is measured by a UV/VIS spectrometer (Hewlett Packard model 8453) to be ~2%. The flow rate of nitric oxide into the glass bulb is adjusted until the brown color in the bulb disappears. The N_2O_5 is trapped for 2 h in an acetone-dry ice bath (approximately at –80°C; cold enough to trap N_2O_5 but not O_3, as condensed O_3 can explode upon warming and is extremely dangerous) as a white solid, and stored between experiments under liquid nitrogen temperature. Once the seed and isoprene concentrations in the chamber stabilize, reaction is initiated by vaporizing N_2O_5 into an evacuated 500 mL glass bulb and introduced into the chamber with an air stream of 5 L min^{-1}.

The amount of N_2O_5 injected is estimated based on the vapor pressure in the glass bulb, which is measured using a capacitance manometer (MKS); this amount corresponds to an initial mixing ratio of ∼1 ppm in the chamber. The thermal decomposition of N_2O_5 forms NO_2 and NO_3 radicals. Impurities in the N_2O_5 starting material are quantified by FTIR spectroscopy (Nicolet model Magna 550). N_2O_5 is vaporized into an evacuated pyrex cell (18 cm in length and 300 cm^3) with CaF_2 windows. Spectra are collected immediately upon addition over the 1000 cm^{-1} to 4000 cm^{-1} window allowing for quantification of NO_2 (1616 cm^{-1} band) and HNO_3 (3550 cm^{-1} band) impurities.

A custom-modified Varian 1200 Chemical Ionization Mass Spectrometer (CIMS) is used to continuously monitor the concentrations of various gas-phase intermediates and products over the course of the experiments. The CIMS instrument is operated mainly in negative mode using CF_3O^- as a reagent ion, which selectively clusters with compounds having high fluorine affinity (e.g., acidic compounds and many hydroxy- and nitrooxy- carbonyls), forming ions at m/z MW+85. In some experiments, the CIMS instrument is also operated in the positive mode using H_2O as a reagent ion forming ions at m/z MW+1. The ionization schemes are as follows:

Negative chemical ionization: $CF_3O^- + HB \text{–>} CF_3O^- \cdot HB$
Positive chemical ionization: $H_3O^+ + D \text{–>} D \cdot H^+ + H_2O$ (where D has a proton affinity $>H_2O$)

The term "product ion" is used throughout this manuscript to describe the ionized products formed through the above chemical reaction schemes. Typically, we scan from m/z 50 to 400. More details about the CIMS technique are given in Crounse et al. (2006) and Ng et al. (2007a). Because authentic standards are not available for the major products, sensitivities are not experimentally determined. We estimate the collision rate of CF_3O^- with these products (which determines the sensitivity) with the empirical method of Su and Chesnavich (1982), which bases its predictions on an analyte's dipole moment and polarizability. Dipole moments and polarizabilities are calculated with the Spartan06 quantum package, and are based on molecular structures optimized with the B3LYP/6-31G(d) method. Further details on estimating CIMS sensitivities based on quantum calculations are described in Paulot et al. (2008). As isomers would have different polarities and hence different sensitivities, in estimating the concentrations it is assumed that the NO_3 attack at C_1-position to C_4-position is 5.5:1 (See Sect. 4.1).

Aerosol physical and chemical properties are monitored by many instruments. Real-time particle mass spectra are obtained with an Aerodyne quadrupole Aerosol Mass Spectrometer (Q-AMS) (Jayne et al., 2000). A Particle-Into-Liquid Sampler (PILS, Brechtel Manufacturing, Inc.) coupled with ion chromatography (IC) is employed for quantitative measurements of water-soluble ions in the aerosol phase (Sorooshian et al., 2006). Duplicate Teflon filters (PALL Life Sciences, 47-mm diameter, 1.0-μm pore size, teflo membrane) are collected from a selected number of experiments for offline chemical analysis. Filter sampling is initiated when the aerosol volume reaches its maximum value. Depending on the total volume concentration of aerosol in the chamber, the filter sampling time is 2–4 h, which results in ∼2–5 m^3 of total chamber air sampled. Teflon filters used for high-resolution electrospray ionization-time-of-flight mass spectrometry (ESI-TOFMS) analysis are extracted in 5 mL of high-purity methanol (LC-MS CHROMASOLV-Grade, Sigma-Aldrich) by 45 min of sonication. Methanol sample extracts are then blown dry under a gentle N_2 stream (without added heat) once the filters are removed and archived at –20°C. Dried residues are then reconstituted with 500 mL of a 1:1 (v/v) solvent mixture of 0.1% acetic acid in water (LC-MS CHROMASOLV-Grade, Sigma-Aldrich) and 0.1% acetic acid in methanol (LC-MS CHROMASOLV-Grade, Sigma Aldrich). All resultant filter extracts are analyzed by a Waters ACQUITY ultra performance liquid chromatography (UPLC) system, coupled to a Waters LCT Premier XT time-of-flight mass spectrometer (TOFMS) equipped with an ESI source that is operated in the negative (–) ionization mode. Detailed operating conditions for the UPLC/(–)ESI-TOFMS instrument have been described previously (Ng et al., 2007a). A Waters ACQUITY UPLC HSS column is selected to separate the SOA components because of its increased retention of water-soluble polar organics; separation is achieved as a result of trifunctionally-bonded (T3) C_{18} alkyl residues on this column, which prevent stationary phase collapse when a 100% aqueous mobile phase is used and result in better retention of water-soluble polar organic compounds. In addition to the UPLC/(–)ESI-TOFMS analysis, all remaining Teflon filters are extracted and analyzed for total peroxide content (sum of ROOR and ROOH) by using an iodometric-spectroscopic method (Docherty et al., 2005; Surratt et al., 2006).

To study the mechanism of SOA formation, in several experiments the experimental protocols are slightly modified: (1) An excess amount of isoprene (relative to N_2O_5 concentration) is injected into the chamber to prevent the further reaction of first-generation gas-phase products, allowing these products to be detected more readily; (2) After the addition of isoprene, pulses of N_2O_5 are introduced into the chamber to study the evolution of different intermediate gas-phase products; (3) With isoprene well mixed in the chamber, N_2O_5 is introduced slowly to maximize the self-reaction of peroxy radicals (see Sect. 4.2). This is achieved by first injecting N_2O_5 into a 65 L Teflon bag; then an air stream of 1 L min^{-1} is passed through the Teflon bag to introduce N_2O_5 into the chamber over a 7 h period. We refer to this as the "slow N_2O_5 injection experiment"; and (4) With N_2O_5 well mixed in the chamber, isoprene is introduced slowly to maximize the reaction between peroxy radicals and nitrate radicals (see Sect. 4.2). This is achieved by first injecting isoprene into a

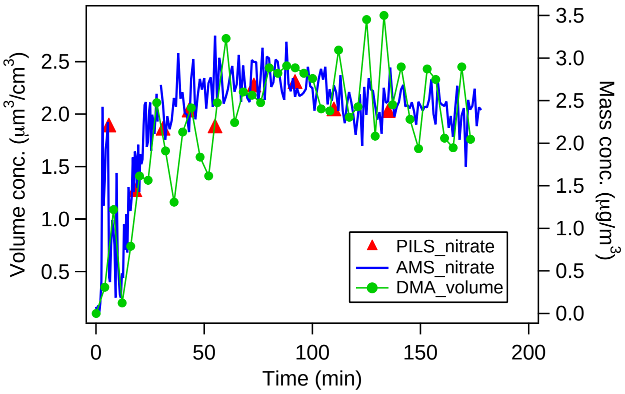

Fig. 1. Time profiles of aerosol volume, inorganic nitrate measured by PILS/IC, and nitrate signals from Q-AMS in a blank experiment (~1 ppm N_2O_5, ammonium sulfate seed, no isoprene).

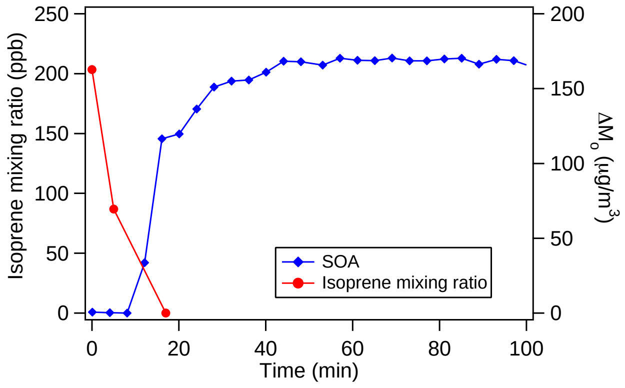

Fig. 2. Reaction profile of the oxidation of an initial mixture containing 203.4 ppb isoprene (573 μg/m^3).

65 L Teflon bag, and then introduced into the chamber with an air stream of 1 L min^{-1} for 7 h. We refer to this as the "slow isoprene injection experiment".

Experimental conditions and results are given in Table 1. In calculating SOA yield (defined as the ratio of the organic aerosol mass formed to the mass of parent hydrocarbon reacted), knowledge of the SOA density is required. By comparing volume distributions from the DMA and mass distributions from the Q-AMS, the effective density for the SOA formed can be estimated (Bahreini et al., 2005; Alfarra et al., 2006).

3 Results

3.1 Blank experiments

Blank experiments are performed to ensure that the aerosol growth observed is from the reaction of isoprene with NO_3 radicals. In these experiments, ~1 ppm N_2O_5 is introduced into chamber after the addition of ammonium sulfate seed aerosol (with no isoprene present). As shown in Fig. 1, aerosol volume increases by ~2 μm^3 cm^{-3} within an hour after the introduction of N_2O_5. About 2.5 μg m^{-3} of inorganic nitrate is measured by PILS/IC, which agrees well with the amount of nitrates detected by Q-AMS. FTIR analysis indicates the presence of ~10% HNO_3 and 4% NO_2 impurity in the N_2O_5 prepared, thus the nitrates measured by PILS/IC and Q-AMS likely arise from the partitioning or reactive uptake of gas-phase HNO_3 into the aerosol phase, or HNO_3 produced from heterogeneous hydrolysis of N_2O_5. As in the Q-AMS analysis, no organic species are detected in the filter samples collected from these blank experiments.

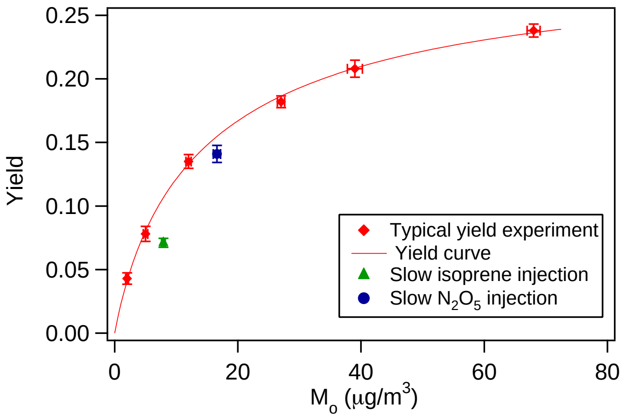

Fig. 3. SOA yield data and yield curve for isoprene-NO_3 reaction. Also shown are SOA yields from the slow N_2O_5 injection experiment and slow isoprene injection experiment.

3.2 Aerosol yields

A series of experiments with different initial isoprene concentrations are carried out (these are referred to as "typical yield experiments" hereafter). The initial isoprene concentration ranged from 18.4 to 203.4 ppb. Figure 2 shows the reaction profile of the oxidation of an initial mixture containing 203.4 ppb isoprene. Since the chamber is NO_x-free at the beginning of the experiment, once N_2O_5 is introduced into the chamber the equilibrium in Reaction (3) favors the formation of NO_3. This generates a relatively high concentration of NO_3 radicals and results in rapid isoprene decay. Aerosol growth is observed and aerosol volume continues to increase even after all the isoprene is consumed. Owing to the rapid isoprene decay and the relatively long time between each GC measurement (12 min), the isoprene decay over time is captured only in experiments in which the initial isoprene concentration is >100 ppb. Based on the observed isoprene decay in these experiments and the isoprene-NO_3 rate constant k_{NO_3}, the average NO_3 concentration in the chamber is estimated to be ~140 ppt.

Table 1. Initial conditions and results for yield experiments.

Date	T (K)	RH (%)	ΔHC (ppb)[a]	ΔM_o (μg/m^3)[b]	SOA Yield (%)
8/9/07	294	5.1	101.6± 0.6	68.1± 1.1	23.8± 0.5
8/10/07	293	4.7	30.2± 0.1	11.5± 0.4	13.5± 0.5
8/11/07	294	5.4	67.1± 0.1	39.3± 1.2	20.8± 0.7
8/12/07	293	6.0	51.7± 0.2	26.7± 0.6	18.2± 0.5
8/13/07	294	5.7	18.4± 0.1	2.2± 0.2	4.3± 0.5
8/14/07	294	5.5	21.8± 0.1	4.8± 0.4	7.8± 0.6
10/4/2007[c]	293	5.5	39.5± 0.1[d]	7.9± 0.3	7.1± 0.6
10/25/2007[e]	294	6.4	42.0± 0.1	16.6± 0.6	14.1± 0.7

[a] Stated uncertainties (1σ) are from scatter in isoprene measurements.
[b] Stated uncertainties (1σ) are from scatter in particle volume measurements.
[c] Slow isoprene injection experiment.
[d] Concentration estimated based on a separate calibration experiment (see Sect. 3.2); the uncertainty in the measured isoprene concentration is assumed to be the same as in the slow N_2O_5 injection experiment.
[e] Slow N_2O_5 injection experiment.

The SOA yield of each experiment (Table 1) is shown in Fig. 3. The density of the SOA is determined to be 1.42 g cm^{-3}. The amount of inorganic nitrate detected by PILS/IC in each experiment ranges from 1.6 to 2.6 $\mu g\,m^{-3}$, which is approximately equal to that measured in the blank experiments. In calculating SOA yield, the organic aerosol mass is corrected for the amount of inorganic nitrate measured in each experiment. For convenience, SOA yields can be parameterized by a semi-empirical model based on absorptive gas-particle partitioning of two semivolatile products (Odum et al., 1996, 1997a,b):

$$Y = \Delta M_o \left[\frac{\alpha_1 K_{om,1}}{1 + K_{om,1} M_o} + \frac{\alpha_2 K_{om,2}}{1 + K_{om,2} M_o} \right] \quad (4)$$

in which Y is the aerosol yield, ΔM_o is the organic aerosol mass produced, M_o is the organic aerosol mass present (equal to ΔM_o in chamber experiments with no absorbing organic mass present initially), α_i is the mass-based gas-phase stoichiometric fraction for semivolatile species i, and $K_{om,i}$ is the gas-particle partitioning coefficient for species i. With this two-product model, Eq. (4) is fit to the experimental yield data (data with $\Delta M_o < 100\,\mu g\,m^{-3}$) and the yield parameters obtained are: α_1=0.089, α_2=0.203, $K_{om,1}$=0.182 $m^3\,\mu g^{-1}$, and $K_{om,2}$=0.046 $m^3\,\mu g^{-1}$. For an organic aerosol mass of ~10 $\mu g\,m^{-3}$, the aerosol yield is ~10%.

Also shown in Fig. 3 are aerosol yields from the slow isoprene/N_2O_5 injection experiments. Since the PILS/IC is not employed in these experiments, in calculating SOA yields it is assumed that the amount of inorganic nitrate formed in these slow injection experiments is roughly the same as that in other experiments. For the slow isoprene injection experiment, no isoprene is observed by GC-FID, indicating that once the isoprene enters the chamber, it is quickly consumed by reaction with NO_3. The time profile of isoprene injection is obtained in a separate experiment, in which the same amount of isoprene is added into the chamber without N_2O_5 present. Assuming the amount of isoprene injected into the chamber is the same as the isoprene reacted, the amount of isoprene reacted over the course of the slow isoprene experiment can be deduced. As seen in Fig. 3, the SOA yield from the slow N_2O_5 injection experiment is roughly the same as those in the other yield experiments; the yield from the slow isoprene injection experiment, however, is lower.

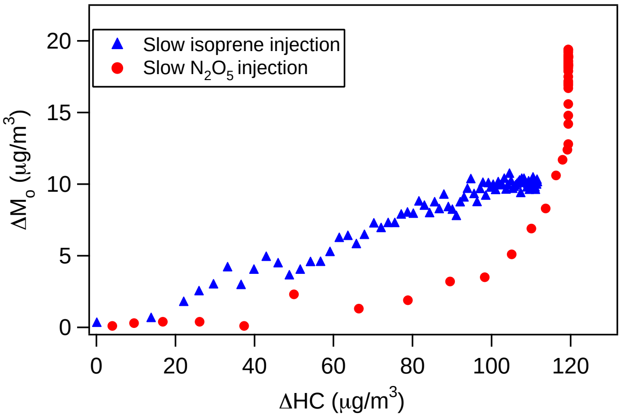

Fig. 4. Time-dependent growth curves for the slow N_2O_5 injection experiment and slow isoprene injection experiment (last two experiments in Table 1).

The time-dependent "growth curves" (organic aerosol, $\Delta M_{o,}$ as a function of hydrocarbon reacted, ΔHC) over the course of the slow N_2O_5 injection experiment and the slow isoprene injection experiment are shown in Fig. 4. As hydrocarbon measurements are made with a lower frequency than particle volume, the isoprene concentrations shown are obtained by interpolating GC-FID measurements. In both

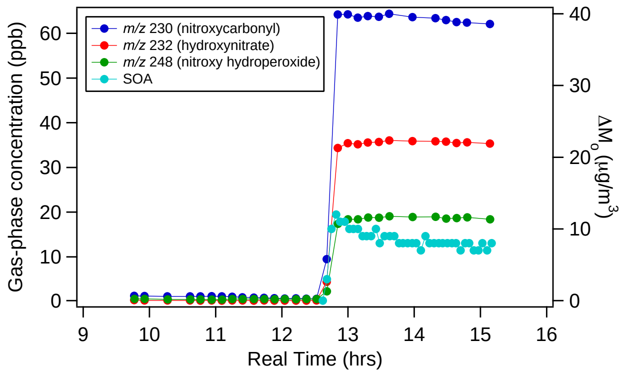

Fig. 5. Time profiles of the major gas-phase products (m/z 230, 232, and 248) and the corresponding aerosol growth from the excess isoprene experiment.

experiments about 40 ppb of isoprene is consumed, the only difference being the order of isoprene/N_2O_5 injection. From Fig. 4 it is clear that as the reaction proceeds, more aerosol is formed in the slow isoprene injection experiment for the same amount of isoprene reacted. However, the final SOA yield under the slow N_2O_5 injection conditions is higher due to continued aerosol formation even after the complete consumption of isoprene. The presence of a "hook" at the end of the growth curve for the slow N_2O_5 injection experiment indicates that further reactions are contributing to aerosol growth after isoprene is consumed (Ng et al., 2006). Higher generation products also contribute to the aerosols formed in the slow isoprene injection experiment; however, their contributions are not readily observed in the growth curve owing to the way the experiment is conducted. This is further discussed in Sect. 4.3.

3.3 Gas-phase measurements

The CIMS technique measures the concentrations of different gas-phase products over the course of the experiments. A series of experiments is carried out to study the mechanisms of SOA formation by varying the relative amount of isoprene and N_2O_5 injected and monitoring the time evolution of the intermediate products. Shown in Fig. 5 are the time profiles of three major gas-phase products and the corresponding aerosol growth from the excess isoprene experiment. In this experiment, ~120 ppb of N_2O_5 is first injected into the chamber, followed by the introduction of ~800 ppb isoprene. The initial concentration of isoprene is estimated based on the volume of the isoprene injected and the chamber volume. Once isoprene is injected, a number of product ions are formed immediately, with m/z 230, 232, and 248 being the most dominant ones. Several minor product ions at m/z 185, 377, and 393 are also observed (not shown). With the presence of excess isoprene, it is expected that the three major products detected are first-generation products. Their further reaction is suppressed, as indicated by the relatively constant concentrations of the product ions once they are formed. At the end of the experiment, 725 ppb of isoprene is measured by GC-FID. A small amount of aerosol is formed instantaneously, likely from the condensation of relatively nonvolatile first-generation products, or from further generation products that are formed at a relatively rapid rate.

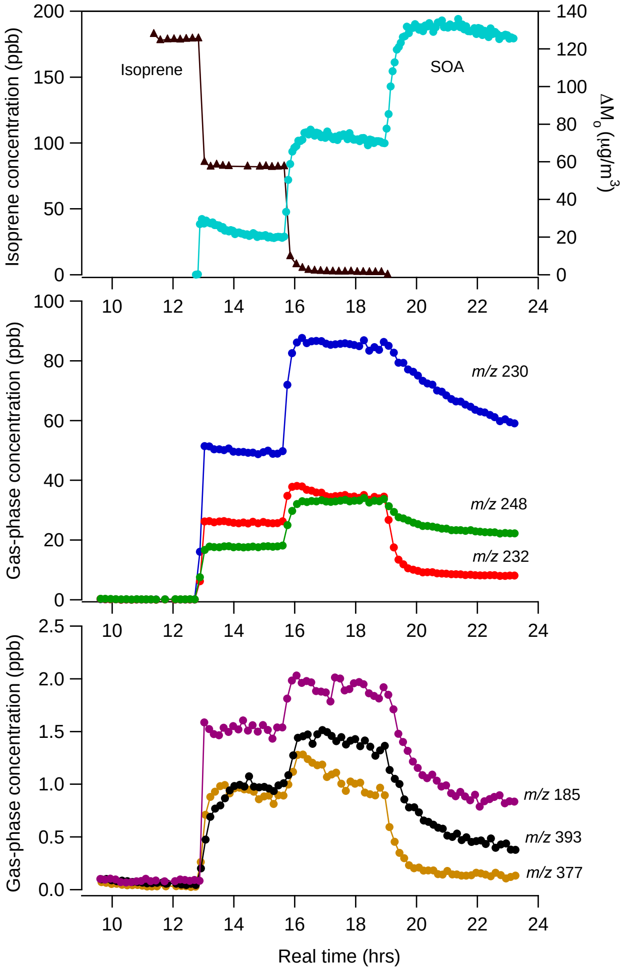

Fig. 6. Time evolution of various gas-phase products in the staggered N_2O_5 injection experiment (Isoprene is first injected into the chamber, followed by the addition of 3 pulses of N_2O_5: ~120, 50, and 210 ppb). The top panel shows the isoprene decay and aerosol formation; the middle panel shows the time profiles of the three major first-generation products (m/z 230, 232, and 248); the bottom panel shows the time profiles of three minor products (m/z 185, 377, and 393). (The likely identities for these products are shown in Fig. 11).

To study further the evolution of the gas-phase products, an experiment is performed in which pulses of N_2O_5 are introduced into the chamber (with isoprene present) (Fig. 6). The top panel shows the isoprene decay and aerosol formation; the middle panel shows the time profiles of the three major first-generation products (m/z 230, 232, and 248); the

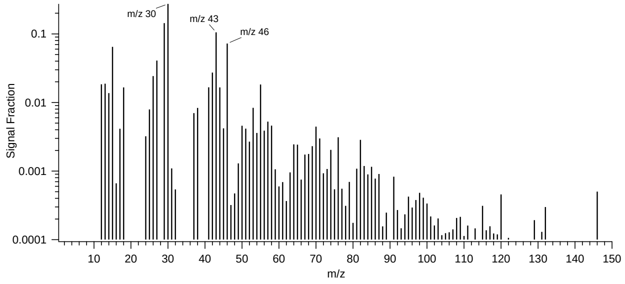

Fig. 7. A typical AMS spectrum for SOA formed in typical yield experiments.

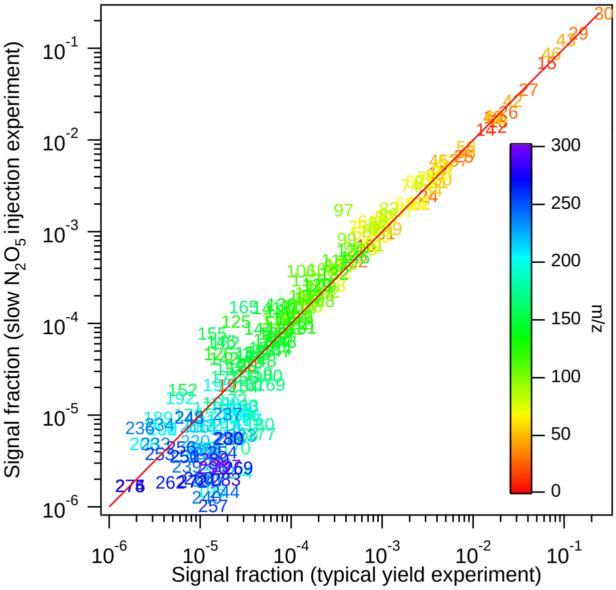

Fig. 8. AMS spectra signal from the slow N_2O_5 injection experiment versus a typical yield experiment. Each mass fragment is normalized by the total signal. The solid red line is the 1:1 line. Note that the higher masses (m/z>165) are dominated by noise.

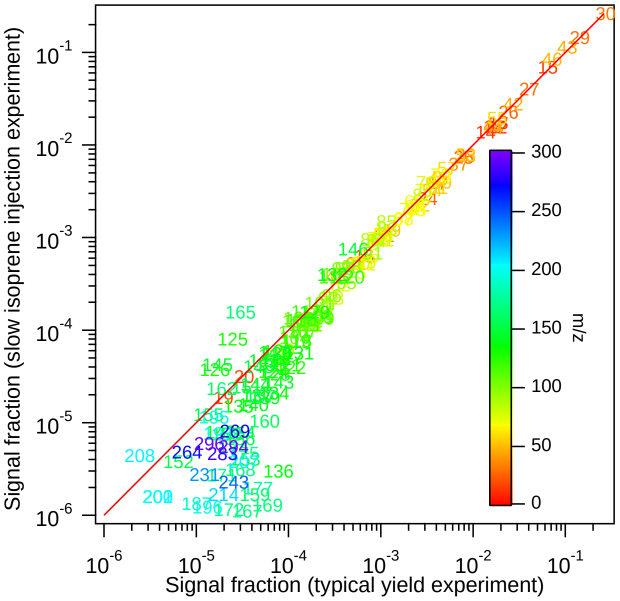

Fig. 9. AMS spectra signal from the slow isoprene injection experiment versus a typical yield experiment. Each mass fragment is normalized by the total signal. The solid red line is the 1:1 line. Note that the higher masses (m/z>165) are dominated by noise.

bottom panel shows the time profiles of three minor products (m/z 185, 377, and 393). In this experiment, 179 ppb of isoprene is first injected into the chamber, followed by the addition of 3 pulses of N_2O_5 (∼120, 50, 210 ppb). The observations after the addition of the first pulse of N_2O_5 are similar to the excess isoprene experiment described above. With the addition of ∼120 ppb N_2O_5, 97 ppb of isoprene is reacted away, m/z 230, 232, and 248 are formed with concentrations of 49.8 ppb, 26.1 ppb, and 17.3 ppb, respectively. Because of the lack of authentic standards, the concentrations are uncertain. Similar to the data in Fig. 5, the concentrations of these product ions stay relatively constant owing to the presence of excess isoprene. The minor products at m/z 185, 377, and 393, are formed with the concentrations 1.4 ppb, 0.9 ppb, and 0.9 ppb, respectively. Because the sum of the ion concentrations derived from our estimated sensitivities is equal to the reacted isoprene, our estimated sensitivity must represent a lower limit for the actual sensitivity of the CIMS technique to these compounds. It is noted that the m/z 393 ion is formed with a relatively slower rate than all other product ions. A small amount of aerosol is observed. At t=15:40, a second pulse of N_2O_5 (∼50 ppb) is introduced into the chamber and the remaining 82 ppb isoprene is completely consumed. As seen from Fig. 6, the concentrations of all intermediate products increase accordingly and more aerosol is produced. The last pulse of N_2O_5 (∼210 ppb) is added at t=19:00. Since all isoprene has been consumed, the additional NO_3 radicals react mainly with the first-generation products, as indicated by the decay of m/z 230, 232, and 248, 185, 377, and 393 ions. Of all of the observed products, it appears that m/z 232 and 377 ions are the most reactive with NO_3 radicals, and their decays in excess NO_3 are strongly correlated with aerosol growth. The rest of the product ions display relatively slower decay kinetics. The decay of the major product ion at m/z 230 does not appear to correlate with aerosol growth, as the concentration of the m/z 230 ion continues to decrease throughout the experiment but there is no further aerosol growth. Since the CIMS instrument has only 0.5 AMU resolution and it cannot distinguish products of similar or identical molecular weight, it is likely that many of observed ions comprise isomers formed from the NO_3 attack at different positions. The fact that many of the observed product ions show two distinct decay time scales indicates that these isomers have substantially different reactivity towards NO_3 radicals.

3.4 Chemical composition of SOA

3.4.1 Aerosol Mass Spectrometer (Q-AMS) measurements

Figure 7 shows the AMS spectrum of SOA formed in the typical yield experiments. Each mass fragment is normalized by the total signal. The SOA exhibits relatively high signals at m/z 30, 43, and 46. The signals at m/z 30 and 46 likely correspond to NO^+(30) and NO_2^+(46) fragments from the nitrates in the aerosol. The spectrum shown in Fig. 7 is obtained when aerosol volume reaches its maximum value; the spectrum obtained several hours after aerosol volume peaks shows minimal changes in the mass fractions of different fragments, indicating that the aerosol composition is not changing significantly over time.

Figure 8 shows the mass spectrum of the slow N_2O_5 injection experiment versus a typical yield experiment; Fig. 9 shows the mass spectrum of the slow isoprene injection experiment versus a typical yield experiment. As shown in both figures, the mass fragments fall on the 1:1 line, suggesting a similar SOA composition under the three different experimental conditions. At higher mass to charge ratios the plots drift below the one-to-one line and it appears that the typical experiments have stronger signals at higher m/z's. However, the signals at these masses ($>$165) are strongly dominated by noise and cannot be interpreted as differences between the spectra.

3.4.2 Offline chemical analysis

Figure 10 shows the representative UPLC/(–)ESI-TOFMS base peak ion chromatograms (BPCs) for different types of experiments conducted. The numbers denoted above the selected chromatographic peaks correspond to the most abundant negative ions observed in their respective mass spectra. Comparison of the BPCs shown in Fig. 10 indicates that the compositions of the SOA are quite similar for the typical yield experiment, slow isoprene injection experiment, and the acid seed experiment, suggesting a common SOA formation pathway. The SOA composition from the excess isoprene experiment, however, is different from these experiments. This will be discussed further in Sect. 4.4.

Accurate mass measurements for all ions observed by the UPLC/(–)ESI-TOFMS technique for a typical yield experiment are listed in Table 2. The error between the measured mass and theoretical mass is reported in two different ways, ppm and mDa. Overall, the error between the measured and theoretical masses is found to be less than $\pm$2 mDa and $\pm$5 ppm, allowing for generally unambiguous identification of molecular formulae. None of the listed ions is observed in solvent blanks and control filters. By combining the elemental SOA composition (i.e. TOFMS suggested ion formula) data and the gas-phase data from CIMS, structures for each of the SOA components are also proposed. As shown in Table 2, the types of compounds formed included nitrooxy-organic acids, hydroxynitrates, nitrooxy-organic peroxides (e.g. nitrooxy-hydroxyperoxides), and nitrooxy-organosulfates. It should be noted that the data presented in Table 2 are also applicable to all other types of experiments conducted in this study; however, none of the organosulfates are observed in the nucleation experiments, consistent with previous work (Liggio et al., 2005; Liggio et al., 2006; Surratt et al., 2007a,b; Iinuma et al., 2007a,b). Surprisingly, previously characterized organosulfates of the 2-methyltetrols and the 2-methyltetrol mono-nitrates detected at m/z 215 and m/z 260 (not listed in Table 2), respectively, which are produced from the photooxidation of isoprene in the presence of acidified sulfate seed aerosol (Surratt et al., 2007a,b; Gómez-González et al., 2007), are also observed in the acid seed experiment shown in Fig. 10, suggesting that nighttime oxidation of isoprene in the presence of acidic seed may also be a viable pathway for these known ambient tracer compounds.

Owing to the implementation of reverse-phase chromatography, the SOA components that are more hydrophilic elute from the column the earliest, while the more hydrophobic components elute the latest. It is clear from Table 2 that compounds with the same carbon number and general functionality (i.e. carboxylic acid, alcohol, or organosulfate), but differing number of nitrooxy groups, exhibit distinctly different chromatographic behaviors. The presence of more nitrooxy groups appears to increase the retention time of the SOA compound. For example, it is found that m/z 194 organic acid compound ($C_5H_8NO_7^-$) containing one nitrooxy group elutes earlier than that of the m/z 239 organic acid compounds ($C_5H_7N_2O_9^-$) containing two nitrooxy groups. Similarly, the m/z 305 organosulfate ($C_5H_9N_2O_{11}S^-$) elutes earlier than that of the m/z 349 organosulfate ($C_5H_8N_3O_{13}S^-$).

SOA components that are either nitrooxy-organic acids or nitrooxy-organosulfates are detected strongly as the $[M–H]^-$ ion, consistent with previous work (Surratt et al., 2006; Surratt et al., 2007a,b; Gao et al., 2004a,b; Gao et al., 2006), whereas the hydroxynitrates and nitrooxy-hydroxyperoxides are detected as both the $[M–H]^-$ and $[M–H + C_2H_4O_2]^-$ ions, with the latter acetic acid adduct ion, in most cases, being the base peak ion (i.e. dominant ion). The acetic acid adduct ions for the hydroxynitrates and the nitrooxy-hydroxyperoxides are formed owing to the presence of acetic acid in the UPLC mobile phase. Previous studies have shown that non-acidic hydroxylated species (such as the 2-methyltetrols) and organic peroxides formed from the photooxidation of isoprene (Claeys et al., 2004; Edney et al., 2005; Surratt et al., 2006) are either undetectable or yield weak negative ions when using (–)ESI-MS techniques. However, it appears that the co-presence of nitrooxy groups in the hydroxylated SOA components allow for these compounds to become acidic enough to be detected by the UPLC/(–)ESI-TOFMS technique, or allow for adduction with acetic acid. Further confirmation for the presence of organic peroxides in the isoprene SOA produced from NO_3 oxidation is provided by the iodometric-spectroscopic measurements shown

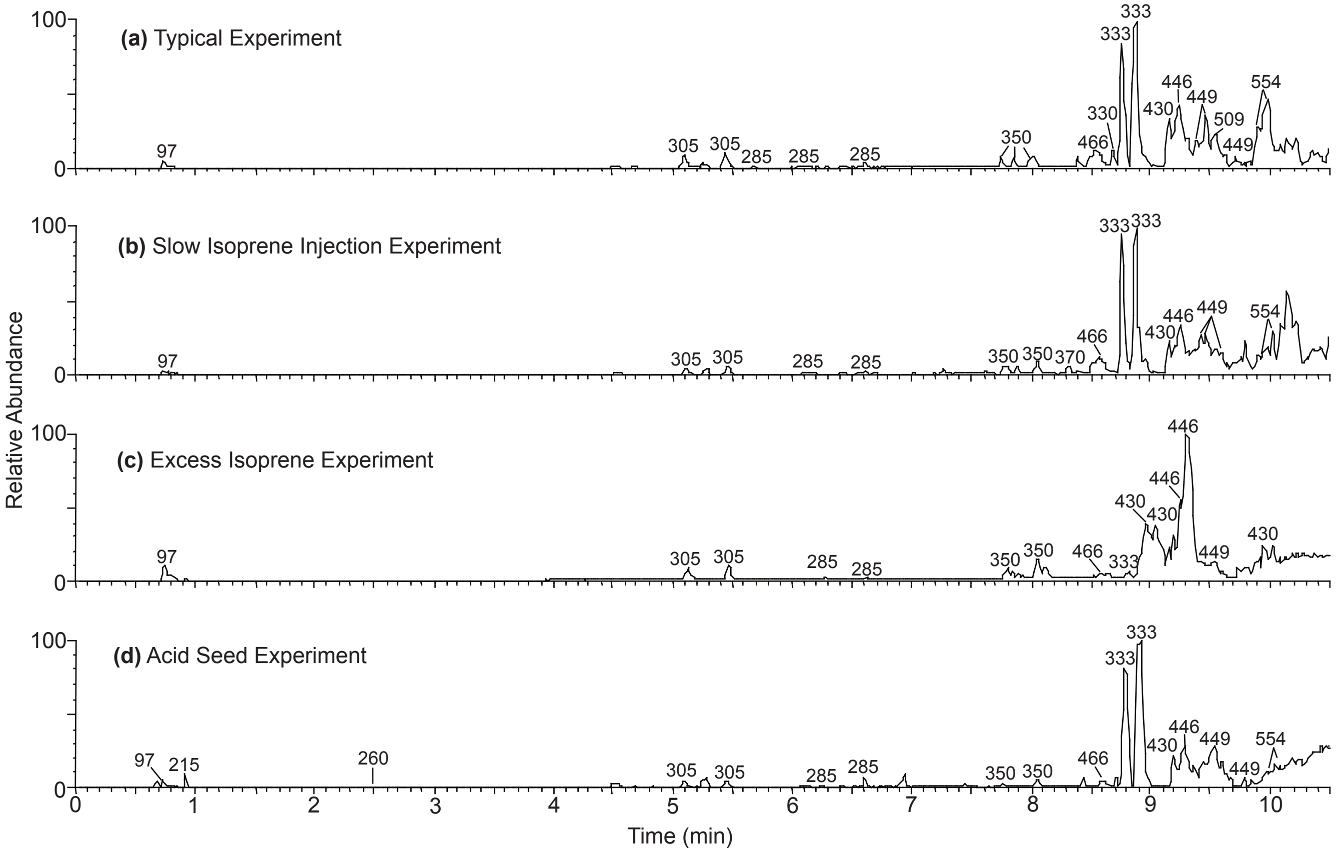

Fig. 10. UPLC/(-)ESI-TOFMS base peak ion chromatograms (BPCs) for the following isoprene-NO_3 oxidation experiments: **(a)** 200 ppb isoprene+1 ppm N_2O_5+seed aerosol generated from 15 mM $(NH_4)_2SO_4$ atomizing solution; **(b)** 300 ppb isoprene+1 ppm N_2O_5+seed aerosol generated from 15 mM $(NH_4)_2SO_4$ atomizing solution; **(c)** 1.2 ppm isoprene+700 ppb N_2O_5+seed aerosol generated from 15 mM $(NH_4)_2SO_4$ atomizing solution; **(d)** 200 ppb isoprene+1 ppm N_2O_5+seed aerosol generated from 30 mM MgSO4+50 mM H_2SO_4 atomizing solution. The numbers indicated above the selected chromatographic peaks correspond to the most abundant negative ion, which is either the $[M–H]^-$ or $[M–H+C_2H_4O_2]^-$ ion.

in Table 3. Based upon the UPLC/(–)ESI-TOFMS measurements shown in Table 2, an average molecular weight of 433 for the organic peroxides is assumed for the calculations shown in Table 3. The contribution of organic peroxides to the SOA mass concentration is found to be fairly reproducible for duplicate typical experiments (i.e., 8/22/07 and 10/24/07). The amount of organic peroxides in the excess isoprene experiment is below detection limits. Owing to the lack of authentic standards, there are large uncertainties associated with the quantification of these products in the aerosol phase. This is further discussed in Sect. 4.4.

4 Gas-phase chemistry and SOA formation

4.1 Formation of various gas-phase products

As seen from Figs. 5 and 6, the three major first-generation products formed from isoprene-NO_3 reaction are the m/z 230, 232, and 248 ions. Since the CIMS technique uses CF_3O^- (anionic mass 85 Da) as the reagent ion, compounds are detected at a m/z value of their molecular weight (MW) plus 85. The product ions at m/z 230, 232, and 248 likely correspond to C_5-nitrooxycarbonyl (MW 145), C_5-hydroxynitrate (MW 147), and C_5-nitrooxyhydroperoxide (MW 163). These products have been observed in previous studies (Jay and Stieglitz, 1989; Skov et al., 1992; Kwok et al., 1996; Berndt and Böge, 1997) and their formation from the isoprene-NO_3 reaction is relatively straightforward (Fig. 11). The reaction proceeds by NO_3 addition to the C=C double bond, forming four possible nitrooxyalkyl radicals depending the position of the NO_3 attack. Previous studies suggest that NO_3 radicals predominantly attack isoprene in the 1-position, with a branching ratio (C_1-position/C_4-position) varying between 3.5 and 7.4 (Skov et al., 1992; Berndt and Boge, 1997; Suh et al., 2001). As mentioned before, the average branching ratio (5.5:1) is used in estimating the sensitivities of the compounds measured by CIMS. In Fig. 11, only the nitrooxyalkyl radical formed from the C1

Table 2. SOA products identified using UPLC/(–)ESI-TOFMS.

Retention Time (min)	Measured $[M–H]^-$ Ion (m/z)	TOFMS Suggested $[M–H]^-$ Ion Formula	Error (mDa, ppm)	Measured $[M–H+C_2H_4O_2]^-$ Ion (m/z)	TOFMS Suggested $[M–H+C_2H_4O_2]^-$ Ion Formula	Error (mDa, ppm)	Proposed Structure[a]
3.68[b]	194.0310	$C_5H_8NO_7^-$	0.9, 4.6	[c]			
4.52[b]	239.0137	$C_5H_7N_2O_9^-$	–1.5, –6.3				
5.09[d]	304.9946	$C_5H_9N_2O_{11}S^-$	1.9, 6.2				
5.24[b]	239.0152	$C_5H_7N_2O_9^-$	0.0, 0.0				
5.43[d]	304.9944	$C_5H_9N_2O_{11}S^-$	1.7, 5.6				
6.07	225.0350	$C_5H_9N_2O_8^-$	–0.9, –4.0				
6.12	225.0342	$C_5H_9N_2O_8^-$	–1.7, –7.6				
6.60	225.0375	$C_5H_9N_2O_8^-$	1.6, 7.1	285.0676	$C_7H_{13}N_2O_{10}^-$	0.6, 2.1	
7.75[d]	349.9775	$C_5H_8N_3O_{13}S^-$	–0.3, –0.9				
7.85[d]	349.9764	$C_5H_8N_3O_{13}S^-$	0.2, 0.6				
8.00[d]	349.9784	$C_5H_8N_3O_{13}S^-$	–0.4, –1.1				
8.48[d]	466.0268	$C_{10}H_{16}N_3O_{16}S^-$	1.7, 3.6				
8.54[d]	466.0264	$C_{10}H_{16}N_3O_{16}S^-$	1.3, 2.8				
8.72[d]	466.0237	$C_{10}H_{16}N_3O_{16}S^-$	–1.4, –3.0				
8.76[e]	270.0199	$C_5H_8N_3O_{10}^-$	–1.1, –4.1	330.0393	$C_7H_{12}N_3O_{12}^-$	–2.8, –8.5	
8.81[d]	466.0237	$C_{10}H_{16}N_3O_{16}S^-$	–1.4, –3.0				
8.85[e]	270.0204	$C_5H_8N_3O_{10}^-$	–0.6, –2.2	330.0379	$C_7H_{12}N_3O_{12}^-$	–4.2, –12.7	
9.15	370.0734	$C_{10}H_{16}N_3O_{12}^-$	0.9, 2.4	430.0940	$C_{12}H_{20}N_3O_{14}^-$	–0.5, –1.2	
9.19	386.0678	$C_{10}H_{16}N_3O_{13}^-$	–0.5, –1.3	446.0888	$C_{12}H_{20}N_3O_{15}^-$	–0.6, –1.3	
9.24	370.0732	$C_{10}H_{16}N_3O_{12}^-$	–0.2, –0.5	430.0937	$C_{12}H_{20}N_3O_{14}^-$	–0.8, –1.9	
9.25	386.0683	$C_{10}H_{16}N_3O_{13}^-$	-0.2, -0.5	446.0893	$C_{12}H_{20}N_3O_{15}^-$	–0.1, –0.2	
9.37	449.0637	$C_{10}H_{17}N_4O_{16}^-$	–0.3, –0.7	509.0854	$C_{12}H_{21}N_4O_{18}^-$	0.3, 0.6	
9.41	386.0684	$C_{10}H_{16}N_3O_{13}^-$	0.1, 0.3	446.0903	$C_{12}H_{20}N_3O_{15}^-$	0.9, 2.0	
9.45	449.0653	$C_{10}H_{17}N_4O_{16}^-$	1.3, 2.9	509.0853	$C_{12}H_{21}N_4O_{18}^-$	0.2, 0.4	
9.90[f]	494.0537	$C_{10}H_{16}N_5O_{18}^-$	4.7, 9.5	554.0669	$C_{12}H_{20}N_5O_{20}^-$	–3.3, –6.0	
9.98[f]	494.0518	$C_{10}H_{16}N_5O_{18}^-$	2.8, 5.7	554.0676	$C_{12}H_{20}N_5O_{20}^-$	–2.6, –4.7	

[a] Structural isomers containing nitrate, sulfate, or hyroxyl groups at other positions are likely; for simplicity, only one isomer is shown.

[b] These compounds appear to be very minor SOA products due to very small chromatographic peak areas, confirming that the further oxidation of the nitrooxycarbonyl and hydroxycarbonyl first-generation gas-phase products do not yield significant quantities of SOA.

[c] A blank cell indicates that the detected SOA product had no observable acetic acid adduct ion (i.e. $[M–H+C_2H_4O_2]^-$).

[d] These organosulfate SOA products were observed only in experiments employing either $(NH_4)_2SO_4$ (i.e. neutral) or $MgSO_4$ +H_2SO_4 (i.e. acidic) seed aerosol. These organosulfate SOA products were also observed in the excess isoprene experiments.

[e] In addition to the acetic acid adduct ion, these compounds also had a significant adduct ion at $[M–H+HNO_3]^-$ (m/z 333), indicating that these compounds are likely not very stable due to the fragmentation of one of the NO_3 groups during the MS analysis.

[f] These compounds were only weakly detected in the excess isoprene experiments.

attack is shown. The nitrooxyalkyl radicals then react with O_2 to form RO_2 radicals, which react further with HO_2, RO_2, or NO_3 radicals under the experimental conditions in this study. The reaction of RO_2 radicals and HO_2 radicals leads to the formation of C_5-nitrooxyhydroperoxide (m/z 248). The reaction of two RO_2 radicals (self reaction or cross reaction) has three different possible channels:

$$RO_2 + RO_2 \rightarrow 2RO + O_2 \quad (5a)$$

$$\rightarrow ROH + RCHO + O_2 \quad (5b)$$

$$\rightarrow ROOR + O_2 \quad (5c)$$

The second channel results in the formation of C_5-nitrooxycarbonyl (m/z 230) and C_5-hydroxynitrate (m/z 232). According to channel (5b), these two products should be formed with a 1:1 ratio; however, C_5-nitrooxycarbonyl can also be formed from alkoxy radicals (alkoxy radicals formed through RO_2+RO_2 reaction or RO_2+NO_3 reaction). In Fig. 6, 49.8 ppb of C_5-nitrooxycarbonyl and 26.1 ppb of C_5-hydroxynitrate are formed after the addition of the first pulse of N_2O_5, indicating ∼24 ppb of C_5-nitrooxycarbonyl is formed from the reaction of alkoxy radicals. The branching ratios for the reaction of small peroxy radicals have been investigated in previous studies. It is found that the branching ratio for channel (5a) for methylperoxy and ethylperoxy radicals is ∼0.3–0.4 and ∼0.6, respectively (Lightfoot et al., 1992; Wallington et al., 1992; Tyndall et al., 1998). It is

Table 3. Peroxide content of SOA formed by NO_3 oxidation of isoprene.

Experiment Date	Seeded[a]/ Nucleation	[Isoprene] (ppb)	$[N_2O_5]$ (ppm)	SOA Volume Growth Observed[b] ($\mu m^3/cm^3$)	Total SOA Mass Concentration[c] ($\mu g/m^3$)	Peroxide Aerosol Mass Concentration ($\mu g/m^3$)	Contriubtion of Peroxides to the SOA Mass Concentration Observed (%)
8/22/07	AS	200	1	102	145	46	32
8/30/07	AMS	200	1	123	174	40	23
10/22/07[d]	AS	1200	0.7	70	100	b.d.l.[e]	[f]
10/23/07	nucleation	200	1	125	177	31	17
10/24/07	AS	200	1	111	158	47	30
10/27/07[g]	AS	300	1	110	156	47	30

[a] AS=ammonium sulfate seed, AMS=acidified magnesium sulfate seed.

[b] Averaged over the course of filter sampling.

[c] Assuming a SOA density of 1.42 g/cm^3. This was based on DMA and Q-AMS measurements.

[d] Excess isoprene experiment.

[e] Below detection limits.

[f] No observable contribution of organic peroxides to the SOA mass concentration.

[g] Slow injection of isoprene in this experiment to enhance the RO_2+NO_3 reaction pathway.

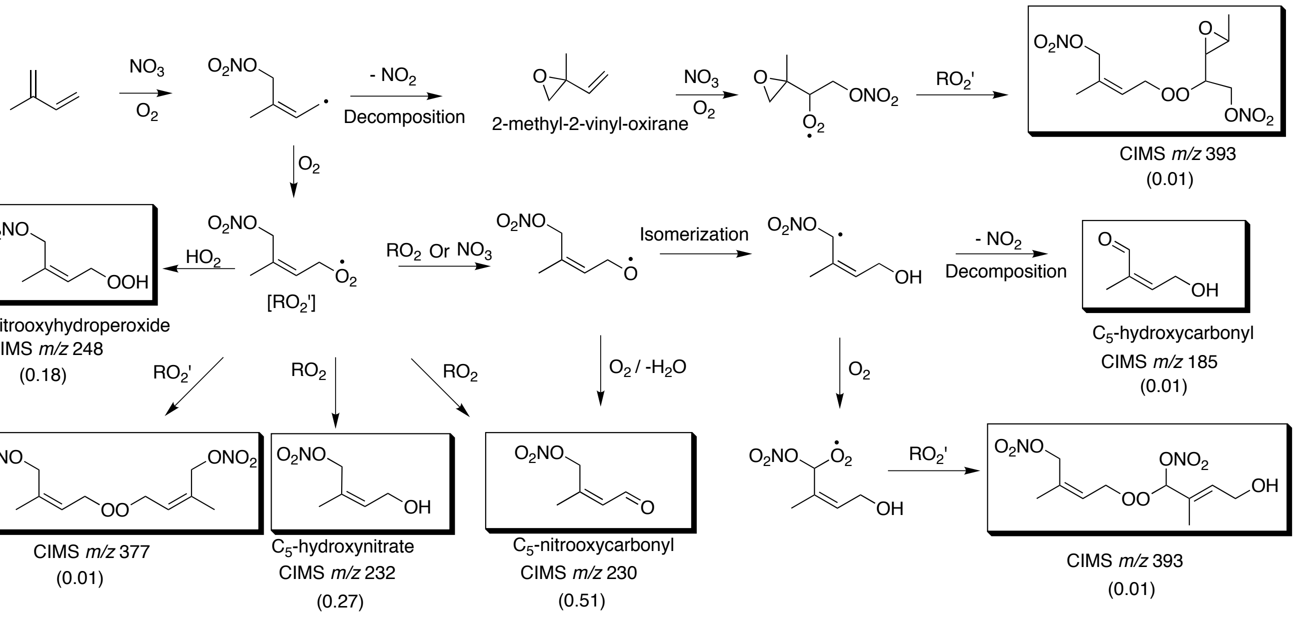

Fig. 11. Proposed mechanisms for the formation of various gas-phase intermediate product ions observed by CIMS. Multiple structural isomers are possible. In this figure, RO_2' refers to the isoprene peroxy radical (nitrooxyperoxy radical), RO_2 refer to a generic peroxy radical. The numbers in the parentheses refer to the molar yields of the products. It is noted that the sensitivity for m/z 393 is not calculated; instead, it is assumed that the sensitivity (and hence the sum of the molar yields of the two isomers shown, since m/z 377 and m/z 393 are formed with the same concentration) to be the same as that for m/z 377.

likely that the isoprene peroxy radicals react via this pathway to form alkoxy radicals and contribute to the "extra" 24 ppb of C_5-nitrooxycarbonyl. This observation is indicative that most RO_2 radicals react with other RO_2 radicals instead with NO_3 or HO_2 radicals.

Other than C_5-nitrooxycarbonyl, C_5-hydroxynitrate, and C_5-nitrooxyhydroperoxide, three other minor products (m/z 185, 377 and 393 ions) are also observed as intermediate products. The proposed mechanisms for the formation of these gas-phase products are also shown in Fig. 11. Although channel (5c) in the RO_2+RO_2 reaction is found to be minor for small peroxy radicals such as methylperoxy and ethylperoxy radicals (Kan et al., 1980; Niki et al., 1981, 1982; Wallington et al., 1989; Tyndall et al., 1998; Tyndall et al., 2001), the product ion at m/z 377 could be the corresponding ROOR product formed from the self reaction of isoprene peroxy radicals. The product ion at m/z 185 likely corresponds to the C_5-hydroxycarbonyl. It has been observed

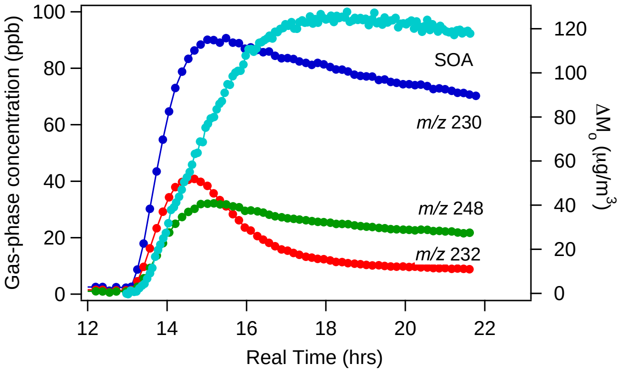

Fig. 12. Time profiles of the major gas-phase products (m/z 230, 232, and 248) and the corresponding aerosol growth from the slow N_2O_5 injection experiment. Note that this experiment has a higher initial isoprene concentration (∼200 ppb) compared to the one shown in Fig. 4.

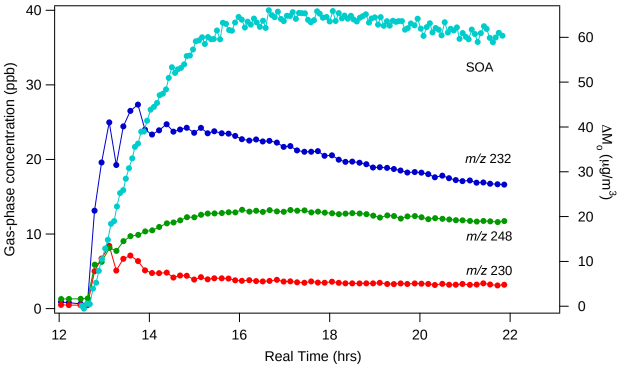

Fig. 13. Time profiles of the major gas-phase products (m/z 230, 232, and 248) and the corresponding aerosol growth from the slow isoprene injection experiment. Note that this experiment has a higher initial isoprene concentration (∼200 ppb) compared to the one shown in Fig. 4.

in previous studies and it likely arises from the isomerization of nitrooxyalkoxy radicals through a 6-member transition state to form a hydroxynitrooxy alkyl radical, which then decomposes to form NO_2 and C_5-hydroxycarbonyl (Kwok et al., 1996). Such isomerization has also been proposed to occur in the photooxidation of isoprene (Paulson and Seinfeld, 1992; Carter and Atkinson, 1996; Dibble, 2002). It is possible that the hydroxynitrooxy alkyl radical formed proceeds to react with O_2 to form a peroxy radical, which then reacts with the isoprene peroxy radical to form the product ion at m/z 393. The product ion at m/z 393 shows a slower rate of formation (Fig. 6) compared to other product ions suggesting that it might also be formed from the further oxidation of a first-generation product. 2-methyl-2-vinyl-oxirane has been observed from isoprene-NO_3 reaction in previous studies at 20 mbar in helium (Berndt and Böge, 1997) and 20 Torr in argon (Skov et al., 1994), respectively. When operated in positive mode with H_3O^+ as the reagent ion (products are observed at m/z=MW+1), CIMS shows a protonated molecule at m/z 85. Although the epoxide yield is found to be <1% of the total reacted isoprene at atmospheric pressure (Skov et al., 1994), the signal at m/z 85 can arise in part from the epoxide. The further oxidation of the epoxide results in the formation of an epoxide peroxy radical, which can react with the isoprene peroxy radical to form the peroxide at m/z 393. It is noted that a product ion at m/z 246 is detected in CIMS, which could arise from the corresponding carbonyl product formed from the reactions of two epoxide peroxy radicals, or from the fragmentation of the epoxide alkoxy radicals. Unlike m/z 393, which decays after the addition of the last pulse of N_2O_5, m/z 246 stays relatively constant suggesting that it is not being further oxidized by NO_3 radicals. To examine further the possibility of peroxide formation (m/z 377 and 393) in the gas phase, an experiment is conducted using 1,3-butadiene as the parent hydrocarbon. The analogous product ions for the 1,3-butadiene system, i.e. m/z 349 and 365, are observed in CIMS, providing further indication that the formation of ROOR products from two RO_2 radicals is occurring in the gas phase. Further details of the gas-phase chemistry of isoprene and 1,3-butadiene will be forthcoming in a future manuscript.

4.2 Effect of peroxy radical chemistry on SOA yield

The SOA yield ranges from 4.3% to 23.8% for an initial isoprene concentration of 18.4 to 101.6 ppb in the typical yield experiments. While the SOA yield from the slow N_2O_5 injection experiment is roughly the same as that in the typical yield experiments, the SOA yield from the slow isoprene injection experiment is lower (Fig. 3). In both cases, ∼ 40 ppb of isoprene is consumed, the main difference being the relative importance of RO_2+RO_2 reaction versus RO_2+NO_3 reaction in each system. In the slow N_2O_5 injection experiment, a relatively small amount of NO_3 is available in the chamber. Once RO_2 radicals are formed, it is expected that they would react primarily with other RO_2 radicals instead of NO_3 radicals owing to the presence of a relatively higher isoprene concentration in the chamber. On the other hand, the slow isoprene injection experiment favors RO_2+NO_3 reaction owing to the presence of excess N_2O_5 in the chamber. Thus the higher SOA yield observed in the slow N_2O_5 injection experiment suggests the products formed via RO_2+RO_2 reaction partition more readily into the aerosol phase, or the RO_2+RO_2 reaction forms products that further react and contribute significantly to aerosol growth. The fact that the SOA yield from the slow N_2O_5 injection experiment is roughly the same as in the typical yield experiments implies that RO_2+RO_2 reaction dominates in typical yield experiments.

The time profile for the three major first-generation gas phase products and SOA growth from the slow N_2O_5 injection experiment and slow isoprene injection experiment are shown in Figs. 12 and 13, respectively. It is noted that this pair of experiments has a higher initial isoprene concentration (~200 ppb) compared to the pair of experiments shown in Fig. 4. In both cases, once the first-generation products are formed they can react further with NO_3 radicals, making it difficult to estimate the formation yields of these products based on the measured concentrations. The extent to which these products react further is expected to be higher in the slow isoprene injection experiment owing to the presence of excess NO_3 in chamber; this is consistent with the relatively lower concentrations of first-generation products observed. As mentioned before, it is possible that the CIMS signal at the observed m/z comprises isomers formed from the NO_3 attack at positions other than the C1 carbon. Such isomers have slightly different structures but they could exhibit a very different reaction rate towards NO_3 radicals. For instance, studies have shown that the reaction rates of NO_3 radicals with unsaturated alcohols and unsaturated carbonyl compounds can vary by several orders of magnitude depending on the position of the substituted methyl group (Noda et al., 2002; Canosa-Mas et al., 2005). It is possible that the minor products formed from NO_3 attack at other positions react much slower with NO_3 radicals, hence the concentrations of the observed product ions do not decay to zero towards the end of the experiment. At the end of the experiment, about 8 ppb and 3 ppb of C_5-hydroxynitrate is left in the slow N_2O_5 injection experiment and slow isoprene injection experiment, respectively. Assuming the amount of reactive isomers and unreactive (or relatively slow reacting) isomers are formed in the same ratio in the slow N_2O_5 injection experiment and the slow isoprene injection experiment, we can deduce that a relatively higher concentration of reactive C_5-hydroxynitrate (as well as the two other first-generation products) is formed in the slow N_2O_5 injection experiment. This is consistent with the larger extent of RO_2+RO_2 reaction (which forms C_5-hydroxynitrate) and the higher SOA yield observed in the slow N_2O_5 injection experiment, as it appears that C_5-hydroxynitrate is an effective SOA precursor (Fig. 6).

4.3 Growth curves: multiple steps in SOA formation

By examining the time-dependent growth curves (organic aerosol, $\Delta M_{o,}$ as a function of hydrocarbon reacted, ΔHC) we can gain insights into the general mechanisms of SOA formation (Ng et al., 2006, 2007a,b). Figure 4 shows the time-dependent growth curves for the slow N_2O_5 injection experiment and the slow isoprene injection experiment, respectively. For the slow N_2O_5 injection experiment, the initial aerosol growth likely arises from the condensation of first-generation products as the presence of excess isoprene in the chamber suppresses their further oxidation. If higher generation products do contribute to SOA formation, they would have to be formed at relatively fast rates. After isoprene is consumed, aerosol mass continue to increase and results in a "hook" in the growth curve. This indicates that secondary products (or higher generation products) also contribute significantly to SOA formation. The same observation can be made if we examine the reaction profile of a typical yield experiment (Fig. 2): there is further SOA growth after all isoprene is reacted away, indicating that the further oxidation of first generation products are contributing to SOA formed. These observations are consistent with the fact that the decay of first-generation products observed in CIMS (especially the m/z 232 and m/z 377 ions) is strongly anticorrelated with further SOA growth (Fig. 6). On the other hand, the slow isoprene injection experiment does not allow us to differentiate the contribution of first- and second-generation products to SOA formation. With the presence of excess NO_3 radicals in the chamber, the first-generation products formed in the slow isoprene injection experiment would be further oxidized once they are formed. The SOA growth observed throughout this experiment is from the partitioning of these highly oxidized and nonvolatile products. Hence, at the beginning of the experiment, for the same amount of ΔHC, the amount of SOA formed in this experiment is higher than that in the slow N_2O_5 injection experiment, in which the aerosol growth is probably from the condensation of relatively more volatile first-generation products. Both the AMS data and filter sample data (Figs. 8, 9, and 10) show a very similar composition for the final SOA formed in slow N_2O_5 injection experiment and the slow isoprene injection experiment, suggesting a common SOA forming channel. Based on the previous discussion on the effect of peroxy radical chemistry on SOA yields, it is likely that the RO_2+RO_2 reaction is the SOA-forming channel in both cases; such a reaction occurs to a large extent in the slow N_2O_5 injection experiments and results in the formation of more SOA.

4.4 Proposed mechanisms of SOA formation

The combination of CIMS gas-phase data and elemental SOA composition data provides substantial insights into the mechanisms of SOA formation. Shown in Figs. 14–17 are the proposed SOA formation mechanisms from the further oxidation of the various gas-phase products measured by CIMS. The compounds in the boxes are the SOA products detected by UPLC/(-)ESI-TOFMS. Owing to multiple chromatographic peaks observed in the UPLC/(–)ESI-TOFMS extracted ion chromatograms (EICs) for the negative ions of the proposed SOA products, structural isomers are likely; however, for simplicity we show only one possible isomer for each product formed from a particular reaction pathway. Many of the SOA products detected are formed from the further oxidation of first- or higher-generation products, which is consistent with the observation of continual SOA growth after the complete consumption of isoprene (hence a "hook" in the growth curve). With the large number of nitrate-substituted compounds detected by UPLC/(–)ESI-TOFMS technique, it is also not surprising that AMS shows strong signals at m/z 30 (NO^+) and m/z 46 (NO_2^+).

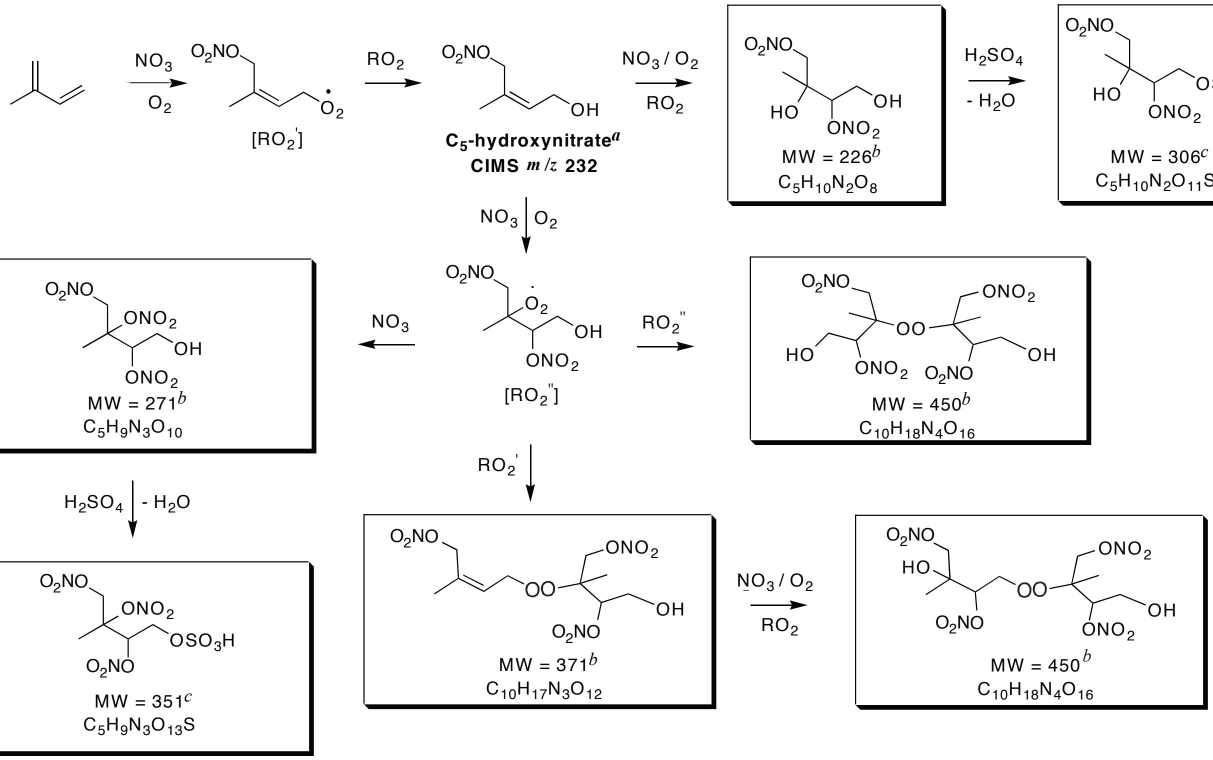

Fig. 14. Proposed mechanism for SOA formation from the formation and decay of the C_5-hydroxynitrate gas-phase product formed from the isoprene + NO_3 reaction. Boxes indicate UPLC/(–)ESI-TOFMS detected SOA products; molecular formulas were confirmed by the accurate mass data provided by the UPLC/(-)ESI-TOFMS. Multiple structural isomers are possible, consistent with the multiple chromatographic peaks observed in the extracted ion chromatograms; however, only one structural isomer is shown for simplicity. [a] This first-generation gas-phase product was previously observed by Jay and Stieglitz (1989), Skov et al. (1992), Kwok et al. (1996), and Berndt and Böge (1997); this gas-phase product was detected as the $[M+CF_3O]^-$ ion by the CIMS instrument. [b] These particle-phase compounds were detected as both their $[M–H]^-$ and $[M–H+C_2H_4O_2]^-$ ions; the acetic acid adduct ($[M–H+C_2H_4O_2]^-$) ion was, in most cases, the molecular ion (i.e. dominant ion). [c]These organosulfate compounds were detected as their $[M–H]^-$ ions and were observed only in ammonium sulfate and acidified magnesium sulfate seeded experiments.

Shown in Figs. 14 and 15 are the proposed SOA formation pathways from the further oxidation of the m/z 232 (i.e. C_5-hydroxynitrate) and 377 gas-phase product ions (as detected by CIMS). The decay of these two products has been found to be strongly correlated with aerosol growth (Fig. 6), which is consistent with the large number of SOA products formed from their further oxidation. The further oxidation of these two gas-phase products also yields SOA compounds of the same molecular weight (compounds of MW 371 and 450). Although m/z 393 is a minor gas-phase product, the further oxidation of this compound leads to formation of several SOA products (Fig. 16). As mentioned before, there are two possible formation routes for m/z 393, and the further oxidation of both products is shown in Fig. 16. The further oxidation of the m/z 393 ion appears to yield SOA products that are specific only to this gas-phase product: these include the SOA products of MW 387 and 467.

Figure 17 shows the proposed SOA formation mechanisms from three other gas-phase products (m/z 185, m/z 230, and m/z 277); the further oxidation of these product ions leads to relatively minor SOA products. Although C_5-nitrooxycarbonyl (m/z 230) is the most abundant gas-phase product detected by CIMS, its further oxidation is not well correlated with aerosol growth (Fig. 6). The further oxidation of m/z 230 yields an SOA product at MW 240. This organic acid product is found to be quite minor when examining the peak area in its corresponding extracted ion chromatogram (EIC). It is noted that no SOA products are detected from the further oxidation of the C_5-nitrooxyhydroperoxide (m/z 248) (also a major gas-phase product); it is possible that these hydroperoxide products are not acidic enough to be detected by the UPLC/(–)ESI-TOFMS technique, or degrade during sample workup and/or analysis procedures. It has been shown that hydroxycarbonyl

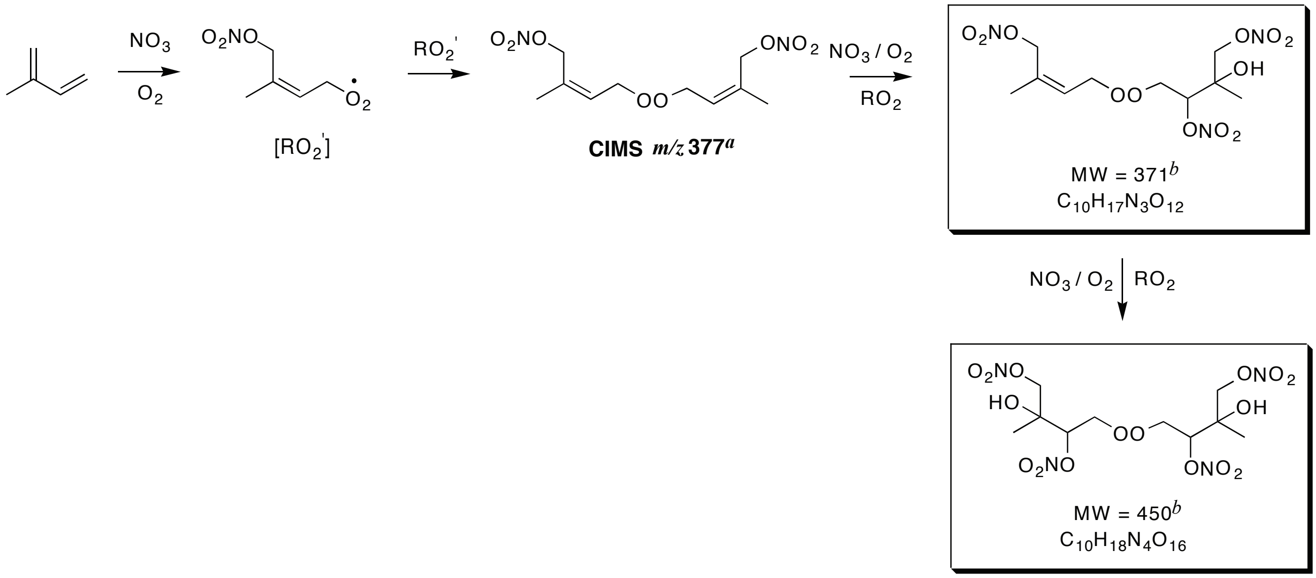

Fig. 15. Proposed mechanism for SOA formation from the formation and decay of the CIMS m/z 377 gas-phase product formed from the isoprene+NO_3 reaction. Boxes indicate UPLC/(–)ESI-TOFMS detected SOA products; molecular formulas were confirmed by the accurate mass data provided by the UPLC/(–)ESI-TOFMS. Multiple structural isomers are possible, consistent with the multiple chromatographic peaks observed in the extracted ion chromatograms; however, only one structural isomer is shown for simplicity. [a] This first-generation gas-phase product was detected as the $[M + CF_3O]^-$ ion by the CIMS instrument. [b] These particle-phase compounds were detected as both their $[M–H]^-$ and $[M–H+C_2H_4O_2]^-$ ions; the acetic acid adduct ($[M-H+C_2H_4O_2]^-$) ion was, in most cases, the molecular ion (i.e. dominant ion).

plays a key role in SOA formation from the reaction of linear alkenes with NO_3 radicals (Gong et al., 2005), however, in the isoprene-NO_3 system, the further oxidation of the minor gas-phase product C_5-hydroxycarbonyl (m/z 185) leads to the formation of only one minor aerosol product at MW 195. Some evidence for the formation of a C_5-dinitrate first-generation gas-phase product is indicated from the CIMS and UPLC/(–)ESI-TOFMS data. This first-generation gas-phase product has been observed previously by Werner et al. (1997). The CIMS shows a weak signal at m/z 277, which could be associated to the dinitrate product; we do not know, however, whether the negative ion efficiently clusters with such compounds. Further evidence for the dinitrate gas-phase product is provided by the UPLC/(–)ESI-TOFMS detection of an SOA product at MW 495, which could result from the further oxidation of a C_5-dinitrate precursor. The precursor compound before the last oxidation step shown in this mechanism in Fig. 17 may exist in the particle phase; however, this compound is not likely to be detected by the UPLC/(–)ESI-TOFMS technique owing to the lack of acidic hydrogens from neighboring hydroxyl and/or carboxyl groups.

The SOA products highlighted in Figs. 14–17 are observed in all major experiments conducted; however, not all of these products are strongly detected in the excess isoprene experiment (Fig. 10c). With the presence of excess isoprene, further oxidations of first-generation products should be minimal and no significant SOA formation is expected. The reaction rate of isoprene and NO_3 radicals is $k_{NO_3}=7\times10^{-13}\,cm^3\,molecule^{-1}\,s^{-1}$. To our knowledge, the reaction rate of the first-generation products and NO_3 radicals has not been studied. The structure of m/z 232 (C_5-hydroxynitrate) is similar to 3-methyl-2-buten-1-ol (MBO321), except that the γ-carbon has one nitro group and one methyl group substitution instead of two methyl group substitutions. The reaction rate coefficient of MBO321 and NO_3 radicals is $k_{NO_3}=1\times10^{-12}\,cm^3\,molecule^{-1}\,s^{-1}$. It is found that the reaction rate with NO_3 radicals increases with increasing number of methyl groups at the γ-carbon (Noda et al., 2002), which is in accordance with the stabilization theory for leaving groups discussed in Atkinson (1997) and Noda et al. (2000). With reference to this, we would expect the reaction rate of C_5-hydroxynitrate and NO_3 radicals to be slower than that of MBO321 due to the presence of the electron withdrawing nitro group. Hence, it is likely that the reaction rate of isoprene and NO_3 radicals and C_5-hydroxynitrate and NO_3 radicals are roughly in the same range. The relative production rate of first- and second-generation products will then be the ratio of the

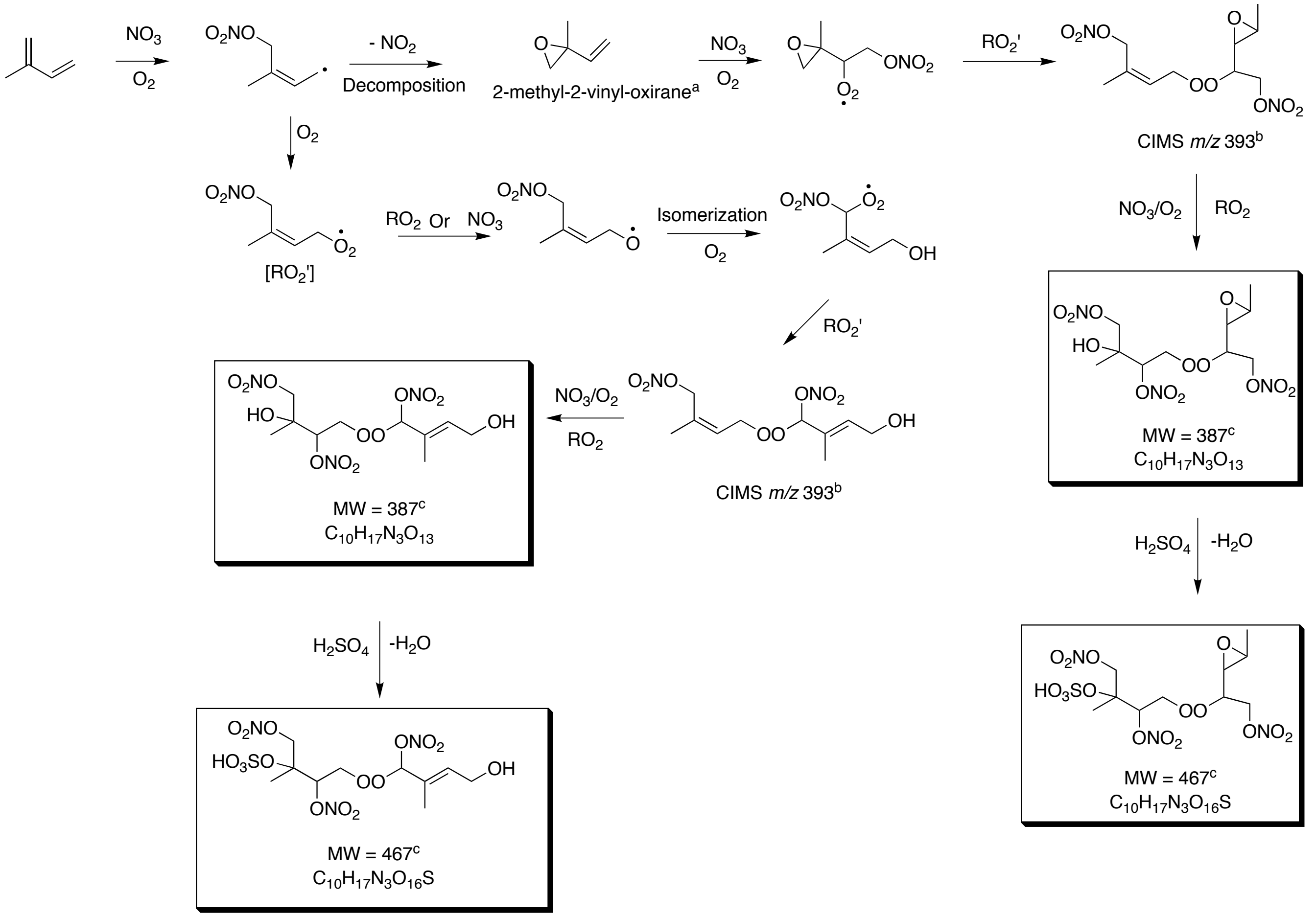

Fig. 16. Proposed mechanism for SOA formation from the formation and decay of the CIMS *m*/*z* 393 gas-phase product formed from the isoprene+NO_3 reaction. Boxes indicate UPLC/(-)ESI-TOFMS detected SOA products; molecular formulas were confirmed by the accurate mass data provided by the UPLC/(–)ESI-TOFMS. Multiple structural isomers are possible, consistent with the multiple chromatographic peaks observed in the extracted ion chromatograms; however, only one structural isomer is shown for simplicity. ^{a} This first-generation gas-phase product was detected as the $[M+H]^+$ ion by the CIMS instrument; this gas-phase product was previously observed by Berndt and Böge (1997) and could also be 2-(1-methyl-vinyl)oxirane. ^{b} This gas-phase product was detected as the $[M+CF_3O]^-$ ion. ^{c} These particle-phase compounds were detected as both their $[M–H]^-$ and $[M–H+C_2H_4O_2]^-$ ions; the acetic acid adduct ($[M–H+C_2H_4O_2]^-$) ion was, in most cases, the molecular ion (i.e. dominant ion). ^{d} This organosulfate compound was detected as its $[M–H]^-$ ion and was observed only in the ammonium sulfate and acidified magnesium sulfate seeded experiments.

concentrations of isoprene and first-generation products, and aerosol can be formed either from the condensation of relatively non-volatile first-generation products (e.g. *m*/*z* 393) or higher generation products that are formed relatively fast in the gas-phase. It appears from the UPLC/(–)ESI-TOFMS data that enough RO_2+RO_2 chemistry is occurring to yield many of the products shown in Figs. 14–17. When comparing the UPLC/(–)ESI-TOFMS BPCs (Fig. 10) of all experiments, it is clear that the *m*/*z* 430 and *m*/*z* 446 are the dominant ions in the excess isoprene experiment, while *m*/*z* 333 is the dominant chromatographic peak in other experiments. The chromatographic peak at *m*/*z* 430 corresponds to the acetic acid cluster ion for the compound at MW 371, which can be formed from the further oxidation of CIMS *m*/*z* 232 and 377 ions (Figs. 14 and 15). The chromatographic peak at *m*/*z* 446 corresponds to the acetic acid cluster ion for the compound at MW 387, which is formed from the further oxidation of CIMS *m*/*z* 393 (Fig. 16). The detection of these two SOA products (MW 371 and MW 387) suggests that further oxidation of *m*/*z* 232, 377, and 393 is occurring in the excess isoprene experiment and contributing to SOA growth. Studies have shown that NO_3 uptake on organic surfaces (even to saturated organic surfaces) be quite rapid (Moise et al., 2002; Knopf et al., 2006; Rudich et al., 2007). Hence, it is also possible that CIMS *m*/*z* 393 (a first-generation product according to one of the formation routes) is nonvolatile enough that it partitions into the aerosol phase and its further oxidation proceeds heterogeneously. Chromatographic peaks

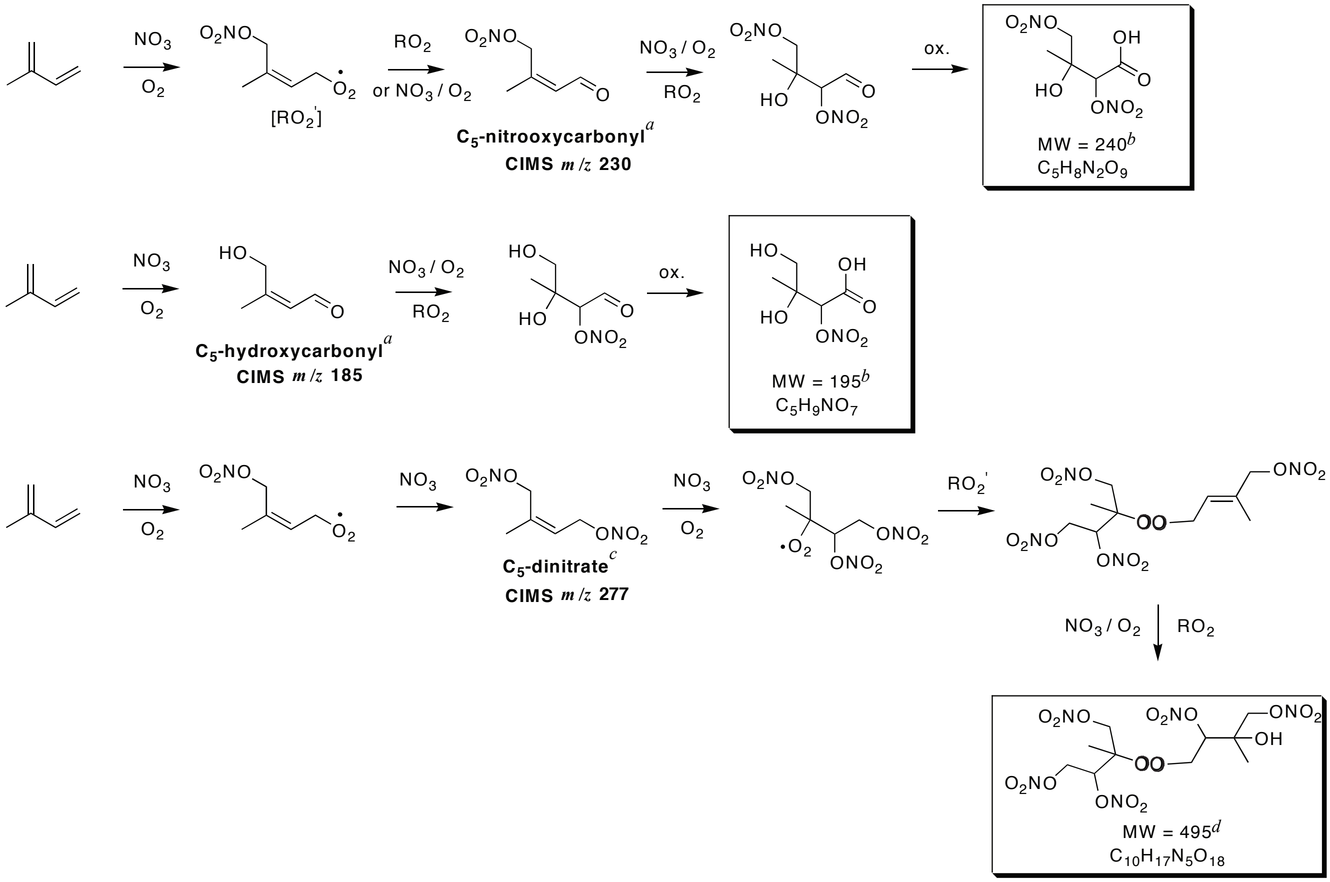

Fig. 17. Proposed mechanism for SOA formation from the formation and decay of the C_5-nitrooxycarbonyl, C_5-hydroxycarbonyl, and C_5-dinitrate first-generation products formed from the isoprene+NO_3 reaction. Boxes indicate UPLC/(–)ESI-TOFMS detected SOA products; molecular formulas were confirmed by the accurate mass data provided by the UPLC/(–)ESI-TOFMS. Multiple structural isomers are possible, consistent with the multiple chromatographic peaks observed in the extracted ion chromatograms; however, only one structural isomer is shown for simplicity. [a] These first-generation gas-phase products were previously observed by Skov et al. (1994) and Kwok et al. (1996); these gas-phase products were detected as the $[M+CF_3O]^-$ ion by the CIMS instrument. [b] These are minor SOA products, confirming that the further oxidation of the C_5-nitrooxycarbonyl and C_5-hydroxycarbonyl first-generation products do not yield significant amounts of SOA. [c] This first-generation gas-phase product was previously observed by Werner et al. (1999); this gas-phase product was also detected as the $[M+CF_3O^-]^-$ ion by the CIMS instrument. [d] This particle-phase compound was detected as both its $[M–H]^-$ and $[M–H+C_2H_4O_2]^-$ ions; the acetic acid adduct ($[M–H+C_2H_4O_2]^-$) ion was the molecular ion (i.e. dominant ion).

such as m/z 333 (associated with MW 271 compound), 449 (MW 450 compound) and 554 (MW 495 compound) are not as strong in the excess isoprene experiment owing to the fact there is not enough NO_3 in the system to allow for the formation of these highly oxidized compounds.

From the UPLC/(–)ESI-TOFMS (Table 2) and PILS/IC measurements, it appears that organic acids are not a major contributor to SOA formation from the oxidation of isoprene by NO_3 radicals. The UPLC/(–)ESI-TOFMS technique detects only two minor organic acids at MW 195 and 240. Additionally, the PILS/IC technique does not detect large quantities of any small organic acids. The sum of formate, acetate, glycolate, lactate, oxalate, and pyruvate are usually between 0.01–0.50 $\mu g\,m^{-3}$. These observations are different from the SOA produced in the photooxidation of isoprene (under high- and low-NO_x conditions), in which a large number of organic acids, such as 2-methylglyceric, formic, and acetic acid, are observed (Surratt et al., 2006; Szmigielski et al., 2007). In the photooxidation experiments, the level of organic acids detected under low-NO_x conditions is lower than under high-NO_x conditions. The low-NO_x isoprene SOA was previously found to also have a significant amount of organic peroxides, as detected in the current study (Table 3); however, organic peroxides detected previously in low-NO_x isoprene SOA were not structurally elucidated through MS techniques performed in the present study (Table 2, Figs. 14–

17), possibly owing to the lack of nitrooxy groups which seem to induce acidity and/or increase the adductive abilities of organic peroxides with acetic acid during the ESI-MS analysis. Overall, it appears that the isoprene-NO_3 SOA is much more similar to the previously studied low-NO_x isoprene SOA. More specifically, it appears that both contain a large amount of organic peroxides, organosulfates (if conducted in the presence of sulfate seed aerosol), and neutral hydroxylated compounds, such as the hydroxynitrates observed in Fig. 14 (e.g. MW 226 and 271 products).

As discussed earlier, the formation yields of ROOR from the reaction of two peroxy radicals is very low for small peroxy radicals (Kan et al., 1980; Niki et al., 1981, 1982; Wallington et al., 1989; Tyndall et al., 1998, 2001). However, according to both gas- phase and aerosol-phase data in this study, it appears that the RO_2+RO_2 reaction (self reaction or cross-reaction) in the gas phase yielding ROOR products is an important SOA formation pathway. Such reaction has been proposed to form low-volatility diacyl peroxides in the SOA formed from cyclohexene ozonolysis (Ziemann, 2002). In the case of self-reaction of peroxy radicals, the molecular weight of the product is essentially doubled, providing an efficient way to form products of low volatility. Based on the iodiometric spectroscopic method the contributions of peroxides (ROOH+ROOR) to the total SOA formed is 17–32% (Table 3). We can estimate the mass yield of peroxides based on their percentage contribution to total SOA and the SOA yield for each of the experiments in Table 3. It is found that the mass yield of peroxides range from ∼6–10%. For the two experiments (i.e., 8/22/07 and 10/24/07) that are carried out under similar conditions as those in the yield experiments, the mass yield of peroxide is 8%.

Based on the shape of the Odum yield curve (Fig. 3), it is expected that the products are semivolatile. Hence, the relatively large contribution of nonvolatile peroxides in the aerosol phase appears to be inconsistent with the observed yield curve behavior. It is evident from the UPLC/(–)ESI-TOFMS data that there exists a wide array of peroxides in the aerosol composition, however, we need to caution that there are large uncertainties associated with the quantification of peroxides owing to the lack of authentic standards. Based on the standard deviations of the measurements, the uncertainty is at least 10%, yet if we take into account the following factors it is expected that the true uncertainty would be larger. In estimating the percentage contribution of peroxides, an average molecular weight of 433 for peroxides is used. The peroxides formed would largely depend on the branching ratio of various reactions and this number may not reflect the molecular weights of the wide array of peroxides formed. Also, the iodiometric spectroscopic method does not allow the distinction between ROOH and ROOR products. Hence, the contribution of the low volatility ROOR products may not be as high as estimated. ROOH standards were run in the ESI-TOFMS to examine the possibility of ROOH further reacting in the mass spectrometer to form ROOR and no ROOR products were detected. As mentioned before, it appears that the presence of nitrooxy groups in ROOR products aids their detection in the MS. Since the ROOH standards used do not have a nitrooxy group, unfortunately we cannot rule out the possibility that ROOR products are formed but just not being detected. Finally, it is worth noting that the initial isoprene concentrations in the yield experiments are much lower than those experiments in which SOA composition is measured. In performing the yield experiments, the initial isoprene concentrations are kept relatively low so as to be closer to atmospheric levels. Because of the lower initial isoprene concentration (hence lower aerosol loading), the partitioning of various products would be different and it is likely that level of peroxides would be lower in the yield experiments. Nevertheless, the higher concentration experiments are necessary to produce enough aerosols for filter analysis and to map out the complete spectrum of oxidation products.

To fully elucidate the relationship between the actual products identified and those inferred from fitting the yield data would require a modeling study that is beyond the scope of this work. However, we emphasize that there are large uncertainties associated with the quantification of peroxides and it is likely that their contributions to total SOA can be overestimated. Indeed, if the mass yield for these nonvolatile peroxides were lower (for instance, ∼2%), this would agree well with the observed yield curve behavior. The measurement of peroxides certainly warrants further study. This work serves as a good example in showing that caution must be taken when interpreting experiments with low aerosol yields, especially when a relatively minor pathway may be responsible for forming the aerosols.

5 Approximate estimate of global production of SOA from isoprene+NO_3

The global chemical transport model GEOS-Chem (v. 7-04-11) (http://www-as.harvard.edu/chemistry/trop/geos/) is used to estimate, roughly, global SOA formation from the isoprene+NO_3 reaction. The current version of GEOS-Chem treats mechanistically SOA formation from isoprene+OH, monoterpenes and sesquiterpenes, and aromatics; here we will estimate SOA formation from isoprene+NO_3 by using an approximate, uniform SOA yield of 10% (corresponding to $M_o \cong 10\,\mu g\,m^{-3}$ in Fig. 3). It is noted that this yield is quite uncertain and the importance of peroxy radical self reactions in this study suggest that the SOA yield in the atmosphere will be highly sensitive to the nature of the nighttime peroxy radical chemistry. Here, we seek to obtain only a "back-of-the-envelope" estimate.

Two global isoprene emissions are available in GEOS-Chem: GEIA (Global Emission Inventory Activity) (Guenther et al., 1995) and MEGAN (Model of Emissions and Gases from Nature) (Guenther et al., 2006). Both models require, as input, meteorological data such as temperature to calculate the amount isoprene emitted. For the present estimate, the meteorological fields employed by Wu et al. (2007), generated by the Goddard Institute for Space Studies (GISS) General Circulation Model III, are used. Meteorological conditions correspond approximately to those of year 2000.

Table 4 presents the annual emissions of isoprene as predicted by each of the emission models, together with the amount of isoprene predicted to react via OH, O_3, and NO_3, the global burden, and lifetime. We note that there is a significant difference between the annual isoprene emissions predicted by the earlier and newer emission models. Isoprene+OH accounts for 300 to 400 Tg yr^{-1} of isoprene consumption. Henze et al. (2007) predict that annual SOA production from isoprene+OH is about 13 Tg yr^{-1} (based on the MEGAN inventory and GEOS-4 meteorological fields, which are assimilated fields from actual year 2004). Note that SOA production from isoprene+OH, or any other pathway for that matter, is sensitive to the production of SOA from other hydrocarbon precursors since gas-aerosol partitioning depends on the total organic aerosol mass.

If we take as a rough estimate a 10% SOA yield from the isoprene+NO_3 pathway from the results in Table 4, 2 to 3 Tg yr^{-1} of SOA results from isoprene+NO_3. This rate of production would make SOA from isoprene+NO_3 as significant as that from sesquiterpenes, biogenic alcohols, and aromatics, each of which is estimated to produce about 2 to 4 Tg yr^{-1} of SOA based on yields measured in chamber studies (Henze et al., 2007). As a reference, the global SOA production is estimated to be 10–70 Tg yr^{-1} (Kanakidou et al., 2005). Recently, Goldstein et al. (2007) provided several alternative approaches to estimate global SOA production: 510–910 Tg C yr^{-1} based on the global mass balance of VOC removal, 225–575 Tg C yr^{-1} based on SOA deposition plus oxidation, 140–540 Tg C yr^{-1} based on comparison with the sulfate budget, and 223–615 Tg C yr^{-1} required to maintain the assumed global mean vertical SOA distribution. If we assume mass carbon/mass organics=0.5, the lower limit for SOA production from these estimates would be 280 Tg yr^{-1}, which is much larger than that estimated from chamber SOA yields. Still, the 3 Tg yr^{-1} of SOA estimated for the isoprene + NO_3 system is worth noticing. Owing to efficient photodissociation, NO_3 achieves its highest concentrations at night. By contrast, isoprene emissions are assumed to be zero at night in both emission models. Consequently, the isoprene+NO_3 reaction occurs only at night, involving isoprene that remains unreacted after each daytime period.

We caution that the estimates above are obtained at the crudest level of approximation, in which a globally uniform SOA yield of 10% from isoprene+NO_3 is applied. As we note from Table 4, there is also as substantial difference between predictions of the two available isoprene emission models; the more recent MEGAN model represents an improved level of understanding over the earlier GEIA model. Predictions of SOA formation from the isoprene+NO_3 pathway are, of course, highly dependent on ambient NO_3 radical concentrations. Nitrate radical concentrations predicted in the current simulations vary from about 0.1 ppt in remote regions of South America to 20 ppt or more in the southeastern USA (in August). Future work will address the simulation of SOA formation from isoprene+NO_3 following the microphysical treatment in GEOS-Chem.

Table 4. Global estimation of isoprene using GEOS-Chem.

	Emission Model	
	GEIA[a]	MEGAN[b]
Isoprene emission (Tg/y)	507	389
Global isoprene burden (Tg)	1.7	1.7
Isoprene lifetime (days)	1.2	1.6
Isoprene reacted (Tg/y) by		
Isoprene+OH	407	304
Isoprene+O_3	69	62
Isoprene+NO_3	29	21

[a] Modification of GEIA for GEOS-Chem are described at Bey et al. (2001c). Original GEIA reference is Guenther et al. (1995).
[b] Guenther et al. (2006).

6 Implications

We report a series of chamber experiments investigating the formation of secondary organic aerosols from the reaction of isoprene with nitrate radicals. For an initial isoprene concentration of 18.4 to 101.6 ppb, the SOA yield ranges from 4.3% to 23.8% (typical yield experiments). The SOA yield from the slow N_2O_5 injection experiment (RO_2+RO_2 reaction dominates) is much higher than that from the slow isoprene injection experiment (RO_2+NO_3 dominates), implying that RO_2+RO_2 is a more effective channel of forming SOA. The SOA yield from the slow N_2O_5 experiment is roughly the same as that in the typical yield experiments, suggesting that SOA yields obtained in this study likely represent conditions in which peroxy-peroxy radical reactions are favored. Using a uniform SOA yield of 10% (corresponding to $M_o \cong 10\,\mu\mathrm{g\,m^{-3}}$), ∼2 to 3 Tg yr^{-1} of SOA results from isoprene+NO_3, which is about 1/4 of the amount of SOA estimated to be formed from isoprene+OH (∼13 Tg yr^{-1}) (Henze et al., 2007).

The extent to which the results from this study can be applied to conditions in the atmosphere depends on the relative importance of the various reaction pathways of peroxy radicals in the nighttime atmosphere: RO_2+RO_2, RO_2+NO_3, RO_2+NO, and RO_2+HO_2. However, the fate of peroxy radicals in the atmosphere is uncertain owing to the large uncertainties in the reaction rate constants and ambient concentrations of the radicals (Skov et al., 1992; Kirchner and Stockwell, 1996; Bey et al., 2001a, b; Vaughan et al., 2006). For instance, a modeling study by Kirchner and Stockwell (1996) suggests that the RO_2+NO_3 reaction is the dominant pathway at night; 77% and 90% of the total RO_2 at night is predicted to react with NO_3 in polluted atmosphere and rural air (mixed with aged air), respectively. The other pathways are not as important; while RO_2+RO_2 can account for about 8–23% of the total RO_2 reaction, RO_2+HO_2 only accounts for 6–10%, and RO_2+NO is minimal (0–1%) (Kirchner and Stockwell, 1996). These results are at odds with the study by Bey et al. (2001a,b), which suggests that NO_3 radicals are not involved significantly in the propagation of RO_2 radicals (<5%). Instead, RO_2+NO (77%) and RO_2+RO_2 (40%) are dominant in the mixed layer in the urban and rural areas, respectively. Although there is no definite conclusion as which reaction pathway dominates in the nighttime atmosphere, both studies seem to suggest that RO_2+HO_2 is relatively not as important. In this work, we investigated situations in which either RO_2+RO_2 or RO_2+NO_3 dominates. In both cases the RO_2+HO_2 reaction is expected to be a minor channel and thus this is in line with the modeling studies. Although RO_2+NO is not considered in this study, this reaction produces the same alkoxy radical as in the RO_2+NO_3 reaction. It is likely that it would result in similar products as those in the case where the RO_2+NO_3 reaction dominates. Currently, only the reaction rate constants for small, relatively simple RO_2 radicals with NO_3 radicals have been reported (e.g. Biggs et al., 1994; Daele et al., 1995; Canosa-Mas et al., 1996; Vaughan et al., 2006) and they are roughly in the range of $(1\text{–}3)\times10^{-12}\,\mathrm{cm}^3\,\mathrm{molecule}^{-1}\,\mathrm{s}^{-1}$. With the oxidation of various volatile organic compounds by O_3 and NO_3 under nighttime conditions, it is expected that multifunctional peroxy radicals would be prevalent; the reaction rates of these complex peroxy radicals warrant future study. Furthermore, more field measurements on the concentrations of various radicals would also help to constrain the relative importance of the different reaction pathways.

In this study, we have shown that the formation of ROOR from the reaction of two peroxy radicals is an effective SOA-forming channel based on gas-phase data and elemental SOA composition data. If the results from this study can be applied to other systems (i.e., the reaction of NO_3 radicals with other volatile organic compounds), the organic peroxides could possibly be formed in all systems; they may not have been identified previously owing to the lack of suitable analytical techniques such as accurate mass measurements from high resolution MS. Since the formation of ROOR from two peroxy radicals has always been considered as a minor channel, the reaction has not been widely studied. Ghigo et al. (2003) ruled out the direct formation of products (RO, ROH, RCHO) from the tetroxide intermediate ROOOOR. Instead, they proposed that the tetroxide breaks up into a weakly bound complex of two RO radicals and O_2, which then fall apart or undergoes intersystem crossing to form the corresponding alcohol and carbonyl products. The formation of ROOR was not discussed in Ghigo et al. (2003) owing to little experimental evidence for the production of ROOR. However, the observation of ROOR formation in this study suggests that this reaction does occur and is potentially important for aerosol formation. As pointed out by Dibble (2008), the mechanism proposed by Ghigo (2003) would seem to allow for easy production of ROOR from the RO-RO-O_2 complex. Therefore, it appears that there are at least two possible pathways for ROOR formation: it can either be formed through the RO-RO-O_2 complex as suggested by Dibble (2008), or there may exist a direct pathway for ROOR formation from ROO+ROO. Certainly more work is needed regarding the formation, detection, and quantification of ROOR products.

It is also worth noting that while most NO_3 chemistry occurs at night, it can also be important during the day at specific locations. Recently, a study by Fuentes et al. (2007) suggested substantial formation of NO_3 radicals can take place in forested environments with moderate to high levels of BVOC production, resulting in a significant oxidation of isoprene and terpenes by NO_3 radicals. For instance, approximately 60% of the terpenes react with NO_3 radicals within the canopy. Clearly, more study is needed to evaluate the importance of NO_3 chemistry of biogenic hydrocarbons under different environments and time of the day.

Acknowledgements. This research was funded by US Department of Energy Biological and Environmental Research Program DE-FG02-05ER63983. This material is based in part on work supported by the National Science Foundation (NSF) under grant ATM-0432377. The Waters LCT Premier XT time-of-flight mass spectrometer interfaced to a Waters UPLC system was purchased in 2006 with a grant from the National Science Foundation, Chemistry Research Instrumentation and Facilities Program (CHE-0541745). The LCQ Ion Trap mass spectrometer was purchased in 1997 with funds from the National Science Foundation through the CRIF program (CHE-9709233). J. D. Surratt is supported in part by the US EPA under the STAR Graduate Fellowship Program. A. J. Kwan and H. O. T. Pye acknowledge the support of NSF graduate research fellowships. The authors would like to thank C. D. Vecitis, J. Cheng, and M. R. Hoffmann for use of and aid with their ozonizer and UV-VIS spectrometer; to K. Takematsu and M. Okumura for helpful advice on preparing N_2O_5; to J. H. Kroll and M. Claeys for helpful discussions and suggestions; to M. N. Chan for assistance with filter sample collection; to H. G. Kjaergaard and F. Paulot for performing the quantum calculations and estimating the sensitivities of CIMS to various gas-phase products; and to Y. Yu and the reviewers for helpful comments on the manuscript.

Edited by: S. Martin

References

Alfarra, M. R., Paulsen, D., Gysel, M., Garforth, A. A., Dommen, J., Prevot, A. S. H., Worsnop, D. R., Baltensperger, U., and Coe, H.: A mass spectrometric study of secondary organic aerosols formed from the photooxidation of anthropogenic and biogenic precursors in a reaction chamber, Atmos. Chem. Phys., 6, 5279–5293, 2006, http://www.atmos-chem-phys.net/6/5279/2006/.

Bahreini, R., Keywood, M. D., Ng, N. L., Varutbangkul, V., Gao, S., Flagan, R. C., and Seinfeld, J. H. Measurements of secondary organic aerosol (SOA) from oxidation of cycloalkenes, terpenes, and m-xylene using an Aerodyne aerosol mass spectrometer. Environ. Sci. Technol., 39, 5674–5688, 2005.

Barnes, I., Bastian, V., Becker, K. H., and Tong, Z.: Kinetics and products of the reactions of NO_3 with monoalkenes, dialkenes, and monoterpenes, J. Phys. Chem., 94, 2413–2419, 1990.

Berndt, T. and Böge, O.: Gas-Phase reaction of NO_3 radicals with isoprene: A kinetic and mechanistic study, Inter. J. Chem. Kinet., 29, 755–765, 1997.

Bey, I., Aumont, B., and Toupance, G.: A modeling study of the nighttime radical chemistry in the lower continental troposphere. 1. Development of a detailed chemical mechanism including nighttime chemistry, J. Geophys. Res., 106(D9), 9959–9990, 2001a.

Bey, I., Aumont, B., and Toupance, G.: A modeling study of the nighttime radical chemistry in the lower continental troposphere. 2. Origin and evolution of HO_x, J. Geophys. Res., 106(D9), 9991–10001, 2001b.

Bey, I., Jacob, D. J., Yantosca, R. M., Logan, J. A., Field, B. D., Fiore, A. M., Li, Q. B., Liu, H. G. Y., Mickley, L. J., and Schultz, M. G.: Global modeling of tropospheric chemistry with assimilated meteorology: Model description and evaluation, J. Geophys. Res., 106(D19), 23 073–23 095, 2001c.

Biggs, P., Canosa-Mas, C. E., Fracheboud, J. M., Shallcross, D. E., and Wayne, R. P.: Investigation into the kinetics and mechanisms of the reaction of NO_3 with CH_3 and CH_3O at 298K between 0.6 Torr and 8.5 Torr – is there a chain decomposition mechanism in operation, J. Chem. Soc., Faraday Trans., 90, 1197–1204, 1994.

Brown, S. S., Ryerson, T. B., Wollny, A. G., Brock, C. A., Peltier, R., Sullivan, A. P., Weber, R. J., Dube, W. P., Trainer, M., Meagher, J. F., Fehsenfeld, F. C., and Ravishankara, A. R.: Variability in nocturnal nitrogen oxide processing and its role in regional air quality, Science, 311, 5757, 67–70, 2006.

Canosa-Mas, C. E., Flugge, M. L., King, M. D., and Wayne, R. P.: An experimental study of the gas-phase reaction of the NO_3 radical with αsβtunsaturated carbonyl compounds, Phys. Chem. Chem. Phys., 7. 643–650, 2005.

Canosa-Mas, C. E., King, M. D., Lopez, R., Percival, C. J., Wayne, R. P., Shallcross, D. E., Pyle, J. A., and Daele, V.: Is the reaction $CH_3C(O)O_2$ and NO_3 important in the night-time troposphere? J. Chem. Soc., Faraday Trans., 92, 2211–2222, 1996.

Carslaw, N., Carpenter, L. J., Plane, J. M. C., Allan, B. J., Burgess, R. A., Clemitshaw, K. C., Coe, H., and Penkett, S. A.: Simultaneous measurements of nitrate and peroxy radicals in the marine boundary layer, J. Geophys. Res., 102, 18 917–18 933. 1997.

Carter, W. P. L. and Atkinson, R.: Development and evaluation of a detailed mechanism for the atmospheric reactions of isoprene and NO_x, Int. J. Chem. Kinet., 28, 497–530, 1996.

Claeys, M., Graham, B., Vas, G., Wang, W., Vermeylen, R., Pashynska, V., Cafmeyer, J., Guyon, P., Andreae, M. O., Artaxo, P., and Maenhaut, W.: Formation of secondary organic aerosols through photooxidation of isoprene, Science, 303, 1173–1176, 2004.

Cocker III, D. R., Flagan, R. C., and Seinfeld, J. H.: State-of-the-art chamber facility for studying atmospheric aerosol chemistry, Environ. Sci. Technol., 35, 2594–2601. 2001.

Crounse, J. D., McKinney, K. A., Kwan, A. J., and Wennberg, P. O.: Measurements of gas-phase hydroperoxides by chemical ionization mass spectrometry, Anal. Chem., 78, 6726–6732, 2006.

Curren, K., Gillespie, T., Steyn, D., Dann, T., and Wang, D.: Biogenic isoprene in the Lower Fraser Valley, British Columbia, J. Geophys. Res., 103, D19, 25467-25477, 1998.

Daele, V., Laverdet, G., Lebras, G., and Poulet, G.: Kinetics of the reactions of CH_3O+NO, CH_3O+NO_3, and CH_3O_2+NO_3, J. Phys. Chem., 99, 1470–1477, 1995.

Davidson, J. A., Viggiano, A. A., Howard, C. J., Fehsenfeld, F. C., Albritton, D. L., and Ferguson, E. E.: Rate constants for the reaction of O_2^+, NO_2^+, NO^+, H_3O^+, CO_3^-, NO_2^-, and halide ions with N_2O_5 at 300 K, J. Chem. Phys., 68, 2085–2087, 1978.

Dibble, T. S.: Isomerization of OH-isoprene adducts and hydroxyalkoxy isoprene radicals, J. Phys. Chem., 106(28), 6643–6650, 2002.

Dibbe T. S.: Failures and limitations of quantum chemistry for two key problems in the atmospheric chemistry of peroxy radicals, Atmos. Environ., in press, 2008.

Docherty, K., Wu, W., Lim, Y., and Ziemann, P.: Contributions of Organic Peroxides to Secondary Aerosol Formed from Reactions of Monoterpenes with O_3, Environ. Sci. Technol., 39, 4049–4059, 2005.

Dommen, J., Metzger, A., Duplissy, J., Kalberer, M., Alfarra, M. R., Gascho, A., Weingartner, E., Prevot, A. S. H., Verheggen, B., and Baltensperger, U.: Laboratory observation of oligomers in the aerosol from isoprene/NO_x photooxidation, Geophys. Res. Lett., 33, L13805, doi:10.1029/2006GL026523, 2006.

Edney, E. O., Kleindienst, T. E., Jaoui, M., Lewandowski, M., Offenberg, J. H., Wang, W., and Claeys, M.: Formation of 2-methyl tetrols and 2-methylglyceric acid in secondary organic aerosol from laboratory irradiated isoprene/NO_x/SO_2/air mixtures and their detection in ambient $PM_{2.5}$ samples collected in the eastern United States, Atmos. Environ., 39, 5281–5289, 2005.

Fan, J. and Zhang, R.: Atmospheric oxidation mechanism of isoprene, Environ. Chem., 1, 140–149, doi:10.1071/EN04045, 2004.

Fuentes, J. D., Wang, D., Rowling, D. R., Potosnak, M., Monson, R. K., Goliff, W. S., and Stockwell, W. R.: Biogenic hydrocarbon chemistry within and above a mixed deciduous forest, J. Atmos. Chem., 56, 165–185. 2007.

Gao, S., Keywood, M. D., Ng, N. L., Surratt, J. D., Varutbangkul, V., Bahreini, R., Flagan, R. C., and Seinfeld, J. H.: Low molecular weight and oligomeric components in secondary organic aerosol from the ozonolysis of cycloalkenes and α-pinene, J. Phys. Chem. A, 108, 10 147–10 164, 2004a.

Gao, S., Ng, N. L., Keywood, M. D., Varutbangkul, V., Bahreini, R., Nenes, A., He, J., Yoo, K. Y., Beauchamp, J. L., Hodyss, R. P., Flagan, R. C., and Seinfeld, J. H.: Particle phase acidity and oligomer formation in secondary organic aerosol, Environ. Sci. Technol., 38, 6582–6589, 2004b.

Gao, S., Surratt, J. D., Knipping, E. M., Edgerton, E. S., Shahgholi, M., and Seinfeld, J. H.: Characterization of polar organic components in fine aerosols in the southeastern United States: Identity, origin, and evolution, J. Geophys. Res., 111, D14314, doi:10.1029/2005JD006601, 2006.

Ghigo, G., Maranzana, A., and Tonachini, G.: Combustion and atmospheric oxidation o hydrocarbons: Theoretical study of the methyl peroxyl self-reaction, J. Chem. Phys., 118, 23, 2003.

Goldstein, A. H. and Galbally, I. E.: Known and unexplored organic constituents in the earth's atmosphere, Environ. Sci. Technol., 41, 1514–1521, 2007.

Gong, H., Matsunaga, A., and Ziemann, P.: Products and mechanism of secondary organic aerosol formation from reactions of linear alkenes with NO_3 radicals, J. Phys. Chem., 109, 4312–4324, 2005.

Gómez-González, Y., Surratt, J. D., Cuyckens, F., Szmigielski, R., Vermeylen, R., Jaoui, M., Lewandowski, M., Offenberg, J. H., Kleindienst, T. E., Edney, E. O., Blockhuys, F., Van Alsenoy, C., Maenhaut, W. and Claeys, M.: Characterization of organosulfates from the photooxidation of isoprene and unsaturated fatty acids in ambient aerosol using liquid chromatography/(–) electrospray ionization mass spectrometry, J. Mass Spectrom., 43(3), 371–382, doi:10.1002/jms.1329, 2007.

Guenther, A., Hewitt, C. N., Erickson, D., Fall, R., Geron, C., Graedel, T., Harley, P., Klinger, L., Lerdau, M., Mckay, W. A., Pierce, T., Scholes, B., Steinbrecher, R., Tallamraju, R., Taylor, J., and Zimmerman, P.: A global-model of natural volatile organic compound emissions, J. Geophys. Res., 100(D5), 8873–8892, 1995.

Guenther, A., Karl, T., Harley, P., Wiedinmyer, C., Palmer, P. I., and Geron, C.: Estimates of global terrestrial isoprene emissions using MEGAN (Model of Emissions of Gases and Aerosols from Nature), Atmos. Chem. Phys., 6, 3181–3210, 2006, http://www.atmos-chem-phys.net/6/3181/2006/.

Heintz, F., Platt, U., Flentje, H., and Dubois, R.: Long-term observation of nitrate radicals at the tor station, Kap Arkona (Rugen), J. Geophys. Res., 101(D17), 22 891–22 910, 1996.

Henze, D. K., Seinfeld, J. H., Ng, N. L., Kroll, J. H., Fu, T.-M., Jacob, D. J., and Heald, C. L.: Global modeling of secondary organic aerosol formation from aromatic hydrocarbons: high- vs. low-yield pathways, Atmos. Chem. Phys., 8, 2405–2420, 2008, http://www.atmos-chem-phys.net/8/2405/2008/.

Horowitz, L. W., Fiore, A. M., Milly, G. P., Cohen, R. C., Perring, A., Wooldridge, P. J., Hess, P.G., Emmons, L. K., and Lamarque, J.: Observational constraints on the chemistry of isoprene nitrates over the eastern United States, J. Geophys. Res., 112, D12S08, doi:10.1029/2006JD007747, 2007.

Iinuma, Y., Müller, C., Berndt, T., Böge, O., Claeys, M., and Herrmann, H.: Evidence for the existence of organosulfates from β-pinene ozonolysis in ambient secondary organic aerosol, Environ. Sci. Technol., 41, 6678–6683, 2007b.

Iinuma, Y., Müller, C., Böge, O., Gnauk, T., and Herrmann, H.: The formation of organic sulfate esters in the limonene ozonolysis secondary organic aerosol (SOA) under acidic conditions, Atmos. Environ., 41, 5571–5583, 2007a.

Jay, K. and Stieglitz, L.: The gas phase addition of NO_x to olefins, Chemosphere, 19, 1939–1950, 1989.

Jayne, J. T., Leard, D. C., Zhang, X., Davidovits, P., Smith, K. A., Kolb, C. E., and Worsnop, D. W.: Development of an Aerosol Mass Spectrometer for size and composition analysis of submicron particles, Aerosol Sci. Technol., 33, 49–70, 2000.

Kan, C. S., Calvert, J. G., and Shaw, J. H.: Reactive channels of the CH_3O_2-CH_3O_2 reaction, J. Phys. Chem., 84, 3411–3417, 1980.

Kanakidou, M., Seinfeld, J. H., Pandis, S. N., Barnes, I., Dentener, F. J., Facchini, M. C., Van Dingenen, R., Ervens, B., Nenes, A., Nielsen, C. J., Swietlicki, E., Putaud, J. P., Balkanski, Y., Fuzzi, S., Horth, J., Moortgat, G. K., Winterhalter, R., Myhre, C. E. L., Tsigaridis, K., Vignati, E., Stephanou, E. G., and Wilson, J.: Organic aerosol and global climate modelling: a review, Atmos. Chem. Phys., 5, 1053–1123, 2005, http://www.atmos-chem-phys.net/5/1053/2005/.

Keywood, M. D., Varutbangkul, V., Bahreini, R., Flagan, R. C., and Seinfeld, J. H.: Secondary organic aerosol formation from the ozonolysis of cycloalkenes and related compounds, Environ. Sci. Technol., 38, 4157–4164, 2004.

Kirchner, F. and Stockwell, W. R.: Effect of peroxy radical reactions on the predicted concentrations of ozone, nitrogenous compounds, and radicals, J. Geophys. Res., 101(D15), 21 007–21 022, 1996.

Knopf, D. A., Mak, J., Gross, S., and Bertram, A. K.: Does atmospheric processing of saturated hydrocarbon surfaces by NO_3 lead to volatilization?, Geophys. Res. Lett., 33, L17816, doi:10.1029/2006GL026884, 2006.

Kroll, J. H., Ng, N. L., Murphy, S. M., Flagan, R. C., and Seinfeld, J. H.: Secondary organic aerosol formation from isoprene photooxidation under high-NO_x conditions, J. Geophys. Res., 32, L18808, doi:10.1029/2005GL023637, 2005.

Kroll, J. H., Ng, N. L., Murphy, S. M., Flagan, R. C., and Seinfeld. J. H.: Secondary organic aerosol formation from isoprene photooxidation, Environ. Sci. Technol., 40. 1869–1877, 2006.

Kwok, E. S. C., Aschmann, S. M., Arey, J., and Atkinson, R.: Product formation from the reaction of the NO_3 radical with isoprene and rate constants for the reactions of methacrolein and methyl vinyl ketone with the NO_3 radical, Inter. J. Chem. Kinet. 28, 925–934, 1996.

Liggio, J. and Li, S. M.: Organosulfate formation during the uptake of pinonaldehyde on acidic sulfate aerosols, Geophys. Res. Lett., 33, L13808, doi:10.1029/2006GL026079, 2006.

Liggio, J., Li, S. M., and McLaren, R.: Heterogeneous reactions of glyoxal on particulate matter: Identification of acetals and sulfate esters, Environ. Sci. Technol., 39, 1532–1541, 2005.

Lightfoot, P. D., Cox, R..A., Crowley, J. N., Destriau, M. Hayman, G. D., Jenkin, M. E., Moortgat G. K., and Zabel, F.: Organic peroxy radicals – kinetics, spectroscopy and tropospheric chemistry, Atmos. Environ., 26, 1805–1961, 1992.

Moise, T., Talukdar, R. K., Frost, G. J., Fox, R. W., and Rudich, Y.: Reactive uptake of NO_3 by liquid and frozen organics, J. Geophys. Res., 107(D2), 4014, doi:10.1029/2001JD000334, 2002.

Ng, N. L., Chhabra, P. S., Chan, A. W. H., Surratt, J. D., Kroll, J. H., Kwan, A. J., McCabe, D. C., Wennberg, P. O., Sorooshian, A., Murphy, S. M., Dalleska, N. F., Flagan, R. C., and Seinfeld, J. H.: Effect of NO_x level on secondary organic aerosol (SOA) formation from the photooxidation of terpenes, Atmos. Chem. Phys., 7, 5159–5174, 2007a, http://www.atmos-chem-phys.net/7/5159/2007/.

Ng, N. L., Kroll, J. H., Chan, A. W. H., Chhabra, P. S., Flagan, R. C., and Seinfeld, J. H.: Secondary organic aerosol formation from *m*-xylene, toluene, and benzene, Atmos. Chem. Phys., 7, 3909–3922, 2007b, http://www.atmos-chem-phys.net/7/3909/2007/.

Ng, N. L., Kroll, J. H., Keywood, M. D., Bahreini, R., Varutbangkul, V., Flagan, R. C., Seinfeld, J. H., Lee, A., and Goldstein, A. H.: Contribution of first- versus second-generation products to secondary organic aerosols formed in the oxidation of biogenic hydrocarbons, Environ. Sci. Technol., 40, 2283–2297, 2006.

Niki, H, Maker, P. D., Savage, C. M., and Breitenbach L.P.: Fourier Transform Infrared studies of the self-reaction of CH_3O_2 radicals, J. Phys. Chem., 85, 877–881, 1981.

Niki, H, Maker, P. D., Savage, C. M., and Breitenbach L.P.: Fourier Transform Infrared studies of the self-reaction of $C_2H_5O_2$ radicals, J. Phys. Chem., 86, 3825–3829, 1982.

Noda, J., Nyman, G., and Langer S.: Kinetics of the gas-phase reaction of some unsaturated alcohols with the nitrate radical, J. Phys. Chem., 106, 945–951, 2002.

Odum, J. R., Hoffmann, T., Bowman, F., Collins, D., R. C. Flagan, R. C., and Seinfeld, J. H.: Gas/particle partitioning and secondary organic aerosol yields, Environ. Sci. Technol., 30, 2580–2585, 1996.

Odum, J. R., Jungkamp, T. P. W., Griffin, R. J., Flagan, R. C., and Seinfeld, J. H.: The atmospheric aerosol-forming potential of whole gasoline vapor, Science, 276, 96–99, 1997a.

Odum, J. R., Jungkamp, T. P. W., Griffin, R. J., Forstner, H. J. L., Flagan, R. C., and Seinfeld, J. H.: Aromatics, reformulated gasoline and atmospheric organic aerosol formation, Environ. Sci. Technol., 31, 1890–1897, 1997b.

Paulot, F., Crounse, J. D., Kjaergaard, H. G., Kroll, J. H., Seinfeld, J. H., and Wennberg, P. O.: Isoprene photooxidation mechanism: resonance channels and implications for the production of nitrates and acids, accepted, Atmos. Chem. Phys. Discuss., 2008.

Paulson, S. E. and Seinfeld, J. H.: Development and evaluation of a photooxidation mechanism for isoprene, J. Geophys. Res., 97(D18), 20 703–20 715, 1992.

Penkett, S. A., Burgess, R. A., Coe, H., Coll, I., Hov, Ø., Lindskog, A., Schmidbauer, N., Solberg, S., Roemer, M., Thijsse, T., Beck, J., and Reeves C. E.: Evidence for large average concentrations of the nitrate radical (NO_3) in Western Europe from the HANSA hydrocarbon database, Atmos. Environ., 41, 3465–3478, 2007.

Platt, U. and Janssen, C.: Observation and role of the free radicals NO_3, ClO, BrO and IO in the troposphere, Faraday Discuss., 100, 175–198, 1995.

Platt, U., Perner, D., Schroder, J., Kessler, C., and Toennissen, A.: The diurnal variation of NO_3, J. Geophys. Res., 86, 11 965–11 970, 1981.

Rudich, Y., Donahue, N. M., and Mentel, T. F.: Aging of organic aerosol: Bridging the gap between laboratory and field studies, Annu. Rev. Phys. Chem., 58, 321–352, 2007.

Sharkey, T. D., Singsaas, E. L., Vanderveer, P. J., and Geron, C.: Field measurements of isoprene emission from trees in response to temperature and light, Tree Physiol., 16, 649–654, 1996.

Skov, H., Benter, Th., Schindler, R. N., Hjorth, J., and Restelli, G.: Epoxide formation in the reactions of the nitrate radical with 2,3-dimethyl-2-butene, cis- and trans-2-butene and isoprene, Atmos. Environ., 28, 1583–1592, 1994.

Skov, H., Hjorth, J., Lohse, C., Jensen, N. R. and Restelli, G.: Products and mechanisms of the reactions of the nitrate radical (NO_3) with isoprene, 1,3-butadiene and 2,3-dimethyl-1,3-butadiene in air, Atmos. Environ., 26A(15), 2771–2783, 1992.

Smith, N., Plane, J. M. C., Nien, C. F., and Solomon, P. A.: Nighttime radical chemistry in the San-Joaquin Valley, Atmos. Environ., 29, 2887–2897, 1995.

Sorooshian, A., Brechtel F. J., Ma, Y. L., Weber R. J., Corless, A., Flagan, R. C., and Seinfeld, J. H.: Modeling and characterization of a particle-into-liquid sampler (PILS), Aerosol Sci. Technol., 40, 396–409, 2006.

Starn, T. K., Shepson, P. B., Bertman, S. B., Riemer, D. D., Zika, R. G. and Olszyna, K.: Nighttime isoprene chemistry at an urban-impacted forest site, J. Geophys. Res., 103(D17), 22 437–22 447, 1998.

Steinbacher, M., Dommen, J. Ordonez, C., Reimann, S., Gruebler, F. C., Staehelin, J., Andreani-Aksoyoglu, S., and Prevot, A. S. H.: Volatile organic compounds in the Po Bason. Part B: Biogenic VOCs, J. Atmos. Chem., 51, 293–315, 2005.

Stroud, C. A., Roberts, J. M., Williams E. J., Hereid, D., Angevine, W. M., Fehsenfeld, F. C., Wisthaler, A., Hansel, A., Martinez-Harder, M., Harder, H., Brune, W. H., Hoenninger, G., Stutz, J., and White, A. B.: Nighttime isoprene trends at an urban forested site during the 1999 Southern Oxidant Study, J. Geophys. Res., 107(D16), 4291, doi:10.1029/2001JD000959, 2002.

Su, T. and Chesnavich, W. J.: Parametrization of the ion–polar molecule collision rate constant by trajectory calculations, The Journal of Chemical Physics, 76, 5183, 1982.

Suh, I., Lei, W., and Zhang, R.: Experimental and theoretical studies of isoprene reaction with NO_3, J. Phys. Chem., 105, 6471–6478, 2001.

Surratt, J. D., Kroll, J. H., Kleindienst, T. E., Edney, E. O., Claeys, M., Sorooshian, A., Ng, N. L., Offenberg, J. H., Lewandowski, M., Jaoui, M., Flagan, R. C., and Seinfeld, J. H.: Evidence for organosulfates in secondary organic aerosol, Environ. Sci. Technol., 41, 517–527, 2007a.

Surratt, J. D., Lewandowski, M., Offenberg, J. H., Jaoui, M., Kleindienst, T. E., Edney, E. O., and Seinfeld, J. H.: Effect of acidity on secondary organic aerosol formation from isoprene, Environ. Sci. Technol., 41, 5363–5369, 2007b.

Surratt, J. D., Murphy, S. M., Kroll, J. H., Ng, N. L., Hildebrandt, L., Sorooshian, A., Szmigielski, R., Vermeylen, R., Maenhaut, W., Claeys, M., Flagan, R. C., and Seinfeld, J. H.: Chemical composition of secondary organic aerosol formed from the photooxidation of isoprene, J. Phys. Chem. A, 110, 9665–9690, 2006.

Szmigielski, R., Surratt, J. D., Vermeylen, R., Szmigielska, K., Kroll, J. H., Ng, N. L., Murphy, S. M., Sorooshian, A., Seinfeld, J. H., and Claeys, M.: Characterization of 2-methylglyceric acid oligomers in secondary organic aerosol formed from the photooxidation of isoprene using trimethylsilylation and gas chromatography/ion trap mass spectrometry, J. Mass Spectrom., 42, 101–116, 2007.

Tyndall, G. S., Cox, R. A., Granier, C., Lesclaux, R., Moortgat, G. K., Pilling, M. J., Ravishankara, A. R., and Wallington, T. J.: Atmospheric chemistry of small peroxy radicals, J. Geophys. Res., 106(D11), 12 157–12 182, 2001.

Tyndall, G. S., Wallington, T. J., and Ball, J. C.: FTIR product study of the reactions of CH_3O_2+CH_3O_2 and CH_3O_2+O_3, J. Phys. Chem., 102, 2547–2554, 1998.

Vaughan, S. Canosa-Mas, C. E., Pfrang, C., Shallcross, D. E., Watson, L., and Wayne, R. P.: Kinetic studies of reactions of the nitrate radical (NO_3) with peroxy radicals (RO_2): an indirect source of OH at night? Phys. Chem. Chem. Phys., 8, 3749–3760, 2006.

von Friedeburg, C., Wagner, T., Geyer, A., Kaiser, N., Platt, U., Vogel, B. and Vogel, H.: Derivation of tropospheric NO_3 profiles using off-axis differential optical absorption spectroscopy measurements during sunrise and comparison with simulations, J. Geophys. Res., 107(D13), 4168, doi:10.1029/2001JD000481, 2002.

Wallington, T. J., Dagaut, P., and Kurylo, M. J.: Ultraviolet absorption cross-sections and reaction kinetics and mechanisms for peroxy radicals in the gas phase, Chem. Rev., 92, 667–710, 1992.

Wallington, T. J., Gierczak, C. A., Ball, J. C., and Japar, S. M.: Fourier Transform Infrared studies of the self-reaction of $C_2H_5O_2$radicals in air at 295 K, Int. J. Chem. Kinet., 21, 1077–1089, 1989.

Werner, G., Kastler, J., Looser, R., and Ballschmiter, K.: Organic nitrates of isoprene as atmospheric trace compounds, Angew. Chem. Int. Ed., 38(11), 1634–1637, 1999.

Wu, S. L., Mickley, L. J., Jacob, D. J. Logan, J. A., Yantosca, R. M., and Rind, D.: Why are there large differences between models in global budgets of tropospheric ozone? J. Geophys. Res., 112(D5), D05302, doi:10.1029/2006JD007801, 2007.

Zhang, D. and Zhang, R.: Unimolecular decomposition of nitrooxyalkyl radicals from NO_3-isoprene reaction, J. Chem. Phys., 116(22), 9721–9728, 2002.

Ziemann, P.: Evidence for low-volatility diacyl peroxides as a nucleating agent and major component of aerosol formed from reactions of O_3 with cyclohexene and homologous compounds, J. Phys. Chem., 106, 4390–4402, 2002.

Appendix E

3-Methyl-1,2,3-Butanetricarboxylic Acid: An Atmospheric Tracer for Terpene Secondary Organic Aerosol*

---

*This chapter is reproduced by permission from "3-Methyl-1,2,3-butanetricarboxylic Acid: An Atmospheric Tracer for Terpene Secondary Organic Aerosol" by Rafal Szmigielski, Jason D. Surratt, Yadian Gómez-González, Pieter Van der Veken, Ivan Kourtchev, Reinhilde Vermeylen, Frank Blockhuys, Mohammed Jaoui, Tadeusz E. Kleindienst, Michael Lewandowski, John H. Offenberg, Edward O. Edney, John H. Seinfeld, Willy Maenhaut, and Magda Claeys, *Geophysical Research Letters*, 34 (24), L24811, 2007. Copyright 2007 by the American Geophysical Union.

GEOPHYSICAL RESEARCH LETTERS, VOL. 34, L24811, doi:10.1029/2007GL031338, 2007

3-methyl-1,2,3-butanetricarboxylic acid: An atmospheric tracer for terpene secondary organic aerosol

Rafal Szmigielski,[1] Jason D. Surratt,[2] Yadian Gómez-González,[1] Pieter Van der Veken,[1]
Ivan Kourtchev,[1] Reinhilde Vermeylen,[1] Frank Blockhuys,[3] Mohammed Jaoui,[4]
Tadeusz E. Kleindienst,[5] Michael Lewandowski,[5] John H. Offenberg,[5] Edward O. Edney,[5]
John H. Seinfeld,[6] Willy Maenhaut,[7] and Magda Claeys[1]

Received 16 July 2007; revised 25 September 2007; accepted 22 October 2007; published 27 December 2007.

[1] Highly oxygenated compounds assigned to be oxidation products of α-pinene have recently been observed in substantial concentrations in ambient aerosols. Here, we confirm the unknown α-pinene tracer compound with molecular weight (MW) 204 as the C_8-tricarboxylic acid 3-methyl-1,2,3-butanetricarboxylic acid. Its gas and liquid chromatographic behaviors and its mass spectral characteristics in electron ionization and negative ion electrospray ionization perfectly agree with those of a synthesized reference compound. The formation of this compound is explained by further reaction of *cis*-pinonic acid involving participation of the OH radical. This study illustrates that complex, multi-generation chemistry holds for the photooxidation of α-pinene in the presence of NO_x. **Citation:** Szmigielski, R., et al. (2007), 3-methyl-1,2,3-butanetricarboxylic acid: An atmospheric tracer for terpene secondary organic aerosol, *Geophys. Res. Lett.*, *34*, L24811, doi:10.1029/2007GL031338.

1. Introduction

[2] Considerable efforts have been devoted in the last two decades to understand secondary organic aerosol (SOA) formation from the photooxidation of volatile organic compounds (VOCs), in particular, the monoterpene, α-pinene. The reasons for these studies are manifold: (1) α-pinene has high emission rates on a global scale estimated at about 127 Tg per year [*Guenther et al.*, 1995]; (2) α-pinene has been shown to give high SOA yields in laboratory smog chamber experiments [e.g., *Griffin et al.*, 1999]; and (3) insight into the underlying mechanisms leading to SOA formation is needed to develop more precise models that allow the prediction of SOA contributions from monoterpenes and other biogenic and anthropogenic VOCs to the ambient aerosol load [e.g., *Kanakidou et al.*, 2005]. SOA is formed from nucleation and/or condensation onto pre-existing aerosol of low-volatility compounds formed by reactions of ozone, OH and NO_3 radicals with biogenic and anthropogenic VOCs. As regards to α-pinene, it has been firmly established that *cis*-pinic, *cis*-norpinic and *cis*-pinonic acids are major products formed by reaction with ozone [e.g., *Yu et al.*, 1999a; *Iinuma et al.*, 2004] and OH radicals [e.g., *Larsen et al.*, 2001]. However, several ambient aerosol studies have shown that the atmospheric concentrations of major α-pinene SOA products (i.e., *cis*-pinic and *cis*-pinonic acid) are rather low during summer episodes [e.g., *Yu et al.*, 1999b; *Warnke et al.*, 2006; *Cahill et al.*, 2006; *Plewka et al.*, 2006; *Gao et al.*, 2006; *Kourtchev et al.*, 2007], while evidence was obtained that highly oxygenated products are formed that could also be generated by irradiating α-pinene in the presence of NO_x through reactions that involve ozone and OH radicals [*Edney et al.*, 2003; *Jaoui et al.*, 2005; *Claeys et al.*, 2007; *Ng et al.*, 2007].

[3] In the present study, we address the chemical identification of a major α-pinene SOA compound with MW 204. This compound was first detected in tropical aerosol from the Amazon basin and summer aerosol from Ghent, Belgium, and based on the mass spectral behavior of the trimethyl ester derivative in the electron ionization (EI) mode it was assigned to a C_8-tricarboxylic acid, i.e., 3-carboxyheptanedioic acid [*Kubátová et al.*, 2000]. In addition to the latter study, a MW 204 compound has also been observed in ambient aerosol collected at other field sites, both in Europe [e.g., *Warnke et al.*, 2004; *Kourtchev et al.*, 2005] and the United States [e.g., *Edney et al.*, 2003; *Gao et al.*, 2006]. Subsequently, laboratory experiments with irradiated α-pinene in the presence of NO_x demonstrated this compound to be an α-pinene SOA product [*Edney et al.*, 2003; *Jaoui et al.*, 2005, *Ng et al.*, 2007]. In addition, it was shown that the MW 204 compound is also a β-pinene SOA product [*Jaoui et al.*, 2005]. A recent study [*Claeys et al.*, 2007] suggested that this compound results from further oxidation of *cis*-pinic acid, and an alternative tentative structure was proposed based on synthesis of an isomeric reference compound, i.e., 2-hydroxy-4-isopropyladipic acid. However, accurate mass measurements using high resolution mass spectrometry indicated a C_8-tricarboxylic acid for the MW 204 α-pinene SOA product and has prompted us to re-address its chemical structure.

[4] The current study consists of the organic synthesis of the proposed unknown compound and comparison of its chromatographic and mass spectral behaviors with

---

[1] Department of Pharmaceutical Sciences, University of Antwerp, Antwerp, Belgium.

[2] Department of Chemistry, California Institute of Technology, Pasadena, California, USA.

[3] Department of Chemistry, University of Antwerp, Antwerp, Belgium.

[4] Alion Science and Technology, Research Triangle Park, North Carolina, USA.

[5] National Exposure Research Laboratory, Office of Research and Development, United States Environmental Protection Agency, Research Triangle Park, North Carolina, USA.

[6] Departments of Chemical Engineering and Environmental Science and Engineering, California Institute of Technology, Pasadena, California, USA.

[7] Department of Analytical Chemistry, Institute for Nuclear Sciences, Ghent University, Ghent, Belgium.

0094-8276/07/2007GL031338$05.00

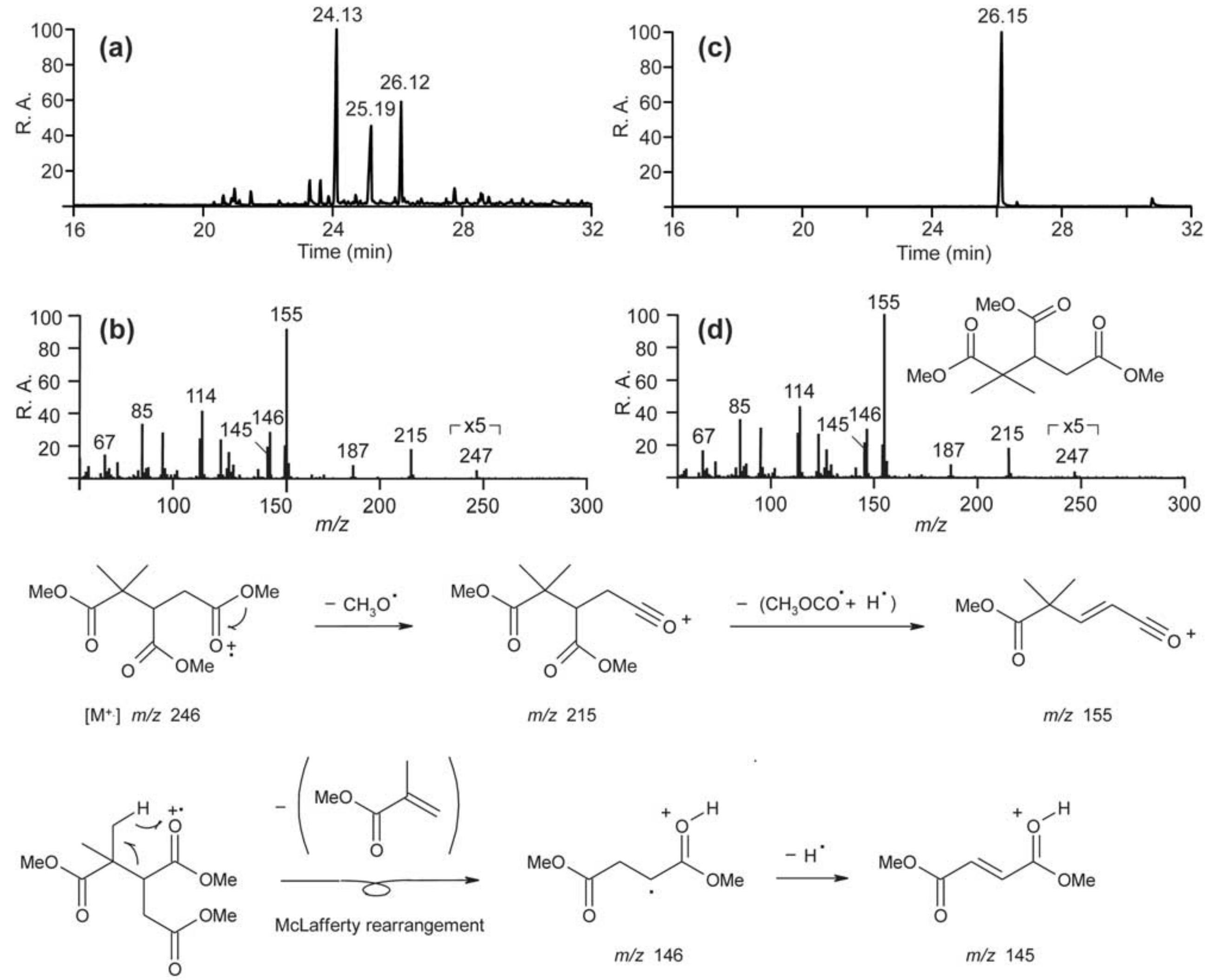

Figure 1. GC/MS data obtained for α-pinene/isoprene SOA (run 1) and synthesized MBTCA trimethyl ester, and EI fragmentation pathways: (a) TIC for α-pinene/isoprene SOA, (b) EI spectrum for compound eluting at 26.12 min, (c) TIC for MBTCA trimethyl ester, and (d) EI spectrum for compound eluting at 26.15 min. Other peaks identified in α-pinene/isoprene SOA (Figure 1a) were *cis*-norpinic acid (24.13 min) and *cis*-pinic acid (25.19 min).

those of the unknown α-pinene SOA product using gas chromatography/mass spectrometry (GC/MS) with EI and prior derivatization into trimethyl ester derivatives as well as liquid chromatography/mass spectrometry (LC/MS) with electrospray ionization in the negative ion mode [(−)ESI]. The unknown α-pinene SOA product is identified as 3-methyl-1,2,3-butanetricarboxylic acid (MBTCA) (trivial name: α,α-dimethyltricarballylic acid), and a plausible formation mechanism is presented.

2. Experimental Methods

[5] Synthesis of the MW 204 α-pinene SOA compound: MBTCA in the trimethyl ester form was prepared by a nucleophilic reaction between methyl 2-bromoisobutyrate (purity >99%; Fluka) with dimethylsuccinate (purity >98%; Fluka) using lithium diisopropylamide as base and tetrahydrofuran as solvent at low temperature. The crude reaction mixture was subjected to distillation under reduced pressure (101–102°C/0.1 mmHg) affording the product of interest as a dense yellowish oil with 56% yield. The structure of the synthesized standard was confirmed by NMR spectroscopy. MBTCA was obtained by hydrolysis of the trimethyl ester with concentrated aqueous HCl under reflux.

[6] Aerosol samples: Archived $PM_{2.5}$ aerosol samples were used. One set of ambient samples was collected at K-puszta, Hungary, a mixed deciduous/coniferous forest site, during a 2003 summer campaign. Details about the aerosol sampling and site conditions are presented in previous work [*Ion et al.*, 2005]. Additional ambient samples were collected at three different sites (i.e., Birmingham, AL; Centerville, AL; and Atlanta, GA) from the southeastern U.S. during the summer 2004 Southeastern Aerosol Research and Characterization (SEARCH) Study. These ambient samples were used only for accurate mass measurements; details of aerosol sampling, site conditions and of gas- and particle-phase measurements conducted can

Table 1. Initial Conditions for the VOC Irradiation Experiments

Exp ID	NO, ppb	SO_2, ppb	α-Pinene, ppmC	Isoprene, ppmC	Toluene, ppmC	T, °C	Initial RH, %
Run 1	270	-	2.27	2.49	-	23.8	30
Run 2	598	296	1.02	2.99	9.81	23.6	30

be found elsewhere [*Gao et al.*, 2006]. The laboratory samples were obtained by irradiating VOC mixtures in the presence of air, NO_x, and with or without SO_2, as described in detail by *Kleindienst et al.* [2006]. The two experiments were carried out in a rectangular 14.5 m^3 smog chamber which was operated in a dynamic or flow mode; the average chamber residence time (τ) was 5.9 and 6.0 h. The samples were collected on glass fiber filters and kept in a freezer at −25°C until analysis. The initial conditions for the chamber experiments are given in Table 1.

[7] Sample preparation: For the ambient samples collected at K-puszta, Hungary, sections of quartz fiber filters from different days and/or nights (containing in total between 30 and 80 μg organic carbon) were pooled, extracted as reported in previous work [*Ion et al.*, 2005] and the extract residues redissolved in 200 μL of water. Details of the extraction procedure for the ambient samples collected from the southeastern U.S. can be found elsewhere [*Gao et al.*, 2006]; however, final residues were redissolved in 500 μL of a 1:1 (v/v) solvent mixture of 0.1% acetic acid in water and 0.1% acetic acid in methanol and were only used for accurate mass measurements. In the case of the laboratory samples, the samples were worked up in the same way as described above. Part of the run 1 filter (3/8) was used for GC/MS and LC/MS analyses, while the run 2 filter was used for accurate mass measurements. Half of the run 1 filter extract was used for LC/MS, while the other half was used for GC/MS and methylated with ethereal diazomethane prior to analysis.

[8] Gas chromatography/mass spectrometry: Details about the GC/MS system and conditions are reported by *Ion et al.* [2005].

[9] Liquid chromatography/mass spectrometry: The LC/MS system consisted of a Surveyor Plus system (pump and autosampler), a linear ion trap mass spectrometer (LXQ), and a data system using Xcalibur version 2.0 software (Thermo Fisher, San Jose, USA). An Atlantis dC18 column (3 μm; 2.1 × 150 mm) (Waters, Milford, USA) was employed. The mobile phases consisted of acetic acid 0.1% (v/v) (A) and methanol (B). The applied 45-min gradient elution program was as follows: the concentration of eluent B was kept at 3% for 2 min, then increased to 90% in 18 min, kept at 90% for 10 min, then decreased to 3% in 5 min, and kept at 3% for 10 min. The injection volume and flow rate were 5 μL and 0.2 mL min^{-1}, respectively. The linear ion trap was operated under the following conditions: sheath gas flow (nitrogen), 50 arbitrary units; auxiliary gas flow (nitrogen), 5 arbitrary units; source voltage, −4.5 kV; capillary tem-

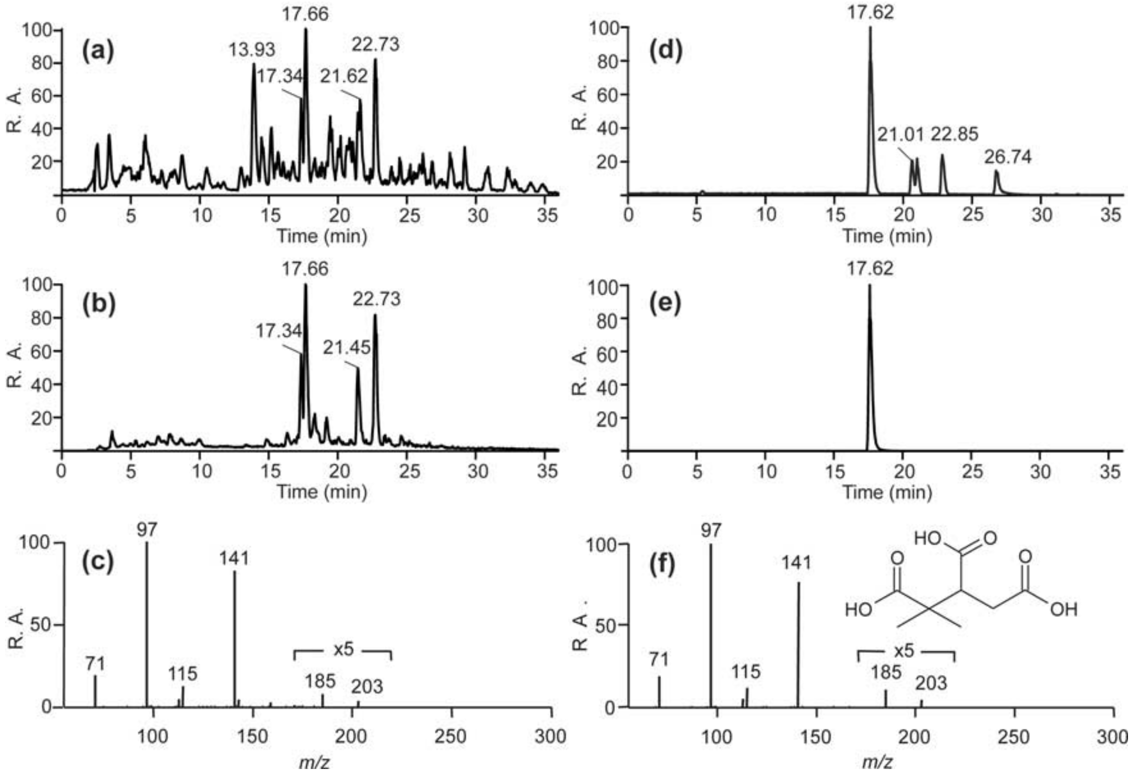

Figure 2. LC/(−)ESI MS data obtained for K-puszta $PM_{2.5}$ aerosol (pooled day- and nighttime sample) and synthesized MBTCA: (a) BPC for K-puszta aerosol, (b) extracted ion chromatogram (EIC) (m/z 203 + 171 + 185 + 183), (c) m/z 203 MS^2 spectrum for compound eluting at 17.66 min, (d) TIC for synthesized MBTCA, (e) EIC (m/z 203), and (f) m/z 203 MS^2 spectrum for compound eluting at 17.62 min.

perature, 350 °C; and maximum ion injection time, 200 ms. For MS^2 experiments, an isolation width of 1 m/z unit, a normalized collision energy level of 35% and broad band activation were applied.

[10] High resolution mass spectrometry: Accurate mass measurements for the run 2 and SEARCH filters were performed with a Waters LCT Premier XT time-of-flight mass spectrometer (TOFMS) equipped with ESI, and interfaced to a Waters ultra performance liquid chromatography (UPLC) system. Details about the UPLC/(-)ESI-TOFMS technique are given by *Ng et al.* [2007].

3. Results and Discussion

[11] Previous studies established that the MW 204 compound detected in ambient aerosol by GC/MS after conversion to different derivatives, including trimethyl ester and trimethylsilyl derivatives, is the same as that formed by irradiating α-pinene in the presence of NO_x [*Edney et al.*, 2003; *Jaoui et al.*, 2005; *Claeys et al.*, 2007] based on similar chromatographic behaviors and EI-MS characteristics. In addition, this compound represents on average 33% of the terpenoic acids (comprising 3-hydroxyglutaric acid, *cis*-pinic acid and the target compound itself) in $PM_{2.5}$ aerosol collected from K-puszta [*Claeys et al.*, 2007], indicating that it is a major terpenoic tracer compound. The structure of this compound was tentatively identified as 2-hydroxy-4-isopropyladipic acid based on the synthesis of an isomeric reference compound [*Claeys et al.*, 2007]. Accurate mass measurements performed in the present study on an irradiated α-pinene/isoprene/toluene mixture (run 2) and the ambient samples collected from the southeastern U.S. using UPLC/(−)ESI-TOFMS at high mass resolution, indicated a composition of $C_8H_{11}O_6$ (measured mass, 203.0558 Da; mass error, 0.2 mDa) for the m/z 203 α-pinene SOA compound, which is consistent with a C_8-tricarboxylic acid proposed in earlier work [*Kubátová et al.*, 2000; *Jaoui et al.*, 2005]. However, the earlier proposed linear structure, i.e., 3-carboxyheptanoic acid, could not be readily explained by oxidation of α-pinene, since the compound lacks the dimethyl methylene moiety $[(CH_3)_2C]$, a specific skeletal feature of α-pinene. Taking into account the EI mass spectral characteristics of the unknown MW 204 compound in the trimethyl ester form, i.e., the formation of characteristic ions at m/z 146/145 through a McLafferty rearrangement reaction [*Kubátová et al.*, 2000], two alternative candidate molecules were considered and synthesized, i.e., 2-methyl-4-carboxyadipic acid (not reported here) and 3-methyl-1,2,3-butanetricarboxylic acid, of which the latter compound is shown in the present study to correspond with the unknown MW 204 α-pinene SOA compound. It is worth noting that retention time and accurate mass measured here for the m/z 203 ion was the same as that observed in recent α-pinene photooxidation experiments conducted under NO_x conditions [*Ng et al.*, 2007], further demonstrating MBTCA as an atmospheric tracer for α-pinene SOA formed in the presence of NO_x.

[12] Figure 1 shows GC/EI-MS data obtained for a methylated extract of α-pinene/isoprene SOA and synthesized MBTCA trimethyl ester. One of the major peaks in the total ion chromatogram (TIC) of methylated α-pinene/isoprene SOA corresponds to MBTCA, since both the chromatographic retention time (26.12 min and 26.15 min for the unknown and synthesized product, respectively) and the EI mass spectrum perfectly agree. Other peaks detected in the methylated α-pinene/isoprene SOA were due to *cis*-norpinic acid (RT 24.13 min) and *cis*-pinic acid (RT 25.19 min), which are known oxidation products of α-pinene. Characteristic ions in the EI mass spectrum of MBTCA trimethyl ester include m/z 215 $[M^{+\bullet} - {}^{\bullet}OCH_3]$, m/z 187 $[M^{+\bullet} - ({}^{\bullet}OCH_3 + CH_3OH)]$, m/z 155 $[M^{+\bullet} - ({}^{\bullet}OCH_3 + 60\ u)]$ (Figure 1), and m/z 145/146 (Figure 1).

[13] Figure 2 shows LC/(−)ESI-MS data obtained for K-puszta $PM_{2.5}$ aerosol and MBTCA which was obtained by partial acid hydrolysis of its trimethyl ester. The major peak in the base peak chromatogram (BPC) of K-puszta $PM_{2.5}$ aerosol corresponds to MBTCA, since its chromatographic retention time (17.66 min) and the m/z 203 MS^2 product ion spectrum perfectly agree with that of synthesized MBTCA (17.62 min). Characteristic ions in the m/z 203 MS^2 product ion spectrum include m/z 185 (loss of H_2O), m/z 141 (combined loss of H_2O and CO_2), and m/z 97 (combined loss of H_2O and twice CO_2). Supporting LC/(−)ESI-MS data (not shown) were also obtained for α-pinene/isoprene SOA. Other terpenoic acids identified in K-puszta $PM_{2.5}$ aerosol include *cis*-pinic acid ($[M - H]^-$ at m/z 185, RT 21.45 min), *cis*-norpinic acid ($[M - H]^-$ at m/z 171, RT 17.34 min), and *cis*-pinonic acid ($[M - H]^-$ at m/z 183, RT 22.73 min) (Figure 2), which are known oxidation products of α-pinene. Additional later-eluting peaks detected in synthesized MBTCA were due to partial hydrolysis of the trimethyl ester derivative ($[M - H]^-$ at m/z 217, *mono*-methyl derivatives; RT 21.01 and 21.33 min; and $[M - H]^-$ at m/z 231, *di*-methyl derivative; RT 22.85 min).

[14] It is worth mentioning that MBTCA has been reported in the early German chemical literature as a liquid-phase oxidation product of terpenes using permanganate as oxidant, but spectroscopic evidence was not available at that time; first, it was reported as a degradation product of pinonic acid [*Tiemann and Semmler*, 1895] and later as a degradation product of the sesquiterpene cedrene which contains a 2,2-dimethylpentane ring [*Treibs*, 1943]. Taking into account these data, it cannot be excluded that MBTCA has, in addition to α- and β-pinene, other BVOC precursors, such as sesquiterpenes containing a 2,2-dimethylpentane or -butane ring.

[15] A plausible mechanism for the formation of MBTCA from *cis*-pinonic acid that involves participation of the OH radical is presented below. It cannot be ruled out that ozone is also involved in the formation of MBTCA; however, laboratory experiments using HONO as oxidant where no ozone formation occurs also resulted in the formation of MBTCA [*Ng et al.*, 2007]. With this pathway it is also possible to better explain smog chamber observations reported in previous work [*Claeys et al.*, 2007], which suggested that the MW 204 compound was formed at the expense of *cis*-pinic acid. The latter observations can be explained with *cis*-pinonic acid following two routes; namely, a short one leading to *cis*-pinic acid, and a longer one, leading to MBTCA. The formation of MBTCA likely takes place in the particle phase, but further work is required to confirm this hypothesis and obtain insights into the reaction mechanism.

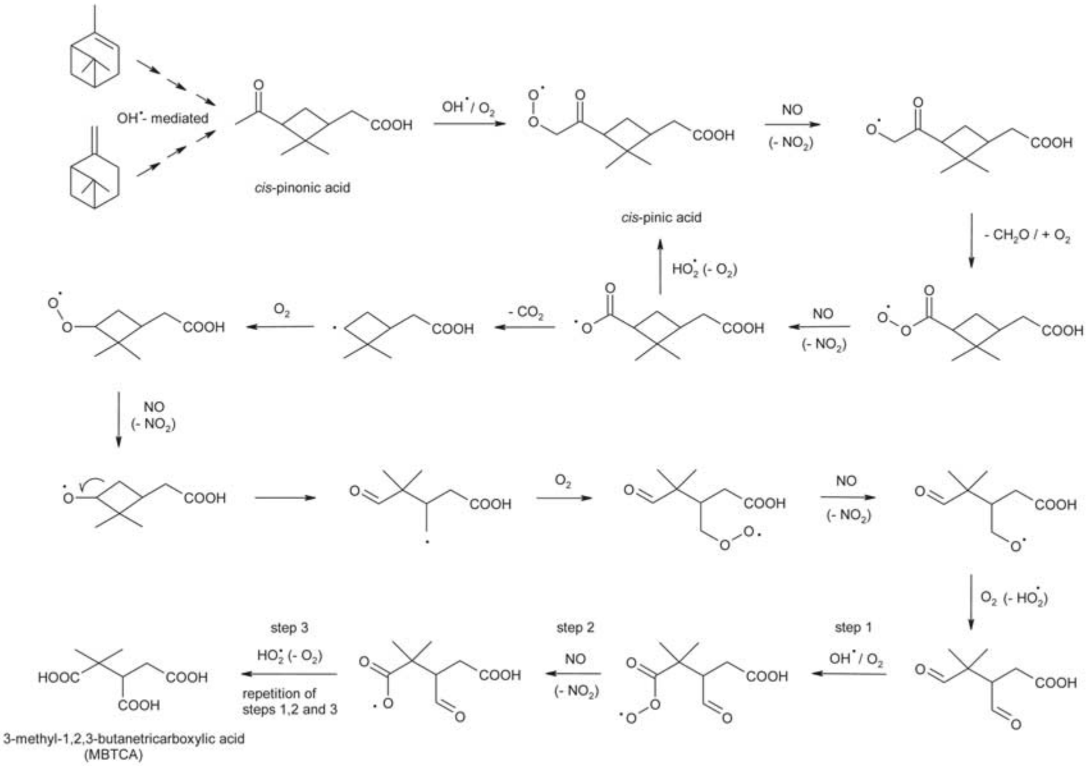

4. Conclusions

[16] This study firmly establishes 3-methyl-1,2,3-butanetricarboxylic acid as the MW 204 α-pinene SOA compound through synthesis of a reference compound and comparison of its gas and liquid chromatographic and mass spectral signatures with those of the unknown compound detected in ambient PM$_{2.5}$ aerosol and α-pinene SOA. MBTCA can be explained by further reaction of *cis*-pinonic acid, involving participation of the OH radical. This study also provides an explanation for the relatively low atmospheric PM concentrations of *cis*-pinic and *cis*-pinonic acid measured in summer that were reported in previous ambient aerosol studies conducted at different sites, both in Europe and the United States. Further research is required to evaluate whether MBTCA has additional BVOC precursors other than α- and β-pinene.

[17] **Acknowledgments.** Research at the Universities of Antwerp and Ghent was supported by the Belgian Federal Science Policy Office (BIOSOL project; contract SD/AT/02A), the Research Foundation – Flanders (FWO) and the Special Research Funds of the Universities of Antwerp and Ghent. The U.S. Environmental Protection Agency through its Office of Research and Development funded and collaborated in the research described here under Contract EP-D-05-065 to Alion Science and Technology. The manuscript has been subjected to external peer review and has been cleared for publication. Mention of trade names or commercial products does not constitute an endorsement or recommendation for use. Rafal Szmigielski was supported by a Marie Curie Intra-European fellowship (contract 039787 – SOAMASS). Jason Surratt was supported in part by the United States Environmental Protection Agency (EPA) under the Science to Achieve Results (STAR) Graduate Fellowship Program. We thank Paul Ziemann (University of California, Riverside) for help with formulating the formation mechanism.

References

Cahill, T. M., V. Y. Seaman, M. J. Charles, R. Holzinger, and A. H. Goldstein (2006), Secondary organic aerosols formed from oxidation of biogenic volatile organic compounds in the Sierra Nevada mountains of California, *J. Geophys. Res.*, *111*, D16312, doi:10.1029/2006JD007178.

Claeys, M., et al. (2007), Hydroxydicarboxylic acids: Markers for secondary organic aerosol from the photooxidation of α-pinene, *Environ. Sci. Technol.*, *41*, 1628–1634.

Edney, E. O., T. E. Kleindienst, T. S. Conver, C. D. McIver, E. W. Corse, and W. S. Weathers (2003), Polar organic oxygenates in PM$_{2.5}$ at a southeastern site in the United States, *Atmos. Environ.*, *37*, 3947–3965.

Gao, S., J. D. Surratt, E. M. Knipping, E. S. Edgerton, M. Shahgholi, and J. H. Seinfeld (2006), Characterization of polar organic components in fine aerosols in the southeastern United States: Identity, origin, and evolution, *J. Geophys. Res.*, *111*, D14314, doi:10.1029/2005JD006601.

Griffin, R. J., D. R. Cocker, R. C. Flagan, and J. H. Seinfeld (1999), Organic aerosol formation from the oxidation of biogenic hydrocarbons, *J. Geophys. Res.*, *104*, 3555–3567.

Guenther, A., et al. (1995), A global model of natural volatile organic compound emissions, *J. Geophys. Res.*, *100*, 8873–8892.

Iinuma, Y., O. Böge, T. Gnauk, and H. Herrmann (2004), Aerosol-chamber study of the α-pinene/O$_3$ reaction: Influence of particle acidity on aerosol yields and products, *Atmos. Environ.*, *38*, 761–773.

Ion, A. C., R. Vermeylen, I. Kourtchev, J. Cafmeyer, X. Chi, A. Gelencsér, W. Maenhaut, and M. Claeys (2005), Polar organic compounds in rural PM$_{2.5}$ aerosols from K-puszta, Hungary, during a 2003 summer field campaign: Sources and diel variations, *Atmos. Chem. Phys.*, *5*, 1805–1814.

Jaoui, M., T. E. Kleindienst, M. Lewandowski, J. H. Offenberg, and E. O. Edney (2005), Identification and quantification of aerosol polar oxygenated compounds bearing carboxylic or hydroxyl groups. 2. Organic tracer compounds from monoterpenes, *Environ. Sci. Technol.*, *39*, 5661–5673.

Kanakidou, M., et al. (2005), Organic aerosol and global climate modelling: A review, *Atmos. Chem. Phys.*, *5*, 1053–1123.

Kleindienst, T. E., E. O. Edney, M. Lewandowski, J. H. Offenberg, and M. Jaoui (2006), Secondary organic carbon and aerosol yields from the irradiations of isoprene and α-pinene in the presence of NO$_x$ and SO$_2$, *Environ. Sci. Technol.*, *40*, 3807–3812.

Kourtchev, I., T. Ruuskanen, W. Maenhaut, M. Kulmala, and M. Claeys (2005), Observation of 2-methyltetrols and related photooxidation products of isoprene in boreal forest aerosols from Hyytiälä, Finland, *Atmos. Chem. Phys.*, *5*, 2761–2770.

Kourtchev, I., et al. (2007), Determination of isoprene and α-/β-pinene oxidation products in boreal forest aerosols from Hyytiälä, Finland: Diel variations and possible link with particle formation events, *Plant Biol.*, doi:10.1055/s-2007-964945.

Kubátová, A., R. Vermeylen, M. Claeys, J. Cafmeyer, W. Maenhaut, G. Roberts, and P. Artaxo (2000), Carbonaceous aerosol characterisation in the Amazon basin, Brazil: Novel dicarboxylic acids and related compounds, *Atmos. Environ.*, *34*, 5037–5051.

Larsen, B. R., D. Di Bella, M. Glasius, R. Winterhalter, N. R. Jensen, and J. Hjorth (2001), Gas-phase OH oxidation of monoterpenes: Gaseous and particulate products, *J. Atmos. Chem.*, *38*, 231–276.

Ng, N. L., et al. (2007), Effect of NO_x level on secondary organic aerosol (SOA) formation from the photooxidation of terpenes, *Atmos. Chem. Phys.*, *7*, 5159–5174.

Plewka, A., T. Gnauk, E. Brüggeman, and H. Herrmann (2006), Biogenic contribution to the chemical composition of airborne particles in a coniferous forest in Germany, *Atmos. Environ.*, *40*, Suppl. 1, S103–S115.

Tiemann, F., and F. W. Semmler (1895), Ueber Pinen, *Ber. Dtsch. Chem. Ges. B. Abh.*, *28*, 1344–1353.

Treibs, W. (1943), Ueber den oxydativen Abbau des Cedrens (III. Mitteil. ueber Cedren und Cedrol), *Ber. Dtsch. Chem. Ges. B. Abh.*, *76*, 160–168.

Warnke, J., R. Bandur, and T. Hoffmann (2004), Quantification of terpenic acids in atmospheric aerosol samples, *J. Aerosol Sci.*, Suppl., S21–S22.

Warnke, J., R. Bandur, and T. Hoffmann (2006), Capillary-HPLC-ESI-MS/MS method for the determination of acidic products from the oxidation of monoterpenes in atmospheric aerosol samples, *Anal. Bioanal. Chem.*, *385*, 34–45.

Yu, J., D. R. Cocker III, R. J. Griffin, R. C. Flagan, and J. H. Seinfeld (1999a), Gas-phase ozone oxidation products of monoterpenes: Gaseous and particulate products, *J. Atmos. Chem.*, *34*, 207–258.

Yu, J., R. J. Griffin, D. R. Cocker III, R. C. Flagan, J. H. Seinfeld, and P. Blanchard (1999b), Observation of gaseous and particulate products of monoterpene oxidation in forest atmospheres, *Geophys. Res. Lett.*, *26*, 1145–1148.

F. Blockhuys, Department of Chemistry, University of Antwerp, BE-2610 Antwerp, Belgium.

M. Claeys, Y. Gómez-González, I. Kourtchev, R. Szmigielski, P. Van der Veken, and R. Vermeylen, Department of Pharmaceutical Sciences, University of Antwerp, BE-2610 Antwerp, Belgium. (magda.claeys@ua.ac.be)

E. O. Edney, T. E. Kleindienst, M. Lewandowski, and J. H. Offenberg, National Exposure Research Laboratory, Office of Research and Development, United States Environmental Protection Agency, Research Triangle Park, NC 27711, USA.

M. Jaoui, Alion Science and Technology, Research Triangle Park, NC 27709, USA.

W. Maenhaut, Department of Analytical Chemistry, Institute for Nuclear Sciences, Ghent University, BE-9000 Ghent, Belgium.

J. H. Seinfeld, Departments of Chemical Engineering and Environmental Science and Engineering, California Institute of Technology, Pasadena, CA 91125, USA.

J. D. Surratt, Department of Chemistry, California Institute of Technology, Pasadena, CA 91125, USA.

Appendix F

Chemical Composition of Gas- and Aerosol-Phase Products from the Photooxidation of Naphthalene*

---

*This chapter is reproduced by permission from "Chemical Composition of Gas- and Aerosol-Phase Products from the Photooxidation of Naphthalene" by Kathryn E. Kautzman, Jason D. Surratt, ManNin Chan, Arthur W. H. Chan, Scott P. Hersey, Puneet S. Chhabra, Nathan F. Dalleska, Paul O. Wennberg, Richard C. Flagan, and John H. Seinfeld, *Journal of Physical Chemistry A*, 114 (2), 913–934, 2010. Copyright 2010 by the American Chemical Society.

J. Phys. Chem. A 2010, *114*, 913–934

Chemical Composition of Gas- and Aerosol-Phase Products from the Photooxidation of Naphthalene

K. E. Kautzman,[†] **J. D. Surratt,**[†] **M. N. Chan,**[‡] **A. W. H. Chan,**[†] **S. P. Hersey,**[‡] **P. S. Chhabra,**[†] **N. F. Dalleska,**[‡] **P. O. Wennberg,**[‡,§] **R. C. Flagan,**[†,‡] **and J. H. Seinfeld***[,†,‡]

Division of Chemistry and Chemical Engineering, Division of Engineering and Applied Science, and Division of Geological and Planetary Sciences, California Institute of Technology, Pasadena, CA

Received: September 3, 2009; Revised Manuscript Received: October 15, 2009

The current work focuses on the detailed evolution of the chemical composition of both the gas- and aerosol-phase constituents produced from the OH-initiated photooxidation of naphthalene under low- and high-NO_x conditions. Under high-NO_x conditions ring-opening products are the primary gas-phase products, suggesting that the mechanism involves dissociation of alkoxy radicals (RO) formed through an $RO_2 + NO$ pathway, or a bicyclic peroxy mechanism. In contrast to the high-NO_x chemistry, ring-retaining compounds appear to dominate the low-NO_x gas-phase products owing to the $RO_2 + HO_2$ pathway. We are able to chemically characterize 53−68% of the secondary organic aerosol (SOA) mass. Atomic oxygen-to-carbon (O/C), hydrogen-to-carbon (H/C), and nitrogen-to-carbon (N/C) ratios measured in bulk samples by high-resolution electrospray ionization time-of-flight mass spectrometry (HR-ESI-TOFMS) are the same as the ratios observed with online high-resolution time-of-flight aerosol mass spectrometry (HR-ToF-AMS), suggesting that the chemical compositions and oxidation levels found in the chemically-characterized fraction of the particle phase are representative of the bulk aerosol. Oligomers, organosulfates ($R-OSO_3$), and other high-molecular-weight (MW) products are not observed in either the low- or high-NO_x SOA; however, in the presence of neutral ammonium sulfate seed aerosol, an organic sulfonic acid ($R-SO_3$), characterized as hydroxybenzene sulfonic acid, is observed in naphthalene SOA produced under both high- and low-NO_x conditions. Acidic compounds and organic peroxides are found to account for a large fraction of the chemically characterized high- and low-NO_x SOA. We propose that the major gas- and aerosol-phase products observed are generated through the formation and further reaction of 2-formylcinnamaldehyde or a bicyclic peroxy intermediate. The chemical similarity between the laboratory SOA and ambient aerosol collected from Birmingham, Alabama (AL) and Pasadena, California (CA) confirm the importance of PAH oxidation in the formation of aerosol within the urban atmosphere.

1. Introduction

A large fraction (80−90% in some locations) of atmospheric organic aerosol is secondary in origin.[1] The formation of secondary organic aerosol (SOA) results from the formation of low-vapor-pressure products in the oxidation of volatile organic compounds (VOCs), where the resultant low-vapor-pressure oxidation products partition between the gas and aerosol phases. Many VOCs, such as monoterpenes (e.g., α-pinene) and single-ringed aromatic hydrocarbons (e.g., toluene), are known to produce SOA. However, the mass of SOA observed in many locations cannot be accounted for by known precursor VOC, suggesting that many sources of SOA are not yet identified or well characterized.[2−4] Recent identification of isoprene oxidation as a significant source of SOA,[5−12] the role of NO_x in forming SOA from the oxidation of aromatics[13−15] and other hydrocarbons,[16−18] the effects of aerosol acidity and heterogeneous chemistry (e.g., oligomer[19−27] and organosulfate formation[24,28−32]), and the contribution of glyoxal to SOA formation[24,33−35] have provided significant insights into potential missing and poorly characterized sources of SOA. Additionally, Robinson et al.[36] have shown that primary organic aerosol (POA), previously considered as nonvolatile, contains gas-phase components of intermediate volatility that themselves are sources of SOA.

Although it is traditionally assumed that small volatile aromatic organic compounds, such as toluene and benzene, are the primary precursors for anthropogenic SOA, it has recently been shown that substantial contributions to SOA formation may also come from compounds of lower volatility,[36] such as polycyclic aromatic hydrocarbons (PAHs). PAHs account for a significant portion of the semivolatile gas-phase emissions from diesel fuels,[37] with substantial emissions also being produced from gasoline engines,[38] wood burning,[39,40] and cooking sources.[41,42] Photooxidation of PAHs has been shown to produce high-MW, low-vapor-pressure, oxygenated compounds.[40,43−47] The nitro PAHs, specifically nitronaphthalenes, have been observed in ambient particulate matter[48] and are of particular importance due to their expected role as carcinogens.[49−52]

We have previously reported SOA yields, defined as the ratio of mass of SOA formed, ΔM_o, to the mass of hydrocarbon reacted, ΔHC, from the photooxidation of naphthalene, 1-methylnaphthalene (1-MN), 2-methylnaphthalene (2-MN), and 1,2-dimethylnaphthalene (1,2-DMN) as a function of organic mass loading under both high- and low-NO_x conditions.[15] Yields for high-NO_x conditions were observed between 0.19 and 0.30 for

---

* Author to whom correspondence should be addressed. Phone: (626) 395-4635, Fax: (626) 796-2591, E-mail: seinfeld@caltech.edu.

[†] Division of Chemistry and Chemical Engineering.

[‡] Division of Engineering and Applied Science.

[§] Division of Geological and Planetary Sciences.

10.1021/jp908530s

TABLE 1: Instruments Employed in Chamber Experiments[a]

instrumentation	measurement	time resolution	detection limit/range
hygrometer (capacitance probe)	temperature	online	10−50 °C
Vaisala HMP233	humidity	online	5−95%
chemiluminescent NO_x analyzer	NO, NO_2 concentrations	online	2 ppb
luminol NO_x analyzer	concentration of NO_2 separated from PAN by GC	online	5 ppb
O_3 analyzer	ozone concentration	online	2 ppb
differential mobility analyzer (DMA)	aerosol number concentration, size distribution, and volume concentration	4 min	0.2 $\mu m^3 cm^{-3}$, 15−780 nm
gas chromatography/flame ionization detector (GC/FID)	parent hydrocarbon concentration	12 min	~1 ppb[b]
chemical ionization mass spectrometry (CIMS)	gas-phase oxidation products	~9 min	~0.1 ppb[b], unit mass resolution
gas chromatography/electron ionization-time-of-flight mass spectrometry (GC/EI-TOFMS)	gas-phase oxidation products, structural indentification	semionline, off-line	0.5 ppb[b], resolution ~7000
ultra performance liquid chromatography/electrospray ionization-time-of-flight mass spectrometry(UPLC/ESI-TOFMS)	particle-phase products, structural identification	off-line	1 ng m^{-3} [b], resolution ~12 000
high performance liquid chromatography electrospray ionization-ion trap mass spectrometry (HPLC/ESI-ITMS)	particle-phase products, structural identification	off-line	1 ng m^{-3} [b], unit mass resolution
high-resolution time-of-flight aerosol mass spectrometry (HR-ToF-AMS)	particle-phase composition	online	0.03 $\mu g\ m^{-3}$, 50−600 nm
particle into liquid sampler-ion chromatography (PILS-IC)	water-soluble aerosol composition	online	~0.1 $\mu g\ m^{-3}$ [b]

[a] Instruments employed at the Caltech dual chamber environmental facility. [b] Detection limits dependent on identity of target species.

naphthalene, 0.19 and 0.39 for 1-MN, 0.26 and 0.45 for 2-MN, and constant at 0.31 for 1, 2-DMN, at aerosol mass loadings between 10 and 40 $\mu g\ m^{-3}$. Under low-NO_x conditions, yields were found to be 0.73, 0.68, and 0.58, for naphthalene, 1-MN, and 2-MN, respectively. Gas-phase products were tentatively identified, and trends involving ring-opening versus ring-retaining oxidation mechanisms were established. Calculations of SOA formation from these PAHs demonstrated that these precursors may contribute significantly to the amount of urban SOA. The suite of instruments associated with the Caltech dual indoor environmental chamber facility (Table 1), by which the data to be presented were obtained, permits a thorough analysis of the generation of SOA commencing with the oxidation of the gas-phase hydrocarbon to the formation of SOA. Here we describe the detailed evaluation of the chemical composition of both the gas- and aerosol-phase constituents produced from the photooxidation of naphthalene, the most abundant PAH in the urban atmosphere.[48]

2. Experimental Section

2.1. Chamber Experiments. All experiments were carried out in the Caltech dual 28 m^3 Teflon chambers. Details of the facilities have been described previously.[53,54] Before each experiment, the chambers were flushed with dried purified air for >24 h, until the particle number concentration was <100 cm^{-3} and the volume concentration was <0.1 $\mu m^3\ cm^{-3}$. In most experiments, ammonium sulfate seed aerosol was used to promote condensation of low volatility oxidation products. The seed aerosol was generated by atomization of a 0.06 M aqueous ammonium sulfate solution. The hydrocarbon was introduced into the chamber by flowing purified air through an FEP tube packed with solid naphthalene at 1 L min^{-1}.

For high-NO_x experiments (NO > 350 ppb initially) nitrous acid (HONO) was used as the OH precursor. HONO was prepared by adding 10 mL of 1 wt % aqueous $NaNO_2$ dropwise into 20 mL of 10 wt % sulfuric acid in a glass bulb. A stream of dry air was then passed through the bulb, sending HONO into the chamber. During this process, NO and NO_2 formed as side products and were also introduced into the chamber. NO/NO_x was measured with a commercial chemiluminescence NO_x monitor (Horiba, APNA-360). In some experiments, NO_2 was monitored by a gas chromatograph with luminol detector (University of California, Riverside, CA) in which NO_2 and peroxyacyl nitrate (PAN) were separated by gas chromatography and detected by chemiluminescence of reaction with luminol.[55] Reaction of HONO with luminol is unlikely, and thus no interference with the NO_2 signal is expected. The NO_2 measurement from the NO_x monitor is higher due to interferences from HONO. The injection of HONO was stopped when the mixing ratio of NO_2 reached about 80 ppb in the chamber as measured by the Riverside NO_2 monitor. Additional NO was added until total NO was about 400 ppb. For all experiments, the concentrations of NO and NO_2 remained approximately constant over the course of photooxidation, and ozone (O_3) concentrations remained insignificant. For low-NO_x experiments, hydrogen peroxide (H_2O_2) was used as the OH precursor. Prior to atomization of the ammonium sulfate seed, H_2O_2 was introduced by bubbling purified air through a 50% aqueous H_2O_2 solution for 2.5 h at 5 L min^{-1} resulting in a mixing ratio of 2−8 ppm of H_2O_2.

The aerosol number concentrations, size distributions, and volume concentrations were measured by a differential mobility analyzer (DMA, TSI model 3081) coupled with a condensation nuclei counter (TSI, CNC-3760). After allowing for all concentrations to stabilize, irradiation was initiated. The temperature (*T*), relative humidity (RH), and concentrations of O_3, NO, and NO_x were continuously monitored. Table 2 summarizes the experimental conditions for the series of naphthalene oxidation experiments conducted.

2.2. Gas-Phase Measurements.

2.2.1. Gas Chromatography/Flame-Ionization Detection (GC/FID). The concentration of naphthalene was continuously monitored by GC/FID. Chamber air was sampled into a 10 mL

TABLE 2: Experimental Conditions from Chamber Experiments

	initial naphthalene (ppb)	oxidant precursor[a]	initial NO_2 (ppb)	initial NO (ppb)	initial O_3 (ppb)	T (°C)[b]	RH (%)[b]	initial seed volume ($\mu m^3/cm^3$)	end volume ($\mu m^3/cm^3$)
1	60	H_2O_2	0	0	6	26	6	14	143
2	25	H_2O_2	0	3	4	26	19	26	50
3	20	H_2O_2	0	2	2	24	10	11	38
4	20	H_2O_2	0	1	1	24	13	11	40
5	48	HONO	166	401	3	28	5	16	65
6	30	HONO	245	455	1	25	7	15	51
7	35	HONO	289	487	3	25	10	15	50
8	30	HONO	260	480	3	26	17	11	n.a.

[a] H_2O_2 is used for low-NO_x conditions; HONO is used for high-NO_x conditions. [b] Reported value is averaged over the course of the experiment.

injection loop and injected onto a HP5 15 m × 0.53 mm ID × 1 μm thickness column installed on a 6890N Agilent GC. The GC was temperature-programmed as follows; initial temp 60 °C, hold 1 min, ramp 35 °C min^{-1} to 140 °C, ramp 20 °C min^{-1} to 200 °C, hold 2 min. The GC response was calibrated by dissolving a known mass of the naphthalene in dichloromethane, and then vaporizing a known volume of that solution into a 38 L Teflon chamber.

2.2.2. Chemical Ionization Mass Spectrometry (CIMS). Monitoring of gas-phase oxidation products was carried out in real time by the use of a CIMS instrument. The details of this instrument are described elsewhere.[17,56,57] Briefly, a 2.5 standard liters per minute (slm) aliquot of air is drawn from the experimental chamber through a 1.6 m long 0.25 in. Teflon tube. 300 standard cubic centimeters per minute (sscm) of this flow is introduced into the CIMS instrument and ionized by a reagent ion. The resultant ions are filtered using a quadrupole mass spectrometer with unit mass resolution. The instrument can operate in both negative mode, using CF_3O^- as a reagent ion, and in positive proton transfer reaction (PTR)-MS mode. Negative mode is found to be more selective toward detection of polar molecules, particularly acids, whereas positive mode detects a broader range of organic compounds. Mass scans were performed covering masses 55−450 amu for negative mode, and 56−350 amu for positive mode, with a total scan time of ~9 min. Mass scans were continuously repeated over the course of each experiment.

2.2.3. Gas Chromatography/Electron Impact Time-of-Flight Mass Spectrometry (GC/EI-TOFMS). The GC/EI-TOFMS instrument (Waters, GCT Premier) is outfitted with a standard 6890N Agilent GC for introduction of volatile samples. The ion source employed here is a traditional 70 eV positive (+)EI source. The ions produced are continuously accelerated across the source to 40 eV and perpendicularly extracted into the TOF mass analyzer at a rate >25 kHz. The ions then pass through a single reflectron with an effective path length of 1.2 m. Ions are subsequently detected by a chevron stack of microchannel plates. The arrival times of the ions are recorded by a time-to-digital converter at a rate of 3.6 GHz, providing high mass accuracy (~7000). All data are acquired and analyzed using MassLynx software version 4.1.

Various components have been added to aid with sample introduction into the GC/EI-TOFMS instrument. A preconcentrator (Entech Instruments, model 7100A) is used to draw, concentrate, and focus gas-phase samples into discrete peaks on the GC column. The preconcentrator extracts air from the environmental chamber and then cryogenically traps and concentrates VOCs in the sample. We have used two different trapping methods with the preconcentrator. The first method, microscale purge and trap (MPT), is a three-stage procedure to efficiently concentrate gas samples. The initial trap, which is filled with glass beads, is used to remove water vapor from the sample and removes bulk atmospheric gases (e.g., O_2 and N_2). The initial concentration step is then followed by trapping of VOCs with a Tenax adsorbent trap, and the sample is subsequently flushed into the cryofocusing module where the sample is focused and rapidly injected onto the GC column. The second method, cold trap dehydration (CTD), uses only the Tenax trap and cryofocusing modules. Although CTD is less effective at removing moisture from humid samples, it is the preferred method of sample concentration for water-soluble compounds such as aldehydes. This method also provides superior handling of samples with high CO_2 levels. Both the MPT and CTD methods have been found to be effective for sampling volatile and semivolatile compounds, although for the highly oxidized products of interest here, the preconcentrator is believed to be the controlling factor for the ultimate detection limit of these latter products. All modules in the preconcentrator have an upper temperature range of 200 °C. Similarly, the transfer line between the preconcentrator and GC can be heated only to a maximum of 150 °C. The upper temperature limit of the preconcentrator makes detection of low-vapor-pressure oxidized compounds challenging.

The concentrations of naphthalene (<40 ppb) employed in the chamber experiments outlined in Table 2 preclude detection of the gas-phase oxidation products by the GC/EI-TOFMS technique as implemented at Caltech. Thus, additional high-concentration experiments were carried out in a separate 3 m^3 Teflon chamber to identify gas-phase products from the photooxidation of naphthalene under high- and low-NO_x conditions using the GC/EI-TOFMS instrument. The initial mixing ratio of the naphthalene in these experiments was ~40 ppm, and the concentration of HONO in high-NO_x experiments was ~10 ppm. For low-NO_x experiments initial mixing ratios of H_2O_2 were ~30−80 ppm. Two methods were used to monitor the formation of gas-phase oxidation products; first, 1000 mL samples were drawn from the 3 m^3 Teflon chamber and introduced directly into the three-step preconcentrator. After preconcentration, the sample was injected onto the GC DB-5MS column (30 m × 0.25 mm ID × 0.25 μm thickness) and temperature-programmed as follows: initial temp 40 °C, hold 2 min, ramp 5 °C min^{-1} to 300 °C. This method has limited time resolution due to the preconcentration and GC steps. In order to improve the time resolution, Tenax tube samples were collected. Air from the 3 m^3 Teflon chamber was drawn through Tenax TA glass tubes (Supelco, 6 mm × 11.5 cm) at a rate of 0.455 L min^{-1} using a critical orifice. Each tube sampled chamber air for 20 min. Subsequently, the tubes were desorbed at 300 °C into the preconcentrator and analyzed as described above. Gas-phase products were identified by NIST library searching the mass spectra,[58] and authentic standards were used when possible. No differences were observed between the preconcentrator MPT and CTD methods.

2.3. Particle-Phase Measurements.

2.3.1. Chamber Filter Sample Collection, Extraction, and Off-Line Detailed Chemical Characterization Protocols. A detailed description of the aerosol filter sample collection and extraction protocol has been previously published.[59] Briefly, aerosol samples are collected on Teflon filters (PALL Life Sciences, 47-mm diameter, 1.0-μm pore size, teflomembrane). Filter samplers employed for aerosol filter sample collection used a front and back-up filter sampling approach, where back-up filters were collected in order to examine if aerosol breakthrough was occurring on the front filter or whether evaporation of semivolatiles from the front filter was occurring during filter sampling. In all experiments outlined in Table 2, no SOA constituents were found on the back-up filters, and as a result, all detailed chemical characterizations are reported only for the front filters. Filter sampling was initiated when the aerosol volume reached its maximum (constant) value, as determined by the DMA. Depending on the total volume concentration of aerosol in the chamber, the duration of filter sampling was 1.8−2.1 h, which resulted in 2.0−2.9 m^3 of total chamber air sampled. Teflon filter extraction protocols in high-purity methanol (LC-MS CHROMASOLV-Grade, Sigma-Aldrich) have been described previously.[59] Additional filter extractions using 5 mL of high-purity acetonitrile (LC-MS CHROMASOLV-Grade, Sigma-Aldrich) were also performed by 45 min of sonication to ensure detection of SOA constituents not soluble in methanol. No additional compounds were recovered using the less-polar acetonitrile solvent. Thus, all results from the off-line ESI-MS measurements are reported only for the methanol filter extractions. The resultant filter extracts were then analyzed by a Waters ACQUITY ultra performance liquid chromatography (UPLC) system, coupled with a Waters LCT Premier TOF mass spectrometer equipped with an ESI source, allowing for accurate mass measurements (i.e., determination of molecular formulas) to be obtained for each observed ion. Operation protocols, including column information and employed chromatographic method, for the UPLC/ESI-TOFMS technique have been described in detail previously.[59]

Selected naphthalene low- and high-NO_x methanol filter extracts were also analyzed by a Thermo Finnigan Surveyor high performance liquid chromatography (HPLC) system (pump and autosampler) coupled to a Thermo Finnigan LCQ ion trap mass spectrometer (ITMS) equipped with an ESI source, allowing for tandem MS measurements (i.e., generation of product ions) to be obtained. The combination of accurate mass and tandem MS measurements significantly aided in detailed structural characterization efforts. Data were acquired and processed using Xcalibur version 1.3 software. A Waters Atlantis T3 column (3 μm particle size; 2.1 × 150 mm) was employed, which is similar to the Water ACQUITY UPLC HSS column used for the UPLC/ESI-TOFMS analysis. The mobile phases consisted of 0.1% acetic acid in water (A) and 0.1% acetic acid in methanol (B). The applied 45 min gradient elution program was as follows: the concentration of eluent B was kept at 3% for 4 min, then increased to 100% in 21 min, holding at 100% for 10 min, then decreased to 3% in 5 min, and kept at 3% for 5 min. The injection volume and flow rate were 10 μL and 0.2 mL min^{-1}, respectively. The ion trap mass analyzer was operated under the following conditions: sheath gas flow (N_2), 65 arbitrary units; auxiliary gas flow (N_2), 3 arbitrary units; source voltage, −4.5 kV; capillary voltage, −14.5 V; tube lens offset, 7 V; capillary temperature, 200 °C; and maximum ion injection time, 200 ms. Two scan events were used during each chromatographic run; scan event 1 was the full scan mode in which data were collected from m/z 120 to 600 in the negative ionization mode and scan event 2 was the MS^2 mode in which product ions were generated from significant base peak ions observed in scan event 1. For MS^2 experiments, an isolation width of 2.5 m/z units and a normalized collision energy level of 35% were applied. The $[M - H]^-$ ion signal optimization was carried out by introducing a 1 mg mL^{-1} malic acid standard solution. Due to the on-axis ESI source that is characteristic of the LCQ ITMS instrument, a solvent delay time of 3.5 min (which diverted the column effluent from the ESI source to waste) was employed to prevent clogging by nonvolatile salts at the entrance of the capillary.

Measurements of total peroxide content from the extracted filter samples were acquired by the UV−vis iodometric spectroscopy method.[19] Filter samples used for this analysis were extracted and prepared differently from the filter samples used in the UPLC/ESI-TOFMS and HPLC/ESI-ITMS analyses.[11] Standard calibration curves were generated using a series of benzoyl peroxide solutions. The structure of the benzoyl peroxide, a peroxy group linking two benzene rings, was judged to be an excellent surrogate for the naphthalene system. Calibrations and measurements were performed on a Hewlett-Packard 8452A diode array spectrophotometer. Peroxides in the form of HOOH, ROOH, and ROOR are quantified by measuring the absorbance at 470 nm of the reaction product I_3^- produced under anaerobic, dark, and acidic conditions by the following reaction scheme:

$$\mathrm{ROOH} + 2\mathrm{I}^- + 2\mathrm{H}^+ \rightarrow \mathrm{I}_2 + \mathrm{H}_2\mathrm{O} + \mathrm{ROH}$$

$$\mathrm{ROOR} + 2\mathrm{I}^- + 2\mathrm{H}^+ \rightarrow \mathrm{I}_2 + 2\mathrm{ROH}$$

$$\mathrm{I}_2 + \mathrm{I}^- \rightarrow \mathrm{I}_3^-$$

Detection of I_3^- at 470 nm is 10 nm to the red from the peak of the characteristic absorbance of I_3^- and has been chosen to avoid interferences with other organic compounds absorbing in this region. Extractions from three high-NO_x and three low-NO_x filters were performed to ensure reproducibility across experiments. No contribution of H_2O_2 to this measurement is expected due to the dry conditions employed in the present experiments, as well as owing to previous quality control experiments demonstrating that no H_2O_2 could be measured on filter samples collected from a nonirradiated chamber mixture containing only gaseous H_2O_2, VOC, and ammonium sulfate seed aerosol. These latter quality control filter samples were collected for the same duration as filter samples collected from SOA chamber experiments.

Of particular concern to the UV−vis measurements is the presence of nitronaphthalenes and nitrobenzenes in high-NO_x filter samples, which in solution have a color similar to the I_3^- produced from the reaction of I^- with the peroxides in solution. 1000 ppm standard solutions of nitronaphthalenes (i.e., 4-nitro-1-naphthol and 2-nitro-1-naphthol), nitrobenzenes (i.e., 2-nitrophenol and 3-hydroxy-4-nitrobenzoic acid), and epoxides (i.e., α-pinene oxide, 2-methyl-2-vinyloxirane, and 2,3-epoxy-1,4-diol) were prepared and tested to confirm that no interferences were present from these compounds in the UV−vis measurement. From the analyses of the 1000 ppm standards, it was found that the nitronaphthalenes and nitrobenzenes were the only classes of compounds to absorb weakly at 470 nm, and as a result, we reanalyzed the nitronaphthalene and nitrobenzene standards at a concentration more relevant to the high-NO_x SOA samples characterized in the current study. Since the highest concentration of the nitronaphthalenes and of the nitrobenzenes was measured at ~5 ppm by the UPLC/(−)ESI-TOFMS technique (Tables 2S−4S, Supporting Information), the absorbance of a 5 ppm standard mixture of the nitronaphthalenes (i.e., 4-nitro-1-naphthol and 2-nitro-1-naphthol) and of the nitrobenzenes (i.e., 2-nitrophenol and 3-hydroxy-4-nitrobenzoic acid) was measured by the UV−vis technique. It was found that the absorbance of this standard mixture, which possessed a yellowish color characteristic of nitroaromatics in solution, was insignificant at this SOA-relevant concentration.

Non-nitro containing benzene standards (i.e., phthalic acid and *trans*-cinnamic acid) were also prepared and analyzed. These compounds did not contribute to the absorbance measurement at 470 nm, consistent with the lack of color observed in their respective standard solutions. As a result of these measurements, it was assumed that the absorbance (peroxide) measurements acquired for the high- and low-NO_x SOA samples were not affected by chemical artifacts. Finally, blank Teflon filters were also extracted and prepared in the same manner as the filter samples collected from chamber experiments; these blank filters produced no significant absorbance at 470 nm, indicating that the filter medium did not interfere with the peroxide measurements.

2.3.2. High-Resolution Time-of-Flight Aerosol Mass Spectrometry (HR-ToF-AMS). Real-time aerosol mass spectra were obtained using an Aerodyne HR-ToF-AMS.[60] The HR-ToF-AMS was operated in both a lower resolution, higher sensitivity "V-mode", and a high-resolution "W" mode, switching between modes once every minute. The V-mode data were analyzed to extract sulfate, ammonium, and organic spectra.[61] Calculation of the SOA densities were achieved by comparing the particle mass distributions obtained using the particle ToF mode and the volume distributions obtained by the DMA in nucleation (seed-free) experiments.[62] O/C, N/C, and H/C ratios were determined from W mode data using the APES toolbox and applying the procedures outlined in Aiken et al.[63,64] The particle-phase signal of CO^+ and the organic contribution to H_xO^+ ions were estimated as described in Aiken et al.[64]

2.3.3. Particle-into-Liquid Sampler/Ion Chromatography (PILS/IC). The PILS/IC instrument is designed to measure aerosol water-soluble ions and is based on the original design of Weber et al.[65] The current instrument has been modified to utilize syringe pumps to introduce the samples from the impactor into vials for later analysis by IC.[66] Chamber air, sampled through a 1 mm cut-size impactor, is passed through three denuders (URG and Sunset Laboratories) to remove gas-phase species. The aerosol is mixed with steam in a condensation chamber and grows by condensation of supersaturated water vapor to diameters >1 μm. Droplets grow sufficiently large to be collected by impingement on a quartz impactor, are washed to the bottom of the impactor, then collected and stored in airtight vials. Vials are analyzed off-line by IC (ICS-2000 with 25 μL sample loop, Dionex Inc.); columns used in the IC and the chromatographic methods employed have been previously described in detail by Sorooshian et al.[66] Vials were collected prior to each experiment to establish background levels of individual species, including Na^+, NH_4^+, K^+, Mg^{2+}, Ca^{2+}, SO_4^{2-}, Cl^-, NO_2^-, NO_3^-, oxalate, pyruvate, formate, and phthalate. Chromatographic peaks were identified and quantified using authentic standards; standards used in the current work are: teraphthalic acid, benzoic acid, *trans*-cinnamic acid, 5-hydroxy isophthalic acid, 1,2,4-benzene tricarboxylic acid, 4-formylcinnamic acid, 2-hydroxy isophthalic acid, 3-hydroxy benzoic acid, 4-hydroxybenzoic acid, 3-formyl benzoic acid, 3-hydroxy-4-nitrobenzoic, 2-nitrophenol, 2-nitro-1-napthol, 4-nitro-1-napthol, and salicylic acid. Additionally, the presence of dicarboxylic acids of C_2 (oxalic), C_3 (malonic), C_4 (succinic), C_5 (glutaric), and C_6 (adipic) compounds were investigated using authentic standards.

2.4. Ambient Aerosol Samples: Filter Collection Protocols and Off-Line Chemical Analysis. Selected archived quartz fiber filters collected from Birmingham, AL during the Southeastern Aerosol Research and Characterization (SEARCH) 2004 campaign were reanalyzed by the UPLC/(−)ESI-TOFMS technique, as described above for the naphthalene SOA chamber filters. Details of the SEARCH network, which includes descriptions of each site, aerosol filter sample collection protocols, gas- and particle-phase measurements conducted, can be found elsewhere.[67,68] Birmingham, AL (denoted as BHM in the SEARCH network) is an urban site consisting of both industrial and residential settings. Quartz fiber filter extractions and sample preparation procedures have been described previously.[69] However, solid-phase extraction (SPE) was not employed in the current study to avoid possible loss of early eluting naphthalene SOA products.

In addition to the ambient aerosol filters samples collected from Birmingham, AL, quartz fiber filters were also collected in Pasadena, CA, during June and July, 2009 using the same high-volume filter sampling approach as used by the SEARCH network. These samples are a part of the Pasadena Aerosol Characterization Observatory (PACO), an ambient sampling study located on the campus of Caltech. Selected PACO filter samples collected on June 3, June 19, and July 14, 2009, were analyzed by the UPLC/(−)ESI-TOFMS technique as described above. These filters represent 4 h integrated morning (7−11 a.m.) and 4 h integrated afternoon (3−7 p.m.) sampling periods. June 19 and July 14 were chosen for this chemical analysis due to the high total organic mass aerosol loadings as measured by a compact time-of-flight AMS instrument (maximum of 21.12 and 11.72 $\mu g\ m^{-3}$, respectively, assuming a collection efficiency of 0.5), O_3 mixing ratios (71 and 56 ppb, respectively), and daytime temperature (29 and 34 °C, respectively). June 3 was chosen as a relatively clean day for comparison with June 19 and July 14, and had a maximum total organic mass aerosol loading of 5.66 $\mu g\ m^{-3}$ (assuming a collection efficiency of 0.5), O_3 mixing ratio of 19 ppb, and daytime temperature of 20 °C. Further results and details from the PACO 2009 campaign will be presented in a forthcoming publication. Here, the chemical characterization data obtained from the ambient filters were compared to that of the naphthalene SOA chamber experiments to identify potential ambient SOA tracer compounds that can be used in source apportionment studies.

2.5. Chemicals. Most of the reagents used in this study were purchased from Sigma Aldrich and their stated purities are listed in Table 1S (Supporting Information). Additionally, 2-formylcinnamaldehyde was synthesized by ozonolysis of naphthalene using the technique of Larson et al.,[70] but was not purified. Identification of both *E*- and *Z*- isomers was confirmed by NMR measurements.

3. Results

3.1. High-NO_x Conditions.

3.1.1. Chemical Characterization of High-NO_x Gas-Phase Oxidation Products. Table 3 lists the gas-phase products detected by the CIMS instrument in positive and negative ion modes and structures identified by the GC/EI-TOFMS technique. These data are compared to aerosol measurements made by the UPLC/ESI-TOFMS technique, thus establishing the connection between the gas and particle phases. When the CIMS is operated

TABLE 3: Summary of Chemically Characterized Gas- and Particle-Phase Products Produced from the Photooxidation of Naphthalene

	Gas-phase measurements					Particle-phase measurements				
	CIMS detection[a]			GC/EI-TOFMS		UPLC/ESI-TOFMS				
MW	$[M + H]^+$	$[M + F]^-$	$[M + CF_3O]^-$	accurate mass	error (mDa)	accurate mass[b]	avg.error (mDa)	% SOA HNO_x[c]	% SOA LNO_x[d]	proposed structure[e]
122	B	B		122.0368	-0.4	121.0301 121.0293 121.0267	0.3	1.57	2.12	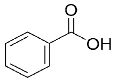
134	B			134.0390	2.4	135.0444	-0.2	n.q.	n.q	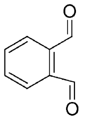
138		B	B			137.0253 137.0228 137.0255 137.0222	-0.05	1.64	3.63	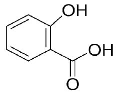
139						138.0225 138.0179 138.0198	1.0	1.13	0	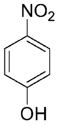
144	B	B	B			143.0531 143.0536	3.7	n.q.	n.q.	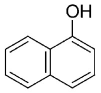
148	B	B	B							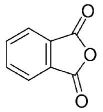
148						147.0432 147.0473 147.0480	1.6	0.25	0.57	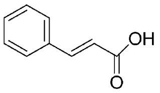
150						151.0401	0.6	n.q	n.q	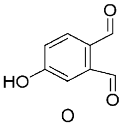
50	B	B	B			149.0231 149.0241 149.0239 149.0248	-0.1	1.24	2.8	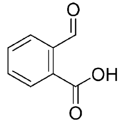
155						154.013	2.5	0.94	0	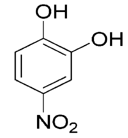
158	B			158.0387	1.9	159.0453	0.7	n.q	n.q	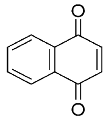
160	B		B	160.0524	0.40					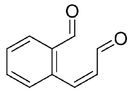
160						161.0578	-2.5	n.q	n.q	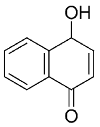
164						165.0539 165.0545 165.0525	-1.6	n.d.	n.q.	
166	B					165.0181 165.0148	2.3	2.71	4.01	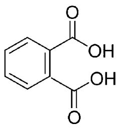

TABLE 3: Continued

	Gas-phase measurements					Particle-phase measurements				
	CIMS detection[a]			GC/EI-TOFMS		UPLC/ESI-TOFMS				
MW	$[M + H]^+$	$[M + F]^-$	$[M + CF_3O]^-$	accurate mass	error (mDa)	accurate mass[b]	avg.error (mDa)	% SOA HNO_x[c]	% SOA LNO_x[d]	proposed structure[e]
173				173.0495 173.0477	1.7 1.3					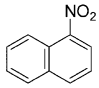
174	B	B	B	174.0328	1.1					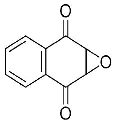
176	B	B	B			175.0377 175.0375 175.0395 175.0403	0.8	1.46	0.53	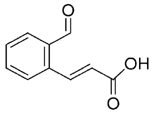
178	B		B			179.069	-1.8	n.q	n.q.	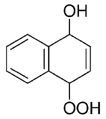
180						179.0325 179.0327 179.0341 179.0320	0.6	2.53	4.56	no tentatitve structure proposed
182						181.0128 181.0146 181.0128	0.3	3.3	9.8	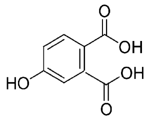
183						182.0096 182.0072	0.5	0.52	0	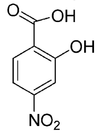
189	H	H		189.0417	-0.9	188.0336 188.0367 188.0310 188.0341 188.0326 188.0357	0.9	0.4	0	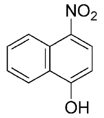
192	B					191.0364 191.0381 191.0345 191.0375	0.0	2.05	1.28	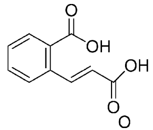
192						193.0511	1.0	n.q	n.q	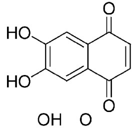
198						197.0108	2.2	n.q	3.5	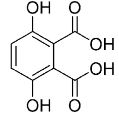
205			H			204.0295 204.0281 204.0286	1.0	0.39	0	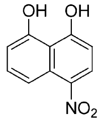
207						206.0477 206.0469	2.0	0.07	0	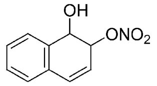
208	B					207.03020 207.02891 207.02930 207.03070 207.02830	-0.6	2.18	4.54	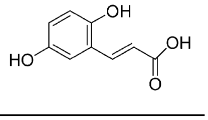

[a] CIMS does not permit structural identification. All proposed structures are derived from either GC/TOFMS, UPLC/TOFMS, or previously identified structures found in the literature. H denotes products observed only under high-NO_x conditions. B denotes products observed under both NO_x conditions. [b] Accurate masses are determined by $[M - H]^-$ or $[M + H]^+$ mode. Reported masses are thus 1 H^+ from the true mass. [c] High-NO_x case (HNO_x). [d] Low-NO_x case (LNO_x). [e] For simplicty only one isomer is shown. Number of observed isomers can be determined by the number of entries in the accurate mass column.

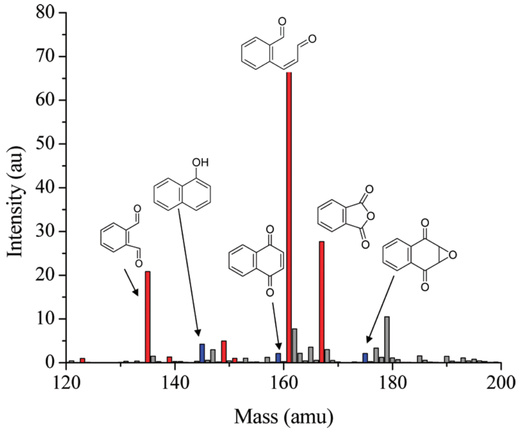

Figure 1. (+)CIMS mass spectrum taken at 70% reacted naphthalene under high-NO$_x$ conditions. Red data indicate ring-opening products. Ring-retaining products are indicated in blue.

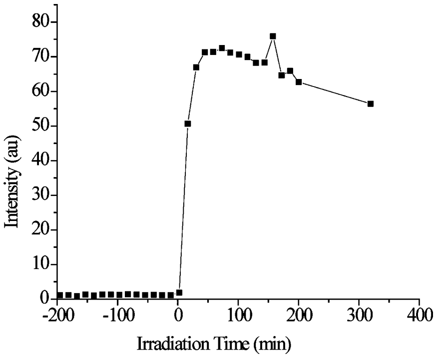

Figure 2. Time trace of 2-formylcinnamaldehyde obtained by the (+)CIMS technique.

in positive mode, compounds with proton affinities higher than that of water extract a proton and are subsequently detected by quadrupole MS; this mode is used for detecting a wide variety of organic compounds. The masses seen in positive mode will generally be detected as $[M + H]^+$ ions and are denoted in the CIMS $[M + H]^+$ column shown in Table 3. The negative mode of operation is highly selective toward acidic and polar molecules. The analyte clusters with CF_3O^- forming an $[M + CF_3O]^-$ cluster ion, or subsequently loses CF_2O to form the $[M + F]^-$ ion. Generally, identification of an $[M + F]^-$ ion corresponds with detecting carboxylic acids, while $[M + CF_3O]^-$ ions may also include hydroxy carbonyls. Owing to the unit-mass resolution of the CIMS technique, structural assignments are based on the results from the GC/EI-TOFMS and from previous results on the photooxidation of naphthalene. Products identified, along with suggested structures and accurate mass measurements obtained by the GC/EI-TOFMS technique are presented in Table 3.

The (+)CIMS mass spectrum from a typical high-NO$_x$ experiment is shown in Figure 1. 2-Formylcinnamaldehyde (at *m*/*z* 161), phthaldialdehyde (at *m*/*z* 135), and phthalic anhydride (at *m*/*z* 167) represent the largest peaks. We refer to these compounds as “ring-opening” products and indicate their presence in Figure 1 by the red mass spectral peaks. These observed compounds are consistent with those of other studies that report products of naphthalene and will be discussed subsequently. Closed-ring or “ring-retaining” compounds, such as isomeric naphthols (at *m*/*z* 145), 1,4-naphthoquinone (at *m*/*z* 159), 2,3-epoxy-1,4-naphthoquinone (at *m*/*z* 175), and isomeric nitronaphthols (at *m*/*z* 190), are also tentatively identified, as indicated by blue mass spectral peaks in Figure 1.

In the CIMS positive mode, the most abundant gas-phase product identified is a compound detected at *m*/*z* 161 (Figure 1). This compound is also observed in the GC/EI-TOFMS data and is positively identified as 2-formylcinnamaldehyde based on a mass spectral comparison with a synthesized standard (as shown in Figure 2S, Supporting Information). The present amounts of this compound are significantly less than found in other studies[71,72] due to losses in the preconcentrator. The time trace for 2-formylcinnamaldehyde under typical high-NO$_x$ conditions in Figure 2 indicates that 2-formylcinnamaldehyde grows rapidly once oxidation is initiated, then decays relatively slowly. From the (−)CIMS measurements, we learn that, after about 2 h of irradiation, all the HONO is consumed; naphthalene concentrations stabilize and generation of 2-formylcinnamaldehyde ends. 2-formylcinnamaldehyde then decays at a rate of 0.06 h^{-1} due to photolysis. After 6 h of irradiation, ∼70% of the initially formed 2-formylcinnamaldehyde remains.

Results from the GC/EI-TOFMS technique demonstrate the presence of both the 1- and 2-nitronaphthalene isomers in the gas phase. 1-Nitronaphthalene has been positively identified using an authentic reference standard (Sigma-Aldrich, 99%) in conjunction with NIST library matching. 2-Nitronaphthalene is identified based on NIST library matching, accurate mass measurements, and comparison of the mass spectrum with the 1-nitronaphthalene isomer. Nitronaphthols are also identified based on NIST library matching. The 4-nitro-1-naphthol authentic standard was run for comparison, but did not match the retention time of the assigned peak. We expect that this is another structural isomer of 4-nitro-1-naphthol, most likely either 1-nitro-2-naphthol or 2-nitro-1-naphthol, both of which have been identified in previous studies.[72,73] Naphthoquinone and 2,3-epoxy-1,4-naphthoquinone are also observed. In addition to these ring-retaining compounds, benzoic acid and phthaldialdehyde are also observed by the GC/EI-TOFMS technique. Chromatograms for selected photooxidation products observed by the GC/EI-TOFMS method are shown in Figure 1S (Supporting Information).

The two methods of sample collection described in Section 2.2.3 yield similar results. Directly introducing the sample into the preconcentrator yielded greater intensities for the nitronaphthalene products; however, the gas-phase product of MW 160 (2-formylcinnamaldehyde) was detected with reduced efficiency using this method. Although the second Tenax tube method detected the gas-phase product of MW 160 with greater efficiency, phthaldialdehyde was not detected. Detection of all other oxidation products was comparable using these two sampling techniques.

3.1.2. Chemical Characterization of High-NO$_x$ SOA.

The chemical composition of naphthalene SOA was probed with the battery of techniques described earlier. HR-ToF-AMS particle-phase data were acquired under a wide range of initial naphthalene mixing ratios. The naphthalene mixing ratios for which aerosol measurements from other instruments were acquired are 20−30 ppb. Hydrocarbon mixing ratios, along with the calculated density and observed aerosol atomic O/C, N/C, and H/C ratios are presented in Table 4. Errors in accuracy associated with AMS compositional ratios are reported as ±30%, ±22%, and ±10% of the measured O/C, N/C, and H/C ratios, respectively, in accordance with findings from Aiken et al.[64] Densities of 1.48 g cm^{-3} were found for high-NO$_x$ SOA.

Under high-NO$_x$ conditions, ∼53% of the overall SOA mass is chemically characterized by off-line chemical analyses of aerosol filter samples using both the UPLC/(−)ESI-TOFMS and total peroxide content measurement techniques. An UPLC/

TABLE 4: Summary of Experimental Conditions and Results from the HR-ToF-AMS Instrument

[naphthalene] (ppb)	NO_x	seed vol ($\mu m^3/cm^3$)	end vol ($\mu m^3/cm^3$)	density (g/cm^3)	SOA mass ($\mu g/m^3$)	O/C ratio	N/C ratio	H/C ratio
5	low	10.64	18.48	1.55	12.15	0.61 ± 0.18	0	0.97 ± 0.1
20	low	10.48	41.48	1.55	48.06	0.72 ± 0.22	0	0.88 ± 0.09
60	low	13	143	1.55	201.5	0.6 ± 0.18	0	0.82 ± 0.08
5	high	12.25	16.23	1.48	6.18	0.55 ± 0.17	0.01 ± 0.02	1.03 ± 0.1
25	high	12.82	39.18	1.48	40.87	0.55 ± 0.17	0.01 ± 0.02	0.90 ± 0.1
30	high	0	26.3	1.48	40.76	0.45 ± 0.15	0.01 ± 0.02	0.90 ± 0.1
40	high	14.67	63.11	1.48	75.08	0.51 ± 0.15	0.01 ± 0.01	0.81 ± 0.08

(−)ESI-TOFMS base peak ion chromatogram (BPC) obtained for a typical high-NO_x naphthalene SOA experiment is shown in Figure 3. Peaks found under both the high- and low-NO_x conditions are denoted in black, while those SOA constituents found only in the high-NO_x case are denoted in green. Due to the use of $(NH_4)SO_4$ seed aerosol, bisulfate (detected as m/z 97) was found to elute first from the reverse-phase C18 column. A complete listing of the high-NO_x SOA constituents identified and quantified by the UPLC/(−)ESI-TOFMS technique is provided in Tables 2S−4S (Supporting Information). As shown in Tables 2S−4S (Supporting Information) and Table 3, ~24−28% of the high-NO_x naphthalene SOA is chemically characterized at the molecular level by the UPLC/(−)ESI-TOFMS technique. These chemical characterizations are further supported by the tandem MS measurements provided by the HPLC/(−)ESI-ITMS technique; major product ions produced for each of the major characterized high-NO_x SOA constituents are also listed in Tables 2S−4S (Supporting Information). All SOA constituents were quantified by calibration with either an authentic or surrogate standard. Dominant contributions to the high-NO_x SOA mass come from phthalic acid and hydroxy benzoic acids. Standard deviations for each UPLC/(−)ESI-TOFMS identified product were calculated across experiments (experiments 2−5 in Table 2). The fraction of SOA mass assigned to each product has a standard deviation of less than 3%, and the average standard deviation for the entire product range was ~2%, indicating the high level of reproducibility of these experiments.

As shown by the time trace in Figure 4, analysis by the PILS/IC technique confirms that phthalic acid is a significant component of the high-NO_x SOA (Retention Time (RT) = 13.88 min), increasing from 0 to 5.23 $\mu g\ m^{-3}$ over the course of the experiment (Experiment 7 in Table 2). Figure 5 shows the ion chromatograms for a high-NO_x chamber sample on the bottom panel. The top panel shows a chromatogram from a 2 ppm standard of phthalic acid. The chromatographic peak with RT of 15.27 min also shows trends of increasing concentration with photochemical age and is not present in background vials, suggesting that this peak corresponds to a SOA constituent; however, this compound could not be identified using available standards. No other water-soluble SOA constituents are observed by the PILS/IC technique, indicating that small organic acids do not account for the unidentified fraction of the SOA mass. This is in contrast to data from the photooxidation of single-ringed aromatic compounds, such as benzene, toluene, and m-xylene, for which small organic acids comprise a substantial portion of the overall SOA mass (unpublished data). Small organic acids have also been observed in SOA generated from the photooxidation of 1,3,5-trimethylbenzene.[74]

On the basis of results from the UPLC/(−)ESI-TOFMS method, N-containing compounds account for ~3% of the total high-NO_x SOA mass formed. Most of the N-containing compounds were quantified using calibration curves generated by either 2-nitro-1-naphthol or 4-nitro-1-naphthol standards. Using 4-nitro-1-naphthol in the quantification of these products yields concentrations that are an order of magnitude reduced from calibrations utilizing the 2-nitro-1-naphthol isomer. Final quantitative results reported here are determined by use of the more conservative mass concentrations. Quantification of these chemically characterized SOA constituents yields an N/C ratio of 0.04. This ratio should be considered as a lower limit for the N/C ratio, because some of the N-containing compounds that are

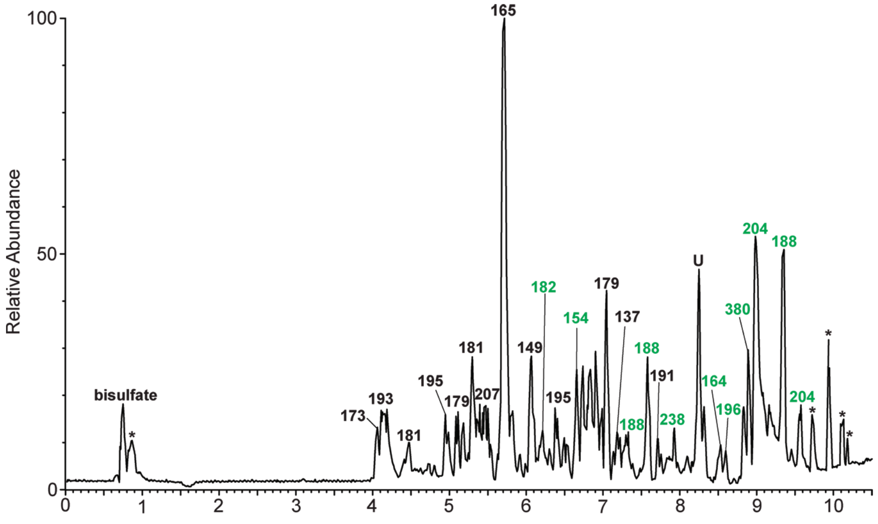

Figure 3. UPLC/(−)ESI-TOFMS base peak ion chromatogram (BPC) of a representative naphthalene high-NO_x SOA sample (Experiment 6). Chromatographic peaks designated with black $[M - H]^-$ ions are also observed in the naphthalene low-NO_x SOA samples. Chromatographic peaks designated with green $[M - H]^-$ ions are only observed in the naphthalene high-NO_x SOA samples. Chromatographic peaks designated with an asterisk, *, were also observed on a blank filter, and they are not considered high-NO_x SOA constituents. Major chromatographic peaks that remain uncharacterized in this study are designated as: U.

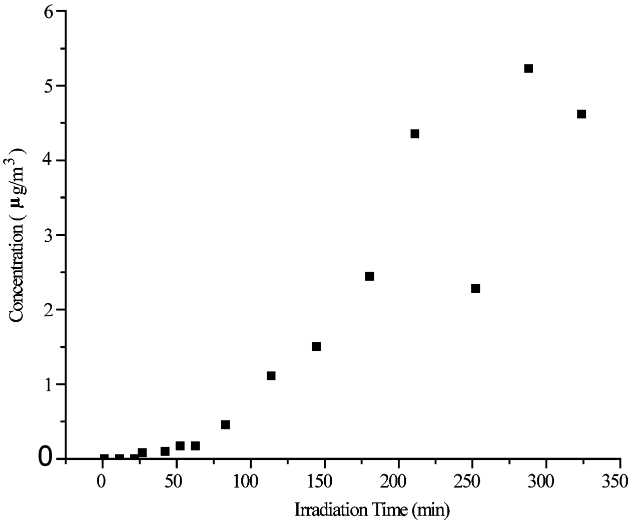

Figure 4. Time trace of phthalic acid acquired from Experiment 6 using the PILS/IC technique.

likely formed are not directly detectable by the UPLC/(−)ESI-TOFMS technique unless the molecule also contains a functional group with an acidic proton that can be abstracted. For example, the UPLC/(−)ESI-TOFMS method detects six isomers of nitronaphthol, as shown in Table 3; however, the 1- and 2-nitronaphthalene compounds identified in the gas phase by the GC/EI-TOFMS technique are not detected, even though the nitronaphthalenes are reported to exist primarily in the particle phase.[46] Given that the 1- and 2-nitronaphthalene isomers are reported to account for 0.3−7%[43,45,72] of the gas-phase yield, and may partition into the particle phase,[46] the detection of these nonacidic nitronaphthalenes in the aerosol phase would likely increase the N/C ratio. We also expect that the formation of PANs, for example from phthaldialdehyde, may play a significant role in SOA formation in the atmosphere. However, owing to the large NO to NO_2 ratio employed in these experiments, and to the difficulty in detecting nonacidic N-containing compounds, PANs are not observed in either the gas-or aerosol-phase.

Bulk HR-ToF-AMS measurements yield measurements of N-containing compounds producing N/C ratios ranging from 0.01−0.044. We place upper and lower bounds on the N/C ratio using calculations with and without the addition of compounds that possess NO^+ and NO_2^+ mass spectral peaks, respectively. Under high-NO_x conditions, OH and NO_2 can react to form nitric acid. Nitric acid can then react with ammonium from the ammonium sulfate seed to produce inorganic nitrates. This process should be of minimal importance for the experiments performed here owing to the dry experimental conditions; however, for the lower-limit calculations, we exclude compounds that have contributions from NO^+ and NO_2^+ mass spectral peaks from the N/C calculation to prevent biasing the chemical composition calculations with the formation of these inorganic nitrates. These lower-limit calculations include only the measurement of organic nitrate (NO_3) functional groups, yielding an atomic N/C ratio of 0.01. Only one organic nitrate is identified by the UPLC/(−)ESI-TOFMS method, supporting the minimal contribution from this class of compounds. However, inclusion of "NO family" ions with mass spectral peaks corresponding to NO^+ and NO_2^+ is necessary to account for the NO_2 groups observed in compounds such as nitronaphthalene, but may introduce artifacts from inorganic nitrates. Inclusion of the NO and NO_2 groups increases the atomic N/C ratio to 0.044, thus providing an upper bound of the N/C ratio. Inclusion of these compounds into the composition calculations also shifts the O/C ratios from 0.51 ± 0.17 (Table 4) to 0.57 ± 0.17. Again, the upper-bound of 0.044 ± 0.01 for the N/C is in good agreement with the lower bound of 0.036 obtained from the UPLC/(−)ESI-TOFMS data as discussed above.

In general, the procedures for compositional analysis determined from high-resolution AMS data are still relatively new, and further studies of the technique are necessary to fully understand the data acquired using this complex instrument. For example, calibrations of compositional ratios performed here are based on AMS data from Aiken et al.,[63] which likely possess a different molecular composition than that of the current experiments. To achieve more accurate ratios, the ionization efficiency of each oxidation product by atomizing standards into

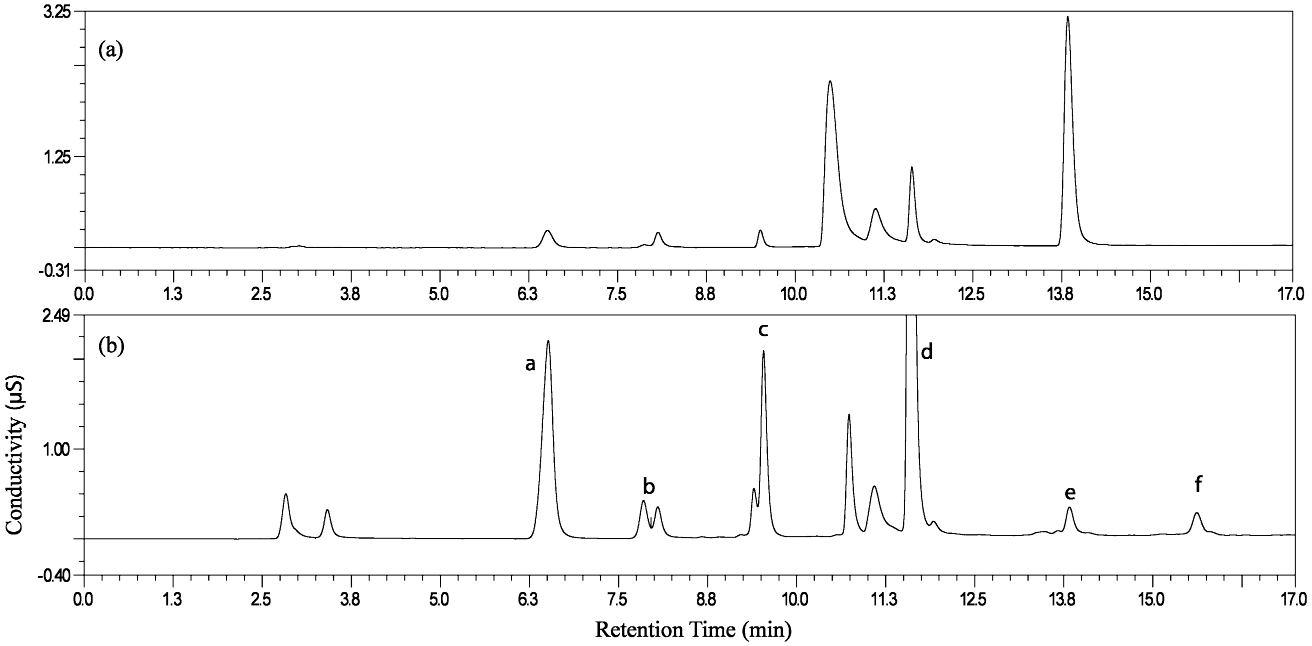

Figure 5. Chromatograms obtained by the PILS/IC technique. The top panel shows a 2 ppm standard of phthalic acid. The bottom panel shows a representative chromatogram of a PILS sample collected under high-NO_x conditions in the presence of ammonium sulfate seed (Experiment 7). Peak assignments are: a-chloride, b-nitrite, c-nitrate, d-sulfate, e-phthalic acid, f-unidentified peak (see text).

the AMS instrument need to be investigated or alternatively, a much larger database of structures would need to be assembled. More work needs to be performed to fully characterize the appropriateness of the compositional ratios acquired by this technique, particularly for the N-containing compounds which have received less attention.

The high-NO_x naphthalene SOA chemically characterized through the filter sampling methods exhibits an average atomic O/C ratio of 0.48. This ratio is largely consistent with the measurements from the HR-ToF-AMS technique, from which an overall O/C ratio of 0.51 ± 0.17 is detected. Atomic H/C ratios of 0.83 calculated from the filter data are also in agreement with the HR-ToF-AMS value of 0.9 ± 0.10, and as stated above, the N/C ratios are also in relative agreement. The implications of the agreement of the O/C, H/C, and N/C ratios between these two analytical techniques is that the 53% of the total SOA mass that has been chemically characterized is an excellent representation of the chemical composition and oxidation level of the entire high-NO_x naphthalene SOA.

The total peroxide measurement based on the iodometric spectroscopic method indicates that under high-NO_x conditions ~28% of the total SOA mass can be attributed to organic peroxides (i.e., ROOH and/or ROOR). Contributions of organic peroxides are calculated by determining the molar concentration of peroxides in the solution. The measured concentration of peroxides obtained by absorption at 470 nm is converted to μg m^{-3} using the known solution volume, molar-weighted average mass, and the volume of chamber air sampled. The molar-weighted average MW is determined by multiplying the MW of each product by the product mole fraction and summing over the individual products. For the high-NO_x system, we have taken a molar-weighted average mass of the chemically characterized SOA constituents listed in Tables 2S−4S (Supporting Information) and assumed this to be the average MW of the unknown organic peroxide structures. The assumption that this average MW would be representative for the unknown organic peroxides is supported by the similar O/C, N/C, and H/C ratios found using both the chemically characterized filter data and the total aerosol HR-ToF-AMS measurements. For the high-NO_x case, the molar-weighted average mass is determined to be 172 amu. As will be discussed subsequently, we believe this is a conservative estimate of the average peroxide mass. If the actual average mass of the peroxides is indeed higher than the assumed mass of 172 amu, then the contribution from peroxides to the total SOA mass would increase. It should be noted that the iodometric spectroscopic method provides no detailed chemical characterization of the quantified organic peroxide content.

3.2. Low-NO_x Conditions.

3.2.1. Chemical Characterization of Low-NO_x Gas-Phase Oxidation Products. A representative (+)CIMS mass spectrum obtained for naphthalene photooxidation under low-NO_x conditions is shown in Figure 6. This mass spectrum was taken at the same fraction of naphthalene reacted as that for the high-NO_x experiment previously shown in Figure 2, and thus the extents of reaction are similar. Whereas the tentatively identified products are the same as those observed under high-NO_x conditions, the relative intensities of the identified compounds are substantially different. In the low-NO_x case, the intensities of the ring-retaining products (e.g., naphthol, naphthoquinone, and epoxyquinone), as denoted by blue mass spectral peaks in Figure 6, are all significantly greater than those found under high-NO_x conditions. Nevertheless, the *m/z* 161 signal continues to dominate the overall (+)CIMS mass spectrum. When compared with data from both the high-NO_x experiments and from injection of the synthesized standard, it is found that the GC retention times, mass spectra, and exact masses (i.e., chemical formulas) obtained using the GC/EI-TOFMS technique match, thus confirming that the compound observed at *m/z* 161 in the (+)CIMS mass spectrum under low-NO_x conditions is 2-formylcinnamaldehyde.

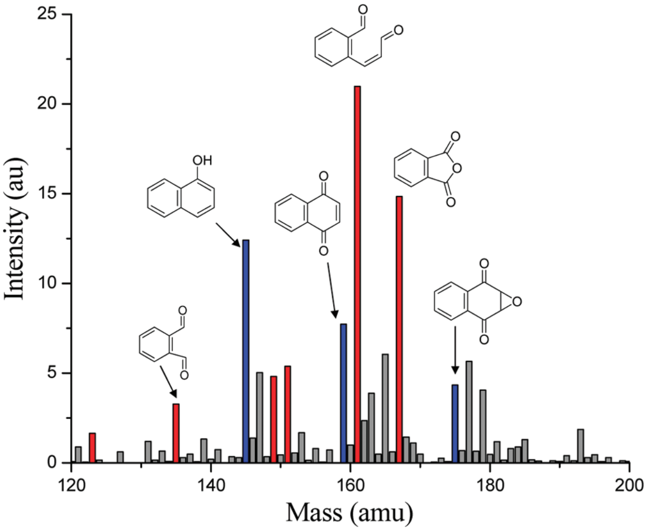

Figure 6. (+)CIMS mass spectrum taken at 70% reacted naphthalene under low-NO_x conditions. Red data indicate ring-opening products. Ring-retaining products are indicated in blue.

3.2.2. Chemical Characterization of Low-NO_x SOA. An UPLC/(−)ESI-TOFMS BPC obtained for a typical low-NO_x naphthalene SOA experiment is shown in Figure 7. Detailed comparison of this chromatogram and the high-NO_x BPC (Figure 3) demonstrates that the aerosol compositions are quite similar. All of the chromatographic peaks are also observed in the naphthalene high-NO_x SOA samples. No N-containing SOA constituents are observed under low-NO_x conditions due to the lack of NO and NO_2 addition reactions. Under low-NO_x conditions, we have been able to chemically characterize ~68% of the SOA mass, as compared to the ~53% identified in the high-NO_x regime. The increase in speciation is the result of a substantial enhancement in the concentration of the acidic species under low-NO_x conditions, with consistent peroxide contributions under both NO_x conditions. As shown in Table 3 and in Supporting Information, the fractions of total SOA mass attributed to phthalic acid and hydroxy phthalic acid, for example, increase by factors of 2 and 3, respectively. Similar increases are observed for benzoic acid, hydroxy benzoic acid, cinnamic acid, and dihydroxy cinnamic acid. The ring-retaining compounds are present in low-NO_x SOA samples, but we cannot remark on their relative abundance compared to the high-NO_x case, owing to the fact that standards are often not available, and these components were not quantified. Detection efficiencies for these nonacidic ring-retaining compounds are lower than those of the acidic ring-opening compounds. Hydroxy cinnamic acid (see Table 3, MW 164) was the only additional compound identified specific to the low-NO_x regime. The atomic O/C compositional ratio from filter sampling methods is 0.50, and the H/C ratio is 0.82. O/C and H/C ratios determined from the HR-ToF-AMS technique are 0.64 ± 0.19 and 0.89 ± 0.1, respectively.

The total organic peroxide contribution was determined in the same manner as that carried out for the high-NO_x experiments as detailed in Section 3.1.2. The molar-weighted average mass was determined to be slightly higher than that of the high-

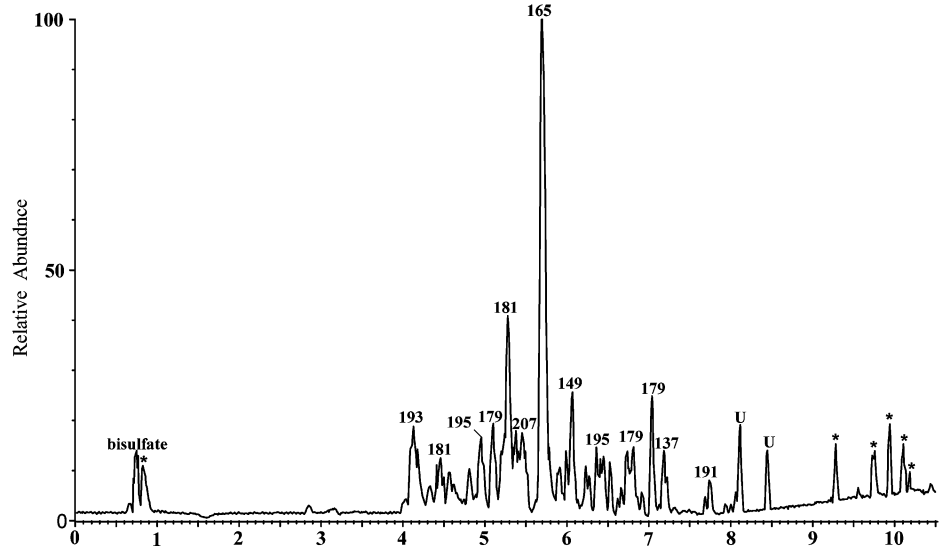

Figure 7. UPLC/(−)ESI-TOFMS base peak ion chromatogram (BPC) of a representative naphthalene low-NO$_x$ SOA sample (Experiment 3). All major chromatographic peaks are marked with their corresponding [M − H]$^-$ base peak ions. Chromatographic peaks designated with an asterisk, *, were also observed on a blank filter, and they are not considered high-NO$_x$ SOA constituents. Major chromatographic peaks that remain uncharacterized in this study are designated as: U.

NO$_x$ SOA at 174 amu due to the increased contribution from larger acids, for example, hydroxy phthalic acid (MW 182 and observed by the UPLC/(−)ESI-TOFMS technique at *m*/*z* 181). The total peroxide contribution under low-NO$_x$ conditions is calculated to be ∼26.2% of the total SOA mass. This is similar to the 28% contribution found in the high-NO$_x$ case. As in the high-NO$_x$ case, we believe this to be a lower limit of the total peroxide contribution to the SOA mass.

4. Discussion

4.1. High-NO$_x$ Conditions.

4.1.1. High-NO$_x$ Gas-Phase Chemistry. The gas-phase mechanism of naphthalene photooxidation has been the subject of considerable study. Our present findings can be viewed within the context of this prior work. We concentrate first on the high-NO$_x$ case, an atmospherically interesting situation owing to the coemissions with other anthropogenic sources and the relatively short lifetime of naphthalene in the urban atmosphere.[43,75−78] Proposed formation mechanisms of the major high-NO$_x$ naphthalene gas-phase products are provided in Scheme 1. The gas-phase photooxidation products detected are boxed, and the MWs of the identified products are highlighted in red. The mechanism presented here does not incorporate all of the chemically characterized products; a complete list of identified products can be found in Tables 2S−4S (Supporting Information). The majority of the gas-phase mechanism has been previously established.[43,45,47,72,79,80] Qu et al.[81] have performed theoretical calculations exploring the OH oxidation of naphthalene in the presence of O$_2$ and NO$_x$, and have detailed much of the gas-phase reaction dynamics. As determined by Wang et al.,[47] 68% of the OH addition occurs at the C$_1$ position to form the hydroxycyclohexadienyl radical. The 1-hydroxycyclohexadienyl radical lies 10 kcal mol^{-1} lower in energy than the 2-isomer.[81] The preference for addition at the 1-site is supported by the fact that 2-nitronaphthalene is ∼2 times more abundant than the 1-nitronaphthalene isomer.[80] The addition, the 1-site also determines the formation of the epoxide, although 2-formylcinnamaldehyde could be formed from either the 1- or 2-hydroxycyclohexadienyl radical.

The OH-naphthalene adduct reacts with either NO$_2$ or O$_2$. GC/FID data combined with GC/MS-negative ion chemical ionization (NCI) data from other chamber studies[80] suggest that the NO$_2$ and O$_2$ reactions with the OH-naphthalene adduct may be of equal importance for NO$_2$ mixing ratios in the range of 60 ppb. The NO$_2$ mixing ratio used in the present high-NO$_x$ experiments is ∼80 ppb, so these pathways should be of roughly equal importance in the present experiments. A detailed description of the importance of the NO/NO$_2$ in these experiments is previously discussed in Section 3.2.1.

The N-containing compounds (i.e., nitronaphthalenes and nitronaphthols) formed through the NO$_2$ reaction pathway are of particular interest due to their mutagenic properties.[50,51] In extensive studies of the nitronaphthalene isomers, along with other nitroarene compounds, Arey and co-workers[43,48,73,80,82] have found that both 1- and 2-nitronaphthalene isomers form during daytime conditions by OH reaction of naphthalene, but actually concentrations of these compounds reach a maximum at night due to N$_2$O$_5$ chemistry.[48] The major loss process for 1- and 2-nitronaphthalene under atmospheric conditions is photolysis, with photolytic lifetimes on the order of 2 h.[73] Photolysis is approximately an order of magnitude more important than OH reaction, for which the reaction rate coefficients are 5.4 × 10^{-12} cm^3 molecule^{-1} s^{-1} and 5.6 × 10^{-12} cm^3 molecule^{-1} s^{-1} for the 1- and 2-nitro isomers, respectively. Arey et al.[73] also suggest that 1-nitronaphthalene is the precursor to the 1,4-naphthoquinone product, which is formed through a photolysis pathway, denoted in Scheme 1 by an open arrow. These OH rates are consistent with the work of Bunce et al.[45] for which lifetimes of 20−34 h against OH reaction for the 1-nitronaphthalene and 2-nitronaphthalene isomers, respectively, were calculated using the same OH concentration, but neglecting the photolysis pathway.

Formation of ring-opening compounds is consistent with decomposition of the alkoxy (RO) radicals formed from the RO$_2$ + NO pathway,[72] which leads to 2-formylcinnamaldehyde (MW 160) and observed by the (+)CIMS technique at *m*/*z* 161, the precursor to the majority of the ring-opening products found in Scheme 2. 2-formylcinnamaldehyde is detected as both *E*- and *Z*- isomers and is the major gas-phase product observed under high-NO$_x$ conditions.[45,71,72] Sasaki et al.[72] suggested a combined yield for the cinnamaldehyde *E*- and *Z*- isomers of 35%. Although two further compounds with MW 160 are identified,

SCHEME 1: Proposed High-NO$_x$ Mechanism for the Formation of Ring-Retaining Products and 2-Formylcinnamaldehyde (MW 160)[a]

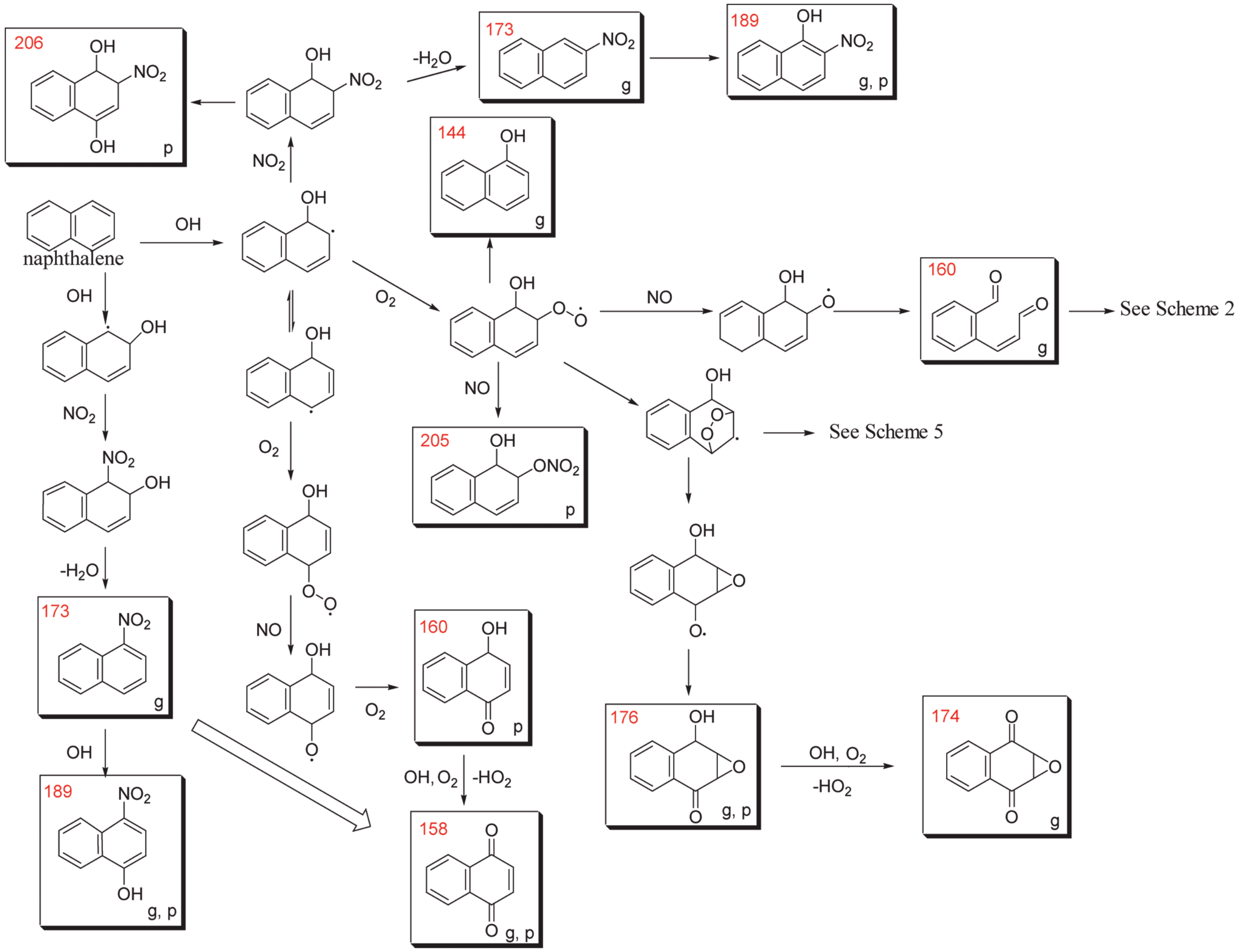

[a] Observed products are boxed. MWs are shown in red, and the phase of the observed product (gas, g, or particle, p) is denoted in the lower right corner.

based on peak intensity, the authors suggest that the *E*- and *Z*-2-formylcinnamaldehyde structures account for ~92% of the products with MW 160. The remaining two compounds with MW 160 have yet to be identified, although data suggest that one of these compounds is an aldehyde isomer, whereas the other compound most likely contains a carbonyl group. The latter structure may be the hydroxy carbonyl identified as MW 160 shown in Scheme 1. We note that dihydroxynaphthalene compounds would also be consistent with this mass.

An alternate route to the formation of 2-formylcinnamaldehyde proposed by Qu et al.[81] involves a hydride shift from the alcohol group on the naphthol peroxy intermediate to form a hydroperoxy intermediate. Subsequent loss of OH and breaking of the C_1-C_2 bond yields the 2-formylcinnamaldehyde. The authors calculate that this reaction is exothermic by 24.88 kcal mol^{-1}. The two mechanisms for the formation of 2-formylcinnamaldehyde are shown in Scheme 3. The first mechanism would result in the formation of NO_2 and HO_2, whereas the second mechanism would result in the formation of OH. It is not possible to confirm one mechanism over the other from our data, and both mechanisms remain as plausible routes to the formation of the major 2-formylcinnamaldehyde oxidation product. 2-Formylcinnamaldehyde undergoes further reaction as shown in Scheme 2 to form ring-opening products, including phthalic anhydride, phthalic acid, and phthaldialdehyde.

In addition to the pathway for ring-opening products through the 2-formylcinnamaldehyde product, the bicyclic peroxy radical may play a crucial role in the formation of not only ring-opened products, but the formation of peroxide and epoxide compounds as well. This alternate pathway will be discussed in Section 4.1.2. An alternate pathway to the formation of ring-opening products is supported by the decay time for 2-formlycinnamaldehyde. As shown in Figure 2, 70% of the 2-formylcinnamaldehyde remains at the completion of the experiment. Given that, under high-NO$_x$ conditions, the SOA mass yield for naphthalene is ~30%,[15] and 2-formylcinnamaldehyde is suggested as the major gas-phase product (30−60%),[72,83] one would expect to see a greater decay in 2-formylcinnamaldehyde in order to produce the observed aerosol yields. This is suggestive that another route to the ring-opening products may play a role in the formation of high-NO$_x$ SOA.

Previous studies present evidence that photolysis plays a significant role in the loss processes for the 2-formylcinnamaldehyde isomers, competing with the various reaction pathways. Wang et al.[47] have detailed the various loss processes for 2-formylcinnamaldehyde and report a ratio of OH reaction to photolysis of 1.8 under blacklamp photolysis conditions with corrections for wall-loss. A further study by Nishino et al.[71] reexamined the competing pathways of 2-formylcinnamaldehyde OH-reaction versus photolysis. Nishino et al. suggest a yield

SCHEME 2: Proposed Mechanism for the Formation of Ring-Opening Products from the Further Reaction of 2-Formylcinnamaldehyde[a]

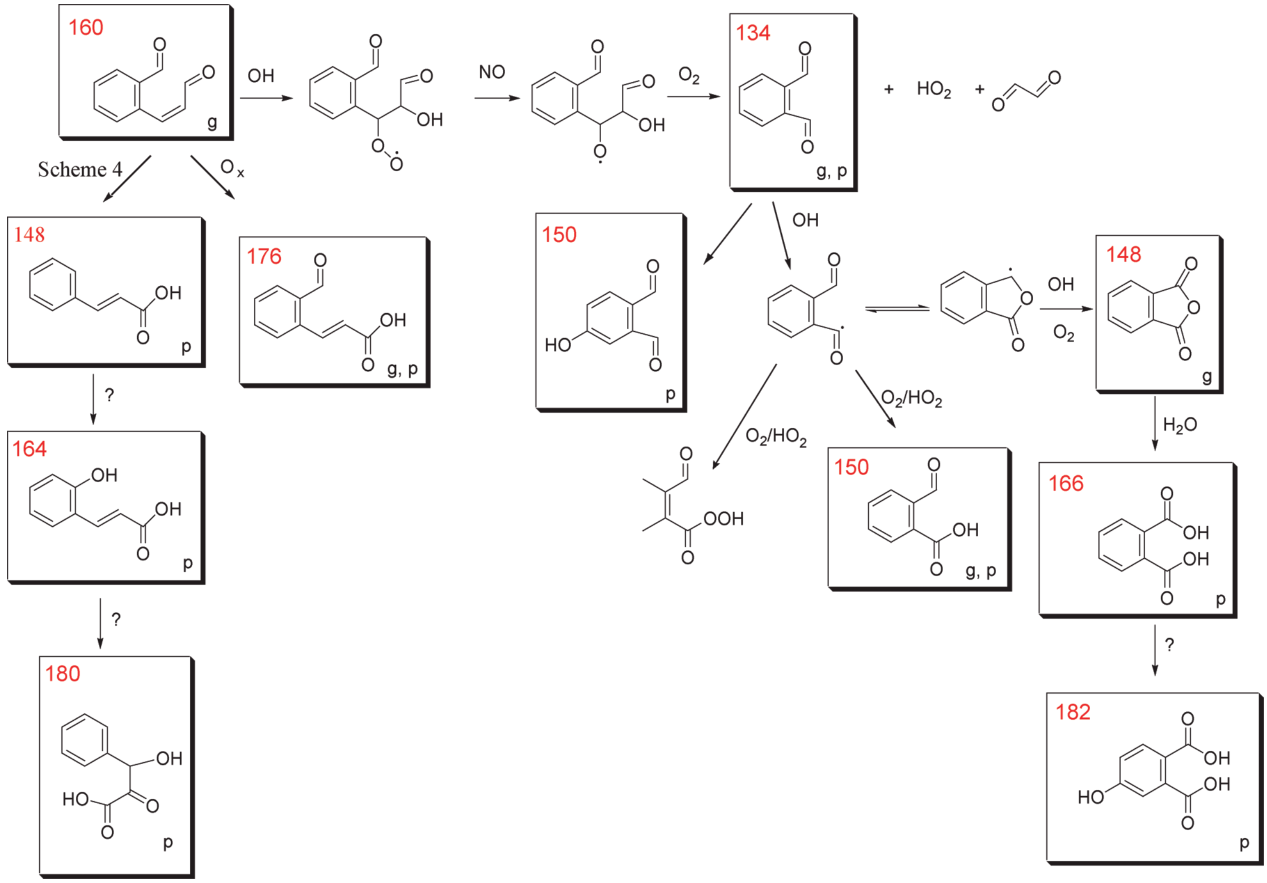

[a] Observed products are boxed. MWs are shown in red, and the phase of the observed product (gas, g, or particle, p,) is denoted in the lower right corner.

SCHEME 3: Suggested Mechanism for the Formation of 2-Formylcinnamaldehyde[a]

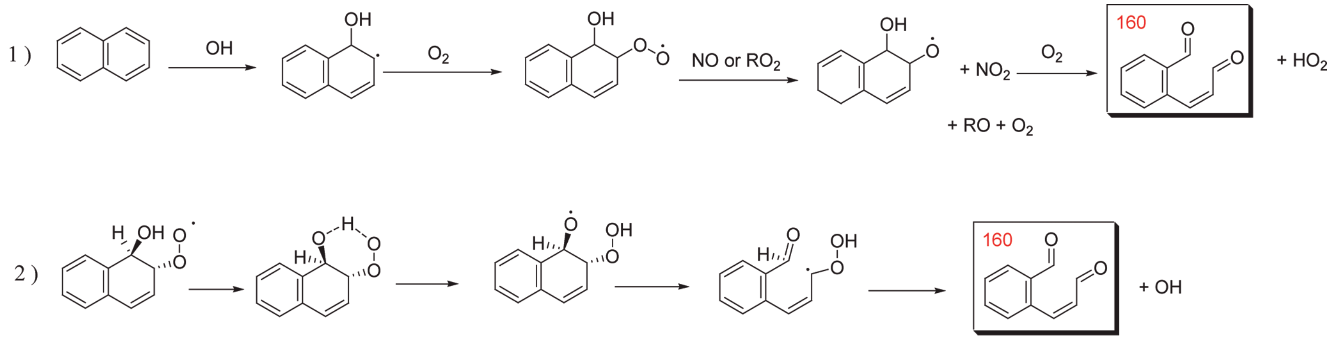

[a] Mechanism 2 from ref 81 begins with the formation of the peroxide assuming the same initial steps as demonstrated in mechanism 1.

of 58−61% for the combined *E*- and *Z*- isomers of 2-formylcinnamaldehyde with the OH-reaction and photolysis decay pathways being of equal importance under experimental conditions.

In addition to the aforementioned products we have identified a range of C_7 and C_9 compounds (benzoic acid, etc) in low abundance. While some of these compounds have been previously observed,[45] a mechanism leading to them has not yet been proposed. We suggest two possible mechanisms as minor routes. Photolytic loss of the formyl group from 2-formlycinnamaldehyde followed by a hydride shift to the benzene ring and further oxidation by O_2 and HO_2 seems to be a plausible mechanism for forming compounds in this class.

Alternatively, as shown in Scheme 4, C_7 and C_9 compounds could be formed through O_2 addition to the radical formed on the formyl group by H-abstraction by OH radical to form a RO_2 radical that subsequently reacts with NO to form an alkoxy radical. Loss of a CO_2 moiety followed by a hydride shift and oxidation of the radical carbonyl to form an acid would generate the observed product with MW 148 denoted in Scheme 2. Similarly, the corresponding peroxyacid would likely be formed in conjunction with the acid (MW 148) during the O_2 addition, and may go on to further react in the aerosol phase.

4.1.2. High-NO$_x$ SOA Chemistry. Two previous studies have addressed the chemical composition of SOA formed from the photooxidation of naphthalene.[46,84] We present here detailed quantitative analysis on the chemical composition and potential reaction pathways relevant to naphthalene high-NO$_x$ SOA formation. The compounds identified from the UPLC/(−)ESI-TOFMS analysis of filter samples yield atomic O/C, N/C, and

SCHEME 4: Possible Mechanism for the Formation of C7 and C9 Compounds

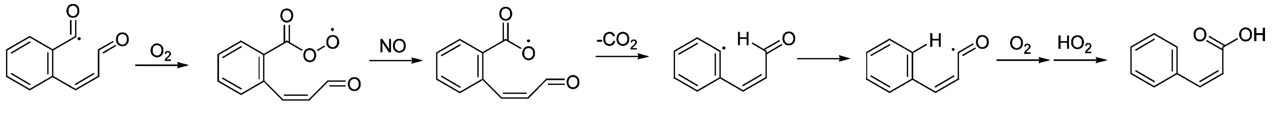

SCHEME 5: Proposed Reaction Mechanisms for Bicyclic Peroxide Structure

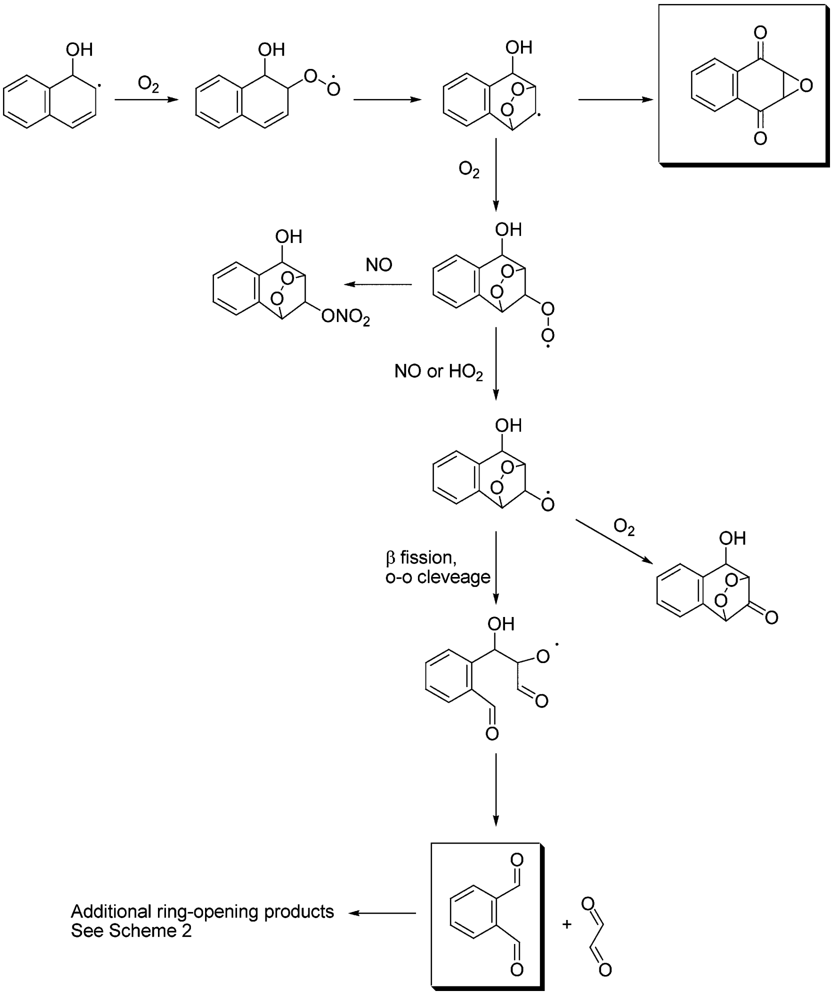

H/C ratios that are in agreement with bulk measurements from HR-ToF-AMS samples. This indicates that the chemical nature of the characterized SOA constituents is a good representation of the bulk aerosol formed from the photooxidation of naphthalene under high-NO_x conditions. The chemical mechanisms shown in Schemes 1 and 2 demonstrate how the gas-phase oxidation products are likely to evolve by further oxidation to form the components identified in the aerosol phase. The "g" and "p" superscripts associated with each product denote the phase of the component. A minor fraction of the SOA mass is attributed to the N-containing compounds such as nitronaphthols. The chemically characterized portion of the aerosol, which we assume to be representative of the bulk aerosol based on detailed composition measurements, is primarily composed of single-ring (ring-opening) acids (e.g., formylcinnamic acid and further oxidized compounds from phthalic acid).

We have performed calculations determining the average number of carbonyls/molecule for the SOA in order to compare with previous FTIR measurements. Dekermenjian et al.[84] reported an average of 3.2 carbonyl/molecule based on the assumption that the average molecule possesses a 10 carbon backbone. As shown in Table 3, many of the compounds with significant yield possess C8 structures, thus calling into question the appropriateness of assuming a 10-carbon backbone. In order to determine the average number of carbonyls/molecule we have counted the number of carbonyl groups on each identified product, and weighted this number by mole fraction, to establish that the average structure possesses ~1.25 carbonyls/molecule. We believe the average we report here is an accurate representation of the degree of molecular oxidation, as it is based on identified structures for which the bulk composition is known. In comparison, the chemical composition determined by FTIR will be strongly dependent on the length of the carbon backbone, the accuracy of the composition calibrations, and the form of the carbonyl group (e.g., acidic, aldehydic, or ketone).[85]

Organic peroxides are found to contribute ~28% of the total high-NO_x SOA mass. We propose that a mechanism for the formation of these compounds may occur through the formation of a bicyclic peroxy radical as shown in Scheme 5. Analogous reaction pathways have been examined in single-ringed aromatic hydrocarbons (SAH). For toluene, benzene, and *m*-xylene it was proposed that isomerization of the primary RO_2 radical to form the bridged bicyclic structure is faster than the competing reaction with NO_2, and a reaction with NO to form the RO

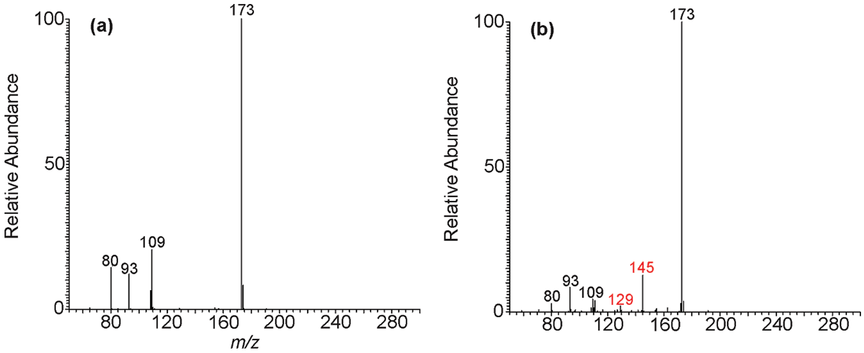

Figure 8. (−)ESI-ITMS MS^2 of *m/z* 173 collected via direct infusion analysis from (a) a 20 ppm 4-hydroxybenzene sulfonic acid standard and from (b) a naphthalene high-NO_x SOA sample (Experiment 6). Due to the generation of these MS^2 spectra via direct infusion, isobaric *m/z* 173 ions were analyzed simultaneously from the high-NO_x SOA sample. As a result, red ions highlighted in (b) are not due to the hydroxybenzene sulfonic acid. Product ions observed at *m/z* 93 and 109 are due to neutral losses of SO_2 and SO_3, respectively, which are neutral losses characteristic of aromatic sulfonates. The product ion observed at *m/z* 80 is due to the production of SO_3^-, which is also a characteristic ion of aromatic sulfonates. The hydroxybenzene sulfonic acids lack the presence of a *m/z* 97 ion (i.e., HSO_4^-) in their MS^2 spectra, which is a characteristic product ion of organosulfate functional groups ($-ROSO_3$).

radical may only occur after O_2 addition.[86] The simplest bicyclic structure from naphthalene, which has molar mass of 192 amu, is shown below in Scheme 5. Thus, structures related to the bicyclic RO_2 radical would yield masses of 192 or higher, and the contributions from peroxides based on the average yield-weighted calculations detailed in Section 3.1.2 would be underestimated. If one uses the single-ringed aromatic compounds as exemplary of the PAH products, then a reasonable mechanism for both peroxides and ring-opening products can be determined as shown in Scheme 5. The initial naphthalene−OH adduct can either undergo hydrogen abstraction through reaction with O_2 to form naphthol or can react with O_2 to form the RO_2 radical. For benzene, master equation calculations suggest that formation of the phenolic compound accounts for 55−65% of the reaction mechanism, and the formation of the bicyclic peroxy radical is the other major pathway.[87] Resonance fluorescence studies for several aromatic species have also shown that the OH-aromatic adduct reacts preferentially with O_2 over both NO_2 and NO to form either the alcohol or the bicyclic peroxide structure, and reaction with NO can only occur after the initial addition of O_2.[86] Reactions of the aromatic-peroxy adduct with NO to form the alkoxy radical are found to be of minor importance for the SAH.[86,88] The bicyclic peroxy radical that forms from the aromatic−OH reaction with O_2 can isomerize to yield an epoxide; however, this route has been suggested based on master equation calculations[87] for benzene, and based on ab initio calculations[86] for toluene, to be of minor importance in the atmosphere, although the epoxide formed from this type of mechanism has been detected in the experiments reported here. For benzene, the pathway to the bicyclic RO_2 structure has a 10 kcal mol^{-1} barrier and is exothermic by ~69 kcal mol^{-1}. Comparatively, the barrier to epoxide formation is 74 kcal mol^{-1} and the reaction is exothermic by 59 kcal mol^{-1}.[87] Once the bicyclic RO_2 radical forms, the radical termination steps can lead to a carbonyl, an organic nitrate, or an RO radical, with the latter undergoing β-fission followed by cleavage of the bridge O−O bond to form ring-opening products. For the SAH, the primary fate of the bicyclic radical is isomerization to form the epoxide or reaction with O_2 to lead to ring-opening products. We include the route through reaction of the alkoxy radical with O_2 to form the carbonyl merely for completeness, but this should be a very minor channel.

Both the mechanism through the bicyclic structure (Scheme 5) and the mechanism shown for the formation of phthaldialedhyde in Scheme 2 are supported by the observed concurrent growth of glyoxal.[47] However, reaction through the bicyclic mechanism generates phthaldialdehyde and glyoxal as first generation products, while further reaction through 2-formylcinnamaldehyde (Scheme 2) leads to second-generation glyoxal and phthaldialdehyde. The bicyclic structure to form ring-opened products has been extensively studied for the single-ringed aromatics,[89] but to the best of our knowledge, has only been suggested in the pathway to epoxide formation for the PAH compounds. Given that about 70% of the 2-formylcinnamaldehyde was found to remain at the completion of the chamber experiments, formation of the ring-opening products through an alternate pathway may be of significance. Further mechanistic studies on the reaction pathways of bicyclic structures related to PAHs could yield important insights into the further gas-phase reactions of this class of compounds.

In addition to the ring-opening and ring-retaining structures previously outlined, an organic sulfonic acid (R-SO_3), which was characterized as hydroxylbenzene sulfonic acid using an authentic standard, is observed here in naphthalene SOA produced under both high- and low-NO_x conditions in the presence of neutral ammonium sulfate seed aerosol. Comparisons of these mass spectra are displayed in Figure 8. Product ions observed at *m/z* 93 and 109 are due to neutral losses of SO_2 and SO_3, respectively. These neutral losses are characteristic of aromatic sulfonates.[90] The product ion observed at *m/z* 80 is due to the production of SO_3^-, which is also a characteristic ion of aromatic sulfonates.[91,92] The hydroxylbenzene sulfonic acids lack the presence of a *m/z* 97 ion (i.e., HSO_4^-) in their MS^2 spectra, which is a characteristic product ion of organosulfate functional groups ($-ROSO_3$).[29,32,59] The absence of this peak clearly suggests that the product identified cannot be an organosulfate. In combination with the accurate mass measurements and similar retention times, the comparison of these MS^2 spectra further supports the identification of hydroxylbenzene sulfonic acids in naphthalene low- and high-NO_x SOA formed in the presence of ammonium sulfate seed. The formation of this product requires reaction with the ammonium sulfate seed, as the seed is the only source of sulfur in the system; however, the mechanism by which an organic sulfonic acid would be produced remains unclear. Methyl sulfonate has been reported in marine layer aerosol due to the oxidation of dimethyl sulfide.[93−95] The presence of sulfonate compounds known as of linear alkylbenzene sulfonates (LAS) has been observed in river and seawater[96] as well. LAS compounds, which are used as surfactants in the manufacturing of cleaning products,[97] are

SCHEME 6: Proposed Low-NO_x Mechanism for the Formation of Ring-Retaining Products and 2-Formylcinnamaldehyde (MW 160) under Low-NO_x Conditions[a]

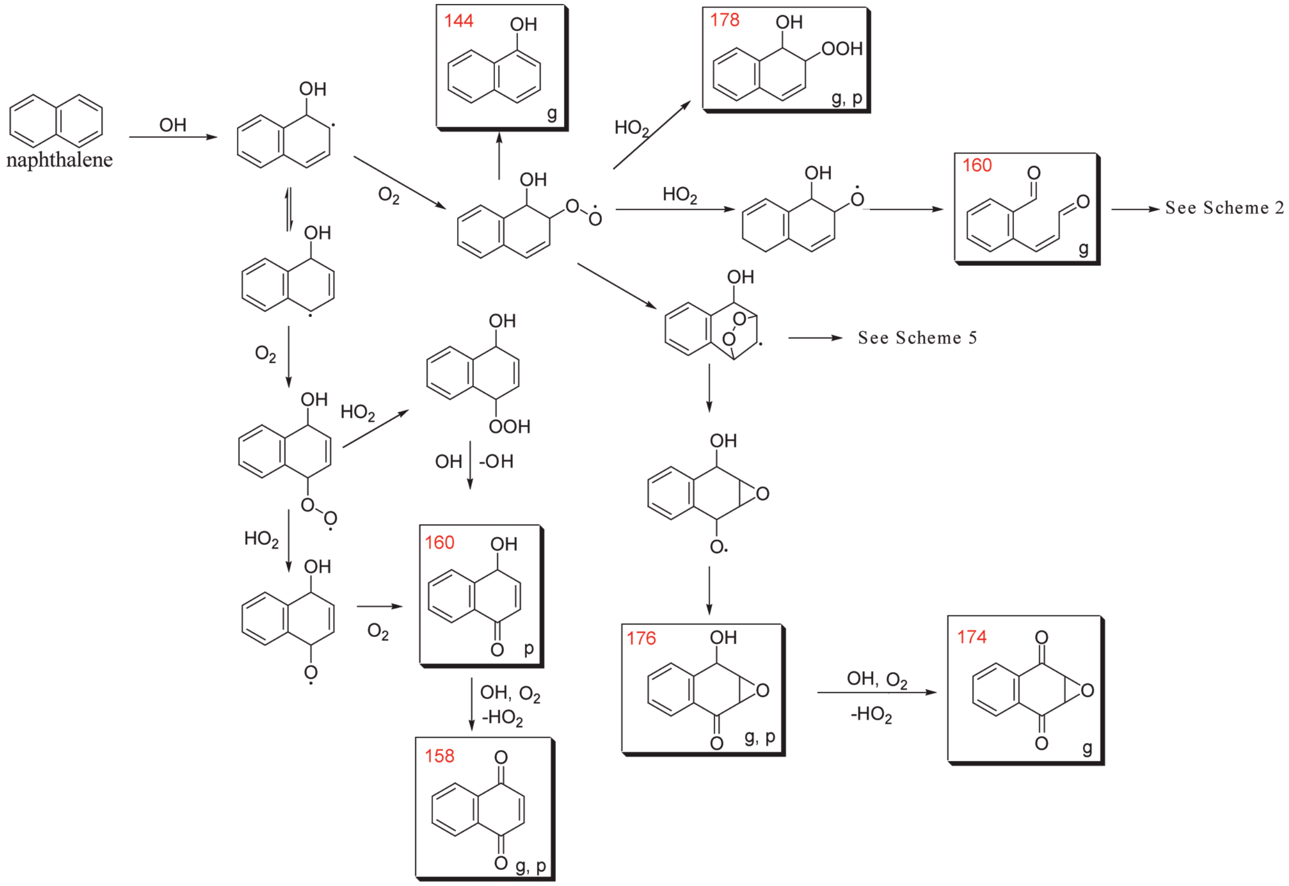

[a] Observed products are boxed. MWs are shown in red, and the phase of the observed product (gas, g, or particle, p) is denoted in the lower right corner.

found in these aquatic systems due to incomplete removal from wastewaters. Most recently, Altieri et al.[98] have observed the presence of LAS directly in precipitation samples. The presence of sulfonates in the environment due to pollution sources does not yield insights into the generation of these compounds in our chamber studies. Nevertheless, the photooxidation of PAHs (e.g., naphthalene) in the presence of sulfur-containing aerosols might yield an additional source of sulfonates found in the environment.

4.2. Low-NO_x Conditions.

4.2.1. Low-NO_x Gas-Phase Chemistry. Although the major gas-phase products observed under low-NO_x conditions are similar to those under high-NO_x conditions, the intensities of the resultant compounds differ dramatically. Scheme 6 shows the proposed mechanism for the formation of the identified products under low-NO_x conditions. Under low-NO_x conditions, the ring-opening products can be formed mechanistically through $RO_2 + RO_2$ or $RO_2 + HO_2$ pathways. Given the high concentrations of HO_2 prevalent in these chamber studies, the $RO_2 + RO_2$ route is calculated to be of minor importance compared to $RO_2 + HO_2$ reactions. A simple kinetic simulation similar to those performed for SAH,[13] indicates that in order for $RO_2 + RO_2$ mechanisms to be competitive with $RO_2 + HO_2$ reactions, $RO_2 + RO_2$ rate constants would need to be at least a factor of 10 larger than $RO_2 + HO_2$ rate constants based on relative concentrations of RO_2 and HO_2 found in the chamber. From the master chemical mechanism (MCM) version 3.1 it is found that $k_{(RO_2+HO_2)}$ are generally on the order of 2.0×10^{-11} cm^3 $molecule^{-1}$ s^{-1}, whereas $k_{(RO_2+RO_2)}$ are no more than 1.0×10^{-12} cm^3 $molecule^{-1}$ s^{-1}, indicating that $RO_2 + HO_2$ pathways should dominate over $RO_2 + RO_2$ reactions under our experimental conditions.

We also acknowledge that a different pathway for the 1,4-naphthoquinone product under low-NO_x conditions may be possible. In their study of the OH-initiated photooxidation of naphthalene, Qu et al.[81] predict that the quinone is formed by addition of HO_2 to 1-naphthol followed by reaction with O_2 to form the 1,4-carbonyl peroxy naphthalene intermediate. Two subsequent reactions with HO_2 yield 1,4-naphthoquinone and OH radical. The overall reaction is exothermic by −58.49 kcal/mol. This type of HO_2 mechanism has not been well established, and reaction rates have not been reported, thus determining the atmospheric importance of such a mechanism is not possible, although it is energetically plausible.

4.2.2. Low-NO_x SOA Composition Chemistry. Under low-NO_x conditions ~68% of the SOA mass has been identified, of which 26.2% is associated with organic peroxide compounds, and the remaining 42% is chemically characterized at the molecular level in Table 3 (and Tables 5S−7S) with dominant contributions coming from acids. Under low-NO_x conditions a significant enhancement in the formation of acids is observed. As shown in Table 3, the contribution of hydroxyphthalic acid to the overall SOA mass increases from 3% in high-NO_x condition to 9% for the low-NO_x case. The increase in the concentration of acidic species is expected in the low-NO_x case as $RO_2 + HO_2$ chemistry dominates over the formation of alkoxy radicals in the absence of NO. However, the formation of alkoxy radicals through an $RO_2 + HO_2$ route still leads to

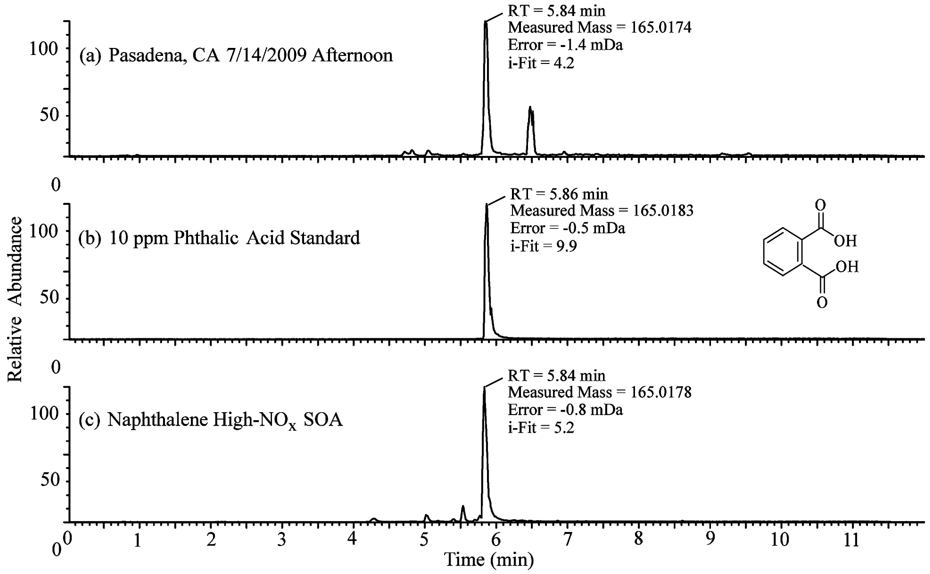

Figure 9. UPLC/(−)ESI-TOFMS EICs of *m/z* 165 from (a) ambient samples collected in Pasadena, CA, (b) a 10 ppm phthalic acid standard, and (c) naphthalene high-NO$_x$ experiments (Experiment 6).

the presence of ring-opening species, as does the bicyclic mechanism shown in Scheme 5. The 28% of SOA mass attributed to organic peroxides, along with the enhancement of acidic species, indicates the importance of $RO_2 + HO_2$ reactions. The further reaction of bicyclic RO_2 radicals may contribute significantly to the generation of ring-opening products, the epoxide, and organic peroxide species. O/C ratios from the filter sampling method are slightly higher than in the high-NO$_x$ data (0.50 vs 0.48, respectively), as is expected given the enhancement of acidic species. AMS data shows that the O/C ratios and H/C ratios are also slightly higher in the low-NO$_x$ experiments, though still within error bars when compared to the high-NO$_x$ experiments. These higher compositional ratios obtained from the AMS technique appear to not only be an effect of increasing acid concentration, but also of aging. Owing to the lower OH concentration achieved in the low-NO$_x$ experiments, longer reaction times are required to reach a constant aerosol volume, thus more oxidation may occur in the aerosol, though the observed affect is small.

4.3. Atmospheric Significance of Naphthalene SOA: Identification of Potential Ambient SOA Tracers in Urban Atmospheres.

Urban aerosol filter samples collected in Birmingham, AL and in Pasadena, CA, were examined for the presence of naphthalene SOA constituents chemically characterized in the present study (Table 3). The UPLC/(−)ESI-TOFMS data obtained from the urban aerosol samples are compared to the laboratory-generated high-NO$_x$ naphthalene SOA. Upon detailed comparison of the UPLC/(−)ESI-TOFMS BPCs obtained from both the laboratory-generated and ambient organic aerosol samples, it becomes evident that several of naphthalene high-NO$_x$ SOA constituents characterized in the present study are observed in the urban aerosol samples. Figure 9 shows the UPLC/(−)ESI-TOFMS extracted ion chromatograms (EICs) of *m/z* 165 obtained from an urban aerosol sample collected from Pasadena, CA, a 10 ppm phthalic acid authentic standard, and a typical naphthalene high-NO$_x$ photooxidation experiment, respectively. The comparison of these 3 EICs suggests that phthalic acid may be a potential ambient naphthalene SOA tracer

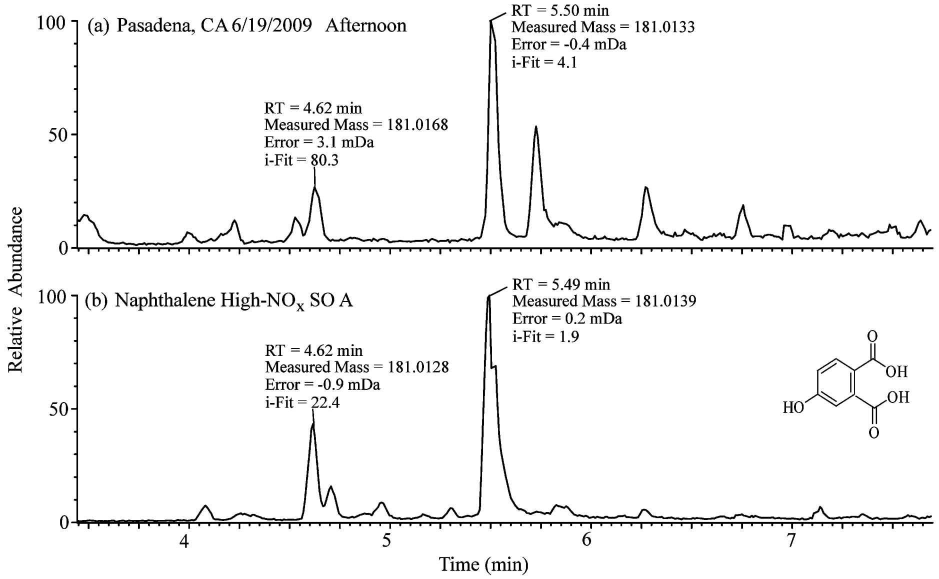

Figure 10. UPLC/(−)ESI-TOFMS EICs of *m/z* 181 from (a) ambient samples collected in Pasadena, CA and (b) naphthalene high-NO$_x$ experiments (Experiment 6).

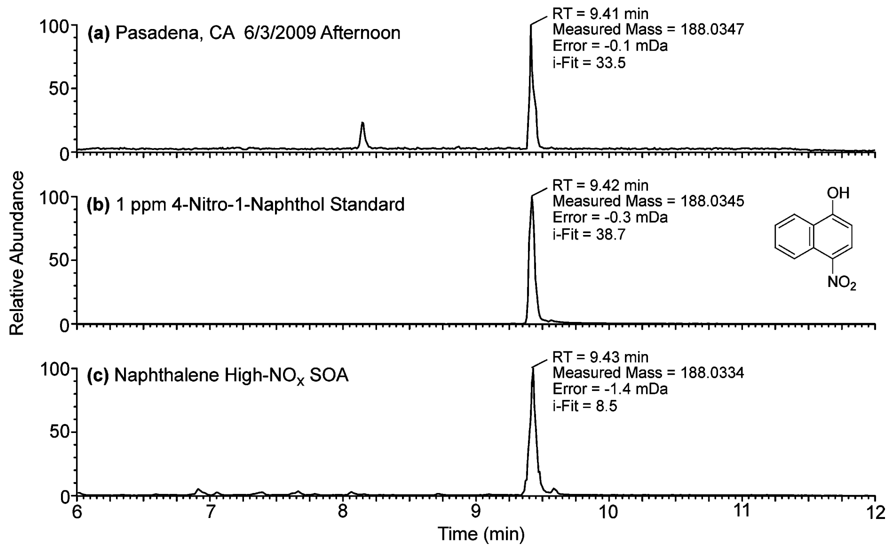

Figure 11. UPLC/(−)ESI-TOFMS EICs of *m/z* 188 from (a) ambient samples collected in Pasadena, CA, (b) a 1 ppm standard of 4-nitro-1-naphthol, and (c) naphthalene high-NO_x experiments (Experiment 6).

that could be used in a SOA source apportionment methods.[99,100] Additionally, Figure 3S (Supporting Information) shows the UPLC/(−)ESI-TOFMS EICs of *m/z* 165 obtained for a typical naphthalene high-NO_x SOA sample, a 10 ppm phthalic acid standard, and an urban aerosol sample collected from Birmingham, AL. The use of phthalic acid as a potential tracer compound for naphthalene photooxidation is tempting due to the large quantities (~14 ng m^{-3}) found in the ambient aerosol sample collected from Birmingham, AL. In comparison, 2-methyltetrols, which are ambient tracer compounds for isoprene SOA, have been measured between 200 pg m^{-3} and 365 ng m^{-3} during the summer in aerosol samples collected from many forested locations.[101] Since isoprene is the most abundant nonmethane hydrocarbon emitted into the atmosphere annually, the mass concentrations of phthalic acid found in urban aerosol samples analyzed in the present study are of some significance. In fact, phthalic acid and other dicarboxylic acids have been previously proposed as tracers.[102,103] However, because phthalic acid/anhydride is known to be formed from a wide variety of sources including sewage sludge[104,105] and plastic processing,[106] its use as a tracer is of questionable value.

Figure 10 shows the UPLC/(−)ESI-TOFMS EICs of *m/z* 181 obtained in a typical naphthalene high-NO_x SOA sample and in an urban aerosol sample collected from Pasadena, CA. The chromatographic peaks eluting at 5.45 min have the same elemental compositions (i.e., molecular formulas) as determined by the accurate mass measurements. This strongly indicates that the hydroxy phthalic acid product characterized in Table 3 can be used as an ambient tracer compound for naphthalene SOA; however, it cannot be ruled out that, as with phthalic acid, other sources may contribute to the formation of hydroxy phthalic acid in ambient aerosol. As a result, we cannot suggest that hydroxy phthalic acid be used solely as an ambient tracer compound for naphthalene SOA.

Another naphthalene high-NO_x SOA constituent found in the urban aerosol samples is 4-nitro-1-naphthol (MW 189). Figure 11 shows the UPLC/(−)ESI-TOFMS EICs of *m/z* 188 obtained for an urban aerosol sample collected from Pasadena, CA, a 1 ppm 4-nitro-1-naphthol authentic standard, and a typical naphthalene high-NO_x SOA sample. The comparison of these EICs clearly demonstrates the presence of this naphthalene high-NO_x SOA compound in ambient aerosol. Additionally, Figure 4S

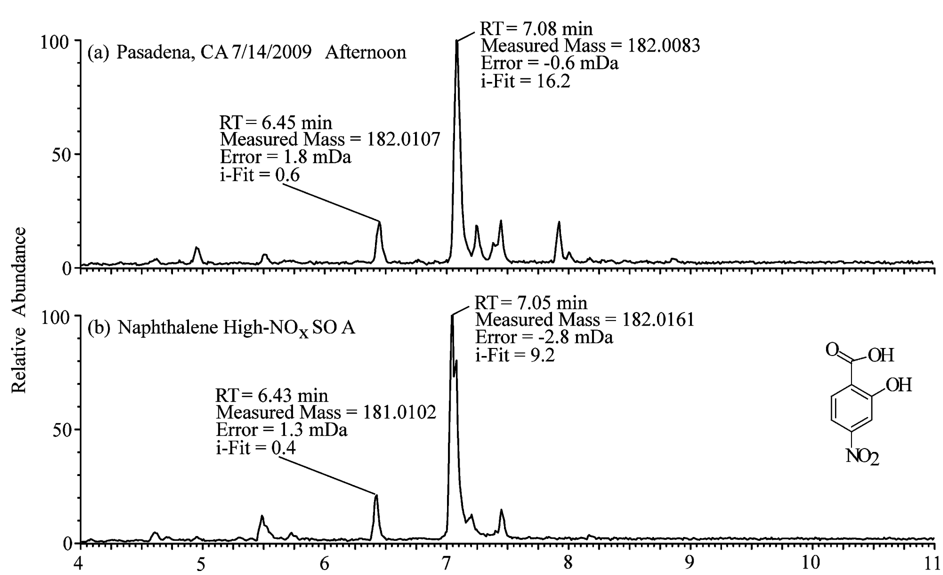

Figure 12. UPLC/(−)ESI-TOFMS EICs of *m/z* 182 from (a) ambient samples collected in Pasadena, CA and (b) naphthalene high-NO_x experiments (Experiment 6).

(Supporting Information) shows the UPLC/(−)ESI-TOFMS EICs of *m*/*z* 188 obtained for a typical naphthalene high-NO_x SOA sample, a 1 ppm 4-nitro-1-naphthol authentic standard, and an urban aerosol sample collected from Birmingham, AL, respectively. Concentrations of 4-nitro-1-naphthol from the Birmingham, AL site were found to be 1.6 ng m^{-3}, and the concentration of 4-nitro-1-naphthol collected from Pasadena, CA during summertime polluted conditions was 228 pg m^{-3}. This compound could prove to be an excellent ambient tracer for anthropogenic PAH chemistry. Apparent from the chamber studies, and Birmingham, AL and Pasadena, CA ambient aerosol samples, this compound, found at concentrations comparable to those of other common tracers (i.e., 2-methyltetrol), appears not to have been reported from alternate biogenic or anthropogenic sources. The added concern of N-containing naphthalene compounds, such as the 4-nitro-1-naphthol found in these ambient aerosol samples, as possible carcinogens makes these compounds of particular interest.

Comparison of the UPLC/(−)ESI-TOFMS EICs of *m*/*z* 182 found in Figure 12 demonstrate that the hydroxy nitrobenzoic acid with MW 183 characterized in the naphthalene high-NO_x SOA (Table 3) is also present in aerosol samples collected from Pasadena, CA. We note that this single-ring aromatic SOA constituent may also form in the atmosphere due to the photooxidation of SAHs (e.g., toluene). However, we have verified that naphthalene is a valid precursor to the presence of this compound in SOA. Since other SAHs and PAHs likely contribute to the formation of this compound in urban aerosol, it is likely not reasonable to use this compound solely as a naphthalene SOA tracer.

As a result of our detailed comparison of the laboratory-generated naphthalene high-NO_x SOA and the urban aerosol samples, we recommend that 4-nitro-1-naphthol might serve as a suitable ambient tracer for naphthalene SOA. It is worth mentioning that other compounds not highlighted here in this discussion were also observed in both the laboratory-generated and ambient aerosol, but these were concluded to be unsuitable ambient tracer compounds for naphthalene SOA; these include the following $[M - H]^-$ ions identified in Table 3: *m*/*z* 137,149,154, 179, 193, and 209.

5. Conclusions

We report extensive studies on the gas- and particle-phase constituents produced from the OH-initiated photooxidation of naphthalene under both high- and low-NO_x conditions. These studies provide significant insights into the chemical mechanisms that lead to SOA formation. For the high-NO_x case, 53% of the SOA mass is chemically identified, of which organic peroxides constitute 28%. The comparison of O/C and H/C ratios between the off-line molecularly characterized analyses are in agreement with measurements from online bulk measurements suggesting that the chemically characterized portion of the aerosol is representative of bulk aerosol components. Additionally, hydroxybenzene sulfonic acid is observed in the aerosol phase for both the low- and high-NO_x cases, although a mechanism for the generation of this product is not established. Under low-NO_x conditions, ∼68% of the SOA mass has been chemically identified, of which 26.2% is associated with organic peroxides. A significant enhancement in the formation of acids is observed relative to the high-NO_x case.

Naphthalene high-NO_x SOA constituents characterized in the present study are compared with urban aerosol samples collected from Birmingham, AL and Pasadena, CA, confirming the presence of SOA from naphthalene photooxidation in the urban atmosphere. In particular, phthalic acid, hydroxy phthalic acid, 4-nitro-1-naphthol and hydroxy nitrobenzoic acid are observed in both the laboratory-generated high-NO_x SOA and the urban organic aerosols. Of these compounds, 4-nitro-1-naphthol appears to be a valid ambient organic tracer for naphthalene high-NO_x SOA.

Acknowledgment. This research was funded by the Office of Science (BER), US Department of Energy Grant No. DE-FG02-05ER63983, US Environmental Protection Agency STAR Research Assistance Agreement No. RD-83374901 and US National Science Foundation grant ATM-0432377. The Electronic Power Research Institute provided support for the SEARCH network field samples. The GC/TOF and CIMS instruments used in this study were purchased as part of a major research instrumentation grant from the National Science Foundation (ATM-0619783). Assembly and testing of the CIMS instrument was supported by the Davidow Discovery Fund. The Waters UPLC/(−)ESI-TOFMS (LCT Premier XT TOFMS) was purchased in 2006 with a grant from the National Science Foundation, Chemistry Research Instrumentation and Facilities Program (CHE-0541745). We thank J. Stockdill for synthesis of 2-formylcinnamaldehyde. We would also like to thank E. S. Edgerton of Atmospheric Research & Analysis (ARA), Inc., for providing the high-volume filter sampler, as well as providing detailed information on its operation procedures, used in the sampling of fine aerosols during PACO. This publication has not been formally reviewed by the EPA. The views expressed in this document are solely those of the authors and EPA does not endorse any products mentioned in this publication.

Note Added in Proof. We proposed the formation of ring-opening products by a bicyclic peroxy intermediate in the text and in Scheme 5. After this work was submitted the following paper came to our attention: Nishino, N.; Arey, J.; Atkinson R. *Environ. Sci. Technol.* **2009**, in press. Nishino et al. also suggest the formation of phthaldialdehyde and glyoxal by the route in Scheme 5.

Supporting Information Available: Table 1S lists the chemicals employed in this study along with their purities. Tables 2S−7S display identification, quantification and (−)ESI-ITMS MS^2 information for experiments 2−8. EICs for selected photooxidation products observed using the GC/EI-TOFMS technique are shown in Figure 1S. Figure 2S compares mass spectra for 2-formylcinnamladehyde (MW 160) from injection of the standard and from chamber studies. Figures 3S and 4S compare ambient data collected in Birmingham, AL and samples collected in Pasadena, CA, with authentic standards. This material is available free of charge via the Internet at http://pubs.acs.org.

References and Notes

(1) Kroll, J. H.; Seinfeld, J. H. *Atmos. Environ.* **2008**, *42*.

(2) Volkamer, R.; Jimenez, J. L.; Martini, F. S.; Dzepina, K.; Zhang, Q.; Salcedo, D.; Molina, L. T.; Worsnop, D. R.; Molina, M. J. *Geophys. Res. Lett.* **2006**, *33*, 4.

(3) Heald, C. L.; Jacob, D. J.; Park, R. J.; Russell, L. M.; Huebert, B. J.; Seinfeld, J. H.; Liao, H.; Weber, R. J. *Geophys. Res. Lett.* **2005**, *32*, 4.

(4) de Gouw, J. A.; Middlebrook, A. M.; Warneke, C.; Goldan, P. D.; Kuster, W. C.; Roberts, J. M.; Fehsenfeld, F. C.; Worsnop, D. R.; Canagaratna, M. R.; Pszenny, A. A. P.; Keene, W. C.; Marchewka, M.; Bertman, S. B.; Bates, T. S. *J. Geophys. Res.* **2005**, *110*.

(5) Claeys, M.; Graham, B.; Vas, G.; Wang, W.; Vermeylen, R.; Pashynska, V.; Cafmeyer, J.; Guyon, P.; Andreae, M. O.; Artaxo, P.; Maenhaut, W. *Science* **2004**, *303*, 1173.

(6) Claeys, M.; Wang, W.; Ion, A. C.; Kourtchev, I.; Gelencsér, A.; Maenhaut, W. *Atmos. Environ.* **2004**, *38*, 4093.

(7) Dommen, J.; Metzger, A.; Duplissy, J.; Kalberer, M.; Alfarra, M. R.; Gascho, A.; Weingartner, E.; Prévôt, A. S. H.; Verheggen, B.; Baltensperger, U. *Geophys. Res. Lett.* **2006**, *33*.

(8) Edney, E. O.; Kleindienst, T. E.; Jaoui, M.; Lewandowski, M.; Offenberg, J. H.; Wang, W.; Claeys, M. *Atmos. Environ.* **2005**, *39*, 5281.

(9) Kroll, J. H.; Ng, N. L.; Murphy, S. M.; Flagan, R. C.; Seinfeld, J. H. *Geophys. Res. Lett.* **2005**, *32*, L18808.

(10) Kroll, J. H.; Ng, N. L.; Murphy, S. M.; Flagan, R. C.; Seinfeld, J. H. *Environ. Sci. Technol.* **2006**, *40*, 1869.

(11) Surratt, J. D.; Murphy, S. M.; Kroll, J. H.; Ng, N. L.; Hildebrandt, L.; Sorooshian, A.; Szmigielski, R.; Vermeylen, R.; Maenhaut, W.; Claeys, M.; Flagan, R. C.; Seinfeld, J. H. *J. Phys. Chem. A* **2006**, *110*, 9665.

(12) Szmigielski, R.; Surratt, J. D.; Vermeylen, R.; Szmigielska, K.; Kroll, J. H.; Ng, N. L.; Murphy, S. M.; Sorooshian, A.; Seinfeld, J. H.; Claeys, M. *J. Mass Spectrom.* **2007**, *42*, 101.

(13) Ng, N. L.; Kroll, J. H.; Chan, A. W. H.; Chhabra, P. S. *Atmos. Chem. Phys.* **2007**, *7*.

(14) Song, C.; Na, K. S.; Cocker, D. R. *Environ. Sci. Technol.* **2005**, *39*, 3143.

(15) Chan, A. W. H.; Kautzman, K. E.; Chhabra, P. S.; Surratt, J. D.; Chan, M. N.; Crounse, J. D.; Kürten, A.; Wennberg, P. O.; Flagan, R. C.; Seinfeld, J. H. *Atmos. Chem. Phys.* **2009**, *9*, 3049.

(16) Hatakeyama, S.; Izumi, K.; Fukuyama, T.; Akimoto, H.; Washida, N. *J. Geophys. Res.* **1991**, *96*, 947.

(17) Ng, N. L.; Chhabra, P. S.; Chan, A. W. H.; Surratt, J. D.; Kroll, J. H.; Kwan, A. J.; McCabe, D. C.; Wennberg, P. O.; Sorooshian, A.; Murphy, S. M.; Dalleska, N. F.; Flagan, R. C.; Seinfeld, J. H. *Atmos. Chem. Phys.* **2007**, *7*, 3909.

(18) Presto, A. A.; Huff Hartz, K. E.; Donahue, N. M. *Environ. Sci. Technol.* **2005**, *39*.

(19) Docherty, K. S.; Wu, W.; Lim, Y. B.; Ziemann, P. J. *Environ. Sci. Technol.* **2005**, *39*, 4049.

(20) Gao, S.; Keywood, M.; Ng, N. L.; Surratt, J.; Varutbangkul, V.; Bahreini, R.; Flagan, R. C.; Seinfeld, J. H. *J. Phys. Chem. A* **2004**, *108*, 10147.

(21) Iinuma, Y.; Böge, O.; Gnauk, T.; Herrmann, H. *Atmos. Environ.* **2004**, *38*, 761.

(22) Jang, M. S.; Czoschke, N. M.; Lee, S.; Kamens, R. M. *Science* **2002**, *298*, 814.

(23) Kalberer, M.; Paulsen, D.; Sax, M.; Steinbacher, M.; Dommen, J.; Prevot, A. S. H.; Fisseha, R.; Weingartner, E.; Frankevich, V.; Zenobi, R.; Baltensperger, U. *Science* **2004**, *303*, 1659.

(24) Liggio, J.; Li, S. M.; McLaren, R. *J. Geophys. Res.* **2005**, *110*.

(25) Liggio, J.; Li, S. M.; McLaren, R. *Environ. Sci. Technol.* **2005**, *39*, 1532.

(26) Tobias, H. J.; Ziemann, P. J. *Environ. Sci. Technol.* **2000**, *34*, 2105.

(27) Tolocka, M. P.; Jang, M.; Ginter, J. M.; Cox, F. J.; Kamens, R. M.; Johnston, M. V. *Environ. Sci. Technol.* **2004**, *38*, 1428.

(28) Gómez-González, Y.; Surratt, J. D.; Cuyckens, F.; Szmigielski, R.; Vermeylen, R.; Jaoui, M.; Lewandowski, M.; Offenberg, J. H.; Kleindienst, T. E.; Edney, E. O.; Blockhuys, F.; Van Alsenoy, C.; Maenhaut, W.; Claeys, M. *J. Mass Spectrom* **2008**, *43*, 371.

(29) Iinuma, Y.; Müller, C.; Berndt, T.; Böge, O.; Claeys, M.; Herrmann, H. *Environ. Sci. Technol.* **2007**, *41*, 6678.

(30) Iinuma, Y.; Müller, C.; Böge, O.; Gnauk, T.; Herrmann, H. *Atmos. Environ.* **2007**, *41*, 5571.

(31) Surratt, J. D.; Gómez-González, Y.; Chan, A. W. H.; Vermeylen, R.; Shahgholi, M.; Kleindienst, T. E.; Edney, E. O.; Offenberg, J. H.; Lewandowski, M.; Jaoui, M.; Maenhaut, W.; Claeys, M.; Flagan, R. C.; Seinfeld, J. H. *J. Phys. Chem. A* **2008**, *112*, 8345.

(32) Surratt, J. D.; Kroll, J. H.; Kleindienst, T. E.; Edney, E. O.; Claeys, M.; Sorooshian, A.; Ng, N. L.; Offenberg, J. H.; Lewandowski, M.; Jaoui, M.; Flagan, R. C.; Seinfeld, J. H. *Environ. Sci. Technol.* **2007**, *41*, 517.

(33) Galloway, M. M.; Chhabra, P. S.; Chan, A. W. H.; Surratt, J. D.; Flagan, R. C.; Seinfeld, J. H.; Keutsch, F. N. *Atmos. Chem. Phys.* **2009**, *9*, 3331.

(34) Kroll, J. H.; Ng, N. L.; Murphy, S. M.; Varutbangkul, V.; Flagan, R. C.; Seinfeld, J. H. *J. Geophys. Res.* **2005**, *110*, 10.

(35) Volkamer, R.; Martini, F. S.; Molina, L. T.; Salcedo, D.; Jimenez, J. L.; Molina, M. J. *Geophys. Res. Lett.* **2007**, *34*.

(36) Robinson, A. L.; Donahue, N. M.; Shrivastava, M. K.; Weitkamp, E. A.; Sage, A. M.; Grieshop, A. P.; Lane, T. E.; Pierce, J. R.; Pandis, S. N. *Science* **2007**, *315*, 1259.

(37) Schauer, J. J.; Kleeman, M. J.; Cass, G. R.; Simoneit, B. R. T. *Environ. Sci. Technol.* **1999**, *33*, 1578.

(38) Schauer, J. J.; Kleeman, M. J.; Cass, G. R.; Simoneit, B. R. T. *Environ. Sci. Technol.* **2002**, *36*, 1169.

(39) Ravindra, K.; Sokhi, R.; Van Grieken, R. *Atmos. Environ.* **2008**, *42*, 2895.

(40) Schauer, J. J.; Kleeman, M. J.; Cass, G. R.; Simoneit, B. R. T. *Environ. Sci. Technol.* **2001**, *35*, 1716.

(41) Schauer, J. J.; Kleeman, M. J.; Cass, G. R.; Simoneit, B. R. T. *Environ. Sci. Technol.* **1999**, *33*, 1566.

(42) Schauer, J. J.; Kleeman, M. J.; Cass, G. R.; Simoneit, B. R. T. *Environ. Sci. Technol.* **2002**, *36*, 567.

(43) Atkinson, R.; Arey, J. *Polycycl. Aromatic Compd.* **2007**, *27*, 15.

(44) Atkinson, R.; Aschmann, S. M.; Arey, J.; Carter, W. P. L. *Int. J. Chem. Kinetics* **1989**, *21*, 801.

(45) Bunce, N. J.; Liu, L.; Zhu, J.; Lane, D. A. *Environ. Sci. Technol.* **1997**, *31*, 2252.

(46) Mihele, C. M.; Wiebe, H. A.; Lane, D. A. *Polycycl. Aromatic Compd.* **2002**, *22*, 729.

(47) Wang, L.; Atkinson, R.; Arey, J. *Environ. Sci. Technol.* **2007**, *41*, 2803.

(48) Arey, J.; Atkinson, R.; Zielinska, B.; McElroy, P. A. *Environ. Sci. Technol.* **1989**, *23*, 321.

(49) Gupta, P.; Harger, W. P.; Arey, J. *Atmos. Environ.* **1996**, *30*, 3157.

(50) Helmig, D.; Arey, J.; Harger, W. P.; Atkinson, R.; Lopezcancio, J. *Environ. Sci. Technol.* **1992**, *26*, 622.

(51) Helmig, D.; Lopezcancio, J.; Arey, J.; Harger, W. P.; Atkinson, R. *Environ. Sci. Technol.* **1992**, *26*, 2207.

(52) Grosovsky, A. J.; Sasaki, J. C.; Arey, J.; Eastmond, D. A.; Parks, K. K.; Atkinson, R. *Res. Rep. Health Eff. Inst.* **1999**, i.

(53) Cocker, D. R.; Flagan, R. C.; Seinfeld, J. H. *Environ. Sci. Technol.* **2001**, *35*, 2594.

(54) Keywood, M. D.; Varutbangkul, V.; Bahreini, R.; Flagan, R. C.; Seinfeld, J. H. *Environ. Sci. Technol.* **2004**, *38*, 4157.

(55) Burkhardt, M. R.; Maniga, N. I.; Stedman, D. H.; Paur, R. *J. Anal. Chem.* **1988**, *60*, 816.

(56) Paulot, F.; Crounse, J. D.; Kjaergaard, H. G.; Kroll, J. H.; Seinfeld, J. H.; Wennberg, P. O. *Atmos. Chem. Phys.* **2009**, *9*, 1479.

(57) Crounse, J. D.; McKinney, K. A.; Kwan, A. J.; Wennberg, P. O. *Anal. Chem.* **2006**, *78*, 6726.

(58) Stein, S. M. Y.; Tchekhovski, D.; Mallard, G.; Mikaia, A.; Zaikin, V.; Zhu, J.; Clifton, C.; Sparkman, D. *The NIST Mass Spectral Search Program for the NIST/EPA/NIH Mass Spectral Library*, 2005 ed.; 2005.

(59) Surratt, J. D.; Gómez-González, Y.; Chan, A. W. H.; Vermeylen, R.; Shahgholi, M.; Kleindienst, T. E.; Edney, E. O.; Offenberg, J. H.; Lewandowski, M.; Jaoui, M.; Maenhaut, W.; Claeys, M.; Flagan, R. C.; Seinfeld, J. H. *J. Phys. Chem. A* **2008**, *112*, 8345.

(60) DeCarlo, P. F.; Kimmel, J. R.; Trimborn, A.; Northway, M. J.; Jayne, J. T.; Aiken, A. C.; Gonin, M.; Fuhrer, K.; Horvath, T.; Docherty, K. S.; Worsnop, D. R.; Jimenez, J. L. *Anal. Chem.* **2006**, *78*, 8281.

(61) Allan, J. D.; Delia, A. E.; Coe, H.; Bower, K. N.; Alfarra, M. R.; Jimenez, J. L.; Middlebrook, A. M.; Drewnick, F.; Onasch, T. B.; Canagaratna, M. R.; Jayne, J. T.; Worsnop, D. R. *J. Aerosol Sci.* **2004**, *35*, 909.

(62) Bahreini, R.; Keywood, M. D.; Ng, N. L.; Varutbangkul, V.; Gao, S.; Flagan, R. C.; Seinfeld, J. H.; Worsnop, D. R.; Jimenez, J. L. *Environ. Sci. Technol.* **2005**, *39*, 5674.

(63) Aiken, A. C.; DeCarlo, P. F.; Jimenez, J. L. *Anal. Chem.* **2007**, *79*, 8350.

(64) Aiken, A. C.; Decarlo, P. F.; Kroll, J. H.; Worsnop, D. R.; Huffman, J. A.; Docherty, K. S.; Ulbrich, I. M.; Mohr, C.; Kimmel, J. R.; Sueper, D.; Sun, Y.; Zhang, Q.; Trimborn, A.; Northway, M.; Ziemann, P. J.; Canagaratna, M. R.; Onasch, T. B.; Alfarra, M. R.; Prevot, A. S. H.; Dommen, J.; Duplissy, J.; Metzger, A.; Baltensperger, U.; Jimenez, J. L. *Environ. Sci. Technol.* **2008**, *42*, 4478.

(65) Weber, R. J.; Orsini, D.; Daun, Y.; Lee, Y. N.; Klotz, P. J.; Brechtel, F. *Aerosol Sci. Technol.* **2001**, *35*, 718.

(66) Sorooshian, A.; Brechtel, F. J.; Ma, Y. L.; Weber, R. J.; Corless, A.; Flagan, R. C.; Seinfeld, J. H. *Aerosol Sci. Technol.* **2006**, *40*, 396.

(67) Edgerton, E. S.; Hartsell, B. E.; Saylor, R. D.; Jansen, J. J.; Hansen, D. A.; Hidy, G. M. *J. Air Waste Manage. Assoc.* **2005**, *55*, 1527.

(68) Hansen, D. A.; Edgerton, E. S.; Hartsell, B. E.; Jansen, J. J.; Kandasamy, N.; Hidy, G. M.; Blanchard, C. L. *J. Air Waste Manage. Assoc.* **2003**, *53*, 1460.

(69) Gao, S.; Surratt, J. D.; Knipping, E. M.; Edgerton, E. S.; Shahgholi, M.; Seinfeld, J. H. *J. Geophys. Res.* **2006**, *111*, D14314.

(70) Larson, R. A.; Garrison, W. J.; Marley, K. A. *Tetrahedron Lett.* **1986**, *27*, 3987.

(71) Nishino, N.; Arey, J.; Atkinson, R. *Environ. Sci. Technol.* 2009.

(72) Sasaki, J.; Aschmann, S. M.; Kwok, E. S. C.; Atkinson, R.; Arey, J. *Environ. Sci. Technol.* **1997**, *31*, 3173.

(73) Atkinson, R.; Aschmann, S. M.; Arey, J.; Zielinska, B.; Schuetzle, D. *Atmos. Environ.* **1989**, *23*, 2679.

(74) Fisseha, R.; Dommen, J.; Sax, M.; Paulsen, D.; Kalberer, M.; Maurer, R.; Hofler, F.; Weingartner, E.; Baltensperger, U. *Anal. Chem.* **2004**, *76*, 6535.

(75) Lu, R.; Wu, J.; Turco, R. P.; Winer, A. M.; Atkinson, R.; Arey, J.; Paulson, S. E.; Lurmann, F. W.; Miguel, A. H.; Eiguren-Fernandez, A. *Atmos. Environ.* **2005**, *39*, 489.

(76) Fraser, M. P.; Cass, G. R.; Simoneit, B. R. T. *Environ. Sci. Technol.* **1998**, *32*, 2051.

(77) Marr, L. C.; Kirchstetter, T. W.; Harley, R. A.; Miguel, A. H.; Hering, S. V.; Hammond, S. K. *Environ. Sci. Technol.* **1999**, *33*, 3091.

(78) Bunce, N. J. D., H. G. *Can. J. Chem.* **1992**, *70*, 1966.

(79) Lane, D. A.; Fielder, S. S.; Townsend, S. J.; Bunce, N. J.; Zhu, J.; Liu, L.; Wiens, B.; Pond, P. *Polycycl. Aromatic Compd.* **1996**, *9*, 53.

(80) Nishino, N.; Atkinson, R.; Arey, J. *Environ. Sci. Technol.* **2008**, *42*, 9203.

(81) Qu, X. H.; Zhang, Q. Z.; Wang, W. X. *Chem. Phys. Lett.* **2006**, *429*, 77.

(82) Atkinson, R.; Arey, J. *Polycycl. Aromatic Compd.* **2007**, *27*, 15.

(83) Nishino, N. A. J.; Atkinson, R. *Environ. Sci. Technol.* 2009.

(84) Dekermenjian, M.; Allen, D. T.; Atkinson, R.; Arey, J. *Aerosol Sci. Technol.* **1999**, *30*, 273.

(85) Palen, E. J.; Allen, D. T.; Pandis, S. N.; Paulson, S. E.; Seinfeld, J. H.; Flagan, R. C. *Atmos. Environ., Part A* **1992**, *26*, 1239.

(86) Koch, R.; Knispel, R.; Elend, M.; Siese, M.; Zetzsch, C. *Atmos. Chem. Phys.* **2007**, *7*, 2057.

(87) Glowacki, D. R.; Wang, L. M.; Pilling, M. J. *J. Phys. Chem. A* **2009**, *113*, 5385.

(88) Suh, I.; Zhang, R. Y.; Molina, L. T.; Molina, M. J. *J. Am. Chem. Soc.* **2003**, *125*, 12655.

(89) Calvert, J. G.; Atkinson, R.; Becker, K. H.; Kamens, R. M.; Seinfeld, J. H.; Wallington, T. J.; Yarwood, G. *The Mechanisms of Atmospheric Oxidation of Aromatic Hydrocarbons*; Oxford University Press, Inc.: New York, 2002.

(90) Reemtsma, T. *J. Chromatogr. A* **2003**, *1000*, 477.

(91) Rodil, R.; Quintana, J. B.; Lopez-Mahia, P.; Muniategui-Lorenzo, S.; Prada-Rodriguez, D. *Anal. Chem.* **2008**, *80*, 1307.

(92) Frömel, T.; Peschka, M.; Fichtner, N.; Hierse, W.; Ignatiev, N. V.; Bauer, K. H.; Knepper, T. P. *Rapid Commun. Mass Spectrom.* **2008**, *22*, 3957.

(93) Barnes, I.; Hjorth, J.; Mihalopoulos, N. *Chem. Rev.* **2006**, *106*, 940.

(94) Johnson, M. T.; Bell, T. G. *Environ. Chem.* **2008**, *5*, 259.

(95) Tang, M. J.; Zhu, T. *Sci. China Ser. B-Chem.* **2009**, *52*, 93.

(96) Lara-Martin, P. A.; Gomez-Parra, A.; Gonzalez-Mazo, E. *Environ. Pollut.* **2008**, *156*, 36.

(97) Lara-Martin, P. A.; Gomez-Parra, A.; Gonzalez-Mazo, E. *J. Chromatogr. A* **2006**, *1137*, 188.

(98) Altieri, K. E.; Turpin, B. J.; Seitzinger, S. P. *Atmos. Chem. Phys.* **2009**, *9*, 2533.

(99) Kleindienst, T. E.; Jaoui, M.; Lewandowski, M.; Offenberg, J. H.; Lewis, C. W.; Bhave, P. V.; Edney, E. O. *Atmos. Environ.* **2007**, *41*, 8288.

(100) Offenberg, J. H.; Lewis, C. W.; Lewandowski, M.; Jaoui, M.; Kleindienst, T. E.; Edney, E. O. *Environ. Sci. Technol.* **2007**, *41*, 3972.

(101) Hallquist, M.; Wenger, J. C.; Baltensperger, U.; Rudich, Y.; Simpson, D.; Claeys, M.; Dommen, J.; Donahue, N. M.; George, C.; Goldstein, A. H.; Hamilton, J. F.; Herrmann, H.; Hoffmann, T.; Iinuma, Y.; Jang, M.; Jenkin, M. E.; Jimenez, J. L.; Kiendler-Scharr, A.; Maenhaut, W.; McFiggans, G.; Mentel, T. F.; Monod, A.; Prevot, A. S. H.; Seinfeld, J. H.; Surratt, J. D.; Szmigielski, R.; Wildt, J. *Atmos. Chem. Phys.* **2009**, *9*, 5155.

(102) Schuetzle, D.; Cronn, D.; Crittenden, A. L.; Charlson, R. J. *Environ. Sci. Technol.* **1975**, *9*, 838.

(103) Chebbi, A.; Carlier, P. *Atmos. Environ.* **1996**, *30*, 4233.

(104) Mougin, C.; Dappozze, F.; Brault, A.; Malosse, C.; Schmidt, J. E.; Amellal-Nassr, N.; Patureau, D. *Environ. Chem. Lett.* **2006**, *4*, 201.

(105) Thiruvenkatachari, R.; Kwon, T. O.; Moon, I. S. *J. Environ. Sci. Health, Part A* **2006**, *41*, 1685.

(106) Butte, W.; Hostrup, O.; Walker, G. *Gefahrstoffe Reinhaltung Der Luft* **2008**, *68*, 79.

JP908530S